Spatial Multiplexing Transmit Diversity Hybrid Schemes For Future Wireless Local Area Network

Hwa Sin Tan

A thesis submitted for the degree of Doctor of Philosophy.
The University of Edinburgh.
March 2005

Abstract

The current development of the IEEE 802.11n wireless local area network (WLAN) standard as an improvement to the current IEEE 802.11a standard open up opportunities into several areas of research. One of the prerequisites of this standard is that the medium access layer (MAC) should support a real data throughput of about 100 Mbps. In order to realise this requirement at reasonable performance, utilising multiple input multiple output (MIMO) technology would be necessary. Preferably, the proposed MIMO system should be implemented at low complexity such that the hardware devices can be manufactured at low cost. The two factors, MIMO systems and low complexity, form the motivation of the work reported in this thesis.

This thesis focuses on several spatial multiplexing, space-time coding and hybrid spatial multiplexing and space-time coding techniques that are capable of delivering high data rates at low complexity. In this context, several MIMO hybrid schemes with low complexity detection algorithms will be developed and investigated.

Initially, three MIMO schemes V-BLAST, Alamouti space time block code (STBC) and Dual Alamouti STBC (i.e., the hybrid technique of concatenating two Alamouti transmitters), which are potential candidates for the IEEE 802.11n standard, are studied and compared with one another. Their potential channel capacity will be analysed while simulations using physically realisable decoders are performed and compared with respect to three parameters, namely, spectral efficiency, number of antennas and channel correlation.

The possibility of exploiting multiuser MIMO transmission in a WLAN leads to the analysis of the V-BLAST and Dual Alamouti STBC in a two users scenario. Using the zero forcing (ZF) and minimum mean square error (MMSE) detectors coupled with interference suppression and cancellation techniques, the robustness of V-BLAST and Dual Alamouti in a two users environment are studied.

Then the possibility using of Alamouti space frequency block code (SFBC) in an OFDM system to replace Alamouti STBC whenever required is investigated. In this context, the implementation of a simplified ZF technique to combat the uncertainty in channel conditions is proposed. Simulation results are generated to compare the performance of this technique with Alamouti STBC and cyclic delay diversity (CDD).

Lastly, three transmit antennas CDD and Alamouti STBC hybrid schemes are suggested in this thesis for IEEE 802.11n to limit the physical size of wireless devices, while still being capable of delivering 100 Mbps MAC throughput. More emphasis has been focused on the latter scheme due to its superior performance. With regards to this, two simplified detection algorithms and a bit loading scheme without channel feedback information at the transmitter are proposed. Finally, a switching scheme between the Alamouti hybrid and Alamouti STBC has been designed to maximised the system throughput and coverage.

Declaration of originality

I hereby declare that the research recorded in this thesis and the thesis itself was composed and originated entirely by myself in the Institute of Digital Communications at University of Edinburgh and Toshiba Telecommunications Research Laboratory in Bristol, Toshiba Research Europe Ltd.

I would like to clarify that some mathematical fuctions in the form of C source code has been obtained from [1].

Acknowledgements

First and foremost, I would like to thank my academic supervisor, John Thompson for his continuous and patient guidance and valuable advice on my PhD study even when I was away from the University and his effort in helping me to deliver this thesis promptly. I would also like to thank my second academic supervisor, Dave Cruickshank for his comments on my work. I am grateful to Steve McLaughlin for his timely effort in reading and providing feedback on my thesis.

I am grateful to my industrial mentor Yong Sun for his timely and valuable advice during my ten month period in Toshiba Telecommunication Research Laboratory (TRL) Europe Ltd at Bristol and Yuk Chow for supervising me at the beginning of my PhD. Also, I would like to thank Steve Parker, Magnus Sandell, Darren Mcnamara, Mong Yee, Paul Strauch and Joe McGeehan for their effort in assisting me both technically and non-technically during my time in TRL.

I would like to express my sincere gratitude to Toshiba Telecommunication Research Laboratory Europe Ltd at Bristol for funding my PhD work.

Special thanks to all my friends in the IDCOM group and colleagues in TRL for sharing their pleasant time with me.

Lastly, I would like to thank my parent and family for whom has been always supportive in my PhD study.

Contents

List of figures

List of tables

Acronyms

A/D	Analogue to Digital
AoA	Angle of Arrival
AP	Access Point
APP	A Posterior Probablity
AS	Angular Spread
BER	Bit Error Probability
BER	Bit Error Ratio
CBTPOS	Coded Bits Transmitted Per OFDM Symbol
CCI	Co-channel Interference
CDD	Cyclic Delay Diversity
CDMA	Code Division Multiple Access
CDDSM	Cyclic Delay Diversity Spatial Multiplexing Scheme
CSMA	Carrier Sense Multiple Acess
CSI	Channel State Information
CP	Cyclic Prefix
D/A	Digital to Analogue
DS-CDMA	Direct Sequence Code Division Multiple Access
FEC	Forward Error Correction Code
FER	Frame Error Rate
FDMA	Frequency Division Multiple Access
FFT	Fast Fourier Transform
FH-CDMA	Frequency Hopping Code Division Multiple Access
IC	Interference Cancellation
ICI	Inter-carrier interference
IFFT	Inverse Fast Fourier Transform
IS	Interference Suppression
ISI	Inter-symbol Interference
LOS	Line-of-sight
LLR	Log-likelihood Ratio

MAC	Medium Access Control
Mbps	Mega bits per second
MC-CDMA	Multi-carrier Code Division Multiple Access
MCS	Modulation Coded Scheme
MHz	Mega Hertz
MIMO	Multiple Input Multiple Output
MMSE	Minimum Mean Square Error
MRC	Maximal Ratio Combining
MT	Mobile Terminal
MUI	Multiuser Interference
NLOS	Non-line-of-sight
OFDM	Orthogonal Frequency Division Multiplexing
OFDMA	Orthogonal Frequency Division Multiple Access
OSIC	Ordered Successive Interference Cancellation
OSTBC	Orthogonal Space Time Block Code
QAM	Quadrature Amplitude Modulation
PAP	Peak to Average Power
PAS	Power Azimuth Spectrum
PDA	Personal Digital Assistant
PHY	Physical layer
POSTBC	Partial Orthogonal Space Time Block Code
P/S	Parallel to Serial
PSD	Power Spectrum Density
RC	Raised Cosine
RTS	Request To Send
SC-DFE	Single Carrier with Decision Feedback Frequency Equalisation
SC-FE	Single Carrier With Frequency Equalisation
SC-LE	Single Carrier with Linear Frequency Equalisation
SDMA	Spatial Division Multiple Access
SFBC	Space Frequency Block Code
SIC	Successive Interference Cancellation
SISO	Single Input Single Output
SINR	Signal-to-Interference-plus-Noise-Ratio

SNR	Signal-to-Noise-Ratio
S/P	Serial to Parallel
STBC	Space Time Block Code
SVD	Singular Value Decomposition
TH-CDMA	Time Division Code Divison Multiple Access
WLAN	Wireless Local Area Network
ZF	Zero Forcing

Nomenclature

ν_s	asynchronous interference shift
b_c	position of bits of modulated symbols
d_{BP}	breakpoint distance of free space path loss
R	Channel Code Rate
h	channel coefficients
$\mathbf{H}$	channel matrix response
$\mathbf{h}$	subchannel matrix response of POSTBC
$\mathbf{H}^{-}$	channel being nulled
c_{const}	constant
α_s	constant for Alamouti SFBC
ν	constant for Alamouti SFBC channel
ψ	constant for BER probability
ξ	constant for BER probability
κ	correlation factor
N_{cons}	constellation bits
δ_{cy}	cyclic delay shift
θ_{cy}	cyclic delay shifted phase
y	detected signal
$\mathbf{y}$	detected signal vector
d	distance
D	Distance in radians
L_{FS}	free space path loss
f	frequency index
G_{Tx}	gain at transmit antenna
G_{Rx}	gain at receive antenna
$\mathbf{\Omega}$	IFFT and CP matrix
$\bar{\mathbf{\Omega}}$	IFFT matrix
$\mathbf{I}_{size}$	identity matrix
X	matrix of Alamouti STBC encoded symbols

$\mathbf{G}$	matrix representation for either MMSE or ZF estimate
l_p	multipath index
γ_{mp}	multipath impulse response
ε_m	multiuser efficiency
η	noise coefficients
$\boldsymbol{\eta}$	noise signal vector
σ_n^2	noise variance
M_{al}	number of Alamouti transmitters
B_c	number of bits per constellation symbol
N_{CP}	length of cyclic prefix
L_{mp}	number of delay multipath impulses
M_q	number of non-Alamouti transmitters
N_{nu}	number of supported users in a non-multiuser detection system
N_u	number of supported users in a multiuser detection system
J_c	number of different constellations in a modulation scheme
N_I	number of interferers
L_{PL}	path loss model
L_{sys}	system loss factor
P_T	Power at transmitter
P_R	Power at receiver
σ_{pd}	pre-detection mean power of multipath signal
$\Pr()$	Probability
ρ_{pdf}	Probabality density function
G_p	processing gain of CDMA system
$Q()$	Quantiser
F_r	ratio of intra-cell interference to total interference
β_R	Rayleigh coefficients
n	receive antenna index
N	receive antenna total
r	receive signal
$\mathbf{r}$	receive signal vector
$\ddot{r}$	receive signal vector of Alamouti SFBC
$\mathbf{r}'$	resultant received signal vector from the 2 simplified Rx POSTBC

$\mathbf{r}''$	resultant received signal vector from the 2 simplified Rx POSTBC
$\mathbf{Z}$	resultant matrix from summation and multiplication of POSTBC MMSE
k_c	subcarrier index
R_c	subcarrier spacing in MC-CDMA
K_c	subcarrier total
T_s	symbol period
T_{sub}	subchannel signalling interval
T_{sam}	sampling period
Γ	SNR
Υ	SINR in the BER probability
m	transmit antenna index
M	transmit antenna total
x	transmit symbol
s	time domain IFFT OFDM symbols
$\ddot{x}$	transmitted Alamouti SFBC symbols
$\hat{\mathbf{x}}$	transmitted symbol estimate vector
$\hat{x}$	transmit symbol estimate
$\hat{\mathbf{x}}$	transmit symbol estimate vector
$\mathbf{x}$	transmit symbols vector
t	time index
k_{Tx}	transmit stream with the highest SINR
λ	one unit wavelength
$\mathbf{w}$	weighting matrix or vector
$\mathbf{w}_1$	weighting matrix of 2 Rx simplified POSTBC detector
$\mathbf{w}_{APP}$	pre-multiplying weighting matrix for POSTBC simplied joint detection
$\mathbf{H_{ZF}}$	ZF estimate
$\mathbf{G_s}$	simplified ZF estimate for Alamouti SFBC
$\mathbf{S}$	singular values matrix
$\mathbf{U}$	left matrix of SVD
$\mathbf{V}$	right matrix of SVD
$\mathbf{s_H}$	singular values of channel
$\boldsymbol{\kappa_r}$	covariance matrix of receiver
$\boldsymbol{\kappa_t}$	covariance matrix of transmitter

$\acute{\boldsymbol{\kappa}}_{\boldsymbol{r}}$	square root covariance matrix of receiver
$\acute{\boldsymbol{\kappa}}_{\boldsymbol{t}}$	square root covariance matrix of transmitter
$\boldsymbol{\kappa}_{\acute{\boldsymbol{M}}\boldsymbol{IMO}}$	square root covariance matrix of MIMO channel
$\boldsymbol{\kappa}_{\boldsymbol{MIMO}}$	covariance matrix of MIMO channel
$\boldsymbol{\Omega}$	eigenvectors matrix
$\boldsymbol{\Sigma}$	eigenvalues matrix
c_p	CDMA chips
δ	Kronecker delta function
S_p	permutation of a set of intergers
α_{MMSE}	constant used for V-BLAST MMSE SNR
β_{MMSE}	constant used for V-BLAST MMSE SNR
τ	time index
$\boldsymbol{\beta_D}$	matrix used in Dual Alamouti STBC equation
$\boldsymbol{\alpha_D}$	matrix used in Dual Alamouti STBC equation
$\boldsymbol{\theta_D}$	matrix used in Dual Alamouti STBC equation
$\ddot{\mathbf{r}}$	received signal vector in Dual Alamouti
$\ddot{\mathbf{H}}$	channel matrix of Alamouti STBC
$\ddot{\mathbf{x}}$	transmitted signal matrix in Dual Alamouti STBC
$\ddot{\boldsymbol{\eta}}$	received signal matrix in Dual Alamouti
$F_c()$	channel funtion
$\acute{\mathbf{H}}$	vectorised MIMO channel
P_{l_p}	power at the l_p channel tap
$\mathbf{H_A}$	channel matrix of Alamouti STBC
$\mathbf{H_D}$	channel matrix of Dual Alamouti STBC
$\mathbf{H_F}$	channel matrix of Alamouti SFBC
$\mathbf{G_F}$	conventional ZF estimates of Alamouti SFBC
$\dot{\mathbf{r}}$	received signal vector in Alamouti SFBC
$\dot{\mathbf{H}}$	channel matrix of Alamouti SFBC
$\dot{\mathbf{x}}$	transmitted signal matrix in Alamouti SFBC
$\mathbf{H_C}$	CDD channel
$\mathbf{H_P}$	channel matrix of POSTBC
$\bar{r}$	received signal envelope of Rayleigh fading channel
$J_i()$	Bessel functions of the first kind and ith order

I_{intra}	magnitude of intra-cell interference
I_{inter}	magnitude of inter-cell interference
P_I	power of interferer
P_D	power of of desired user
P_c	power of user at a particular constellation
s_H	singular values
N_{CD}	number of different constellations in the modulation
C_{VB}	capacity of V-BLAST
C_{Al}	capacity of Alamouti STBC
C_{DA}	capacity of Dual Alamouti STBC
p_c	occurence probability of constellation point
ξ_i	coefficients of bit error probability of a QAM constellation
ψ_i	coefficients of bit error probability of a QAM constellation

Chapter 1
Introduction

The migration of wireless technology from analogue radio transmission to digital application has led the world of communication into a new modern era. A few examples in the advances of wireless applications are wide area digital mobile telephony within hundred of miles radius, wireless internet, digital radio and video transmission, etc. The trend of communication systems moving into wireless applications provides ongoing improvements and advancements in digital communication technologies and signal processing techniques.

It is only until the recent development of robust micron VLSI technology which has led to a sudden surge in wireless systems over past ten years as the implementation of compact wireless devices becomes realisable. Such systems like the migration from analog to digital mobile telephony system, e.g. GSM [3] and 3G [4], IEEE 802.11 [5] wireless local area networks (WLAN), IEEE 802.16 [6] wireless access and IEEE 802.15 [7] wireless personal area network (WPAN) are a few examples of the ongoing wireless development. Innovations in digital communication techniques, namely, code division multiple access (CDMA) used for 3G and IEEE 802.11b, orthogonal division frequency multiplexing (OFDM) for IEEE 802.11a and the ultra wideband (UWB) [8] proposal for IEEE 802.15, single carrier with frequency domain equalisation (SC-FE) proposed for IEEE 802.16 and multicarrier CDMA (MC-CDMA) proposed for 4G are some of the practical applications of digital communications. In this thesis, the development for future IEEE 802.11 WLAN standard will be the focus of the work.

1.1 Overview of Thesis Topic

With the high throughput study group (HTSG) [9] working towards the IEEE 802.11n standard, which is the next generation wireless local area network (WLAN), research into improvements to the current IEEE 802.11a is required. One of the areas that should be considered is the choice of modulation scheme. Since OFDM [10–16] had been proposed for the IEEE 802.11a, several modulation schemes have then been developed. Some of the schemes worth considering are MC-CDMA [10, 15, 17–19], SC-FE [2, 20–24] and flash OFDM [25]. Several papers [26–

31] have investigated one of these modulation schemes and compared relative to the others. Nonetheless, a comprehensive comparison of all these schemes from the perspective of WLAN has not yet been established.

One of the requirements imposed on the new standard requires that the medium access control (MAC) layer support data rate up to 100 Mbps. This means that the physical layer (PHY) must transmit data at 200 Mbps, with an approximate 50% MAC overhead efficiency. Whether or not IEEE 802.11n will be allocated a 20 or 40 MHz bandwidth channel, persisting with the single input single output (SISO) techniques as in IEEE 802.11a will not reach the 100 Mbps MAC pre-requisite at reasonable performance. For instance, the largest available constellation of 64 QAM with 3/4 code rate used over 40 MHz channel, will only yield an equivalent MAC data rate of 90Mbps. Moreover, such constellation and code rate requires a high operating SNR. To meet this requirement, moving to MIMO techniques is highly recommended. The well-known low complexity MIMO technique that was developed in [32–34], the so called the V-BLAST transmit scheme, is capable of delivering reasonable performance provided the number of antenna elements at the receiver is not less than that at the transmitter. The drawback of this scheme is the lack of diversity that can be exploited at the transmitter. This is then followed by the invention of a powerful and low complexity transmit diversity scheme in [35], Alamouti space time block code (STBC). Contrary to V-BLAST, this scheme is limited by its data throughput capability, which is the same as a SISO system. In order to compromise between the advantages of these two schemes, [36–38] develop a hybrid of V-BLAST and Alamouti STBC. Since then, improvements on these three techniques have been developed [39–41]. Despite this, there is still a lack of understanding among the performance of these three schemes relative to one another.

The possibility of IEEE 802.11n supporting multiple users simultaneously should be investigated as an optional mode for the system. This results in interference [42–49] among users. Although several interference mitigation techniques [45–49] have been suggested, appropriate mitigation technique at low complexity that can be applied to mitigate multiuser WLAN interference has not been properly compared with one another.

For low data rate transmission, Alamouti STBC can deliver high performance at low cost. However, two drawbacks exist, namely latency and wasting resources. Because Alamouti STBC need to transmit over two OFDM symbols, small packet sizes might not be able to fill up all the available subcarriers over two OFDM symbols, which is a waste of resources. Also, the

receiver would need to buffer signal over two OFDM symbols before detection can take place resulting in latency. This leads to the Alamouti space frequency block code (SFBC) [50–53], in which adjacent OFDM subcarriers are assumed to be highly correlated with each other. In practice, this is not always the case and may degrade system performance significantly. Although, [53] proposes the use of zero forcing technique to combat this uncertainty in channel condition, decoding is done at the expense of higher complexity. Furthermore, it is important to understand the performance difference between this Alamouti SFBC technique with the recently developed cyclic delay diversity (CDD) scheme [54–56] which also eliminates the above mentioned disadvantages of Alamouti STBC. This will enable the choice of either these two schemes to replace Alamouti STBC whenever the above problems cannot be tolerated.

Due to the physical limit of future wireless devices and high cost of radio frequency (RF) chains, it is better to limit the number of antennas in which the above mentioned hybrid is no longer implementable (it requires four transmit antennas). In practice, two transmit antennas spatial multiplexing scheme is sufficient to deliver the required 100 Mbps prerequisite, (two 64 QAM modulated antennas over 20 MHz bandwidth channel). However, this does not allow channel coding to be deployed into the system, which would decrease the data rate significantly. Hence, poor system performance is expected in this case. Even though three transmit V-BLAST is capable of achieving this throughput, this would require considerable decoding complexity to obtain reasonable performance due to the lack of diversity in the system. Therefore, improvement to three transmit diversity technique using low complexity decoder can still be further developed.

1.2 Objective

On the basis of the above issues, a number of studies have been conducted which form the motivation of the research work reported here. The objective of this thesis is to investigate the best solution that can be deployed into future WLAN from the PHY layer perspective. With regard to this, improvements to current IEEE 802.11a to support higher throughput, larger range coverage and the possibility of multiple users transmission form the three major pieces of work covered here. Subsets of the work discuss the trade off for several MIMO techniques suggested with various parameters, choosing the best modulation schemes, developing receiver algorithms, system optimisation and modelling. Practical implementation is also considered in these studies.

1.3 Contributions To Knowledge

Contributions from this research for future WLAN systems can be summarised as follows:

- Mathematical analysis and modelling of two possible interference scenarios, synchronous and asynchronous in a WLAN. The closed form error probabilities in the presence of synchronous interference are derived. Details of these mathematical modelling are found in Chapter 4.

- Understanding that interference cancellation (IC) (in Section 4.4.1) technique is the better solution over interference suppression (IS) (in Section 4.4.1) in mitigating synchronous interference provided the degrees of spatial freedom is sufficient. (Details of these interference mitigation technique are found in Chapter 4). From simulation results, it is apparent that IS has poorer performance than the IC technique with respect to increasing interference power. Also, it is observed that Dual Alamouti STBC is more robust to interference than V-BLAST given that the same number of receive antennas are deployed in both schemes. Also, it is observed that using IS technique to mitigate synchronous and asynchronous interference results in the same performance based on results generated from the simulator.

- The channel capacity and simulation results (in Chapter 3) in uncorrelated channels show that Dual Alamouti STBC outperforms both V-BLAST and Alamouti STBC. However, the performance of Dual Alamouti STBC is slightly worse than Alamouti STBC for very high antenna correlation. Dual Alamouti STBC is much more robust to correlation than V-BLAST.

- Developed a simplified zero forcing (ZF) (in Chapter 5) solution to combat the uncertainty in channel conditions of an Alamouti SFBC transmit technique. Using this simplified detector, Alamouti SFBC achieves similar performance as Alamouti STBC for low to moderate frequency selective channels. For very frequency selective channels, the frequency encoded version is significantly worse than its temporal encoded version. Unless the channel is extremely frequency selective, Alamouti SFBC performs better than CDD transmit scheme.

- Studied the hybrid three transmit antennas technique (in Chapter 6) where simplified detection algorithms have been developed. Although the CDD hybrid performs better than

V-BLAST, its performance is still marginally worse than the Alamouti STBC hybrid. This Alamouti hybrid study leads to the development of two simplified successive interference cancellation (SIC) algorithms which are comparable to the ordered successive interference cancellation (OSIC) detector in error performance. Bit loading on different Alamouti hybrid antennas shows that channel feedback information is not necessarily required in order to allocate the higher constellation size to the better (Alamouti STBC) channel.

- The design of a modulation coded scheme (MCS) (in Chapter 6) switching between the 3 transmit Alamouti STBC hybrid and Alamouti STBC. The simulation results indicate that the Alamouti STBC performs better at lower throughput while the hybrid is preferred at high throughput. The range covered by switching between the designed MCS modes shows a significant increase in coverage as compared to non switching.

1.4 Organisation Of Thesis

Following this chapter, the rest of the thesis is structured as follows:

Chapter 2

This chapter introduces the concept of OFDM, MC-CDMA, SC-FE and flash OFDM. Analysing each scheme and comparing them, supported by results from existing literature are presented. The best choice of modulation scheme to suit a WLAN will then be discussed. This is followed by a brief introduction to MIMO systems, the V-BLAST scheme and Alamouti STBC.

Chapter 3

This chapter analyses and compares the capacity of V-BLAST, Alamouti STBC and Dual Alamouti STBC. The simulation of these schemes using a low complexity decoder is presented with respect to three parameters: spectral efficiency, number of antennas and channel correlation. The similarities and differences between the capacity and simulation results are discussed. From the perspective of WLAN, the efficiency of the above three MIMO techniques is discussed. In this context, efficiency is referred to as 80% error performance and 20% complexity.

Chapter 4

This chapter models two different types of interference that can possibly exist in a WLAN. They are synchronous and asynchronous interference. There is a description of the two models

followed by the mathematical analysis and closed form bit error probability (BEP) analysis. Then, the application of IC and IS interference techniques to V-BLAST and Dual Alamouti STBC are studied.

Chapter 5

The use of a simplified ZF decoder to combat the uncertainty of channel conditions in Alamouti SFBC is studied. Simulation results comparing the SFBC to STBC and CDD are investigated under different channel conditions.

Chapter 6

In this chapter, three transmit hybrid CDD and Alamouti STBC are studied with more attention paid to the latter due to its better performance. Several simplified SIC algorithms comparable to the well known OSIC detector have been developed for the Alamouti hybrid. Bit loading on antennas for this hybrid scheme is investigated. Later, a MCS switching scheme using both Alamouti STBC and its hybrid are presented. The range covered by this MCS design will be demonstrated.

Chapter 7

Finally, some concluding remarks are presented and possible future work is described.

Chapter 2
Choice of Modulation and MIMO system

A wireless local area network (WLAN) is a system that enables data communication between a central control unit and a wireless or mobile terminal (MT). The MT can come in the form of a computer, personal digital assistant (PDA), etc. The central control unit is normally termed as an access point (AP). The WLAN offers several advantages over wired LAN as follows:

- Mobility
  Users are not restricted to designated AP, like wired ethernet. They have access to real-time information anywhere within the coverage area.
- Flexibility
  Wireless devices can be used in areas where installation of cables are not available.
- Cost
  Installation of cables in older building is costly. With the use of a wireless network, this incurred cost is eliminated.

Two of the well known WLAN families are Hiperlan and IEEE 802.11 [57–59]. The latter standard is focused in this thesis because its products are more widely available in the current market.

The evolution of IEEE 802.11b [60] to IEEE 802.11a in the past few years outlines the push in WLAN to compete with its wired counterpart. IEEE 802.11b uses either frequency hopping or direct sequence spread spectrum that supports data rates up to 11 Mbits/sec in the 2.4 GHz band. Frequency hopping uses Gaussian frequency shift keying while direct sequence employs differential BPSK. The newer IEEE 802.11a standard, introduces the concept of orthogonal frequency division multiplexing (OFDM) that operates in the 5.2 GHz band. This system can support data rates up to 54 Mbps.

The upcoming future IEEE 802.11n WLAN standard which is currently under study is required to support data rates up to approximately four times more than the IEEE 802.11a standard. In order to realise this data rates at reasonable performance, the new standard might require to use multiple input multiple output (MIMO) systems. Even though OFDM is likely to be the modulation format used, the recent development of other schemes, namely, multi-carrier code division multiple access (MC-CDMA), flash OFDM and single carrier with frequency domain equalisation (SC-FE) show comparable performance with OFDM.

Therefore, this chapter shall briefly introduce and compare the performance of the above modulation schemes, with results based on existing literature. The best modulation format to suit future WLAN implementation will be discussed. Then, the advantages of MIMO technique in increasing data rate will be briefly explained. Two well known MIMO schemes, V-BLAST and Alamouti STBC will be introduced.

2.1 Orthogonal Frequency Division Multiplexing (OFDM)

OFDM [10] as shown in Figure 2.1, is a modulation scheme splitting a single stream of high rate serial data into parallel streams each with a lower data rate. These sub-streams of symbols, conventionally encoded using BPSK, QPSK, 16 QAM or 64 QAM as used in the IEEE 802.11a standard, are then mapped onto their respective carrier frequencies. By doing so, the bandwidth of each subcarrier becomes smaller than the coherence bandwidth of the channel provided the number of subcarriers is sufficiently large. This implies that the symbol's duration is made longer than the delay spread of the channel.

The symbols mapped at each subcarrier are summed via the IFFT to produce the time domain signal as [61]:

$$s(t) = \sum_{k_c=0}^{K_c-1} x_{k_c} e^{j2\pi \frac{k_c}{T_{sub}} t} \tag{2.1}$$

where K_c is the total number of subcarriers, T_{sub} is the sub-channel signalling interval and x_{k_c} is the modulated symbol at subcarrier k_c.

This summation leads to a multicarrier system where all subcarriers overlap with one another. Despite the overlapping nature of OFDM, intercarrier interference (ICI) is absent because the carriers in this summation are orthogonal to one another. Figure 2.2 illustrates the difference between an OFDM and single carrier signal in the frequency domain. Unlike conventional

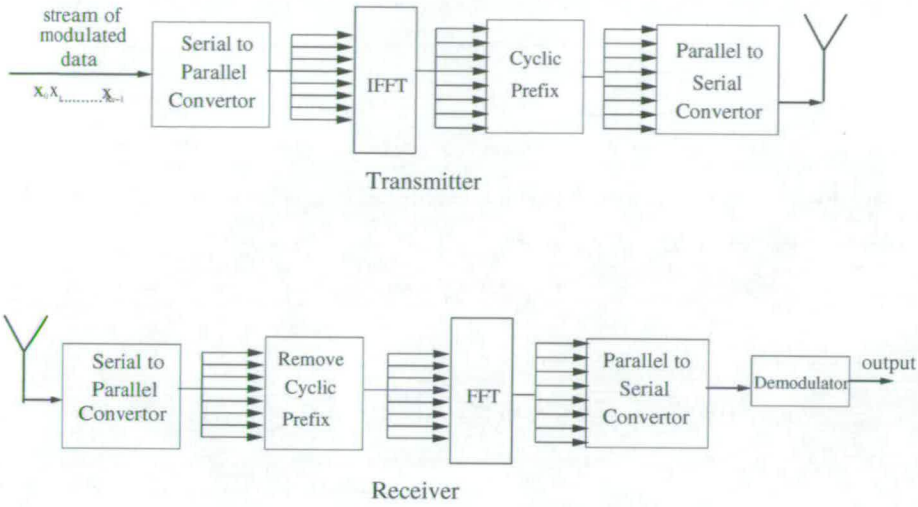

Figure 2.1: *Architecture of an OFDM system*

frequency division multiple access (FDMA), OFDM occupies approximately 50% [10] of the required bandwidth in FDMA.

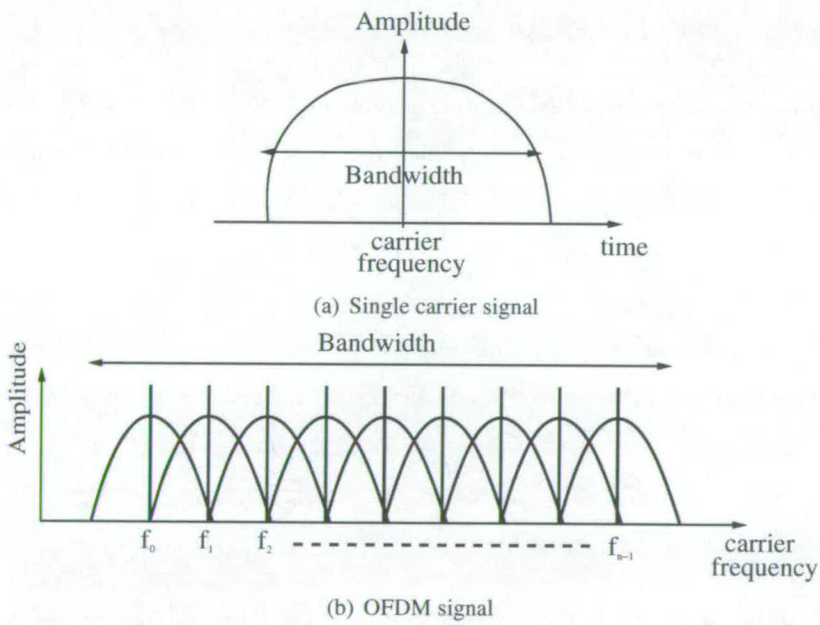

Figure 2.2: *Frequency power spectra of (a) Single carrier frequency domain signal and (b) OFDM*

In order to prevent inter-symbol interference (ISI), a guard time longer than the delay spread of the channel is zero padded at the beginning of each OFDM symbol. However, this can cause

ICI between subcarriers due to the time dispersive effect of the multipath channel. In order to eliminate ICI, the guard interval can be replaced by cyclically extending part of the OFDM symbol end at the beginning of each symbol. The cyclic prefix makes the transmitted signal periodic and eliminates the time dispersive effect of the channel. To illustrate this, Figure 2.3 shows a time domain signal for one OFDM symbol ,i.e., the IFFT of the data symbols with its cyclic prefix. In this figure, K_c is assumed.

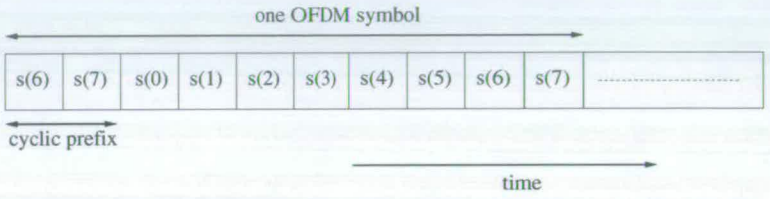

Figure 2.3: *Time domain signal for one OFDM symbol*

At the receiver, the cyclic prefix is first removed, the remaining signal is transformed into the frequency domain via FFT for equalisation, and lastly detected.

One significant advantage of OFDM over conventional single carrier time domain equalisation [12], such as maximum likelihood and decision feedback equaliser, is the reduction in complexity and digital signal processing. The complexity [28] of frequency domain equalisation is proportional to $N \log_2 L_{mp}$, where N is the number of receive antennas and L_{mp} is the length of the channel impulse response in symbols. The complexity of time domain equalisation [28] is proportional to NL_{mp} or even $N^2 L_{mp}^2$ depending on the algorithm used. To illustrate this, Figure 2.4 (similar to the one in [2]) compares the complexity between time domain and frequency domain equalisation for $N = 2$. The complexity of the time domain equaliser becomes significant as L_{mp} increases. This highlights the advantage of OFDM over single carrier with time domain equalisation.

One of the disadvantages of OFDM is the peak-to-average-power (PAP) ratio. This is due to the adding of symbols at all subcarriers which can be constructive. This requires the use of highly linear amplifiers at the transmitter to avoid undesirable inter-modulation products. On the other hand destructive addition results in low power efficiency. Secondly, the carriers are more difficult to synchronise as compared to single carrier techniques, which can lead to ICI and ISI.

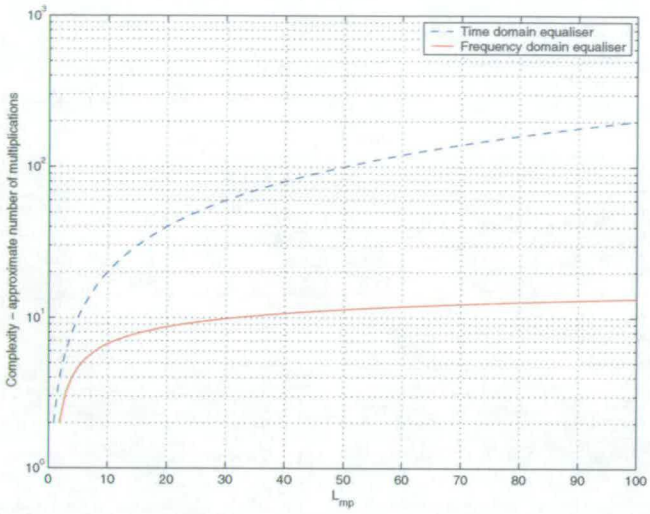

Figure 2.4: *Complexity graph between frequency and time domain equalisation for* $N = 2$

2.2 Single Carrier With Frequency Domain Equaliser (SC-FE)

SC-FE is an alternative technique to reduce the equalisation complexity of time domain equaliser for large delay spread channels. This technique attains similar equalisation complexity as that of OFDM. The architecture of single carrier frequency domain linear equalisation (SC-LE) is shown in Figure 2.5. A cyclic prefix is attached to a several blocks of K_c symbols, where K_c is the FFT size, as in an OFDM transmitter. At the receiver, several blocks of K_c received symbols are fed into the FFT and the output in the frequency domain is then equalised. After equalisation, the signal is transformed into the time domain for detection. A decision feedback equaliser (SC-DFE) can be embedded into the receiver for better performance as shown in Figure 2.5 at the expense of higher complexity.

2.3 Comparison Between OFDM and Single Carrier System

Both OFDM and SC-FE share similar complexity unlike the time domain equaliser. However SC-FE does not have the problems of PAP ratio. Secondly, frequency offset in SC-FE only leads to degradation in SNR but in OFDM it results in ISI and ICI as well.

The comparison of SC-FE and OFDM compiled from [2, 26, 27] will be summarised in this section. Refer to Appendix B for more details. For an uncoded system, SC-LE performs significantly better than OFDM due to the lack of frequency diversity being exploited by the OFDM

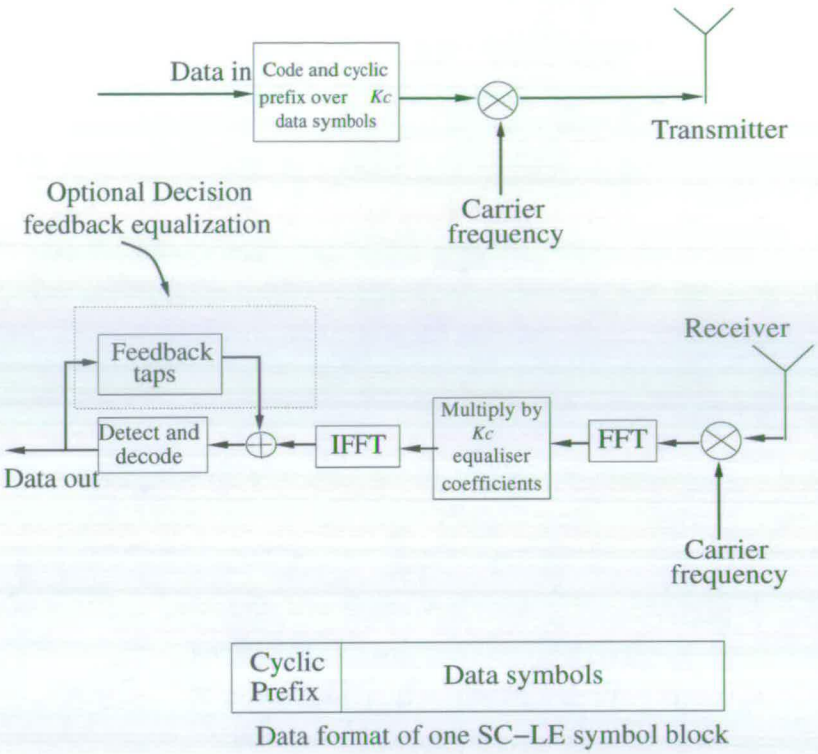

Figure 2.5: *Transceiver of a SC-LE*

system. When coding is employed, the higher code rate systems still favour SC-LE and SC-DFE slightly. On the other hand the lower code rate SC-LE system can only outperform OFDM when smaller constellations such as BPSK and QPSK are used. Increases in constellation size to 16 QAM and 64 QAM show that OFDM outperforms SC-LE while achieving similar performance as SC-DFE for the 64 QAM system. However, SC-DFE requires a higher complexity due to the feedback loop.

2.3.1 Direct Sequence Code Division Multiple Access(DS-CDMA)

The transceiver model of DS-CDMA is shown in Figure 2.6. The modulated data is multiplied by a spreading sequence before transmission. Similarly, at the receiver the observed signal is multiplied with the despreading sequence (i.e. the complex conjugate of the spreading sequence) before detection. The processing gain of the system is defined as :

$$G_p = \frac{T_s}{T_c} = \text{No. of chips per symbol} \tag{2.2}$$

where T_c is the period of one chip and T_s is the symbol period.

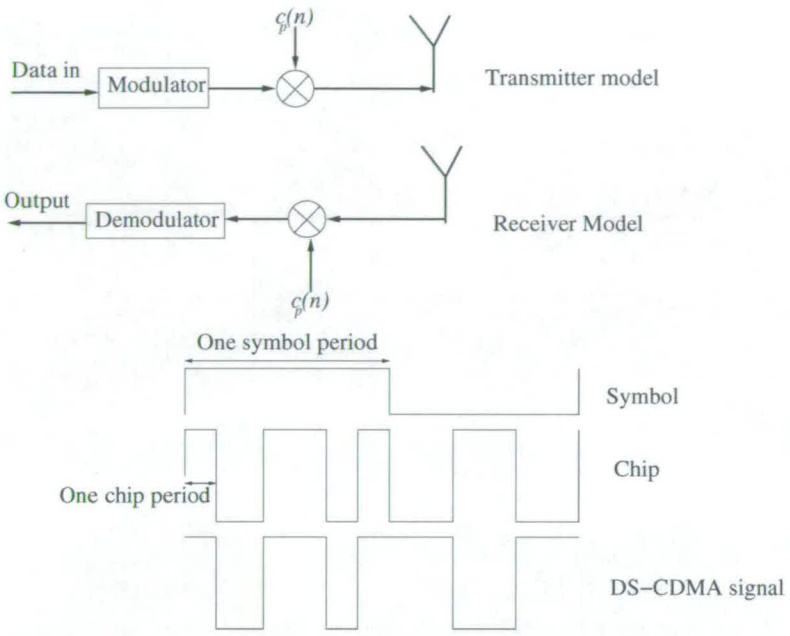

Figure 2.6: *Architecture of DS-CDMA structure*

The spreading codes for different users should have small cross-correlations so that the receiver is able to differentiate between them. If the received signal is multiplied by the code of the desired user with the correct time delay, the signal power peaks, otherwise, it will be spread over the entire bandwidth with low power. This means that the time of arrival of each spread spectrum symbol can be measured accurately.

2.4 Multi-carrier Code Division Multiple Access

MC-CDMA [10, 62–64], as shown in Figure 2.7, is a hybrid technique, which exploits the advantages of both CDMA and OFDM. Contrary to DS-CDMA, the spreading operation of this multi-carrier technique is conventionally performed in the frequency domain. The data at each subcarrier, where the subcarrier is spaced by R_c/T_{sub} (R_c an integer and T_{sub} is the sub-channel interval), is multiplied by its unique spreading code to support multiple users. When both G_p and R_c are equal to 1, this system is equivalent to OFDM. When R_c is large, more frequency diversity gain can be achieved but at the expense of spectral efficiency.

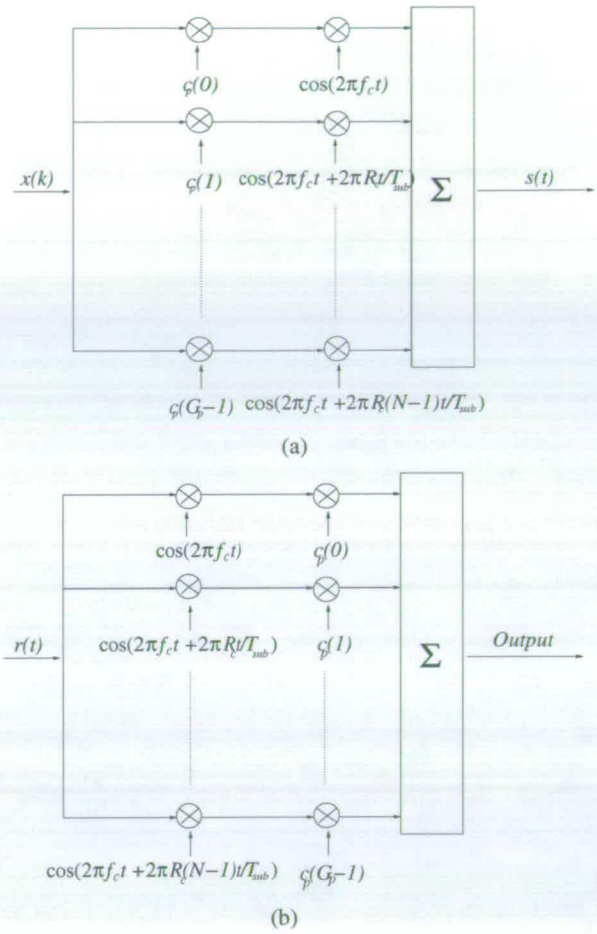

Figure 2.7: *(a) MC-CDMA transmitter, (b) MC-CDMA receiver*

2.4.1 Frequency Hopping CDMA

This spread spectrum technique [10] is different from DS-CDMA in that the carrier frequency changes from time to time. A block diagram of the transceiver is shown in Figure 2.8. Two types of frequency hopping exist, namely, fast frequency hopping where the hopping rate is greater than or equal to the symbol rate and slow frequency hopping where the hopping rate is much less than symbol rate. In this chapter, all the discussed FH-CDMA configurations assume the fast hopped version.

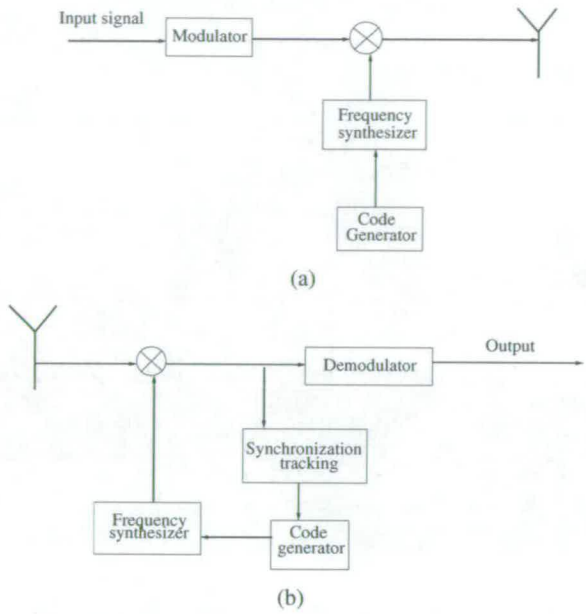

Figure 2.8: *(a) FH-CDMA transmitter (b) FH-CDMA receiver*

2.5 Flash OFDM

This technique developed in [65] can be considered a hybrid of fast frequency hopping and OFDM which avoids the use of a frequency synthesiser. The architecture is similar to that of a normal OFDM transceiver with a special arrangement of users to subcarriers. Figure 2.9 shows an example of the allocation for 8 subcarriers supporting 5 users in a flash OFDM system.

Each user is allocated a different subcarrier in every OFDM symbol. By doing so, each user is effectively varying its carrier frequency over multiple symbol periods which can be thought of as a fast hopping pattern over the entire OFDM bandwidth. Hence, this architecture permits multiple access but also maintains orthogonality between users even in multi-path channels. The number of users that this system can support without interference in one cell is equal to the number of subcarriers allocated to the system.

2.5.1 Capacity Comparison of DS-CDMA, Multi-user Detection and Flash OFDM

In this section, we compare the capacity of the three techniques relative to the number of users that can be supported in the system, coupled with a multiuser detection technique. Multiuser detection technique [66, 67] gives an indication of the number of users that can be successfully

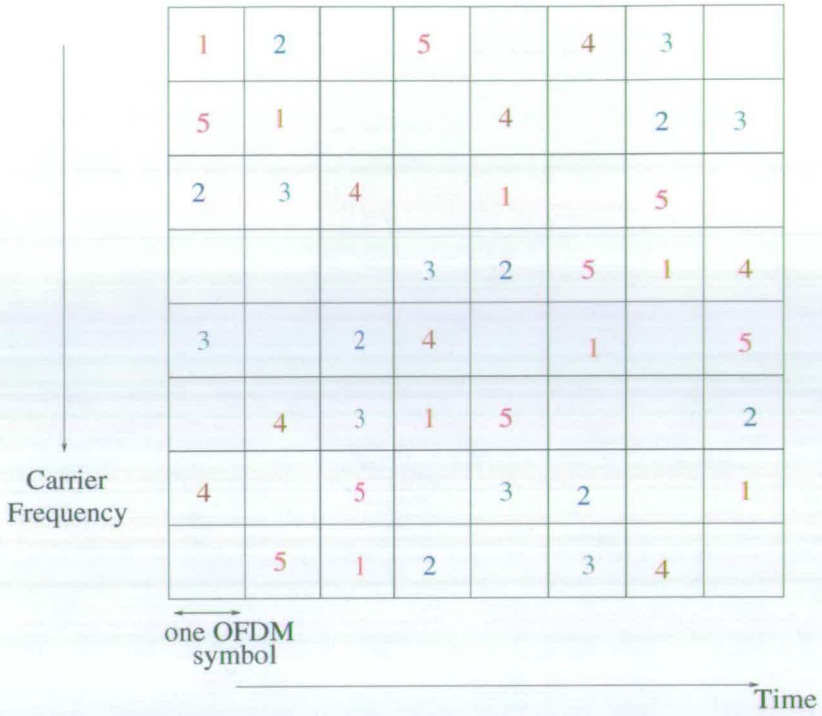

Figure 2.9: *Allocation of subcarriers to 5 active users in flash OFDM with 8 subcarriers*

detected by the system.

In DS-CDMA, without multi-user detection, the number of users that can be supported in a single cell of a DS-CDMA network is [68] :

$$N_{nu} = F_r \left(\frac{G_p}{\Gamma} + 1 \right) \tag{2.3}$$

where G_p is the processing gain

Γ is the required signal-to-noise-ratio

F_r is the ratio of intra-cell interference to total interference given by the equation:

$$F_r = \frac{I_{intra}}{I_{intra} + I_{inter}} \tag{2.4}$$

$$= \left(1 + \frac{I_{inter}}{I_{intra}} \right)^{-1} \tag{2.5}$$

When multiuser detection is used, the equation is expressed as [68]

$$N_u = F_r \left(\frac{\frac{G_p}{\Gamma} - (\varepsilon_m - 1)}{1 - \varepsilon_m F_r} \right) \tag{2.6}$$

where $0 < \varepsilon_m < 1$ represents the multi-user efficiency. This is the proportion of in-cell interference that is removed by multi-user detection.

Dividing equation (2.6) by (2.3) represents the capacity increase of using multi-user detection. It is approximated by [68]:

$$C \approx \frac{1}{(1 - \varepsilon_m F_r)} \tag{2.7}$$

When ε_m is one, this represents the capacity of a flash OFDM system where in-cell interference is absent. Setting ε_m to zero corresponds to a normal DS-CDMA without multi-user detection. Thus flash OFDM achieves the capacity of a DS-CDMA system with ideal multi-user detection that cancels all in-cell interference. A simulation has been performed for various F_r and the results are plotted in Figure 2.10.

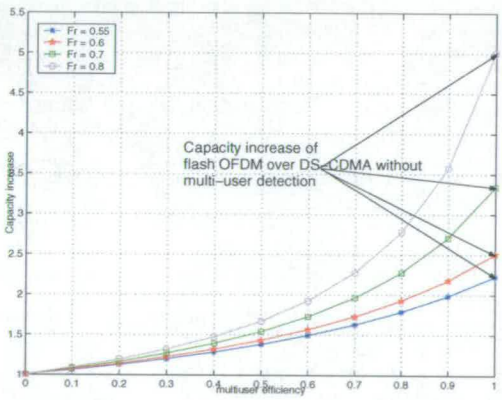

Figure 2.10: *Capacity increase for various F_r*

The graph shows that as F_r increases, which corresponds to a decrease in inter to intra cell interference, the capacity of the system increases. Also apparent is that the capacity of the system is maximised for ε_m equal to one which corresponds to flash OFDM. In practice, despite their complexity, most multi-user detection schemes will not be able to achieve a ε_m value anywhere close to 1. This means flash OFDM will have a higher capacity than the more complex DS-CDMA systems which incorporate multi-user detection. For a value of $F_r = 0.6$, which is the typical value for a homogeneous base station with a uniformly distributed population of

power controlled users in each cell and appropriate distance based propagation model [68], the increase in capacity of flash OFDM over conventional DS-CDMA is approximately 2.5 times.

2.6 Comparison of OFDMA and MC-CDMA

MC-CDMA has the advantage over orthogonal frequency division multiple access (OFDMA) of universal frequency reuse among all cells. OFDMA is a downlink technique in an OFDM system where users are assigned to different subcarriers. Generally, OFDMA would require careful frequency planning to minimise interference among adjacent cells' users. On the other hand, MC-CDMA tends to lose its codes' orthogonality in a frequency selective fading channel [69]. This is not a problem in OFDM due to the cyclic prefix (assuming that the length of the cyclic prefix is long enough to cover the multipath). Due to the spreading of each symbol into several chips in a MC-CDMA system, the spectral efficiency is reduced by factor equal to the processing gain, G_p as compared to OFDM.

Based on three papers [29–31], this section compares some properties of MC-CDMA and OFDMA. Refer to Appendix C for more details. The performance of OFDMA can be thought to be similar to that of an OFDM system supporting multiple users.

For a single input multiple output (SIMO) system, MC-CDMA performs significantly better than OFDMA when 1 receive antenna is used [29]. In that paper it is shown that, as the number of antennas increase, the performance of OFDMA improves and equals the performance as MC-CDMA when four or more antennas are used. This is due to the inherent frequency diversity in MC-CDMA that differentiates its performance from OFDMA for low number of antennas where spatial diversity gain is negligible.

The simulation results from [30] show that the performance of OFDMA is insensitive to the number of users supported in the system. MC-CDMA outperforms OFDMA in terms of bit error ratio (BER) results for small number of users while the performance gap becomes small for subsequent increases in the number of users. This is because interference between the spreading codes of MC-CDMA is less for small number of users while higher interference is incurred for a fully loaded system.

In a single cell environment, OFDMA performs better than MC-CDMA due to inter-code interference among the MC-CDMA users. On the other hand, MC-CDMA is preferable in a cellular

environment because of the universal frequency reuse, in which inter-cell interference becomes more significant than inter-code interference.

2.7 Comparison Between Flash OFDM, OFDM And MC-CDMA

Some general comparisons of OFDM, MC-CDMA and flash OFDM are summarised in this section.

Advantages of flash OFDM over OFDM are as follows:

1. Multiple access

   Since flash OFDM is a form of FH-CDMA, it is possible to achieve a frequency reuse factor of one, unlike OFDMA. Since there is no interference between users in one cell, capacity is limited only by interference from other cells.

2. Multi-path interference

   Since the carrier frequency in flash OFDM keeps changing, the interference is averaged out over the multiple hops, so performance is not degraded by carriers with poor signal-to-interference-plus-noise ratio (SINR).

3. Frequency diversity

   By hopping to a different frequency every symbol period, frequency diversity against fading can be achieved in a frequency selective fading channel. In flash OFDM this is achieved by allocating each user to a different frequency for each OFDM symbol period.

4. PAP ratio

   PAP ratio in flash OFDM depends on the number of carriers in use simultaneously during one OFDM symbol period. If only a user is using a system at a particular instant, then the PAP ratio is similar to that of a single carrier because for every symbol period, the user is only occupying only a carrier while the other carriers can be padded with zeros. However, if the system is loaded with more users, then the number of subcarriers being used for one OFDM symbol is higher. In fact, the PAP ratio is proportional to the number of users in the system.

Comparing flash OFDM with MC-CDMA:

1. The main advantage of flash OFDM over DS-CDMA/MC-CDMA is the absence of in-cell interference in flash OFDM. The lack of in-cell interference can lead to an increase in capacity which will be shown below.

The advantage of flash OFDM over conventional FH-CDMA is :

1. Frequency synthesiser

   It is expensive to buy a synthesiser that will be able to change its frequency regularly with low latency. This is because each user's data in a flash OFDM system is spread over several subcarriers, thus not requiring a frequency synthesiser at the receiver to synchronise every users' data. In flash OFDM there is no latency due to the absent of frequency synthesiser, thus improving spectrum efficiency.

The advantage of OFDM over flash OFDM is:

1. Spectral efficiency

   In order to utilise flash OFDM efficiently, each user must be allocated at different subcarriers over every OFDM symbol. This does not cause any problem in a fully loaded system. On the other hand, when the system is not fully loaded, some subcarriers are bound to be unused. This reduces the overall spectral efficiency of the system as compare to the conventional OFDM system. In fact a fully loaded flash OFDM is equivalent to a traditional OFDM system. Consequently, flash OFDM system is not recommended for use in the uplink as each user would require several OFDM symbols to transmit a finite size of packet information. This results in latency.

2.8 Best Choice of Modulation Scheme

Several issues comparing the similarities and differences between SC-FE, OFDM, MC-CDMA and flash OFDM have been discussed. SC-LE seems to be the natural choice over OFDM because the single carrier scheme has a better PAP ratio and synchronisation is simpler . However, the performance for low code rate and high order modulation favours OFDM over SC-LE. In this case, OFDM serves as a more suitable compromise for future WLAN systems capable of delivering high throughput. SC-DFE can outperform OFDM for lower order modulation but is equal for higher order modulation, e.g., 64 QAM. However, in a wideband channel, e.g. indoor

environment, potentially with multi-path dispersion, SC-DFE maybe significantly more complex than OFDM. The problem is that SC-DFE requires lots of feedback taps which makes the filter difficult to train [12].

The BER performance of MC-CDMA and OFDM is similar to each other when multiple antennas are used in the system due to spatial diversity being made available for the OFDM system to exploit. However, sensitivity to system loading and better BER performance in a multi-cell environment (for the case of a large indoor environment where access points are located in different parts of the building) lead us to MC-CDMA which could suit WLAN systems. However, in a typical indoor environment, e.g. office, generally one base station is enough to serve the active area. Hence, this would favour the use of OFDM. Despite the advantages of MC-CDMA over OFDM, the significant decrease in spectral efficiency is a major problem, especially for future WLANs supporting high data throughput.

Flash OFDM, which is a hybrid of OFDM and FH-CDMA but without the use of frequency synthesiser can also exploit the properties of MC-CDMA with an additional advantage, i.e., the absence of in-cell interference that leads to an increase in capacity. Unlike MC-CDMA, flash OFDM does not suffer code distortion in a frequency selective fading channel. However, flash OFDM can be spectrally inefficient when the number of users is less than the FFT size. Also, this technique is not suitable for uplink transmission as each user data need to be split across several time periods, introducing latency in the system.

Therefore, OFDM is the compromise modulation scheme over SC-LE, SC-DFE, MC-CDMA and flash OFDM for future wireless LAN implementation based on the comparisons that have been presented here.

2.9 MIMO Schemes

MIMO technology is essential in fulfilling the potential of high data rates for the IEEE 802.11n WLAN standard. The capacity of a MIMO system was derived in [70, 71] and is given as:

$$C = \log_2(\det(\mathbf{I_N} + \frac{P_T}{\sigma_n^2 M}\mathbf{H}\mathbf{H}^H)) \tag{2.8}$$

where $\mathbf{I}$ is the identity matrix, $\mathbf{H}$ is the $N \times M$ MIMO channel and σ_n^2 is the noise variance. M and N are the number of transmitters and receivers respectively.

The effect on the average capacity for increasing number of antennas is shown in Figure 2.11. In these results, each of the channel coefficient in $\mathbf{H}$ is a zero mean, unit variance, complex, independent Gaussian identically distributed random variable. It is shown that increasing the

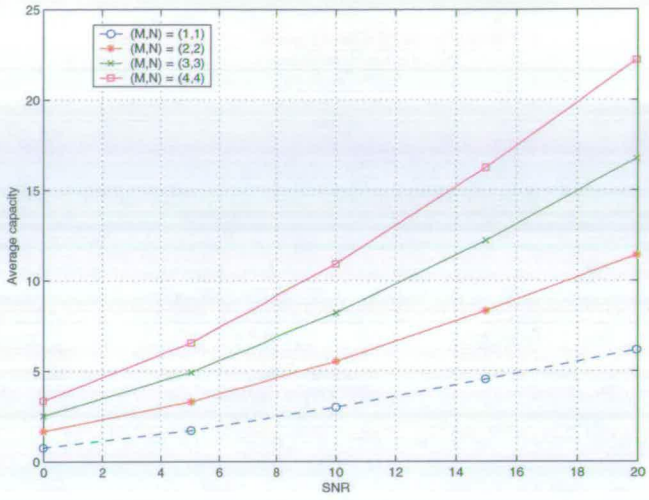

Figure 2.11: *Average Capacity of MIMO*

number of antennas, M and N in a (M, N) configuration gives significant increase in the capacity. The increase in capacity is more significant at high SNR due to the higher diversity gain for more number of antennas.

As supported by the results in Figure 2.11, MIMO seems to be the best way for future WLAN to enable high throughput spectrally efficient data transmission. Further capacity analysis of MIMO systems will be presented in Chapter 3. In this chapter, two well-known MIMO schemes, V-BLAST and Alamouti STBC will be introduced.

2.10 Vertical Bell Lab Space Time (V-BLAST)

V-BLAST [32] is a spatial multiplexing transmission scheme that has the capability to support high data rates which are linearly proportional to the number of transmit and receive antennas used. The architecture of V-BLAST as shown in Figure 2.12 consists of M spatially multiplexed substreams at the transmitter, which are measured at N receive antennas. Each transmitter is a conventional QAM OFDM modulator while the receiver reverses the process with the help of an additional V-BLAST signal processor. The V-BLAST signal processor is similar to that of a conventional multi-user detector [72] with an optimal ordering algorithm to select

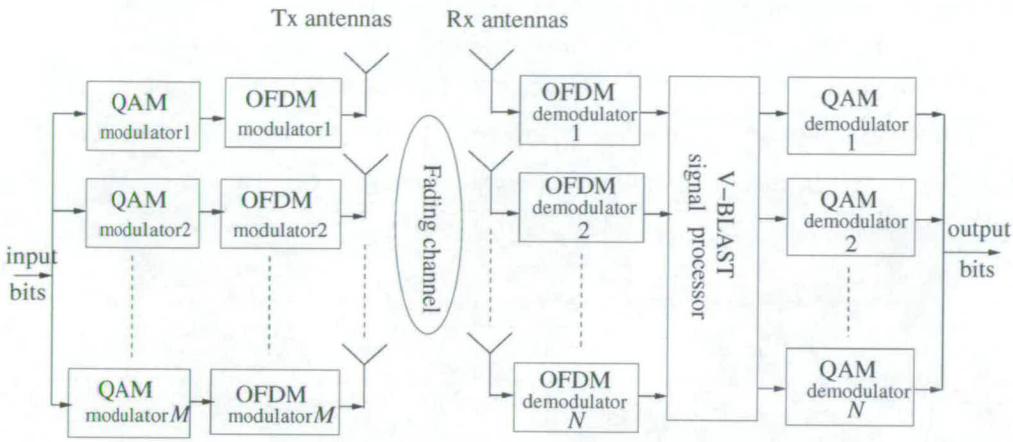

Figure 2.12: *Architecture of an OFDM BLAST system*

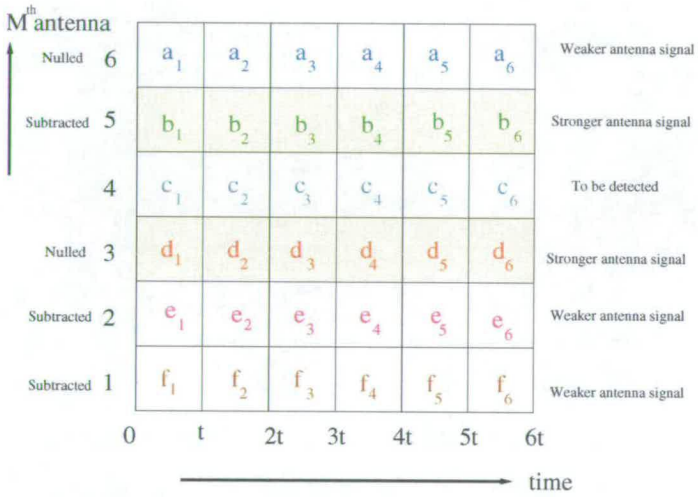

Figure 2.13: *Optimal ordering and selection process of BLAST*

the detection order. The ordering algorithm, so called ordered successive interference cancellation (OSIC), selects the antenna with the strongest signal followed by the next strongest until every antenna signal has been detected. Reconstructed signals for the detected antennas are then subtracted from the received signal to remove interference from the remaining undetected antennas. This choice of the strongest antenna's signal at each stage ensures that the largest interference signal is removed, so that subsequent detection are less affected by interference. Figure 2.13 illustrates the detection process. To implement an operational V-BLAST system, the number of antennas at the receiver must be greater or equal to the number of transmitter ($N \geq M$).

2.10.1 Mathematical Analysis Of V-BLAST Detection

During the detection process, except for the antenna signal to be detected, the interference from the remaining antennas are being nulled or suppressed. The nulling is performed by linearly weighting the received signals so as to satisfy certain performance related criteria such as zero forcing (ZF) or minimum mean squared error (MMSE) [39].

For simplicity, the ZF weighting vectors w_i, i = 1, 2, ..., M can be chosen such that:

$$\mathbf{w}_i^T(\mathbf{H})_j = \delta_{ij} \tag{2.9}$$

where $\mathbf{H}_j$ is the jth column vector of $\mathbf{H}$ $N \times M$ size channel matrix, and δ is the Kronecker delta function. Thus, the decision statistic for the ith substream is $y_i = \mathbf{w}_i^T\mathbf{r}$. In the ZF nulling criterion, the weighting vector $\mathbf{w_i}$ is the ith row vector of the pseudoinverse of the channel matrix $\mathbf{H}$ expressed as:

$$\mathbf{G} = \mathbf{H}^H(\mathbf{H}\mathbf{H}^H)^{-1} \tag{2.10}$$

This matrix $\mathbf{G}$ spatially separates each antenna data from one another so that the detection can be performed independently.

The optimal ordering for detection and symbol cancellation made V-BLAST different from the conventional linear combinatorial nulling. Let $S_p = \{k_1, k_2, ...k_M\}$ be a permutation of integers from 1 to M specifying the order of detecting the symbol vector $\mathbf{x}$.

The decision statistic can be formed by multiplying the nulling vector and received signal.

$$y_{k_i} = \mathbf{w}_{k_i}^T\mathbf{r}_i \tag{2.11}$$

where $\mathbf{r}_i$ denotes the received signal after subtracting $(i-1)$ detected signal.

The decision statistic is then quantised in accordance to the constellation in use.

$$\hat{x}_{k_i} = \mathrm{Q}(y_{k_i}) \tag{2.12}$$

where $Q()$ is the slicer for the respective constellation in use.

The detected data are subtracted from the received signal while the column vectors of $\mathbf{H}$ due to

the detected symbols are nulled.

$$\mathbf{r}_{i+1} = \mathbf{r}_i - \hat{x}_{k_i}(\mathbf{H}_i)_{k_i} \tag{2.13}$$

where $(\mathbf{H}_i)_{k_i}$ denotes the k_i column of $\mathbf{H_i}$ after zeroing its $(i-1)$ columns matching the $(i-1)$ previously detected signals. The subtraction of the detected data from the received signal aims to minimise errors in the subsequent detection process provided the detected data possesses a certain degree of accuracy. Hence, for proper performance of V-BLAST the estimate of the channel $\mathbf{H}$ must be close to the true one, otherwise the system may fail drastically due to the subtraction of incorrectly reconstructed data from the received signal.

The ordering of the detection is done in accordance to the received signals' SNR values. The signal with the highest SNR is prioritised for detection followed by the next highest SNR until all the M substreams are detected. The SNR of transmitter antenna m for the ZF technique can be determined as follows:

$$\text{SNR(m)} = \frac{(\mathbf{w}_m\mathbf{H}_m)(\mathbf{w}_m\mathbf{H}_m)^* E(|x_m|^2)}{\mathbf{w}_m\mathbf{w}_m^*\sigma_n^2} \tag{2.14}$$

$$= \frac{E(|x_m|^2)}{||\mathbf{w}_m||^2\sigma_n^2} \tag{2.15}$$

where $\mathbf{w}_m\mathbf{H}_m = \mathbf{I}_m$ using the ZF solution and $\mathbf{I}_m$ is the m^{th} row of the identity matrix, $E(|x_m|^2)$ is the expectation of the data symbol used and σ_n^2 is the noise variance. Hence from equation (2.15), the lowest norm value of $\mathbf{w_m}$ would be equivalent to the highest SNR of substream x_m.

MMSE detection differs from the ZF technique in that the weighting vectors take account of the noise present at each receiver. The MMSE detector is defined as:

$$\mathbf{G} = \mathbf{H}^H(\mathbf{H}\mathbf{H}^H + \frac{\sigma_n^2}{P_T}\mathbf{I})^{-1} \tag{2.16}$$

where $\mathbf{I}$ is the identity matrix and P_T is the power at the transmitter. Due to the trade off between interference and noise in MMSE detection, the maximum SNR determination is not as straight forward as the ZF technique. The SNR at each receiver is calculated as follows:

$$SNR(m) = \frac{|\alpha_{MMSE}|^2 E(|x_m|^2)}{\beta_{MMSE}} \tag{2.17}$$

$$\alpha_{MMSE} = (\mathbf{G}_m)_{k_i}(\mathbf{H}_m)_{k_i} \tag{2.18}$$

$$\beta_{MMSE} = |(\mathbf{G}_m)_{k_i}|^2\sigma_n^2 + \sum_{\forall p \neq k_1,k_2,\ldots,k_{i-1}}^{M} |(\mathbf{G}_m)_{k_i}\mathbf{H}_p|^2 E(|x_p|^2) \tag{2.19}$$

where $(\mathbf{G}_m)_{k_i}$ is the k_i-th row and column of $\mathbf{G}_m$ and $\mathbf{H}_m$ respectively after $(m-1)$ detection cycles.

Using the OSIC detector, the diversity order achieved by the V-BLAST transmit scheme can be approximated as [73] $N - M + 1$.

2.11 Alamouti Space Time Block Code (STBC)

Diversity is a well known technique that has been employed to improve the BER performance of any system. The well known combining technique for spatial diversity, maximal ratio combining (MRC) [74], uses multiple antennas at the receiver to exploit diversity. Despite the enhanced performance, this technique might not always be feasible due to a larger physical receiver being required to accommodate the extra antennas. Recently, Alamouti [35] suggested the idea of exploiting diversity by employing multiple antennas at the transmitter. The transmitted data is encoded in both the spatial and temporal domains. The diversity order achieved is equivalent to the product of the number of transmit and receive antennas, (MN). However, this is done at the expense of reduced spectral efficiency, which equals $1/M$ of the achievable spectral efficiency in V-BLAST. The Alamouti STBC architecture is shown in Figure 2.14.

2.11.1 Transmission Encoding scheme

The data of Alamouti STBC is encoded in both the spatial and temporal domain at the two transmit antennas over two consecutive symbol periods as shown in (2.20).

$$\mathbf{X} = \begin{bmatrix} x_0 & -x_1^* \\ x_1 & x_0^* \end{bmatrix} \tag{2.20}$$

The columns and rows of this matrix map onto the space and time domain of the transmitted data respectively. The symbol x_0 and x_1 are transmitted from antenna 1 and 2 respectively at time t_0 followed by $-x_1^*$ and x_0^* respectively at the next symbol period t_1. In order for the

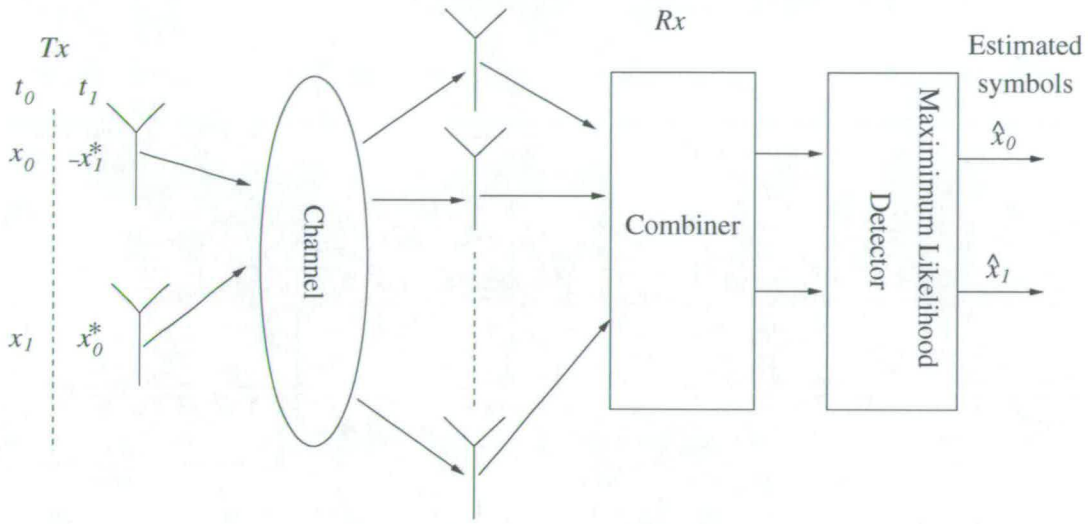

Figure 2.14: *Architecture of the STBC*

decoding to achieve a maximum diversity effect, this matrix $\mathbf{X}$ must be orthogonal such that

$$\mathbf{X}.\mathbf{X}^H = (|x_o|^2 + |x_1|^2)\mathbf{I} \tag{2.21}$$

Another important assumption for this scheme to work properly is that the channel coefficients must remain unchanged over 2 consecutive symbol periods, T_s.

$$h_{n,m}(t) = h_{n,m}(t + T_s) \tag{2.22}$$

where n and m are the index of the receiver and transmitter respectively, while $h_{n,m}$ is the channel response at receiver n due to transmitter m.

2.11.2 Decoding of Alamouti Space Time Block Code

In order to decode the signal, the received signal can be expressed as:

$$\begin{aligned} \mathbf{r} &= \mathbf{H_A x} + \boldsymbol{\eta} \\ \begin{bmatrix} \acute{\mathbf{r}}_1 \\ \acute{\mathbf{r}}_2 \\ \vdots \\ \vdots \\ \acute{\mathbf{r}}_N \end{bmatrix} &= \begin{bmatrix} \ddot{\mathbf{H}}_1 \\ \ddot{\mathbf{H}}_2 \\ \vdots \\ \vdots \\ \ddot{\mathbf{H}}_N \end{bmatrix} \begin{bmatrix} \acute{\mathbf{x}} \end{bmatrix} + \begin{bmatrix} \acute{\boldsymbol{\eta}}_1 \\ \acute{\boldsymbol{\eta}}_2 \\ \vdots \\ \vdots \\ \acute{\boldsymbol{\eta}}_N \end{bmatrix} \end{aligned} \tag{2.23}$$

where the following definitions are used [37]

$$\acute{\mathbf{r}} = \begin{bmatrix} r_{t_0} \\ r^*_{t_1} \end{bmatrix} \quad \acute{\mathbf{x}} = \begin{bmatrix} x_0 \\ x_1 \end{bmatrix} \quad \acute{\boldsymbol{\eta}} = \begin{bmatrix} \eta_{t_0} \\ \eta^*_{t_1} \end{bmatrix} \quad \ddot{\mathbf{H}}_\mathbf{n} = \begin{bmatrix} h_{n,1} & h_{n,2} \\ h^*_{n,2} & -h^*_{n,1} \end{bmatrix} \tag{2.24}$$

where $\acute{\mathbf{r}}_\mathbf{n}$ is the received signal vector at receiver n during time t_0 and t_1, $\acute{\boldsymbol{\eta}}$ is the noise vector for receiver n at time t_0 and t_1, $\acute{\mathbf{x}}$ is the transmitted signal vector from the pair of Alamouti transmitter antennas and $\ddot{\mathbf{H}}_\mathbf{n}$ is the matrix channel response of receiver antenna n due to the Alamouti transmitter.

The decoding can be done by multiplying the received signal with the channel matrix as:

$$\begin{aligned} \hat{\mathbf{x}} &= \mathbf{H_A}^H \mathbf{r} \\ &= \mathbf{H_A}^H \mathbf{H_A x} + \mathbf{H_A}^H \boldsymbol{\eta} \\ \begin{bmatrix} \hat{x_0} \\ \hat{x_1} \end{bmatrix} &= \begin{bmatrix} \sum_{m=1}^{2} \sum_{n=1}^{N} |h_{(n,m)}|^2 & 0 \\ 0 & \sum_{m=1}^{2} \sum_{n=1}^{N} |h_{(n,m)}|^2 \end{bmatrix} \begin{bmatrix} x_0 \\ x_1 \end{bmatrix} \\ &\quad + \mathbf{H_A}^H \boldsymbol{\eta} \end{aligned} \tag{2.25}$$

2.12 Conclusion

Several modulation schemes have been introduced and their behaviour from the existing literature has been compiled and compared with one another. The OFDM modulation is suggested as a compromise over SC-FE, MC-CDMA and flash OFDM for future WLAN. In the later part

of this chapter, it was shown that MIMO technique improves the channel capacity significantly. Then, two MIMO schemes have been introduced based on the OFDM system which are potential candidates for future WLAN. The V-BLAST technique improves the the spectral efficiency of the system while Alamouti STBC provides significant diversity gain by reducing the number of antennas at the receiver. These schemes will be further discussed in Chapter 3, along with the recent hybrid MIMO architecture that combine elements of both V-BLAST and Alamouti STBC.

Chapter 3

Feasibility Of Existing MIMO And Transmit Diversity Schemes For Future WLAN

3.1 Introduction

Support for high data rates and low implementation complexity form two of the prerequisites for future wireless local area network (WLAN), and in particular for candidate architectures for the IEEE 802.11n working group. Spatial multiplexing and space time block codes (STBC) techniques, by virtue of their multiple input and multiple output (MIMO) structure, are attractive schemes to fulfil the two requirements. Specifically, Alamouti STBC [35], V-BLAST [32] and Dual Alamouti STBC [37] (which is the hybrid of V-BLAST/Alamouti STBC by concatenating two Alamouti STBC transmitters) are three MIMO candidates that can achieve favourable link layer performance.

In this chapter, the capacity of these three MIMO techniques will be derived, analysed and compared with one another both in the uncorrelated and correlated scenarios. The capacity gives an impression on the performance limits of these MIMO techniques when the maximum likelihood detector coupled with an infinitely powerful outer code are used. In practice, due to constraints on the processing power and physical size, it is impossible to support detector and an outer code at infinite complexity to reach the capacity result. Therefore, these three MIMO techniques using low complexity, physically realisable decoders will be studied by means of simulation with respect to three parameters, namely spectral efficiency, number of antennas used and channel correlation.

3.2 Channel Model

In this thesis, all simulations assume a quasi-static channel with symbol spaced taps. Each tap follows a Rayleigh fading distribution governed by:

$$\rho_{pdf}(\bar{r}) = \begin{cases} \frac{\bar{r}}{\sigma_{pd}^2} \exp[\frac{\bar{r}^2}{2\sigma_{pd}^2}] & \text{for } r \geq 0 \\ 0 & \text{otherwise} \end{cases} \tag{3.1}$$

where $\bar{r}$ is the received signal envelope and $2\sigma_{pd}^2$ is the pre-detection mean power of the multi-path signal. The channel with L_{mp} impulses can be mathematically expressed as:

$$\gamma_{mp}(\tau) = \sum_{l_p=0}^{L_{mp}-1} P_{l_p} \beta_R \delta(\tau - l_p T_{sam}) \tag{3.2}$$

where β_R is the Rayleigh fading coefficient, $l_p T_{sam}$ is the delay of the l_pth impulse, P_{l_p} is the power at the l_p pulse and T_{sam} is the sampling period of the OFDM system. The sum of the power of all channel taps is normalised to one.

In this thesis, a channel function with several input parameters has been defined as:

$$F_c(\text{Correlation}, \text{Channel model}, \text{AoA}_{Tx}, \text{AS}_{Tx}, d_{Tx}, \text{AoA}_{Rx}, \text{AS}_{Rx}, d_{Rx}) \tag{3.3}$$

where AoA, AS and d denote the angle of arrival, angular spread and antenna spacing respectively. The choice of input parameters to the function in (3.3) are tabulated in Table 3.1. In the

Parameter	Input Value
Correlation	U = uncorrelated, C = correlated
Channel model	An integer = denotes number of equal power taps A = power delay profile of Hiperlan channel model A D = power delay profile of IEEE 802.11n channel model D
Angle of arrival	-90^o to 90^o Left empty if uncorrelated Var - variable
Angular spread	0^o to 180^o Left empty if uncorrelated Var - variable
Antenna spacing	Left empty if uncorrelated Var - variable

Table 3.1: *Channel function input*

case of uncorrelated channels, the F_c function only requires the first two inputs while the rest is left blank. Note that an equal power tap channel is not physically realistic - it is only used for study purposes to reflect the frequency selectivity in a channel. The power delay profile of Hiperlan channel model A is depicted in Appendix A. The default antenna spacing of the IEEE 802.11n channel model D is set to 1 and 0.5 unit wavelength at the transmitter and receiver respectively. The angle of arrival is assumed to be perpendicular to linear array. More details of this model is not available as this data has been provided by Toshiba Telecommunication Research Laboratory Europe Ltd at Bristol. [1] Therefore when the channel model parameter input is D, the channel function will also acquires only two input parameters, in which the rest is assumed to default to the above. In all simulations, the delay spread of the channel is set to 50 ns, which is a 20 MHz bandwidth channel.

When generating cross-correlation coefficients for correlated channels, the power azimuth spectrum (PAS) follows a uniform distribution [76]. These coefficients are generated as:

$$\kappa = |\kappa_x + \mathrm{j}\kappa_y|^2 \tag{3.4}$$

where

$$\kappa_x = J_0(D) + \frac{2}{\mathrm{AS}} \sum_{i=1}^{+\infty} \frac{J_{2i}(D)}{2i} \cos(2i\mathrm{AoA}) \sin(2i\mathrm{AS}) \tag{3.5}$$

$$\kappa_y = \frac{2}{\mathrm{AS}} \sum_{i=0}^{+\infty} \frac{J_{2i+1}(D)}{2i+1} \cos((2i+1)\mathrm{AoA}) \sin((2i+1)\mathrm{AS}) \tag{3.6}$$

$J_i(.)$ denotes the Bessel function of the first kind and ith order while D is given by:

$$D = \frac{2\pi d}{\lambda} \tag{3.7}$$

where λ is one unit wavelength spacing.

Using equation (3.4) to generate the $N \times N$ $\boldsymbol{\kappa_r}$ and $M \times M$ $\boldsymbol{\kappa_t}$ covariance matrices of the

[1] The author gratefully acknowledge Toshiba Telecommunication Research Laboratory Europe Ltd at Bristol for providing the IEEE 802.11n channel data for his simulations. In regards to this channel the author would also like to acknowledge
<http://cpk.auc.dk/cellular> AAU-CSys' and FUNDP-INFO's parenthood on the
<http://www.mathworks.com> MATLAB(c) packages,
<http://www.info.fundp.ac.be/ lsc/Publications/2002/JSAC/01021913.pdf> [75] for the information on generating MIMO channel model
and IST project IST-2000-30148 <http://www.ist-imetra.org>I-METRA.

receiver and transmitter respectively, the spatial correlation matrix of the MIMO channel is modelled by [76]

$$\boldsymbol{\kappa_{MIMO}} = \boldsymbol{\kappa_r} \otimes \boldsymbol{\kappa_t} \tag{3.8}$$

where $\otimes$ denotes Kroneckor product. Therefore the $N \times M$ size channel matrix $\mathbf{H}$ vectorised MIMO channel, $\acute{\mathbf{H}}$ given by:

$$\acute{\mathbf{H}} = \begin{bmatrix} h_{0,0} & \dots & h_{N-1,0} & h_{0,1} & \dots & h_{N-1,1} & \dots & \dots & h_{N-1,M-1} \end{bmatrix} \tag{3.9}$$

where $\mathbf{H}$ is represented by:

$$\mathbf{H} = \begin{bmatrix} h_{0,0} & h_{0,1} & \ddots & h_{0,M-1} \\ \vdots & \ddots & \dots & \vdots \\ \vdots & \dots & \ddots & \vdots \\ h_{N-1,0} & h_{N-1,1} & \dots & h_{N-1,M-1} \end{bmatrix} \tag{3.10}$$

can be calculated as:

$$\acute{\mathbf{H}}^T = \acute{\boldsymbol{\kappa}}_{\boldsymbol{MIMO}} \boldsymbol{\beta} \tag{3.11}$$

where

$$\acute{\boldsymbol{\kappa}}_{\boldsymbol{MIMO}} = \boldsymbol{\Omega}_{\mathrm{MIMO}} \sqrt{\boldsymbol{\Sigma}_{\mathrm{MIMO}}} \boldsymbol{\Omega}_{\mathrm{MIMO}}{}^{-1} \tag{3.12}$$

$$\boldsymbol{\beta} = \begin{bmatrix} \beta_0 & \beta_1 & \dots & \dots & \beta_{NM-1} \end{bmatrix}^T \tag{3.13}$$

where β_i is the zero mean unit variance complex independent identically distributed random variables and $\boldsymbol{\Omega}_{\mathrm{MIMO}}$ and $\boldsymbol{\Sigma}_{\mathrm{MIMO}}$ are the eigenvector and diagonal eigenvalue matrices respectively obtained from the eigenvalue decomposition of $\boldsymbol{\kappa_{MIMO}}$

3.3 System Model

A block diagram of the transmitter used for generating simulation results is pictured in Figure 3.1. Blocks of randomly generated binary data are encoded with a rate R = 1/2, constraint length 7, convolutional encoder. The generator matrix used has the octal form of 133 171. Where higher code rates are required, the encoded bits are punctured. These encoded bits are then randomly interleaved and mapped to the constellation in use. In this thesis, only symmetric square QAM constellations are considered, in which each constellation consists of

2^{B_c} symbols, where $B_c = \{1, 2, 4, 6\}$, is the number of bits per symbol. These symbols are spatially and temporally encoded with respect to the chosen transmission scheme and then OFDM modulated separately at each of M antennas. The modulated signals are transmitted out to the channel.

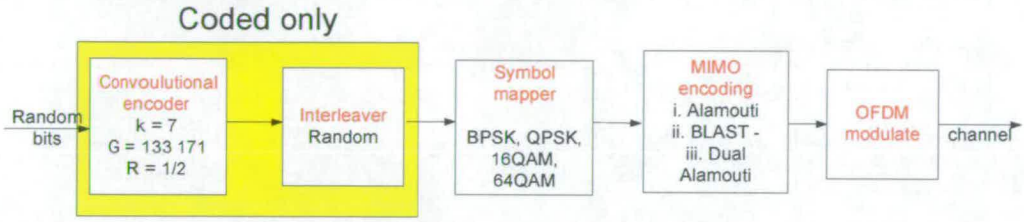

Figure 3.1: *Transmit system model*

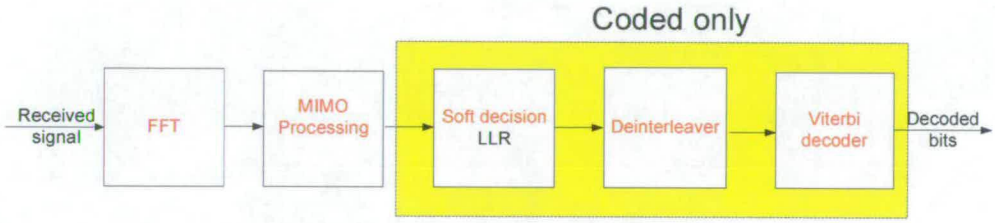

Figure 3.2: *Receive system model*

At each of the N received antennas, the signals are OFDM demodulated and the (M, N) MIMO received signal at each subcarrier can be represented as:

$$\mathbf{r} = \mathbf{H}\mathbf{x} + \boldsymbol{\eta} \tag{3.14}$$

where $\mathbf{r}$ and $\boldsymbol{\eta}$ are the received signal and noise vector of size $N \times 1$ respectively. $\mathbf{x}$ is the $M \times 1$ transmitted signal vector and $\mathbf{H}$ the size $N \times M$ channel matrix. For simplicity the subcarrier index of the signal has been dropped out from equation (3.14) and all future equations. The received signal are then processed and decoded to obtain the estimated transmitted bits using the Viterbi algorithm.

If the system is uncoded, the filled region in Figure 3.1 and 3.2 are omitted from the transmitter and receiver respectively.

3.4 Hybrid of V-BLAST/Alamouti STBC

In Section 2.11 on Alamouti STBC, it is seen that with M transmit antennas to achieve full diversity the spectral efficiency of the system is only $1/M$ of the achievable spectral efficiency in V-BLAST for M antennas. In this section, a V-BLAST hybrid [37] with Alamouti STBC to exploit both diversity and higher spectral efficiency will be studied. The architecture of this hybrid is shown in Figure 3.3.

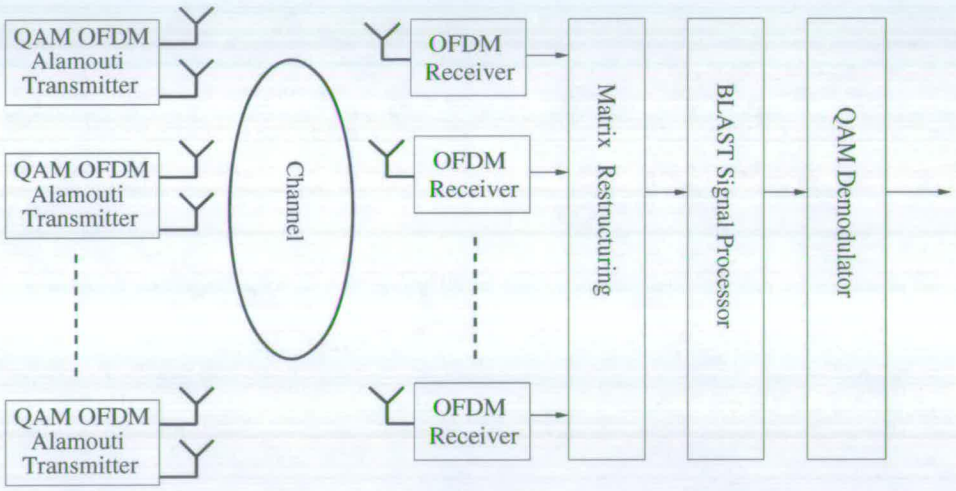

Figure 3.3: *Hybrid of Alamouti and BLAST*

Assuming that two Alamouti transmitters are concatenated, the so called the Dual Alamouti STBC, the received signal can be expressed as:

$$\begin{bmatrix} \ddot{\mathbf{r}}_0 \\ \ddot{\mathbf{r}}_1 \\ \vdots \\ \ddot{\mathbf{r}}_{N-1} \end{bmatrix} = \begin{bmatrix} \ddot{\mathbf{H}}_{0,0} & \ddot{\mathbf{H}}_{0,1} \\ \ddot{\mathbf{H}}_{1,0} & \ddot{\mathbf{H}}_{1,1} \\ \vdots & \vdots \\ \ddot{\mathbf{H}}_{N-1,0} & \ddot{\mathbf{H}}_{N-1,1} \end{bmatrix} \begin{bmatrix} \ddot{\mathbf{x}}_0 \\ \ddot{\mathbf{x}}_1 \end{bmatrix} + \begin{bmatrix} \ddot{\boldsymbol{\eta}}_0 \\ \ddot{\boldsymbol{\eta}}_1 \\ \vdots \\ \ddot{\boldsymbol{\eta}}_{N-1} \end{bmatrix} \tag{3.15}$$

where

$$\ddot{\mathbf{r}}_n = \begin{bmatrix} r_{n,\tau_0} \\ r^*_{n,\tau_1} \end{bmatrix} \quad \ddot{\boldsymbol{\eta}}_n = \begin{bmatrix} \eta_{n,\tau_0} \\ \eta^*_{n,\tau_1} \end{bmatrix} \quad \ddot{\mathbf{x}}_m = \begin{bmatrix} x_{2m} \\ x_{2m+1} \end{bmatrix}$$
$$\ddot{\mathbf{H}}_{n,m} = \begin{bmatrix} h_{n,2m} & h_{n,2m+1} \\ h^*_{n,2m+1} & -h^*_{n,2m} \end{bmatrix} \tag{3.16}$$

where τ_t is the time index. Similarly the received signal in equation (3.15) can be detected using the OSIC algorithm as described in Section 2.10.1. In this case, the Alamouti block with the higher SNR will be detected first. This is because the SNR at each antenna from the same Alamouti block is equal and orthogonal to each other.

From equation (3.15) and (3.16), it can be seen that the dimension of $\mathbf{r}$ has been increased to $2N$. The expansion of this dimension means that there can be a reduction in number of receive antennas required. In this hybrid scheme, the minimum number of receive antennas required to perform the OSIC algorithm efficiently is only half the number of transmit antennas used, i.e, $N \geq M/2$. This means that the number of receive antennas required is half of that needed for the V-BLAST scheme given that the same number of transmit antennas is used. The order of diversity from this scheme using the OSIC algorithm is approximately equal to $2(N-1)$ [37]. The penalty for this is the reduction in the number of spatial multiplexing streams by a factor of two.

Assuming the minimum number of two antennas are used, the MMSE solution can be mathematically expressed as [77]:

$$\mathbf{G} = \begin{bmatrix} \boldsymbol{\alpha_D}\boldsymbol{\beta_D}^* & -\boldsymbol{\alpha_D}\boldsymbol{\beta_D}^*\ddot{\mathbf{H}}_{0,1}\ddot{\mathbf{H}}_{1,1}^{-1} \\ -\boldsymbol{\gamma_D}\boldsymbol{\theta_D}^*\ddot{\mathbf{H}}_{1,0}\ddot{\mathbf{H}}_{0,0}^{-1} & \boldsymbol{\gamma_D}\boldsymbol{\theta_D}^* \end{bmatrix} \tag{3.17}$$

where

$$\begin{aligned} \boldsymbol{\beta_D} &= \ddot{\mathbf{H}}_{0,0} - \ddot{\mathbf{H}}_{0,1}\ddot{\mathbf{H}}_{1,1}^{-1}\ddot{\mathbf{H}}_{1,0} \qquad \boldsymbol{\theta_D} = \ddot{\mathbf{H}}_{1,1} - \ddot{\mathbf{H}}_{1,0}\ddot{\mathbf{H}}_{0,0}^{-1}\ddot{\mathbf{H}}_{0,1} \\ \boldsymbol{\alpha_D} &= (\boldsymbol{\beta_D}^*\boldsymbol{\beta_D} + \sigma_n^2\mathrm{I})^{-1} \qquad \boldsymbol{\gamma_D} = (\boldsymbol{\theta_D}^*\boldsymbol{\theta_D} + \sigma_n^2\mathrm{I})^{-1} \end{aligned}$$

3.5 Capacity Analysis of V-BLAST, Alamouti STBC and Dual Alamouti STBC

In this section the capacity of V-BLAST, Alamouti STBC and Dual Alamouti STBC will be analytically derived. Their capacity for both uncorrelated and correlated Rayleigh fading channels will be compared with one another.

3.5.1 Capacity of V-BLAST

The channel capacity of MIMO developed in [70, 71] can be applied to a (M, N) V-BLAST configuration expressed as:

$$C_{VB} = \log_2 \det(\mathbf{I_N} + \frac{P_T}{M\sigma_n^2}\mathbf{H}\mathbf{H}^H) \tag{3.18}$$

where $\mathbf{I_N}$ is the N size identity matrix, P_T is the power transmitted and σ_n^2 is the noise variance.

Applying singular values decomposition (SVD) to the channel matrix

$$C_{VB} = \log_2 \det(\mathbf{I_N} + \frac{P_T}{M\sigma_n^2}\mathbf{U_H}\mathbf{S_H}\mathbf{V_H}^H\mathbf{V_H}\mathbf{S_H}^H\mathbf{U_H}^H) \tag{3.19}$$

where $\mathbf{S_H}$, $\mathbf{U_H}$ and $\mathbf{V_H}$ are the decomposed matrices such that

$$\mathbf{H} = \mathbf{U_H}\mathbf{S_H}\mathbf{V_H}^H \tag{3.20}$$

Given the relationship [71],

$$\log(\det(A + BC)) = \log(\det(A + CB)) \tag{3.21}$$

the expression in (3.19) can be simplified to

$$C_{VB} = \log_2 \det(\mathbf{I_N} + \frac{P_T}{M\sigma_n^2}\mathbf{S_H}^H\mathbf{S_H}) \tag{3.22}$$

$$= \log_2 \prod_{k=0}^{\min(N,M)-1} (1 + \frac{P_T}{M\sigma_n^2}s_H^2(k)) \tag{3.23}$$

$$= \sum_{k=0}^{\min(N,M)-1} \log_2(1 + \frac{P_T}{M\sigma_n^2}s_H^2(k)) \tag{3.24}$$

where $s_H(k)$ is the off-diagonal singular values of $\mathbf{S_H}$.

When the channel is correlated, equation (3.18) can be modified such that [78]

$$C_{VB} = \log_2 \det(\mathbf{I_N} + \frac{P_T}{M\sigma_n^2}\boldsymbol{\kappa_r}\mathbf{H}\boldsymbol{\kappa_t}\mathbf{H}^H) \tag{3.25}$$

where $\boldsymbol{\kappa_r}$ and $\boldsymbol{\kappa_t}$ are the covariance matrices of the receiver and transmitter respectively.

3.5.2 Capacity of Alamouti STBC

On the basis of the uncorrelated channel capacity from equation (3.18), the channel capacity for a two transmit and N receive antennas Alamouti STBC transmit diversity scheme is expressed as:

$$C_{Al} = \frac{1}{2}\log_2 \det(\mathbf{I_2} + \frac{P_T}{2\sigma_n^2}\mathbf{H_A}^H\mathbf{H_A}) \tag{3.26}$$

such that $\mathbf{H_A}$ is the orthogonal structure spanned from the channel matrix $\mathbf{H}$ where at one receive antenna

$$\mathbf{H} = \begin{bmatrix} h_{n,m} & h_{n,m+1} \end{bmatrix} \tag{3.27}$$

$$\mathbf{H_A} = \begin{bmatrix} h_{n,m} & h_{n,m+1} \\ h^*_{n,m+1} & -h^*_{n,m} \end{bmatrix} \tag{3.28}$$

and the factor 1/2 compensates for the two signalling intervals spanned in the received signal. Expanding equation (3.26)

$$C_{Al} = \frac{1}{2}\log_2 \det\left(\mathbf{I_2} + \frac{P_T}{2\sigma_n^2}\begin{bmatrix} \sum_{n=0}^{N-1}\sum_{m=0}^{M-1}|h_{n,m}|^2 & 0 \\ 0 & \sum_{n=0}^{N-1}\sum_{m=0}^{M-1}|h_{n,m}|^2 \end{bmatrix}\right) \tag{3.29}$$

$$= \frac{1}{2}\log_2(1 + \frac{P_T}{2\sigma_n^2}(\sum_{n=0}^{N-1}\sum_{m=0}^{M-1}|h_{n,m}|^2))^2 \tag{3.30}$$

$$= \frac{1}{2}\log_2(1 + \frac{P_T}{2\sigma_n^2}||\mathbf{H_A}||^2)^2 \tag{3.31}$$

$$= \log_2(1 + \frac{P_T}{2\sigma_n^2}||\mathbf{H_A}||^2) \tag{3.32}$$

where $||\mathbf{A}||$ denotes the norm of matrix $\mathbf{A}$ calculated as:

$$||\mathbf{A}|| = \sum_{n=0}^{N-1}\sum_{m=0}^{M-1}|a_{n,m}|^2 \tag{3.33}$$

and $a_{n,m}$ are the elements of $\mathbf{A}$ at the nth row of the mth column.

For correlated channels, the expression in equation (3.26) can include the effect of correlation such that

$$C_{Al} = \frac{1}{2}\log_2 \det(\mathbf{I_2} + \frac{P_T}{2\sigma_n^2}\boldsymbol{\kappa_t}\mathbf{H_A}^H\boldsymbol{\kappa_r}\mathbf{H_A}) \tag{3.34}$$

where the covariance matrix of the receiver, κ_r is expressed as:

$$\begin{bmatrix} \kappa_{0,0} & 0 & \kappa_{0,1} & 0 & \dots & \dots & \kappa_{0,N-1} & 0 \\ 0 & \kappa_{0,0} & 0 & \kappa_{0,1} & \dots & \dots & 0 & \kappa_{0,N-1} \\ \vdots & \dots & \ddots & & & & & \\ \vdots & \dots & \dots & \ddots & & & & \end{bmatrix} \tag{3.35}$$

where $\kappa_{m,n}$ is the cross correlation coefficient between receive antenna m and n. Refer to Appendix E for proof of the matrix structure.

3.5.3 Capacity of Dual Alamouti STBC

Given that Dual Alamouti STBC is a hybrid of both V-BLAST and Alamouti STBC, the uncorrelated channel capacity of this transmit scheme can be formulated as:

$$C_{DA} = \frac{1}{2}\log_2 \det(\mathbf{I_4} + \frac{P_T}{4\sigma_n^2}\mathbf{H_D}^H\mathbf{H_D}) \tag{3.36}$$

$$= \frac{1}{2}\log_2 \det(\mathbf{I_4} + \frac{P_T}{4\sigma_n^2}\mathbf{S_H}^H\mathbf{S_H}) \tag{3.37}$$

$$= \frac{1}{2}\log_2 \det\left(\mathbf{I_4} + \frac{P_T}{4\sigma_n^2}\begin{bmatrix} s_H(0) & 0 & 0 & 0 \\ 0 & s_H(1) & 0 & 0 \\ 0 & 0 & s_H(2) & 0 \\ 0 & 0 & 0 & s_H(3) \end{bmatrix}^2\right) \tag{3.38}$$

Due to the orthogonality between each Alamouti pair, $s_H(2m) = s_H(2m+1)$, where $m = 0, 1$. Therefore, the expression in equation (3.38) can be simplified to

$$C_{DA} = \frac{1}{2}\log_2(\frac{P_T}{4\sigma_n^2}(1 + s_H(0))^2(1 + s_H(2))^2) \tag{3.39}$$

$$= \log_2(\frac{P_T}{4\sigma_n^2}(1 + s_H(0))(1 + s_H(2))) \tag{3.40}$$

$$= \log_2 \sum_{m=0}^{1}(1 + \frac{P_T}{4\sigma_n^2}s_H(2m)) \tag{3.41}$$

Similarly for correlated channel, the correlated channel capacity for Dual Alamouti STBC can

be expressed as:

$$C_{DA} = \frac{1}{2}\log_2 \det(\mathbf{I_4} + \frac{P_T}{4\sigma_n^2}\boldsymbol{\kappa_t}\mathbf{H_D}^H\boldsymbol{\kappa_r}\mathbf{H_D}) \tag{3.42}$$

where $\boldsymbol{\kappa_r}$ has the same expression as equation (3.35)

3.5.4 Capacity Comparison between V-BLAST, Alamouti STBC and Dual Alamouti STBC

In the capacity comparison between the three MIMO schemes, the results obtained from evaluating the formula for C_{VB}, C_{Al} and C_{DA} are compared. This is done by generating 10000 sample $\mathbf{H}$ matrices and using these to evaluate the channel capacity at different signal-to-noise-ratio (SNR) and angular spread (AS) in case of correlated channels. Each element in the $\mathbf{H}$ matrix is generated from zero mean, unit variance, complex, independent, identically distributed Gaussian random variables. The ergodic capacity, which is the average capacity of all the channel realisations and 1% outage capacity, the capacity that is exceeded for 99% of all channel realisations will be analysed. The ergodic capacity gives an indication on the performance of an adaptive system adapting to instantaneous channel condition while the 1% outage indicates the performance for systems with fixed transmission scheme.

The ergodic and 1% outage capacity of V-BLAST, Alamouti STBC and Dual Alamouti STBC for two and four receive antennas are plotted in Figure 3.4 and 3.5 respectively. For the 2 Rx case, Alamouti STBC 1% outage capacity outperforms V-BLAST for SNR up to 15 dB while Dual Alamouti STBC achieves the highest outage capacity for all SNR ranges. Alamouti STBC performs better than V-BLAST at lower capacity due to the latter's lack of spatial degrees of freedom to exploit any means of diversity. At higher SNRs, Alamouti STBC has a shallower capacity gradient than the other methods and loses out to V-BLAST. The ergodic capacity sees a similar trend except that the V-BLAST curve moves closer to Dual Alamouti STBC while the Alamouti STBC capacity is only better than V-BLAST at a lower SNR up to a value of 6.3 dB. Also, the capacity of Alamouti STBC is higher than Dual Alamouti for SNR up to 5 dB because of higher interference due to two extra antennas from the latter. At higher SNR, diversity becomes more effective and therefore Dual Alamouti STBC performs better than Alamouti STBC.

In the case of 4 Rx, the 1% outage capacity for Alamouti STBC is only better than V-BLAST for SNRs up to 2.8 dB which is 12.2 dB less than the 2 Rx scenario. This is due to the extra

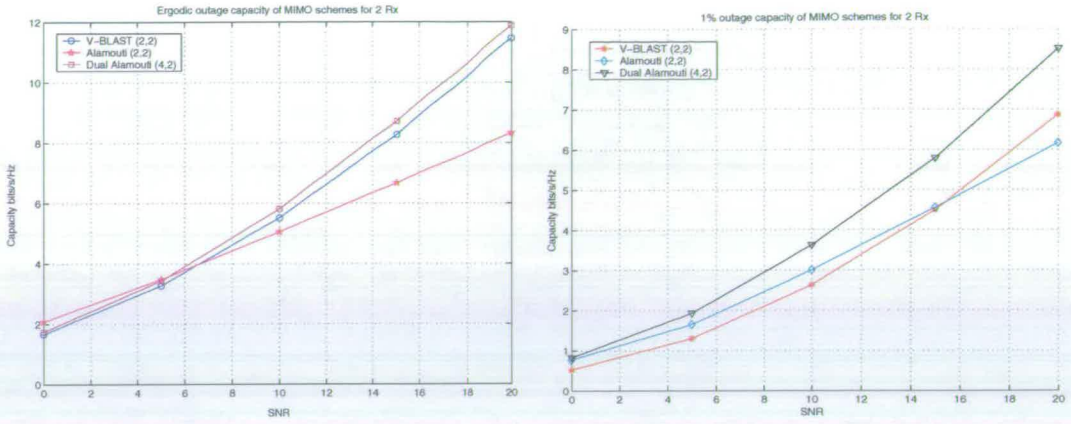

(a) Ergodic capacity of MIMO schemes (b) 1% capacity of MIMO schemes

Figure 3.4: *Capacity of MIMO schemes with two receive antennas*

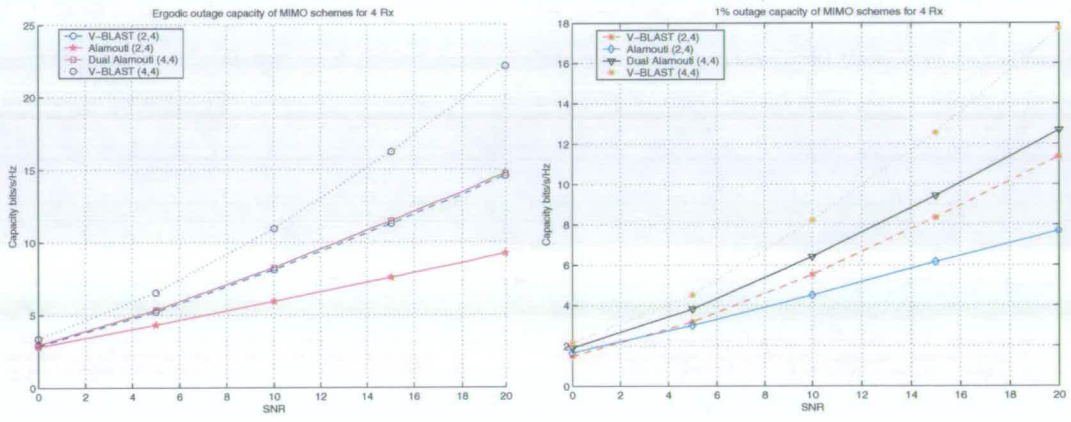

(a) Ergodic capacity of MIMO schemes (b) 1% capacity of MIMO schemes

Figure 3.5: *Capacity of MIMO schemes with four receive antennas*

antennas at the receiver which enables V-BLAST to exploit diversity efficiently even at low SNR. Unlike the 2 Rx scenario, the ergodic capacity of Alamouti is significantly worse than V-BLAST and Dual Alamouti STBC. Otherwise, similar trends to the 2 Rx results are observed. Also, included is the (4,4) V-BLAST scheme whose capacity is significantly higher than the others for all SNR values.

The sensitivity of the three MIMO schemes for both two and four receive antennas is shown in

Figure 3.6. Sensitivity here is defined as

$$\text{Sensitivity} = \frac{\text{ergodic capacity - 1\% outage capacity}}{\text{ergodic capacity}} \text{x100}$$

Sensitivity reflects the deviation on the MIMO performance with respect to channel variation in an adaptive system. In other words, sensitivity shows the difference in performance between and adaptive and fixed transmission system. It is observed that the two receive antennas case is more sensitive than the four Rx scenario due to the extra diversity exploited in every scheme with four antennas. With the exception that the Alamouti STBC is less sensitive than Dual Alamouti STBC for the 2 Rx case at higher SNR (>14.8 dB), the algorithms can be ordered according to increasing sensitivity as Dual Alamouti STBC, Alamouti STBC, V-BLAST. The exception is due to the interference caused from the spatial multiplexing of two Alamouti STBC pairs in Dual Alamouti, while at higher SNR diversity becomes more significant. The 4 Tx V-BLAST is less sensitive than the 2 Tx V-BLAST. At lower SNRs, the 4 Tx V-BLAST is less sensitive than Alamouti STBC due to the V-BLAST scheme being less able to exploit diversity at low SNRs while at higher SNRs diversity becomes more significant.

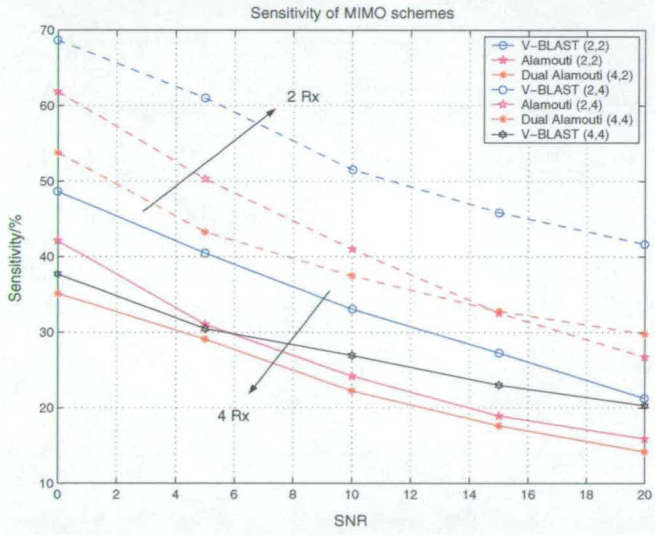

Figure 3.6: *Sensitivity of MIMO schemes*

The 1% outage capacity at an SNR value of 20 dB for the three MIMO schemes in correlated fading channels are shown in Figure 3.7 and 3.8 varying only either the receiver and transmitter correlation respectively. Four antennas are deployed at the receiver. The angular spread (AS) is used as a measure of correlation. Note that there is an inverse relationship between correlation

and AS so that low angular spread implies high correlation and vice versa. When either the Tx or Rx AS is used as the varying parameter, the other parameter is kept constant at an AS of 90^o. The spacing between antennas is 0.5 wavelengths and the angle of arrival at the receiver and departure from the transmitter is perpendicular to the linear array.

Comparing the 2 Tx and 4 Tx V-BLAST and Dual Alamouti STBC, the latter scheme is much more robust to correlation as it requires a lower AS value as shown in Figure 3.8 to provide higher capacity than Alamouti STBC when the transmit correlation is varied. In spite of its high spectrally efficiency, the 4 Tx scheme still performs worse than Dual Alamouti for low AS values, $\leq 12^0$. On the other hand, when the receive correlation is varied as shown in Figure 3.7, the 2 Tx V-BLAST still performs worse than Alamouti STBC at low AS while Dual Alamouti STBC achieves higher capacity than Alamouti STBC for all AS values. This time, the 4 Tx V-BLAST performs better than Alamouti STBC for all AS values. As observed from the two graphs, the Dual Alamouti scheme is more sensitive to transmit correlation than receive correlation because it is more difficult to distinguish between the transmitted stream for very high correlated transmitter.

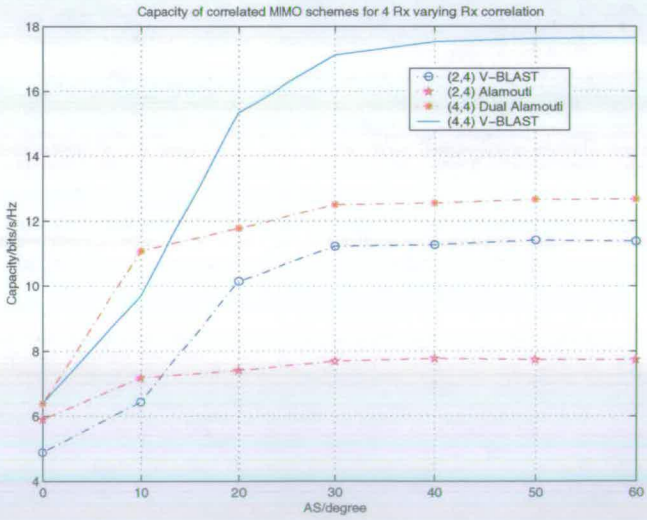

Figure 3.7: *1% outage capacity of MIMO schemes for correlated fading using 4 Rx varying Rx correlation for R=1/2*

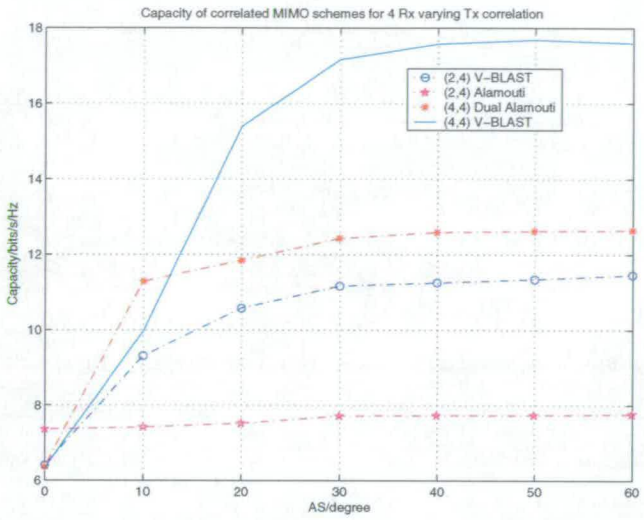

Figure 3.8: *1% outage capacity of MIMO schemes for correlated fading using 4 Rx varying Tx correlation for R=1/2*

3.6 Simulations Comparison of V-BLAST, Alamouti STBC and Dual Alamouti STBC

It is known that V-BLAST transmit scheme is potentially vulnerable to correlated fading channels as the receiver is unable to clearly differentiate among the received signals due to the linearly dependent channels. On the other hand, the inherent transmit diversity in the Alamouti transmit scheme makes this system much more robust to this parameter, but it is incapable of achieving as high spectral efficiencies as compare to V-BLAST. This leads to the hybrid of these two techniques, the Dual Alamouti STBC [37]. Its performance with respect to V-BLAST and Alamouti STBC has not studied so far. Although this performance has been compared in the previous capacity analysis section, the capacity analysis assumes an ideal channel coder and detector are used. This does not necessarily reflect a real implementation as this requires infinite complexity to realise the capacity results. Therefore, this section only considers low complexity decoders where V-BLAST and Dual Alamouti STBC uses the MMSE ordered successive interference cancellation (OSIC) algorithm and Alamouti STBC with its MRC combiner and linear maximum likelihood (ML) detector as described in Section 2.11.2. In this section, the error and throughput performance of these three MIMO schemes with respect to three parameters that will be significant when considering future MIMO wireless LAN implementation are as follows:

i. Spectral efficiency:

It is known that for Alamouti STBC to achieve the same spectral efficiency as V-BLAST requires the use of higher order modulation, which can severely degrades its error performance. This section shall investigate how Dual Alamouti STBC overcomes this problem while attaining considerable diversity gain. The spectral efficiency is varied as a function of either number of transmit antennas used or modulation order.

ii. Number of antennas used:

The number of antennas used determines the diversity gain for the MIMO schemes. The simulation results show how the number of antennas can affect the performance of the three MIMO techniques when varied, i.e., how each scheme can exploit diversity gain when available.

iii. Channel correlation:

Through the combination of V-BLAST and Alamouti STBC, we aim to increase the robustness of Dual Alamouti STBC in the presence of correlated fading channels. The correlation as a function of angular spread will be analysed in this section. The required SNR values at 1% frame error rate (FER) are compared and analysed.

3.6.1 Uncoded MIMO comparison

In this section, comparisons of the three MIMO techniques using a fixed spectral efficiency will be presented using results from the simulations. In order to achieve a fair comparison, the number of receive antennas is set to be the same. The performance of the three techniques for the spectral efficiency of 2, 4 and 8 b/s/Hz is shown in Figure 3.9, 3.10 and 3.11 respectively. The channel model has the function as in (3.3), F_c(U, 1). The transmitter and receiver follow the system as depicted in Figure 3.1 and 3.2 respectively without the shaded regions.

The spectral efficiency of 2 b/s/Hz achieved by STBC, BLAST and the hybrid scheme in Figure 3.9 use constellations of QPSK, BPSK and BPSK respectively. There are 2 antennas used at the receiver. It can be seen from this figure that V-BLAST performs worse due to achieving only a diversity of order one as compared to four and two for the Alamouti STBC and Dual Alamouti STBC respectively.

Figure 3.10 displays the results of the three MIMO techniques achieving a spectral efficiency of 4 b/s/Hz. The order of algorithms for 2 receive antennas starting from the worst is in the

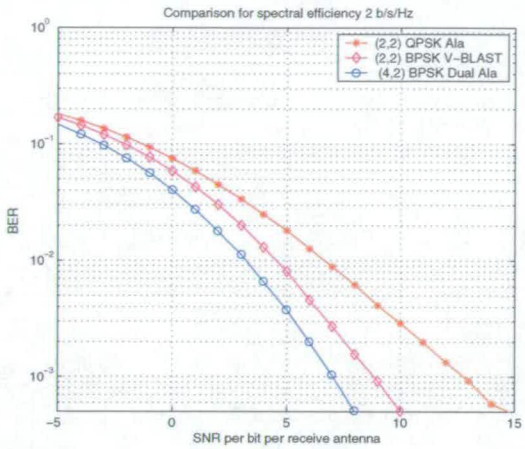

Figure 3.9: *Uncoded BER vs E_b/N_O for spectral efficiency of 2 b/s/Hz in a $F_c(U,1)$ channel*

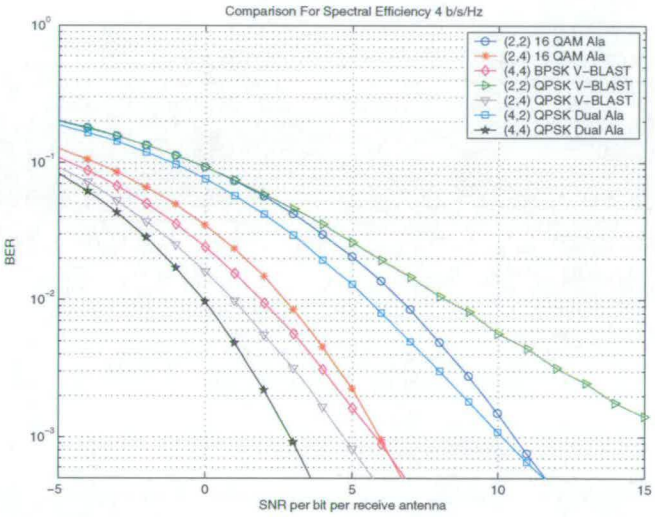

Figure 3.10: *Uncoded BER vs E_b/N_O for spectral efficiency of 4 b/s/Hz in a $F_c(U,1)$ channel*

order QPSK V-BLAST, 16 QAM Alamouti STBC and then the QPSK Dual Alamouti scheme. The poor performance of V-BLAST is due to no diversity achieved in the (2,2) configuration. Although the Alamouti STBC and hybrid scheme possess a diversity order of 4 which is a factor of 2 more than Dual Alamouti STBC, Alamouti STBC is outperformed due to the higher order modulation (16 QAM) being used.

When employing 4 antennas at receiver, Alamouti STBC gives the worst performance while the Dual Alamouti scheme remains the best. Also shown is the QPSK V-BLAST with 2 transmitting antennas and the BPSK V-BLAST with 4 transmitting antennas. Despite the QPSK

V-BLAST employing a higher constellation than its equivalent BPSK system, the performance of the QPSK is better due a diversity gain of order 3 fold in the (2,4) configuration as compared to 1 in the (4,4) configuration. Comparing the QPSK (2,4) V-BLAST and (4,4) Dual Alamouti scheme shows that both employ the same constellation, but because the V-BLAST technique has less interfering antennas, one would expect better performance than the hybrid scheme. However, this is not the case due to the doubling in receiver degrees of freedom in the Dual Alamouti scheme.

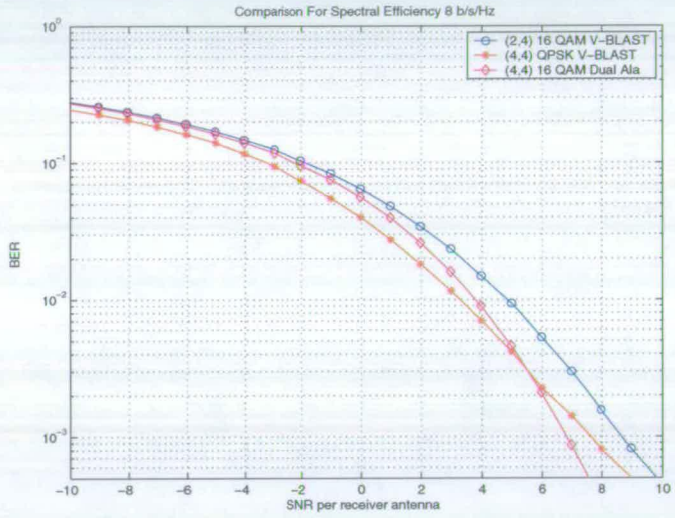

Figure 3.11: *Uncoded BER vs E_b/N_O for spectral efficiency of 8 b/s/Hz in a $F_c(U,1)$ channel*

Lastly, Figure 3.11 shows the results for V-BLAST and Dual Alamouti for a spectral efficiency of 8 b/s/Hz. In this scenario, a mixed performance is seen where for lower SNR values, QPSK (4,4) V-BLAST performs better than the 16 QAM (4,4) Dual Alamouti scheme while the opposite performance comparison is seen for the higher SNR values. This is because at higher SNR, diversity gain is the dominant factor on BER performance. Also included in this figure is the performance of (2,4) 16QAM V-BLAST. This time the performance of this technique is worse than the other two techniques due to a higher constellation modulation being used.

3.6.2 Coded Systems

At the receiver of a coded system as shown in Figure 3.2, each subcarrier's symbol at every antenna is spatially and temporally processed while its outputs are sent to a soft decision metric generator [79] prior to the Viterbi decoder governed by the log-likelihood ratio (LLR) to obtain

its *a posteriori* probability (APP). Assuming perfect channel knowledge, the LLR for a SISO system at bits b_c can be calculated as:

$$\mathrm{LLR}(b_c) = \ln \frac{\Pr(b_c = +1|r)}{\Pr(b_c = -1|r)} \tag{3.43}$$

$$\mathrm{LLR}(b_c) = \ln \sum_{x^+ \in \{x:b_c=+1\}}^{N_{cons}} \exp\left(-\frac{|r - hx^+|^2}{\sigma_n^2}\right) - \ln \sum_{x^- \in \{x:b_c=-1\}}^{N_{cons}} \exp\left(-\frac{|r - hx^-|^2}{\sigma_n^2}\right) \tag{3.44}$$

where x belongs to a set of all possible symbols in the QAM constellation, $x \in \{x_0, x_1, \ldots, x_{2^{B_c}-1}\}$, and B_c is equal to $\log_2(N_{cons})$, N_{cons} being the number of points in the constellation size.

The equation in (3.44) represents the APP for a single input single output (SISO) system. This soft output gives an indication of the likely bits being +1 or -1 by calculating the distances between the received signal and all possible symbols in the constellation. This can be extended to the MIMO perspective, so called the APP detection. The MIMO APP detector modifies the expression in (3.44) such that

$$\mathrm{LLR}(b_c) = \ln \sum_{\mathbf{x}^+ \in \{\mathbf{x}:b_c=+1\}}^{N_{cons}} \exp\left(-\frac{||\mathbf{r} - \mathbf{H}\mathbf{x}^+||^2}{\sigma_n^2}\right) - \ln \sum_{\mathbf{x}^- \in \{\mathbf{x}:b_c=-1\}}^{N_{cons}} \exp\left(-\frac{||\mathbf{r} - \mathbf{H}\mathbf{x}^-||^2}{\sigma_n^2}\right) \tag{3.45}$$

where $\mathbf{r}$ is the N size received signal vector, $\mathbf{x}$ is the M size transmitted signal vector and $\mathbf{H}$ is the $N \times M$ size channel matrix. The number of bits generated, b_c, is equal to $M \log_2(N_{cons})$. The complexity of this detector grows exponentially with the number of transmitter used, N_{cons}^M, which is hardly physically realisable for a large constellation size.

In the case of using the MMSE OSIC algorithm for either the V-BLAST or Dual Alamouti STBC, the soft outputs generator in equation (3.44) is slightly modified such that:

$$\mathrm{LLR}(b_c) = \ln \sum_{x^+ \in \{x:b_c=+1\}}^{N_{cons}} \exp\left(-\frac{|\breve{r} - \breve{h}x^+|^2}{\breve{\sigma}_n^2}\right) - \ln \sum_{x^- \in \{x:b_c=-1\}}^{N_{cons}} \exp\left(-\frac{|\breve{r} - \breve{h}x^-|^2}{\breve{\sigma}_n^2}\right) \tag{3.46}$$

where

$$\breve{r} = \mathbf{G}_m \mathbf{r} \tag{3.47}$$

$$\breve{h} = \mathbf{G}_m \mathbf{H}_m \tag{3.48}$$

$$\breve{\sigma}_n^2 = |(\mathbf{G}_m)|^2 \sigma_n^2 + \sum_{\forall p}^{M} |(\mathbf{G}_m)\mathbf{H}_p|^2 E(|x_p|^2) \tag{3.49}$$

where $\mathbf{G}_m$ is the mth row vector of the MMSE/ZF beamformer, $\mathbf{H}_m$ is the mth column vector of the channel matrix and p is the undetected streams. m represents the stream that is being detected.

A separate replicate of signal before the LLR calculator in (3.47) are being quantised and subtracted from the received signal as in Section 2.10.1 as part of the OSIC algorithm.

The full system setup is depicted in Figure 3.1 and 3.2. 3066 bits per frame has been used in the simulation for this section.

3.6.3 Performance of Spectral Efficiency And Number Of Antennas For Coded Systems

The error performance of V-BLAST, Alamouti STBC and Dual Alamouti STBC attaining spectral efficiency of 2, 4 and 6 bits/s/Hz employing both two and four antennas at the receiver are shown in Figure 3.12, 3.13 and 3.14 respectively. Unless stated, the channel code rate is assumed to be 1/2 and the channel function is set to F_c(U, A). The spectral efficiency of a MIMO scheme can be calculated as follows:

$$B_c * R * M * \text{Number of period per retransmitted information} \tag{3.50}$$

The achieved spectral efficiencies compared with respect to their MIMO scheme, code rate and number of antennas are tabulated in Table 3.2

The choice of increasing number of antennas for spatial transmission or using a higher constellation size in a V-BLAST technique is illustrated in Figure 3.12, 3.13 and 3.14 for the $R = 1/2$ QPSK (2,4) and $R = 1/2$ BPSK (4,4), $R = 1/2$ 16 QAM (2,4) and $R = 1/2$ QPSK (4,4) and $R = 1/2$ 64 QAM (2,4) and $R = 3/4$ 64 QAM (4,4) respectively. Despite a low error probability constellation used in the (4,4) configuration, the performance still favours the (2,4)

Spectral efficiency	Compared schemes
2 bits/s/Hz	(2,2) 16 QAM Alamouti, R = 1/2
	(2,4) 16 QAM Alamouti, R = 1/2
	(4,4) BPSK V-BLAST, R = 1/2
	(2,2) QPSK V-BLAST, R = 1/2
	(2,4) QPSK V-BLAST, R = 1/2
	(4,2) Dual Alamouti STBC, R = 1/2
	(4,4) Dual Alamouti STBC, R = 1/2
4 bits/s/Hz	(2,2) 16 QAM V-BLAST, R = 1/2
	(2,4) 16 QAM V-BLAST, R = 1/2
	(4,4) QPSK V-BLAST, R = 1/2
	(4,2) 16 QAM Dual Alamouti, R = 1/2
	(4,4) 16 QAM Dual Alamouti, R = 1/2
6 bits/s/Hz	(2,2) 64 QAM V-BLAST, R = 1/2
	(2,4) 64 QAM V-BLAST, R = 1/2
	(4,4) QPSK V-BLAST, R = 3/4
	(4,2) 64 QAM Dual Alamouti, R = 1/2
	(4,4) 64 QAM Dual Alamouti, R = 1/2

Table 3.2: *Simulation MIMO schemes with different spectral efficiencies*

configuration. The three fold diversity gain in (2,4) introduces robustness and overshadows the higher error probability caused by the higher size constellation. Similar trend is observed in the uncoded case as shown in Figure 3.10 where the (2,2) QPSK V-BLAST performs better than the (4,4) BPSK V-BLAST.

Irrespective of the spectral efficiency attained by any of the three MIMO schemes, the V-BLAST scheme using two antennas at the receiver performs significantly worse than the other two schemes (similar trend as the uncoded case in Figure 3.9 and 3.10). This is due to the absence of diversity, i.e. 1, in the V-BLAST scheme, because having an equal number of antennas at both the transmitter and receiver provides virtually no means of exploiting spatial diversity. Comparing the 4 receive antennas case for both the V-BLAST and Dual Alamouti STBC achieving 2, 4 and 6 bits/s/Hz, the SNR difference between both schemes at 1% FER is 1.6 dB, 2.1 dB and 2.0 dB respectively with the performance favouring the Dual Alamouti scheme. However, this difference becomes more apparent when 2 receive antennas are used at the receiving terminals. The differences in values at 10% FER are 4.7 dB, 6.2 dB and 7.3 dB for spectral efficiency 2, 4 and 6 bits/s/Hz respectively, while the expected difference would be larger at 1% FER. The 1% FER is not simulated for the V-BLAST because it would require a much higher SNR to reach to this error margin.

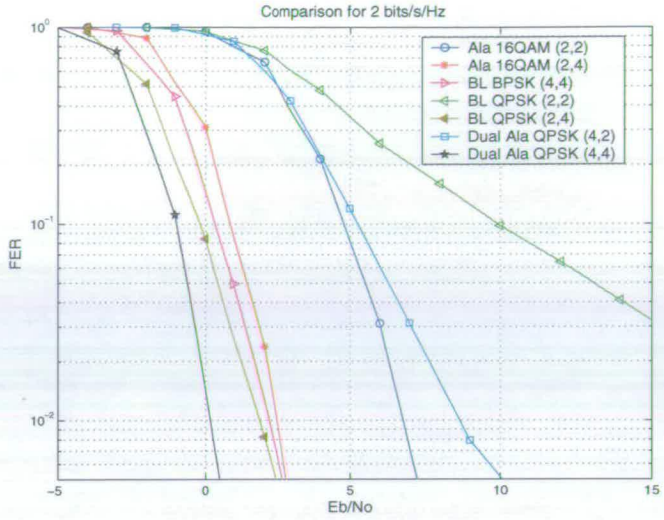

Figure 3.12: *Coded FER vs E_b/N_O for spectral efficiency of 2 b/s/Hz in a $F_c(U,A)$ channel for R = 1/2 comparing Alamouti STBC, MMSE OSIC V-BLAST and MMSE OSIC Dual Alamouti*

Even though the 4 receive antennas case of Dual Alamouti scheme achieves a diversity double that of V-BLAST, the performance gain is not as significant as the 2 antennas case due to V-BLAST achieving an approximate diversity order of three fold. Further increase in diversity order higher than three results in a slight gain in performance (Refer to Appendix F). Due to the lack of diversity being exploited in the V-BLAST 2 receive antennas case, its relative performance to Dual Alamouti STBC scheme is seen to be more sensitive to spectral efficiency. This is because the more spectrally efficient system requires a larger constellation that results in more interference between the transmitted streams. In this case, the transmit diversity inherent in the Dual Alamouti scheme is useful in minimising the error propagation effect in the OSIC algorithm.

The Alamouti STBC scheme performs better than both the V-BLAST and Dual Alamouti schemes when two antennas are used at the receiver (similar as the uncoded case in Figure 3.9). The achievable diversity gain from the Dual Alamouti scheme is minimum when two receive antennas are used, in addition to interference between the two Alamouti concatenated pairs. As the number of receive antennas increases, the Dual Alamouti and V-BLAST schemes become more robust than Alamouti STBC because the latter scheme requires a larger constellation size to achieve the same spectral efficiency as compared to the other two MIMO techniques.

To understand the optimum performance of these MIMO schemes, the V-BLAST and Dual

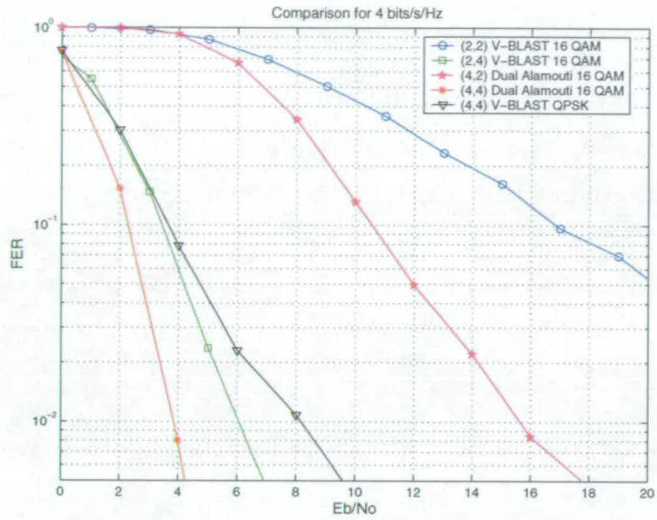

Figure 3.13: *Coded FER vs E_b/N_O for spectral efficiency of 4 b/s/Hz in a F_c(U,A) channel for R = 1/2 comparing Alamouti STBC, MMSE OSIC V-BLAST and MMSE OSIC Dual Alamouti*

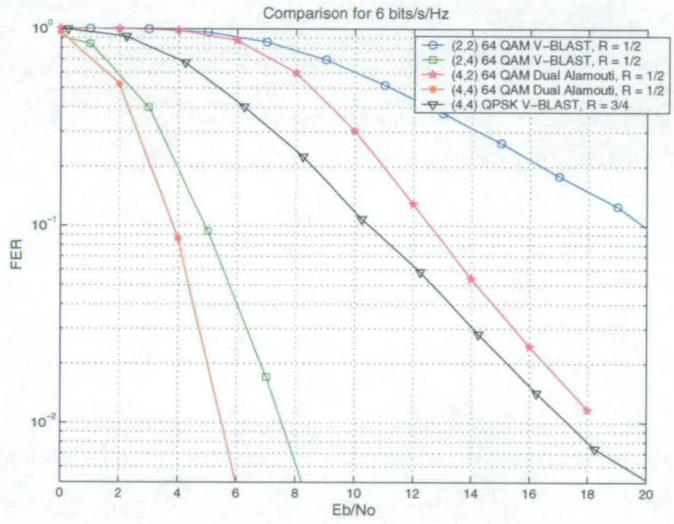

Figure 3.14: *Coded FER vs E_b/N_O for spectral efficiency of 6 b/s/Hz in a F_c(U,A) channel comparing Alamouti STBC, MMSE OSIC V-BLAST and MMSE OSIC Dual Alamouti*

Alamouti STBC deploying the APP detector simulation results for 2 bits/s/Hz are plotted in Figure 3.15. Similar channel function, F_c(U, A) and channel code rate of 1/2 for all schemes have been used. Other than the performance of the (4,4) BPSK V-BLAST being better than the (2,4) QPSK V-BLAST when 4 Rx are used, similar trend to the 4 Rx OSIC performance is observed as in Figure 3.12. Unlike the OSIC detector, where spatial freedom is more sig-

nificant to improve diversity, the APP detector runs through all possible solutions in search of the minimum distance. Hence, using a lower error propagation constellation becomes more advantageous. Contrary to the OSIC detector, the 2 Rx Alamouti STBC scheme using a higher constellation gives the worse performance. Dual Alamouti STBC which has both transmit diversity gain and as spectrally efficient as V-BLAST is seen to perform among the best.

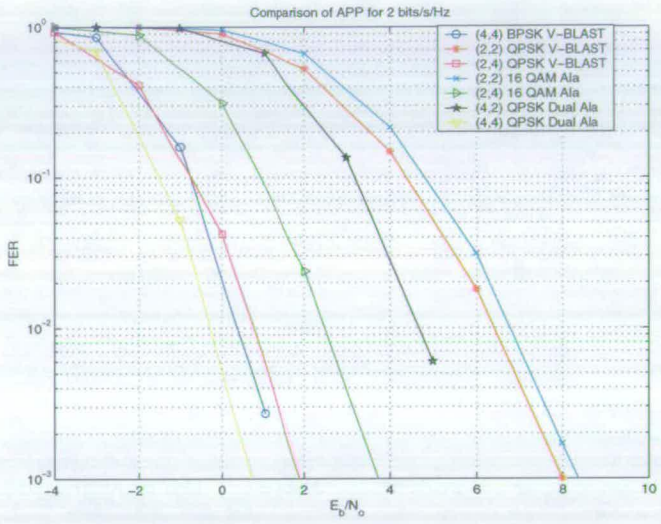

Figure 3.15: *Coded FER vs E_b/N_O for spectral efficiency of 2 b/s/Hz in a F_c(U,A) channel for R = 1/2 using the APP detector*

3.6.4 Channel Correlations

The results for comparing the 16 QAM (2,4) Alamouti STBC, QPSK (2,4) V-BLAST, BPSK (4,4) V-BLAST and QPSK (4,4) Dual Alamouti schemes in a correlated fading channel are illustrated in Figure 3.16. All the MIMO schemes are convolutionally coded with , R = 1/2. In this simulation, the AS at the receiver is varied while that for the transmitter is fixed at an AS of 90^o where the channel function is set to F_s(C, A, 0^o, 90^0, 0.5λ, 0^o, Var, 0.5λ). As expected, V-BLAST performance is significantly affected by low AS while Alamouti STBC is fairly robust to variations in correlation. The plots show that at low correlation (AS > 100), the FER performance for Dual Alamouti is approximately 2.0 dB better than the other techniques. However, at very low angular spread the Dual Alamouti scheme suffers some degradation compared to Alamouti STBC. Comparing V-BLAST and Dual Alamouti, Dual Alamouti attains similar performance to Alamouti STBC at an AS of 50^o while V-BLAST requires a much higher AS of 115^o at the receiver to achieve similar performance. The robustness to correlation is due to

the orthogonal nature of Alamouti STBC which makes each stream from the same Alamouti pair non-interfering unlike V-BLAST where every stream interferes with one another. Despite attaining a lower correlation at 180^o, it is observed that the required SNR for the 160^o AS is lower for the latter case. This is due to the correlation being generated using a sum of Bessel function that oscillate in a similar manner to a sinc function as the angle spread increases.

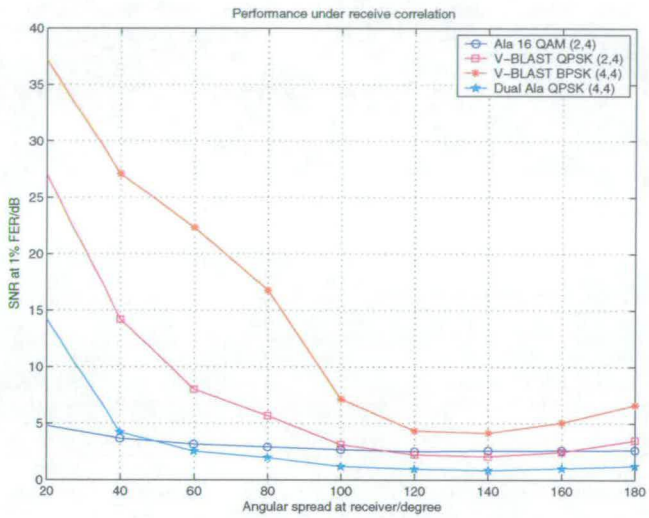

Figure 3.16: *Required SNR at 1% FER vs Rx AS in a $F_c(U,A,0^o,90^0,0.5\lambda,0^o,Var,0.5\lambda)$ channel for R = 1/2 comparing Alamouti STBC, MMSE OSIC V-BLAST and MMSE OSIC Dual Alamouti*

Similar simulations to the previous correlation study is shown in Figure 3.17, but this time the receiver AS is fixed at 90^o while the transmit correlations are varied. The channel function is set to F_s(C, A, 0^o, Var, 0.5λ, 0^o, 90^o, 0.5λ). The relative performance of each scheme is similar to the Figure 3.16. Unlike the previous case, the (2,4) V-BLAST required SNR is observed to be less than the Dual Alamouti for very low AS, approximately 30^o and less. This is because the number of transmit elements is doubled in the latter scheme, hence increasing its effective correlation as compared to two antenna transmit V-BLAST. Also, the Dual Alamouti scheme requires an AS of 60^o to equal and outperform the performance of Alamouti STBC, which is 10^o more than the previous case. This can be explained by the MMSE beamformer being less able to spatially separate the more correlated transmitted streams.

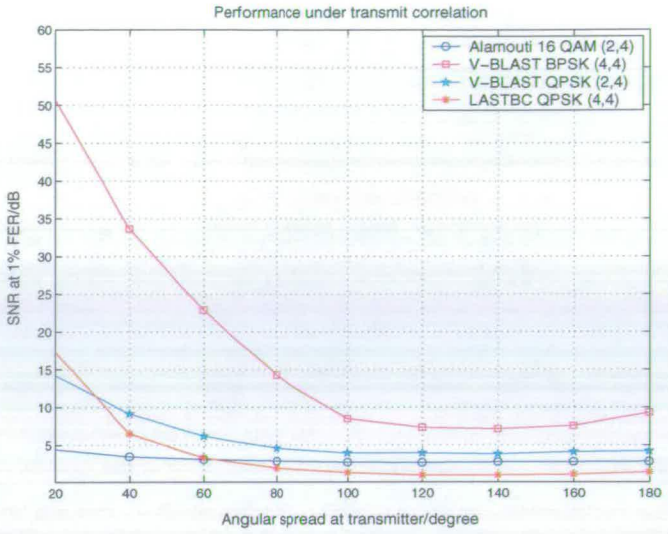

Figure 3.17: *Required SNR at 1% FER vs Tx AS in a F_c(U, A, 0^o, Var, 0.5λ, 0^o, 90^0, 0.5λ) channel for R = 1/2 comparing Alamouti STBC, MMSE OSIC V-BLAST and MMSE OSIC Dual Alamouti*

3.7 Conclusion

In this chapter the relative performance of three MIMO schemes, namely Alamouti STBC, V-BLAST and Dual Alamouti STBC was studied. The capacity of these schemes were analysed for both the uncorrelated and correlated scenarios. In both cases Dual Alamouti STBC was generally better than the other two. The stand alone (2,N) Alamouti STBC is seen to outperform (2,N) V-BLAST for lower SNRs while at higher SNRs V-BLAST becomes better. In the correlated case, Alamouti is the most robust followed by Dual Alamouti and V-BLAST. For extremely high correlation Alamouti STBC performs the best among the three MIMO techniques.

The coded simulation results using less complex decoders in Section 3.6.2 compares the three techniques with respect to three parameters that will be important when considering future wireless LAN implementation. The three parameters are spectral efficiency, number of antennas used and channel correlation. The simulation results show that Alamouti STBC is preferred at low complexity when the spectral efficiency is low while the number of Tx and Rx are restricted to two. Without this restriction, increasing the number of Tx or Rx favours the hybrid Dual Alamouti STBC scheme, supporting higher spectral efficiency transmission. On the other hand, where the number of transmitting antennas is less than that for the receiving terminal, e.g. a (2,4) scheme, then the V-BLAST is capable of delivering good performance at

the expense of a small degradation as compared to Dual Alamouti STBC for the same number of Rx used. Similar results have been observed in the uncoded case too.

Under the influence of correlated fading channels, which is the case in a real scenario, the V-BLAST scheme is severely affected as compared to Alamouti STBC. Also, the hybrid of Dual Alamouti STBC is more robust to channel correlation than V-BLAST.

Comparing the theoretical capacity analysis and simulation results, some similarities and differences will be discussed. Firstly and analogously, for the uncorrelated 2 Rx case, the Alamouti STBC is better than V-BLAST for low spectral efficiency. When 4 Rx are used, then V-BLAST performs better than Alamouti STBC. Dual Alamouti STBC performs better in the 4 Rx case but there is a contradiction between the the theory and simulation results for the 2 Rx. In the 2 Rx simulation results case, Alamouti STBC performs better than Dual Alamouti while the theoretical analysis predicts the opposite effect. The difference can be explained by the fact that Dual Alamouti STBC uses the sub-optimal MMSE OSIC detector in the simulation. In the case of correlated fading channels, both theoretical analysis and simulation results match each others' trends. For very high correlation, Alamouti STBC is preferred over the other two schemes. The inherent transmit diversity in Dual Alamouti STBC makes it more robust to correlation relative to V-BLAST. While the MIMO schemes using the optimum APP detector, its performance follows a similar trend as the theoretical capacity results.

Since the uncoded and coded systems show similar relative performance for the MIMO detection algorithms, the next chapter comparing the robustness of MIMO techniques in the presence of interference will be simulated with the uncoded system.

Chapter 4
Interference Modelling And MIMO Multiuser Interference Mitigation

4.1 Introduction

The use a of wireless local area network (WLAN) in unlicensed frequency bands means that it is vulnerable to a considerable amount of cochannel interference (CCI), not only from its own system but also other systems and devices, e.g. Bluetooth, microwave ovens, etc. The error performance of the system degrades severely as the power of the CCI increases. In these circumstances, a WLAN system can only tolerate a fixed amount of interference before the link layer performance fails to operate .

Pre-equalisation [44] is an effective way of mitigating interference, but is reasonably complicated to implement because channel knowledge of all users are required prior to transmission. Also, this technique does not allow suppression of interference from external sources. One of the most efficient techniques to tackle CCI is to implement an antenna array receiver [80], in which the number of antenna elements at the receiver is more than that at the transmitter. The antenna weights can be varied such that a strong beam of signal is directed in the direction of the desired user and nulled in the direction of the interferers. Subtractive interference cancellation [45] can also be effective provided the CCI user's signal is correctly estimated.

Two possible CCI models for a SISO OFDM system, namely, synchronous and asynchronous interference scenarios are modelled. Detailed explanations of these models and their corresponding mathematical analysis, which was verified with simulation results in a Rayleigh flat fading channel, will be shown. Then, interference mitigation techniques which are extension to the ordered successive interference cancellation (OSIC) algorithm are suggested. In order to mitigate interference efficiently at low cost, two types of interference mitigation techniques will be defined and studied, namely interference cancellation (IC) and interference suppression (IS). IC processing is similar to that of the OSIC algorithm where transmitted signals from each antenna of all users are ordered according to the highest SNR, detected and then subtracted

from the received signal. On the other hand, IS processing only detects the desired user's signals while nulling the interferers. Single user performance analysis using these two techniques comparing the robustness of V-BLAST and Dual Alamouti STBC in the presence of CCI will be analysed. Alamouti STBC is dropped in this chapter due to its low spectral efficiency.

4.2 System description

A wireless OFDM system with one CCI user from the same system is shown in Figure 4.1. Both the data of the desired user and the CCI from one user are extended using a cyclic prefix to eliminate ISI completely.

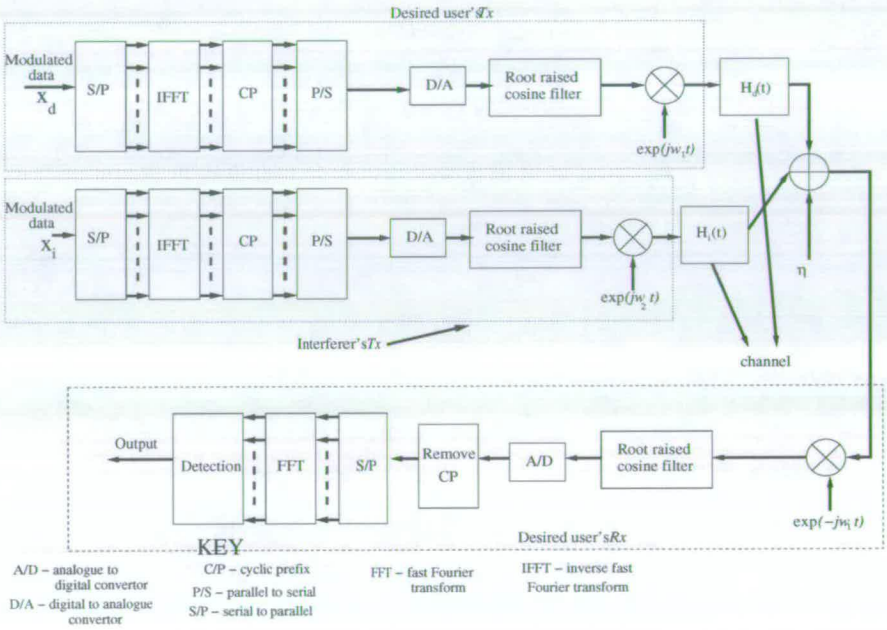

Figure 4.1: *A passband OFDM system*

Repeating the baseband OFDM signal in equation (2.1), the time domain signal of each user is given by:

$$s(t) = \sum_{k_c=0}^{K_c-1} x_{k_c} e^{j2\pi \frac{k_c}{T_{sub}} t}$$

where K_c is the total number of carriers, T_{sub} is the sub-channel signalling interval and x_{k_c} is the modulated symbol at sub-carrier k_c.

4.3 Mathematical Analysis and Simulation of CCI in a Rayleigh Flat Fading Channel

In a wireless system, CCI that appears at the receiver when not properly removed is treated as an additional noise, which will distort the desired user's signal significantly if the signal strength of the CCI is sufficiently high. Clearly, the system will not function properly when the number of CCI users interfering at the same time becomes sufficiently large. In this section two models of interference will be considered, namely, synchronous and asynchronous. Mathematical analysis supported by simulation results on the basis of one desired user and one CCI user are investigated. The analysis will determine the behaviour of the interference and bit error probability (BEP).

4.3.1 Synchronous Interference

This type of model represents a good starting point to understand how interference can affect the BER performance of a system. Synchronous interference is modelled in such a way that the transmission of both the desired user and CCI user start at the same time, which is illustrated in Figure 4.2. Both the desired user's and the CCI user's data lengths are assumed to be equal.

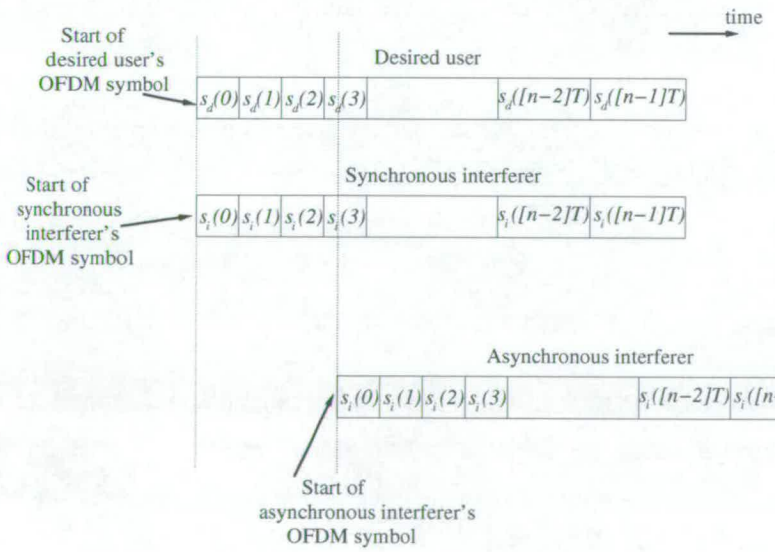

Figure 4.2: *Synchronous and asynchronous OFDM interference*

In the presence of interference (synchronous), the time domain signal at the receiver can be

expressed as:

$$\begin{aligned} r(t) &= h_d(t) \otimes s_d(t) + h_i(t) \otimes s_i(t) + \eta(t) \\ &= h_d \otimes (t) \sum_{k_c=0}^{K_c-1} x_d e^{j2\pi \frac{k_c}{T_{sub}} t} + h_i(t) \otimes \sum_{k_c=0}^{K_c-1} x_i e^{j2\pi \frac{k_c}{T_{sub}} t} + \eta(t) \end{aligned} \tag{4.1}$$

where $\otimes$ denotes the convolution operation; $s_d(t)$ and $s_i(t)$ are the transmitted time domain signal of the desired user and interferer respectively; $h_d(t)$ and $h_i(t)$ are the time domain channel response of the desired user and interferer respectively; x_d and x_i are the frequency domain QAM symbols at subcarrier k_c of the desired user and interferer respectively and $\eta(t)$ is complex additive white Gaussian noise (AWGN). Note that the subcarrier index has been dropped from the equations for simplicity.

Because of the synchronous transmission between the user and its interferer, the received signal at each subcarrier k_c can be expressed as:

$$r = h_d x_d + h_i x_i + \eta \tag{4.2}$$

Note that, the equation in (4.2) illustrates that for a desired user being interfered with by one synchronous user, the received signal at each subcarrier is equivalent to adding the symbol multiplied with its channel response (which is flat fading for an OFDM system) of both the desired user and interferer at the same subcarrier

Recall from [61] that for a $m-ary$ QAM modulated signal received over a Rayleigh flat fading channel, the bit error probability (BEP) can be expressed as:

$$P(\overline{\Gamma}) = \sum_{i=1}^{J_c} \frac{1}{2} \xi_i \left(1 - \sqrt{\frac{\psi_i \Gamma}{2 + \psi_i \Gamma}} \right) \tag{4.3}$$

where Γ is the signal-to-noise ratio (SNR) of the received signal and J_c is the total number of coefficients of ξ_i and ψ_i which are tabulated in [61]. These coefficients vary accordingly to the constellation size. Refer to Appendix D for the coefficients with respect to the constellation size used.

In the presence of synchronous interference, the BEP of a Rayleigh flat fading system is further

developed in this thesis by slight modification of (4.3)

$$P(\overline{\Gamma}) = \frac{1}{2}\sum_{i=1}^{J_c}\sum_{c=1}^{N_{CD}} p_c\xi_i\left(1-\sqrt{\frac{\psi_i\frac{P_D}{P_c+\sigma_n^2}}{2+\psi_i\frac{P_D}{P_c+\sigma_n^2}}}\right) \tag{4.4}$$

$$= \frac{1}{2}\sum_{i=1}^{J_c}\sum_{c=1}^{N_{CD}} p_c\xi_i\left(1-\sqrt{\frac{\psi_i\Upsilon_c}{2+\psi_i\Upsilon_c}}\right) \tag{4.5}$$

where N_{CD} is the number of different constellation points used in the modulation scheme for the interferer, P_D is the signal power of desired user, P_c is the signal power of the interferer at constellation point c, σ_n^2 is the noise power and p_c is the occurrence probability of constellation point c. The ratio $\frac{P_D}{P_c+\sigma_n^2}$, which is the signal-to-interference-plus-noise ratio (SINR), is denoted by Υ_c. In this case, the Rayleigh faded interferer is modelled as additional noise in the system. This result may be extended to an arbitrary number of interferers, but every possible combination of transmitted constellation points must be considered.

Results of BER vs SNR performance for various CCI signal power levels are shown in Figure 4.3. Figure 4.3(a), 4.3(b), 4.3(c) and 4.3(d), show a QPSK and a 16 QAM desired user with an identically modulated CCI user, QPSK with a 16 QAM CCI user and 16 QAM with a QPSK CCI user respectively. For every BER curve, the interference-to-noise ratio (INR) is set to a constant value in the range -20 to 20 dB. Simulation results are shown as lines and theoretical results from (4.5) as points.

From these graphs, it can be seen that when the level of CCI signal power is well below that of desired user, the BER is barely affected by the presence of interference. However, as the CCI signal power increases to a similar level as that of the desired user, the link layer performance degrades significantly so that the coverage of the system reduces. This situation is likely to happen, for example, when a user is at the edge of one cell and the interferer is located at the edge of a nearby AP boundary.

4.3.2 Asynchronous Interference

In Section 4.3.1, the link layer performance with a synchronous CCI user is studied. However, this scenario can only exist in a single cell where all users are being controlled by one AP. Where users from neighbouring cells sharing the same frequency band interfering with one another, the symbol timing of the interferer does not necessarily coincide with that of the desired user as

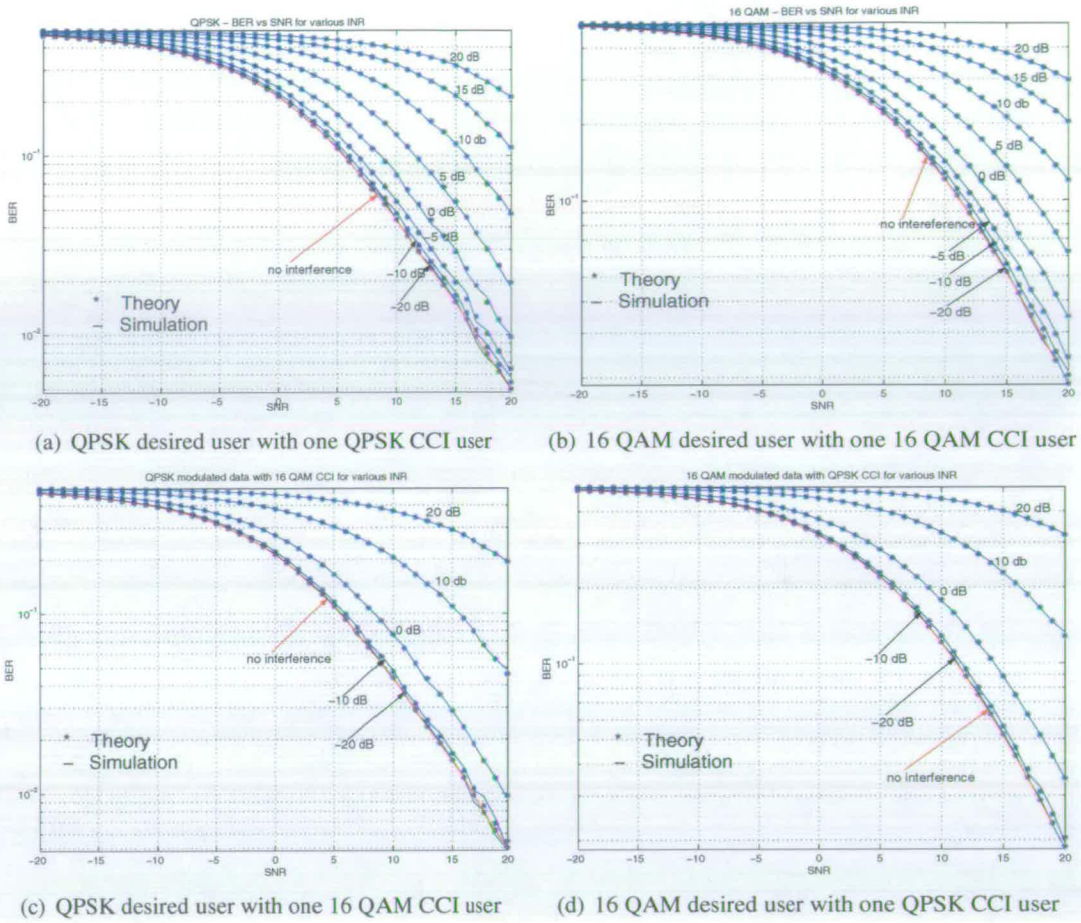

(a) QPSK desired user with one QPSK CCI user

(b) 16 QAM desired user with one 16 QAM CCI user

(c) QPSK desired user with one 16 QAM CCI user

(d) 16 QAM desired user with one QPSK CCI user

Figure 4.3: *BER vs SNR for various INR levels in a Rayleigh flat fading channel with synchronous interference employing matched filter at the receiver*

illustrated in Figure 4.2. In this case, mitigation of CCI becomes more challenging as the timing of interference is not known, which makes it very difficult to estimate the channel response of the interferer.

Assuming that one asynchronous interferer is present and that the channel is constant over one FFT size frame length, the time domain OFDM signal can be expressed as:

$$\mathbf{r}(t) = \mathbf{H_d}(t)\mathbf{s_d}(t) + \mathbf{H_i}(t)\mathbf{s_i}(t) + \boldsymbol{\eta}(t) \tag{4.6}$$

where $\mathbf{r}(t), \mathbf{s}(t), \boldsymbol{\eta}(t)$ are the $(K_c + N_{CP})$ received signal (N_{CP} is the length of cyclic prefix), transmitted signal and noise signal vector respectively. Assuming a (M, N) = (1,1) OFDM

system for both users, the $(K_c + N_{CP})$ size circulant square channel matrix, $\mathbf{H_d}(t)$ and $\mathbf{H_i}(t)$ of the desired user and interferer respectively, assuming a cyclic prefix equal to the length the channel memory can be represented as:

$$\mathbf{H_d}(t) = \begin{bmatrix} h_d(0) & 0 & \dots & 0 & h_d(N_{CP}-1) & h_d(N_{CP}-2) & \dots & h_d(1) \\ h_d(1) & h_d(0) & 0 & \dots & 0 & h_d(N_{CP}-2) & \dots & h_d(2) \\ \\ h_d(N_{CP}-1) & h_d(N_{CP}-2) & \dots & h_d(0) & 0 & 0 & 0 & 0 \\ 0 & 0 & \dots & 0 & h_d(0) & 0 & 0 & 0 \\ \vdots & & & & h_d(1) & h_d(0) & 0 & 0 \\ \\ 0 & 0 & 0 & 0 & h_d(N_{CP}-1) & h_d(N_{CP}-2) & \dots & h_d(0) \end{bmatrix} \tag{4.7}$$

where $h_d(t)$ is the channel response of the desired user at time t. Similarly, $\mathbf{H_i}(t)$ possesses the same structure as (4.7)

Expanding the expression in equation (4.6) to:

$$\mathbf{r}(t) = \mathbf{H_d}(t)\mathbf{\Omega_d}\mathbf{x_d}(t) + \mathbf{H_i}(t)\mathbf{\Omega_i}\mathbf{x_i}(t) + \boldsymbol{\eta}(t) \tag{4.8}$$

and

$$\mathbf{\Omega_d} = \begin{bmatrix} \bar{\mathbf{\Omega}} \\ \begin{bmatrix} \bar{\mathbf{\Omega}}(K_c - N_{CP}, 0) & \dots & \bar{\mathbf{\Omega}}(K_c - N_{CP}, K_c - 1) \\ \vdots & \ddots & \dots \\ \bar{\mathbf{\Omega}}(K_c - 1, 0) & \dots & \bar{\mathbf{\Omega}}(K_c - 1, K_c - 1) \end{bmatrix} \end{bmatrix} \tag{4.9}$$

$$\mathbf{\Omega_i} = \begin{bmatrix} \begin{bmatrix} \bar{\mathbf{\Omega}}(\nu_s, 0) & \dots & \bar{\mathbf{\Omega}}(\nu_s, K_c - 1) \\ \vdots & \ddots & \dots \\ \bar{\mathbf{\Omega}}(K_c + N_{CP} - 1 - \nu_s, 0) & \dots & \bar{\mathbf{\Omega}}(K_c + N_{CP} - 1 - \nu_s, K_c - 1) \end{bmatrix} \\ \begin{bmatrix} \bar{\mathbf{\Omega}}(K_c + N_{CP} - \nu_s, 0) & \dots & \bar{\mathbf{\Omega}}(K_c + N_{CP} - \nu_s, K_c - 1) \\ \vdots & \ddots & \dots \\ \bar{\mathbf{\Omega}}(K_c - 1, 0) & \dots & \bar{\mathbf{\Omega}}(K_c - 1, K_c - 1) \end{bmatrix} \end{bmatrix} \tag{4.10}$$

where $\bar{\mathbf{\Omega}}$ is the standard K_c size IFFT square matrix and A(c_1, c_2) denotes the element at the c_1 row of column c_2. The parameter ν_s is defined to be the asynchronous shift of the interferer

relative to the user as seen by the receiver.

Removing the CP and transforming the received signal into the frequency domain via FFT, the received signal vector can be expressed as:

$$\mathbf{r} = \mathbf{\Omega_d}^H \mathbf{H_d}(t)\mathbf{\Omega_d}\mathbf{x_d}(t) + \mathbf{\Omega_d}^H \mathbf{H_i}(t)\mathbf{\Omega_i}\mathbf{x_i}(t) + \boldsymbol{\eta} \tag{4.11}$$

In the case where $\nu_s = 0$, in which the interference is synchronous, $\mathbf{\Omega_d}^H \mathbf{H_i}(t)\mathbf{\Omega_i}$ becomes a diagonal matrix and the received signal can be expressed as in equation (4.2). However, in the asynchronous scenario, i.e., $\nu_s \neq 0$, then the off-diagonal elements are no longer non-zero, causing interference among subcarriers, intercarrier interference (ICI). This interference disrupts the channel response which results in a potentially frequency selective interference channel depending on the relative delay in transmission time between the user and interferer. Despite this interference, the maximum received power remains the same as in the synchronous case. This is because the FFT and IFFT operate by summing the multiplication of each transmitted symbol at each subcarrier by an unique phase shift. To understand the behaviour of the channel response to the parameter ν_s, the effective power spectrum density (PSD) of the frequency channel response with respect to each subcarrier is shown in Figure 4.4

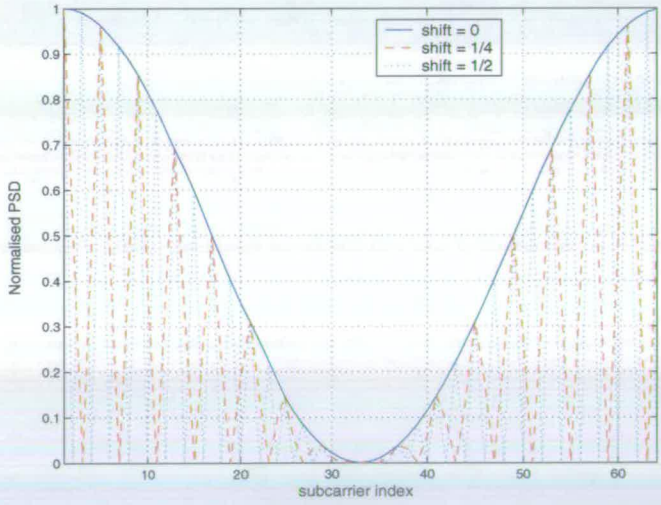

Figure 4.4: *PSD vs subcarrier index of channel response due to the parameter ν_s*

The simulation is set up such that both the desired user and the interferer channel have 2 equal power multipath Rayleigh fading taps. When the parameter ν_s is zero, the overall channels response is similar to that of a two tap channel. When this parameter is set to 1/4 of K_c, the

overall channel response becomes more frequency selective. This is because, the off-diagonal values of $\mathbf{\Omega_d}^H \mathbf{H_i}(t)\mathbf{\Omega_i}$ in equation (4.11) are no longer zero, which results in inter-carrier interference (ICI). Further increase of ν_s to 1/2 of K_c results in the channel response being twice as frequency selective as ν_s = 1/4 of K_c. Not shown in this simulation is the channel response for $\nu_s \geq 1/2$ as the channel response in this range of value is equivalent to the channel response as 1-ν_s due to one of the cyclic delay properties of FFT. Irrespective of the value of the parameter ν_s, the maximum power at the each subcarrier stays constant. Due to the frequency selectivity caused by the asynchronous interference, the BEP is not derived for this case. In the case of Rayleigh flat fading environment, the BEP is similar to that of the synchronous case in equation (4.5).

4.3.3 Degrees of Freedom and Successive Interference Cancellation

Given the two possible multiuser scenarios that can commonly exist in a cellular WLAN environment as explained in Section 4.3.1 and 4.3.2, it is important to understand the concept behind mitigating this interference. Using spatial separation technology, more commonly known as spatial division multiple access (SDMA) technique [81, 82], the available degrees of freedom required at the receiver to successfully separate the desired user from its interferer is very important. Assuming a flat fading channel for each user, the received signal at one antenna as observed by the desired user can be mathematically expressed as:

$$r = h_d x_d + h_{i_0} x_{i_0} + h_{i_1} x_{i_1} + h_{i_1} x_{i_1} + h_{N_I-1} x_{N_I-1} + \eta \tag{4.12}$$

$$= h_d x_d + \sum_{u=0}^{N_I-1} h_{i_u} x_{i_u} + \eta \tag{4.13}$$

The equation in (4.13) can be expressed in its matrix notation as:

$$r = \begin{bmatrix} h_d & h_{i_0} & h_{i_1} & \dots & h_{N_I-1} \end{bmatrix} \begin{bmatrix} x_d \\ x_{i_0} \\ x_{i_1} \\ \vdots \\ x_{N_I-1} \end{bmatrix} + \eta \tag{4.14}$$

Provided the channels of all users can be estimated to a certain degree of accuracy, the minimum means square error (MMSE) estimate can be applied to minimise the interference-plus-noise

error terms to provide interference *suppression*. This suppression technique nulls the interference signals, so that the desired user signal can be detected with minimum interference. The MMSE estimate separate the desired user from the interferer so that the desired user's signal can be detected without being interfered. Alternatively, the receiver can spatially separate all users and detect them in turn using the successive interference cancellation technique (SIC) termed as *cancellation*.

The SIC technique can only be applied to spatially separate all users provided the degrees of spatial freedom [32] is sufficiently enough at the receiver. Given that there are N_I interferers, the degrees of freedom required at the receiver must be at least equal or greater than $N(N_I+1)$. In the later section, the zero forcing (ZF) and MMSE solution applied to the SIC technique will be explained in detail.

4.4 Interference Mitigation Techniques - Single user Analysis in a Multiuser Interference MIMO environment

In this section, we assume two user environment where one is the desired user and the other acts as its interferer. Unless specified, the interference is assumed to be synchronous with the desired user. In the event that this interference is not properly mitigated, it can cause severe degradation to the overall system performance. A code division multiple access (CDMA) system supporting multiple user transmission can mitigate multiuser interference (MUI) efficiently because the receiver is able to identify each user's unique code and decorrelates the desired user from all others. However, this is not as straightforward in an OFDM multiple access scheme employed in a wireless system where no spreading codes are assigned to each individual user. Furthermore, systems supporting high data rates implementing MIMO techniques cause more problems in mitigating interference because more spatial degrees of freedom are required at the receiver.

In a multiuser environment, the two interference mitigation techniques suggested are extensions to that in [39,83,84] where multiple users are considered. In order to mitigate interference efficiently, two types of interference mitigation techniques will be defined and considered, namely interference cancellation (IC) and interference suppression (IS). In order to study the behaviour of these two interference mitigation techniques, both V-BLAST and the Dual Alamouti STBC schemes are used. Also, the robustness of these two schemes in the presence of multiuser

interference will be studied.

In the presence of synchronous interference, the received signal vector of size $N \times 1$ for the desired user can be mathematically modelled as:

$$\mathbf{r} = \mathbf{H_D x_D} + \mathbf{H_I x_I} + \boldsymbol{\eta} \tag{4.15}$$

where $\mathbf{H_D}$ and $\mathbf{H_I}$ are the matrix channel responses of size $N \times M$ for the desired user and interferer respectively, $\mathbf{x_D}$ and $\mathbf{x_I}$ are the $M \times 1$ data vector of the desired user and interferer respectively while $\boldsymbol{\eta}$ is the noise vector signal of size $N \times 1$.

The signal model in equation (4.15) can be translated into its matrix form as:

$$\mathbf{r} = \begin{bmatrix} \mathbf{H_D} & \mathbf{H_I} \end{bmatrix} \begin{bmatrix} \mathbf{x_D} \\ \mathbf{x_I} \end{bmatrix} + \boldsymbol{\eta} \tag{4.16}$$

4.4.1 Interference Cancellation (IC) Mitigation Technique

IC processing is similar to that of OSIC algorithm where transmitted signals from each antenna of both the desired user and interferer are ordered according to the highest SNR, detected and removed from the received signal. By detecting and subtracting the interferer's signal successively, non-linear processing is applied to both the desired user and interferer signals. In order to perform this technique, both the desired user and interferer channels need to be estimated as accurately as possible. Therefore, it is only restricted to mitigating interference where both the desired user and interferer are controlled by the same AP, in which synchronised transmission can be expected. The ZF and MMSE IC weighting matrix can be mathematically expressed as:

$$\mathbf{G} = [\mathbf{H_D H_I}]^H (\mathbf{H_D}(\mathbf{H_D})^H + \frac{P_I}{P_D}\mathbf{H_I}(\mathbf{H_I})^H)^{-1} \qquad \text{ZF} \tag{4.17}$$

$$\mathbf{G} = [\mathbf{H_D H_I}]^H (\mathbf{H_D}(\mathbf{H_D})^H + \frac{P_I}{P_D}\mathbf{H_I}(\mathbf{H_I})^H + \frac{\sigma_n^2}{P_D}\mathbf{I})^{-1} \qquad \text{MMSE} \tag{4.18}$$

where P_D and P_I are the power of the desired user and interferer respectively. In this case, equal power is assumed to be allocated at each transmit antenna for both users.

4.4.2 Simulation of Interference Cancellation

The simulation results for one V-BLAST and Dual Alamouti STBC user being interfered with by one synchronous cochannel interferer using the same transmission system with BPSK OFDM modulated data are shown in Figure 4.5. The channel model of $F_c(U, 1)$ has been used. The IC technique is used to mitigate the interference. The 2 transmit and 4 receive antennas ZF and MMSE V-BLAST system and 4 transmit and 4 receive antennas MMSE Dual Alamouti STBC scheme are shown in Figure 4.5(a), 4.5(b) and 4.5(c) respectively. The results displayed in all the figures show the BER vs SNR performance for various INR values. The INR in the MIMO case is defined as the INR at the receiver due to one interfering transmit antenna.

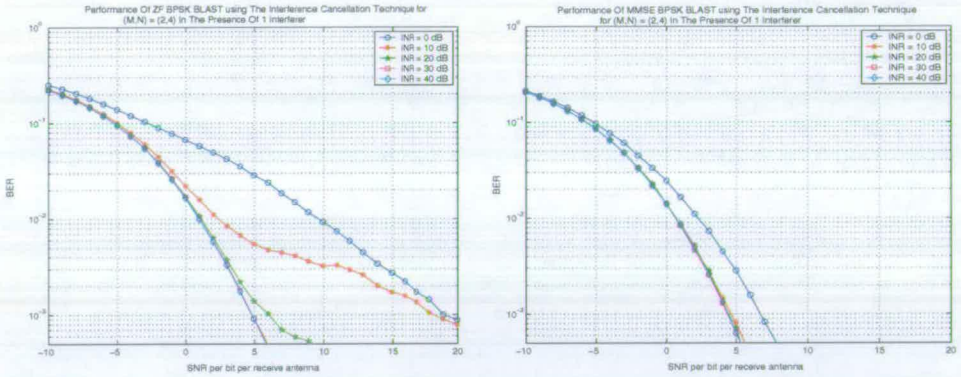

(a) BER vs SNR for ZF V-BLAST interference cancellation

(b) BER vs SNR for MMSE V-BLAST interference cancellation

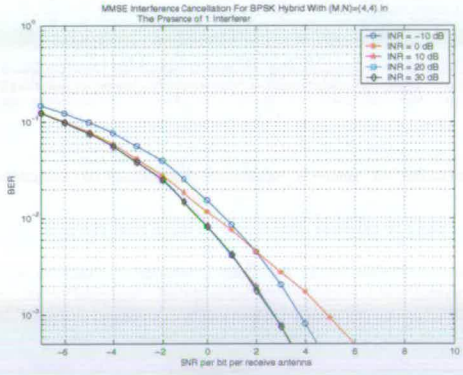

(c) BER vs SNR for MMSE Dual Alamouti STBC interference cancellation

Figure 4.5: *BER vs SNR ZF interference cancellation techniques for the three techniques for various INR*

It is observed from the three figures that employing the IC scheme gives better BER performance at low SNR values with higher INRs. This is because the high INR values lead to the

interference being detected and cancelled from the received signal first with a higher degree of accuracy. The remaining received signal, consisting only of the desired user's data, can then be detected with only occasional interference due to errors caused from wrongly detected interfering symbols. The overlapping of BER curves for very high INR values is due to the saturation effect where the interferer's signal is effectively being perfectly cancelled.

In Figure 4.5(b) and 4.5(c), crossover points of 0 dB and 10 dB INR for the first figure and -10 dB and 0 dB in the latter figure can be seen. This is because at lower SNR, the higher INR interferer can be detected and subtracted successfully from the desired user's data, hence improving the BER performance slightly. As the SNR increases the optimal ordering priority switches from the interferer to the desired user's data. This time, the higher SNR desired user's data will be detected first with only spatial suppression of the interferer. The ordering of the streams to be detected first around the crossover region would be a mixture between the desired user and interferer ones.

4.4.3 Interference Suppression (IS) Mitigation Technique

IS processing differs to IC such that only the desired user's data are being detected successively and cancelled from the received signal while the interferer's signals are nulled. Contrary to IC, linear filtering is applied to the interferer's signal. The ZF and MMSE weighting vector for this mitigation technique can be expressed as:

$$\mathbf{G} = [\mathbf{H_D}]^H(\mathbf{H_D}(\mathbf{H_D})^H + \frac{P_I}{P_D}(\mathbf{H_I}\mathbf{H_I})^H)^{-1} \quad \text{ZF} \quad (4.19)$$

$$\mathbf{G} = [\mathbf{H_D}]^H(\mathbf{H_D}(\mathbf{H_D})^H + \frac{P_I}{P_D}\mathbf{H_I}(\mathbf{H_I})^H + \frac{\sigma_n^2}{P_D}\mathbf{I})^{-1} \quad \text{MMSE} \quad (4.20)$$

Provided that the MMSE solution is used, unlike IC, this interference mitigation technique is not only restricted to interferer transmitting from the same cell. Also, irrespective of the interferer being synchronous or asynchronous this mitigation technique can be applied. This technique is advantageous compared to the IC because the interferer's channel need not to be estimated. This is because the interferer's channel information using the MMSE detector can be estimated from the covariance matrix of the received signal assuming that the channel and transmitted symbol between the desired user and interferer are independent from each other.

The covariance matrix can be calculated as:

$$\begin{aligned} E(\mathbf{r}\mathbf{r}^H) &= E((\sqrt{P_D}\mathbf{H_D}\mathbf{x_D} + \sqrt{P_I}\mathbf{H_I}\mathbf{x_I} + \boldsymbol{\eta})(\sqrt{P_D}\mathbf{H_D}\mathbf{x_D} + \sqrt{P_I}\mathbf{H_I}\mathbf{x_I} + \boldsymbol{\eta})^H) \\ &= P_D\mathbf{H_D}\mathbf{x_D}\mathbf{x_D}^H\mathbf{H_D}^H + P_I\mathbf{H_I}\mathbf{x_I}\mathbf{x_I}^H\mathbf{H_I}^H + \sigma_n^2\mathbf{I} \\ &= P_D\mathbf{H_D}\mathbf{H_D}^H + P_I\mathbf{H_I}\mathbf{H_I}^H + \sigma_n^2\mathbf{I} \end{aligned} \tag{4.21}$$

which is the matrix to be inverted in equation (4.20)

Given that the channel of the desired user can be estimated, the interference can be suppressed from the covariance matrix of the received signal combining equation (4.20) and (4.21). Unlike the IC technique, the degrees of spatial freedom at the receiver need not to be equal the total number of spatial transmission of the desired user and interferer. In this case, the number of antennas at the receiver must be at least equal to the number of the antennas at the transmitter.

4.4.4 Simulation of Interference Suppression

A set of four figures showing the results of IS technique is shown in Figure 4.6. One interferer is assumed for all simulation results. A similar set up to Figure 4.5(a) for this interference mitigation technique for ZF V-BLAST has been used. The ZF results in Figure 4.6(a) show that the BER performance is independent of the INR values, i.e., all curves overlap. This is because the IS technique can successfully suppress the interference (assuming perfect channel knowledge) leaving only the user's data to be detected. However, the performance of this detector is significantly poorer than the cancellation technique (Figure 4.5(a)), especially at high INRs. This is because the suppression technique does not detect and remove the interference from the received signal, instead it is only nulled and treated as coloured noise resulting in a lower SINR as seen by the desired user's signal as compared to the cancellation technique.

The results displayed in Figure 4.6(b) show the same set up as Figure 4.6(a) but with a MMSE detector. The curves do not overlap one another like the ZF case (Figure 4.6(a)) because MMSE detector takes into account both the interference and noise in the beamformer. Unlike the cancellation technique, the BER performance degrades for higher values of the INR. However, even at an INR = 40 dB, the MMSE performance is about 3 dB better than ZF (Figure 4.6(a)). Also with MMSE detector for V-BLAST, the results shown in Figure 4.6(c) is a 4 transmit and 4 receive antennas system so that the total number of transmitters is greater than the number of receivers. The results show that for low INR values, the BER performance is still tolerable but

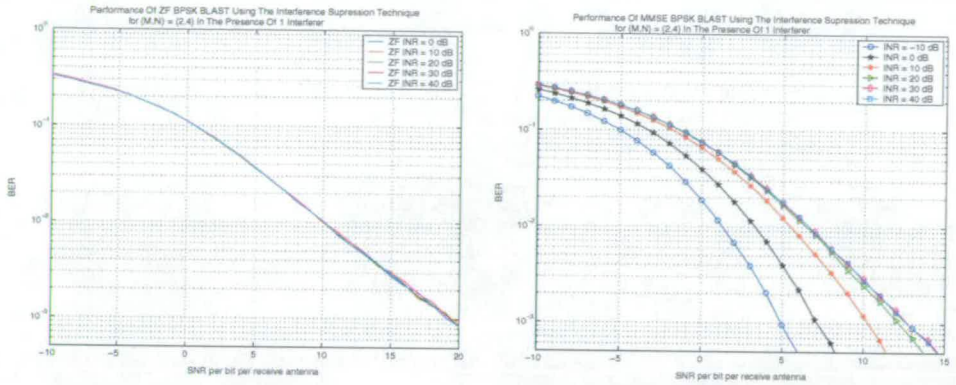

(a) BER vs SNR for ZF V-BLAST interference suppression for (M, N) = (2,4)

(b) BER vs SNR for MMSE V-BLAST interference suppression for (M, N)=(2,4)

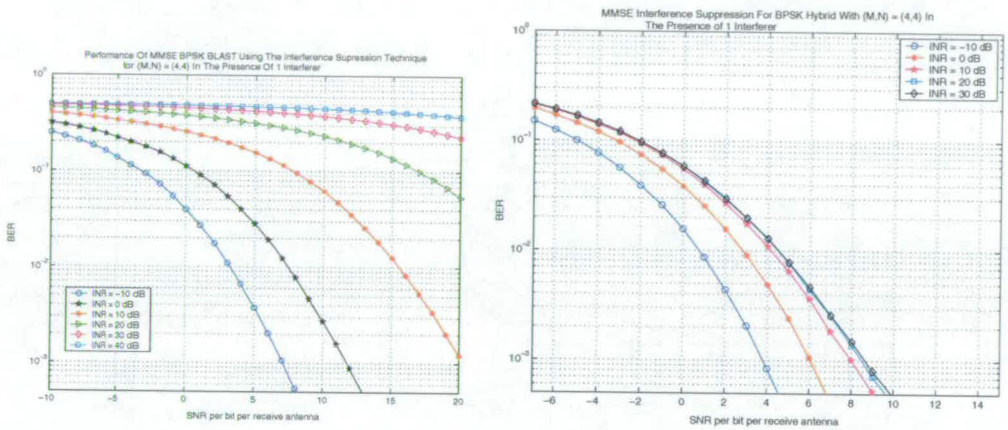

(c) BER vs SNR for MMSE V-BLAST interference suppression for (M, N)=(4,4)

(d) BER vs SNR for MMSE Dual Alamouti STBC interference suppression (M, N) = (4,4)

Figure 4.6: *BER vs SNR interference suppression techniques for the for various INR*

degrades significantly at high INRs.

Lastly Figure 4.6(d) shows the BER performance of the Dual Alamouti STBC scheme with BPSK. Similarly, this set of results have a pattern of poorer BER performance for higher INR values.

4.4.5 Robustness of Dual Alamouti STBC and V-BLAST To Interference

This section briefly compares the performance of V-BLAST and the Dual Alamouti STBC scheme for a spectral efficiency of 2 b/s/Hz using 4 antennas at the receiver. One cochannel interferer is assumed to be present. Table 4.1 shows the SNR values with its respective INR

values achieving a spectral efficiency of 2 b/s/Hz for both MMSE V-BLAST and the Dual Alamouti STBC scheme at BER value of 10^{-2}. This comparison shows that the Dual Alamouti STBC scheme significantly outperforms V-BLAST in the presence of interference using the interference cancellation mitigation technique.

Interferer's INR/dB	BPSK Dual Alamouti STBC(4,4)/dB	BPSK BLAST(2,4)/dB
0	0.3	2.3
$10 \rightarrow 30$	-0.45	0.8

Table 4.1: *Comparison of required SNR for interference cancellation for spectral efficiency of 2 b/s/Hz at BER* 10^{-2}

Similarly the values compared in Table 4.2 illustrates that using interference suppression mitigation technique at spectral efficiency of 2 b/s/Hz, the Dual Alamouti STBC scheme required SNR for a particular INR value is lower as compared to MMSE V-BLAST. This is because the diversity achieved in the Dual Alamouti STBC scheme is twice approximately that of the V-BLAST and the doubling in the effective receiver dimension gives more degrees of freedom to mitigate interference.

Interferer's INR/dB	BPSK Dual Alamouti STBC(4,4)/dB	BPSK BLAST(2,4)/dB
-10	0.75	1.30
0	2.78	3.30
10	4.20	5.50
20	4.50	6.50
30	4.50	7.10

Table 4.2: *Comparison of required SNR for interference suppression for spectral efficiency of 2 b/s/Hz at BER* 10^{-2}

4.4.6 Comparison Of Synchronous and Asynchronous Interference

As mentioned in Section 4.4.3, the MMSE IS technique can be operated by estimating the covariance matrix of the received signal and then inverting it to obtain the MMSE beamformer, can be applied for both synchronous and asynchronous interference. In order to understand the performance using this mitigation technique for both the synchronous and asynchronous scenarios, a 1/2 rate convolutionally coded OFDM with 2 transmit 4 receive antennas using a QPSK V-BLAST system is implemented. For simplicity, the power delay profile of the channel assumes a Rayleigh frequency selective fading environment with equal power taps.

The simulation results for both scenarios in a F_c(U,2) and F_c(U,4) environment for an INR value of 5 dB are shown in Figure 4.7. Despite the more unpredictable nature of asynchronous interference, the performance for both the 2 and 4 taps cases matches with that of the synchronous interference. Referring to the PSD of asynchronous interference in Figure 4.4, the nature of this interference only induces more frequency selectivity to the channel response but the maximum power remains the same as in the synchronous scenario. This suggests that the IS beamformer must suppress interference of a magnitude which is equal for both the synchronous and asynchronous scenarios for the same INR value.

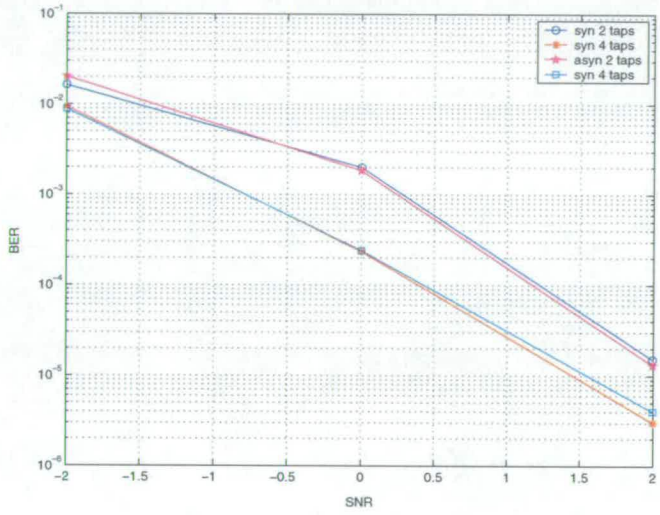

Figure 4.7: *Performance of IS technique for both synchronous and asynchronous interference*

4.5 Conclusion

Two common interference models that can appear at the received signal of the desired user, namely synchronous and asynchronous have been modelled. The characteristic of these models has been described and the BEP for the synchronous scenario, has been derived and benchmarked with simulation results. However, in a typical WLAN environment supporting multiuser transmission, synchronous interference can be expected from users transmitting from a cell as they can be controlled by the same access point. The asynchronous interference model can also exists but mitigating this interference is relatively more difficult.

In order to mitigate synchronous interference efficiently, two techniques, IC and IS have been introduced. The performance of these two techniques applied to the V-BLAST and Dual Alam-

outi STBC techniques have been studied and compared. Even though the IC technique performs better than IS, the restriction of IC technique, in terms of the degrees of spatial freedom along with the requirements for synchronous transmission and channel state information (CSI) of the interferer are the drawbacks of this technique. Comparing the performance of synchronous and asynchronous interference using the IS technique where the CSI of the interferer is estimated from the covariance matrix of the received signal, similar results are observed for both cases as the maximum SINR is the same for both scenarios.

Given that the number of receive antennas employed are equal for both the V-BLAST and Dual Alamouti STBC transmit scheme employing the OSIC algorithm, Dual Alamouti STBC is relatively more robust to interference due to the inherent extra diversity at the transmitter and extra degrees of freedom at the receiver.

The next chapter shall study alternative space-time coding technique that can be applied to an OFDM system, feasible for small packets transmission with resource saving.

Chapter 5

OFDM Diversity Transmit Structures

5.1 Introduction

The Alamouti STBC scheme introduced in Section 2.11 achieves diversity gain even though the number of antennas at the transmitter is less than that at the receiver. The simulation results comparing both V-BLAST and Dual Alamouti STBC in Figure 3.12 (Section 3.6.3), show that for 2 bits/s/Hz spectral efficiency, Alamouti STBC outperforms the other two MIMO schemes given that two antennas are used at the receiver, which is the minimum number of antennas required for a 2 Tx V-BLAST and Dual Alamouti STBC.

However, in spite of its high performance gain for this case, Alamouti STBC has two major drawbacks. The first being the need to allocate two OFDM symbols for spatial-temporal encoding which can be a waste of resources for transmission of small packets. Secondly, detection could only take place after a delay of one OFDM transmission period which results in latency. Due to this several papers [50–53] translate this encoding technique from the temporal to the frequency domain giving the so called the Alamouti space-frequency block code (SFBC). However, most papers [50–52] assume that the adjacent subcarriers are correlated to each other in an OFDM system and detect using the maximal ratio combining (MRC) technique in Section 2.11.2. Otherwise, the zero forcing (ZF) [53] estimate can be employed to combat the uncertainty in channel conditions. An alternative to overcome these problems was recently introduced in [54–56], called the cyclic delay diversity (CDD) transmit scheme, which exploits frequency diversity in a coded OFDM system.

In this chapter, both the CDD and Alamouti SFBC will be introduced. A simplified ZF decoding technique will be proposed for the Alamouti SFBC transmit structure. The performance degradation with respect to Alamouti STBC will be analysed while its comparison with CDD will be studied.

5.2 Cyclic Delay Diversity

Figure 5.1 shows a two transmit CDD scheme. In this figure, we assume that the FFT is of size 64. Note that this scheme can be extended to any number of transmitters, but for simplicity the analysis considers only two transmit antennas.

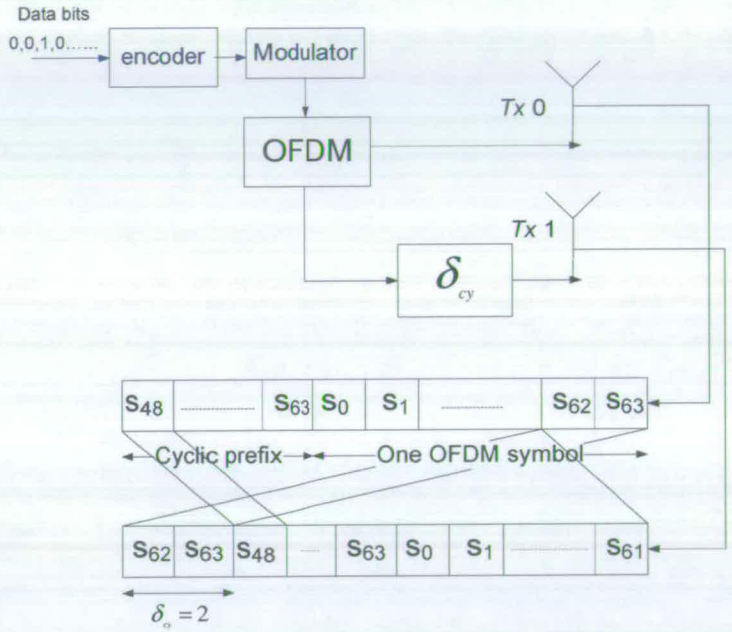

Figure 5.1: *Transmit Structure of CDD*

Transmit antenna 0 consists of a conventional OFDM system while transmit antenna 1 is a cyclic delay shifted version of transmit antenna 1 by a factor of δ_{cy} (in this Figure $\delta_{cy} = 2$), where δ_{cy} is defined as the cyclic delay shift. The cyclic delay version of antenna 1 is obtained by removing the last δ_{cy} samples of the OFDM symbol and placing them instead at the beginning of the OFDM symbol. By doing so, the frequency domain symbol at each subcarrier, k_c, is phase shifted by a factor of θ_{cy}, where

$$\theta_{cy} = \frac{2\pi k_c S_{cy}}{K_c} \tag{5.1}$$

where k_c is the subcarrier index and K_c is the FFT size.

The phase shifted signal induces an artificial channel with higher frequency selectivity so that more frequency diversity can be exploited from the OFDM system coupled with its outer channel code.

Assuming that two antennas are used, the received signal at subcarrier k_c can be expressed as:

$$\begin{bmatrix} r_0 \\ r_1 \end{bmatrix} = \begin{bmatrix} h_{0,0} & h_{0,1} \\ h_{1,0} & h_{1,1} \end{bmatrix} \begin{bmatrix} x \\ x\exp(-j\theta_{cy}) \end{bmatrix} + \begin{bmatrix} \eta_0 \\ \eta_1 \end{bmatrix} \tag{5.2}$$

$$= \begin{bmatrix} h_{0,0} + h_{0,1}\exp(-j\theta_{cy}) \\ h_{1,0} + h_{1,1}\exp(-j\theta_{cy}) \end{bmatrix} \begin{bmatrix} x \end{bmatrix} + \begin{bmatrix} \eta_0 \\ \eta_1 \end{bmatrix} \tag{5.3}$$

$$= \mathbf{H_C}x + \boldsymbol{\eta} \tag{5.4}$$

where r_n and η_n are the received signal and noise at the nth antenna, x is the transmitted signal and $h_{n,m}$ is the channel response at the nth receive antenna from transmit antenna m. For simplicity the subcarrier index k_c has been dropped from the equations.

The received signal at the two antennas can be further enhanced by MRC to obtain the estimated symbol as:

$$\hat{x} = \mathbf{H_C}^H\mathbf{H_C}x + \mathbf{H_C}^H\boldsymbol{\eta} \tag{5.5}$$

$$= (c_1 + c_2)x + \sqrt{c_1}\eta_0 + \sqrt{c_2}\eta_1 \tag{5.6}$$

where

$$c_1 = |h_{0,0} + h_{0,1}\exp(-j\theta_{cy})|^2$$
$$c_2 = |h_{1,0} + h_{1,1}\exp(-j\theta_{cy})|^2$$

In an uncoded system, a (M,N) CDD system performs the same as a SISO OFDM system due to the absence of any channel coder to exploit frequency diversity in the OFDM system. Also, in an uncoded OFDM system, the channel at each subcarrier is flat fading, therefore no frequency diversity is exploitable.

5.2.1 Backward Compatibility of CDD with SISO system

In addition to the advantages of good resource management and latency reduction as compared to Alamouti STBC, CDD benefits from supporting backward compatibility with the current WLAN single input single output (SISO) system, i.e., IEEE 802.11a. Consider a 2 Tx CDD source received by an IEEE 802.11a single antenna, the received signal as seen by the receiver

can be expressed as:

$$r = h_{0,0} + h_{0,1} \exp(-j\theta_{cy})x + \eta \tag{5.7}$$

Although, the transmitted signals come from two different antennas, the receiver adds the two channel response as shown in equation (5.7), viewing it as a signal from a single source. Hence, the transmitted CDD signal can be detected by the legacy terminal (IEEE 802.11a).

However, this backward compatibility can suffer setback unless minor amendment is made to the receiver. The problem lies with any OFDM receiver employing a time domain channel estimator [85], which will be briefly described. A simple time domain channel estimator would firstly zero pad all subcarriers that have not been trained in the preamble or pilot sequence, remove the effect of the trained symbols and feed into a size K_c IFFT hardware. The IFFT outputs are then truncated to a fixed number of channel taps to obtain the estimated time domain channel impulse response. Then, this truncated channel response is fed into a size K_c FFT hardware where the outputs represent the estimated channel response at every subcarrier.

In a conventional OFDM system, the truncation step to obtain the time domain channel taps would normally be fixed to a known number based on the real channel response. However, this number would normally be much higher in a CDD system due to the extra multipath generated from the cyclic delay shift. Thus, the conventional truncation process can result in a falsely estimated channel response which is likely to cause a very poor system performance. In order to ensure backward compatibility between SISO OFDM and CDD, the channel estimation algorithm must increase the number of multipath channel taps required during the truncation process.

Also, the δ_{cy} value is preferably not set to be too large because this might induce too much frequency selectively, which results in the channel memory being longer than the cyclic prefix. However, this is not too much of a problem in most system with reasonable cyclic prefix length, because the power of the larger delayed channel taps tend to be small and redundant. The slight performance degradation from this problem is compensated by the frequency diversity gain from the CDD system.

5.3 Alamouti Space Frequency Block Code

The Alamouti SFBC technique is encoded over two transmit antennas such that the k_{2n} subcarriers consists of the original transmitted symbols, while the conjugated symbols are allocated to the k_{2n+1} subcarriers, n =0, 1, ...$K_c - 1$. Figure 5.2 shows the arrangement of symbols with respect to their subcarriers over the two transmit antennas.

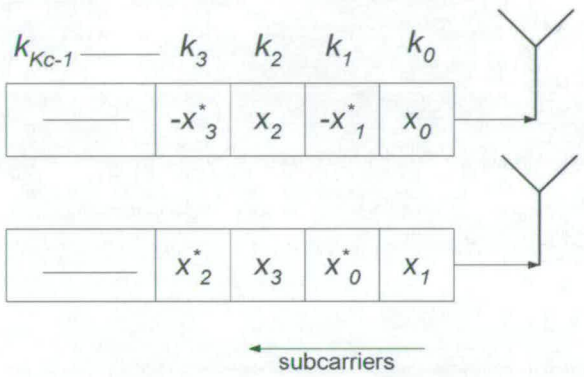

Figure 5.2: *Architecture of Alamouti SFBC*

5.3.1 Decoding

The received signal in equation (3.14) can be expressed for this case as:

$$\begin{bmatrix} \dot{\mathbf{r}}_0 \\ \dot{\mathbf{r}}_1 \\ \vdots \\ \dot{\mathbf{r}}_{N-1} \end{bmatrix} = \begin{bmatrix} \dot{\mathbf{H}}_{0,0} \\ \dot{\mathbf{H}}_{1,0} \\ \vdots \\ \dot{\mathbf{H}}_{N-1,0} \end{bmatrix} \dot{\mathbf{x}} + \begin{bmatrix} \dot{\boldsymbol{\eta}}_0 \\ \dot{\boldsymbol{\eta}}_1 \\ \vdots \\ \dot{\boldsymbol{\eta}}_{N-1} \end{bmatrix} \tag{5.8}$$

$$= \mathbf{H_F}\dot{\mathbf{x}} + \dot{\boldsymbol{\eta}} \tag{5.9}$$

where

$$\dot{\mathbf{r}}_n = \begin{bmatrix} r_n(k_{2c}) \\ r^*_n(k_{2c+1}) \end{bmatrix} \qquad \dot{\boldsymbol{\eta}}_n = \begin{bmatrix} \eta_n(k_{2c}) \\ \eta^*_n(k_{2c+1}) \end{bmatrix} \qquad \dot{\mathbf{x}} = \begin{bmatrix} x_{2m}(2k_c) \\ x_{2m+1}(2k_c) \end{bmatrix}$$

$$\dot{\mathbf{H}}_{n,m} = \begin{bmatrix} h_{n,2m}(k_{2c}) & h_{n,2m+1}(k_{2c}) \\ h^*_{n,2m+1}(k_{2c+1}) & -h^*_{n,2m}(k_{2c+1}) \end{bmatrix}$$

where $r_n(k_c)$ and $\eta_n(k_c)$ are the received signal and noise of the k_c subcarrier at receive antenna n, $x_m(k_c)$ is the transmitted symbol at transmit antenna m mapped onto subcarrier k_c and $h_{n,m}(k_c)$ is the channel response from subcarrier k_c at receive antenna n due to transmit antenna m.

It was assumed that the channel between adjacent subcarriers are highly correlated with each other. Hence, the symbols can be detected using the Alamouti decoding technique as:

$$\hat{\dot{\mathbf{x}}} = \mathbf{H_F}^H \mathbf{H_F} \dot{\mathbf{x}} + \mathbf{H_F}^H \dot{\boldsymbol{\eta}} \tag{5.10}$$

where $\hat{\dot{\mathbf{x}}}$ is the estimated symbol vector expressed as:

$$\hat{\dot{\mathbf{x}}} = \begin{bmatrix} \hat{x}_{2m}(2k_c) \\ \hat{x}_{2m+1}(2k_c) \end{bmatrix} \tag{5.11}$$

and the assumption that adjacent subcarriers are correlated such that:

$$\begin{aligned} h_{n,2m}(k_{2c}) &= h_{n,2m}(k_{2c+1}) \\ h_{n,2m+1}(k_{2c}) &= h_{n,2m+1}(k_{2c+1}) \end{aligned}$$

However, this method of detection, assuming that adjacent subcarriers' channels are highly correlated, is only applicable for channel characterised by low frequency selectivity. In the case where channels are highly frequency selective this assumption is invalid. Therefore, [53] suggested the use of the ZF estimate to combat the uncorrelated adjacent subcarriers' channels where detected symbols can be expressed as:

$$\hat{\dot{\mathbf{x}}} = \mathbf{G_F} \mathbf{H_F} \dot{\mathbf{x}} + \mathbf{G_F} \dot{\boldsymbol{\eta}} \tag{5.12}$$

and the weighting matrix $\mathbf{G_F}$ can be computed as:

$$\mathbf{G_F} = (\mathbf{H_F}^H \mathbf{H_F})^{-1} \mathbf{H_F}^H \tag{5.13}$$

Although the technique in equation (5.13) permits four different channels coefficients at the two subcarriers, $h_{n,2m}(k_{2c})$, $h_{n,2m+1}(k_{2c})$, $h^*_{n,2m}(k_{2c+1})$, $h^*_{n,2m+1}(k_{2c+1})$, per decoding process, the ZF beamformer consists of several multiplications to form a $2 \times 2N$ size channel matrix. However, this ZF solution in equation (5.13) can be avoided by concatenating the adjoint chan-

nel matrix of the response at each receiver as:

$$\mathbf{G}_s = \left[\begin{array}{cccc} adj(\dot{\mathbf{H}}_{0,0}) & adj(\dot{\mathbf{H}}_{1,0}) & \dots & adj(\dot{\mathbf{H}}_{N-1,0}) \end{array} \right] \tag{5.14}$$

where $adj(\mathbf{A})$ is the adjoint matrix defined as:

$$\mathbf{A} = \left[\begin{array}{cc} a_{0,0} & a_{0,1} \\ a_{1,0} & a_{1,1} \end{array} \right], \qquad adj(\mathbf{A}) = \left[\begin{array}{cc} a_{1,1} & -a_{0,1} \\ -a_{1,0} & a_{0,0} \end{array} \right]$$

Multiplying $\mathbf{G}_s$ in (5.14) by the received signal in (5.9) yields the equivalent ZF solution as:

$$\hat{\dot{\mathbf{x}}} = \mathbf{G}_s(\mathbf{H_F}\dot{\mathbf{x}} + \dot{\boldsymbol{\eta}}) \tag{5.15}$$

$$= \left[\begin{array}{cccc} adj(\dot{\mathbf{H}}_{0,0}) & adj(\dot{\mathbf{H}}_{1,0}) & \dots & adj(\dot{\mathbf{H}}_{N-1,0}) \end{array} \right] \tag{5.16}$$

$$\left(\left[\begin{array}{c} \dot{\mathbf{H}}_{0,0} \\ \dot{\mathbf{H}}_{1,0} \\ \vdots \\ \dot{\mathbf{H}}_{N-1,0} \end{array} \right] \dot{\mathbf{x}} + \left[\begin{array}{c} \dot{\boldsymbol{\eta}}_0 \\ \dot{\boldsymbol{\eta}}_1 \\ \vdots \\ \dot{\boldsymbol{\eta}}_{N-1} \end{array} \right] \right) \tag{5.17}$$

$$= \left[\begin{array}{cc} -\alpha_{s1} & 0 \\ 0 & -\alpha_{s2} \end{array} \right] \left[\begin{array}{c} x_m(2k_c) \\ x_m(2k_c+1) \end{array} \right] + \mathbf{G}_s\dot{\boldsymbol{\eta}} \tag{5.18}$$

where

$$\alpha_{s1} = \sum_{n=0}^{N-1} \sum_{m=1}^{1} h^*_{n,2m}(k_{2c+1}) h_{n,2m}(k_{2c}) \tag{5.19}$$

$$\alpha_{s2} = \sum_{n=0}^{N-1} \sum_{m=1}^{1} h_{n,2m+1}(k_{2c}) h^*_{n,2m+1}(k_{2c+1}) \tag{5.20}$$

Hence, as illustrated in equation (5.18), the equivalent ZF solution can be obtained without performing the full pseudoinverse as shown in equation (5.13). In this case the complexity can be reduced by the number of multiplications required to generate the ZF solution in equation (5.13). A similar technique to this simplified ZF solution was proposed for Alamouti STBC in [86] for fast fading channel, where the channels over two OFDM symbols are different.

5.3.2 SNR Analysis Under Differently Correlated Subcarriers

In order to verify the system performance for different correlation coefficients between subcarriers, the SNR parameter which has direct impact on the performance will be analysed. Consider a (2,1) Alamouti STBC system, the SNR for each of the two transmitted orthogonal symbols can be expressed as follows:

$$\text{SNR} = \frac{|h_{0,0}|^2 + |h_{0,1}|^2}{\sigma_n^2} \tag{5.21}$$

Given the same system, but for the frequency encoded version, the combined received signal can be expressed as:

$$\begin{aligned}
\begin{bmatrix} r(2k) \\ r^*(2k+1) \end{bmatrix} &= \begin{bmatrix} -\nu_3^* & -\nu_1 \\ -\nu_2^* & \nu_0 \end{bmatrix} \left(\begin{bmatrix} \nu_0 & \nu_1 \\ \nu_2^* & -\nu_3^* \end{bmatrix} \begin{bmatrix} x_0(2k) \\ x_1(2k) \end{bmatrix} + \begin{bmatrix} \eta_0(2k) \\ \eta_0^*(2k+1) \end{bmatrix} \right) \\
&= \begin{bmatrix} -\nu_3^*\nu_0 - \nu_1\nu_2^* & 0 \\ 0 & -\nu_2^*\nu_1 - \nu_3\nu_0^* \end{bmatrix} \begin{bmatrix} x_0(2k) \\ x_1(2k) \end{bmatrix} + \\
&\quad \begin{bmatrix} -\nu_3^*\eta_0(2k) - \nu_1\eta_0(2k+1) \\ -\nu_2^*\eta_0(2k) + \nu_0\eta_0(2k+1) \end{bmatrix}
\end{aligned} \tag{5.22}$$

where

$$\begin{bmatrix} \nu_0 & \nu_1 \\ \nu_2 & \nu_3 \end{bmatrix} = \begin{bmatrix} h_{0,0}(2k) & h_{0,1}(2k) \\ h_{0,1}(2k+1) & h_{0,0}(2k+1) \end{bmatrix}$$

The SNR of $x_0(2k)$ in (5.22) can be expressed as:

$$\begin{aligned}
\text{SNR} &= \frac{|-\nu_3^*\nu_0 - \nu_1\nu_2^*|^2}{\sigma_n^2(|\nu_1|^2 + |\nu_3|^2|)} \\
&= \frac{(-\nu_3^*\nu_0 - \nu_1\nu_2^*)(-\nu_3\nu_0^* - \nu_1^*\nu_2)}{\sigma_n^2(|\nu_1|^2 + |\nu_3|^2|)} \\
&= \frac{|\nu_3|^2|\nu_0|^2 + \nu_3^*\nu_0\nu_1^*\nu_2 + \nu_1\nu_2^*\nu_3\nu_0^* + |\nu_1|^2|\nu_2|^2}{\sigma_n^2(|\nu_1|^2 + |\nu_3|^2|)}
\end{aligned} \tag{5.23}$$

Similarly, the SNR of $x_1(2k)$ is equal to:

$$\text{SNR} = \frac{|\nu_3|^2|\nu_0|^2 + \nu_2^*\nu_1\nu_3^*\nu_0 + \nu_3\nu_0^*\nu_2\nu_0^* + |\nu_1|^2|\nu_2|^2}{\sigma_n^2(|\nu_0|^2 + |\nu_2|^2|)} \tag{5.24}$$

If the channel is non frequency selective, i.e., the adjacent channel coefficients are equal to one

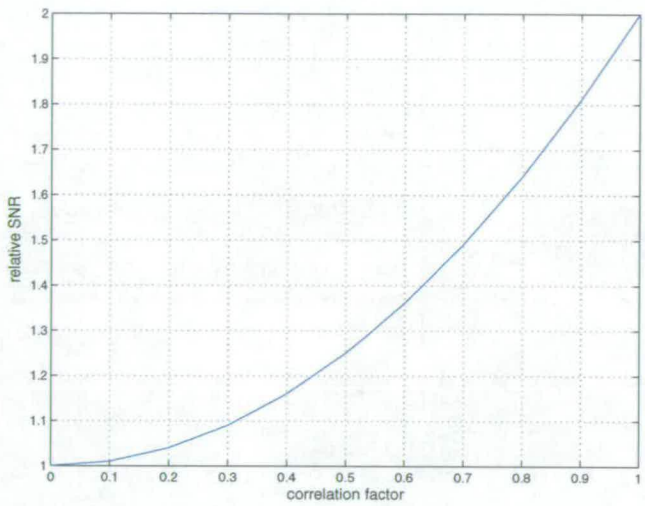

Figure 5.3: *Achievable relative SNR for different correlated adjacent subcarriers*

another, the SNR in (5.23) is equal to that of the temporal encoded version given by:

$$\text{SNR} = \frac{|\nu_0|^2 + |\nu_1|^2}{\sigma_n^2} \tag{5.25}$$

To analyse the SNR performance, the adjacent subcarriers' coefficients from both transmit antenna are varied simultaneously to produce different correlation factors, κ. Assuming that

$$E(|\nu_0|^2) = E(|\nu_1|^2) = E(|\nu_2|^2) = E(|\nu_3|^2) = 1 \tag{5.26}$$

and that

$$E(|\nu_0\nu_3^*|^2) = E(|\nu_3\nu_0^*|^2) = \kappa_0 \tag{5.27}$$

$$E(|\nu_1\nu_2^*|^2) = E(|\nu_2\nu_1^*|^2) = \kappa_1 \tag{5.28}$$

where κ_0 and κ_1 are the correlation coefficients between the adjacent subcarriers at transmit antenna $m = 0$ and $m = 1$ respectively.

Therefore, the relative normalised SNR obtained as a function of its adjacent subcarriers' correlation by substituting equation (5.26)-(5.28), into (5.23) or (5.24) giving:

$$\text{SNR} = \frac{1 + \kappa_0\kappa_1}{\sigma_n^2} \tag{5.29}$$

The normalised achievable SNR with respect to its correlation factor, assuming $\kappa_0 = \kappa_1$ and $\sigma_n^2 = 1$ is shown in Figure 5.3. From this graph it can be seen that the SNR increases as the adjacent subcarriers become more correlated with each other. When $\kappa_0 = \kappa_1 = 1$, i.e., adjacent subcarriers are fully correlated, the performance of Alamouti SFBC equals to that of STBC. On the other hand, if $\kappa_0 = \kappa_1 = 0$, i.e., adjacent subcarriers are uncorrelated, Alamouti SFBC is 3 dB worse in achievable SNR than STBC.

5.3.3 Simulations

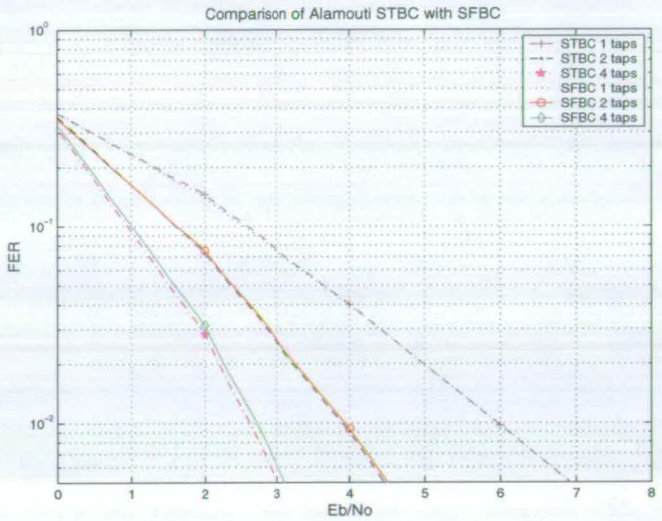

Figure 5.4: *Comparison of (2,2) Alamouti STBC and (2,2) Alamouti SFBC using QPSK symbols for 1 to 4 taps*

The results for comparing (2,2) QPSK Alamouti STBC and (2,2) QPSK Alamouti SFBC is shown in Figure 5.4 for channels F_c(U,1), F_c(U,2) and F_c(U,4) while F_c(U,8) and F_c(U,16) in Figure 5.5. Here, we consider 1-16 sample spaced multipath equal power taps. The cyclic delay shift, δ_{cy} is set to 8, so that maximum frequency diversity [56] can be achieved. When the channel is flat fading, the performance of the temporal and frequency coded system is the same as to each other. This is because the adjacent channel subcarriers are fully correlated with one another and both schemes achieve the same SNR as shown in Figure 5.3. However, the performance advantage of STBC over SFBC increases for subsequent increments in the number of channel taps. Even though the Alamouti SFBC 16 taps system can exploit more frequency diversity inherent in the OFDM symbol coupled with the channel decoder, the performance for this scenario is worse than the 8 taps STBC system due to the highly uncorrelated adjacent

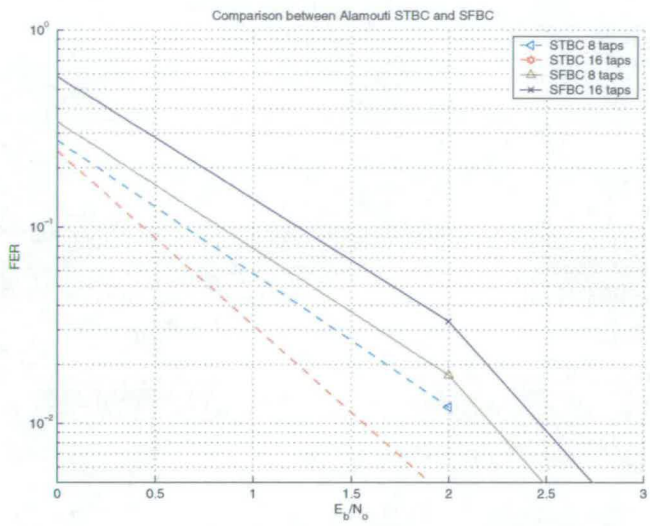

Figure 5.5: *Comparison of (2,2) Alamouti STBC and (2,2) Alamouti SFBC using QPSK symbols 8 and 16 taps*

subcarriers, which destroys the orthogonality of the Alamouti code.

The next set of results comparing (2,2) QPSK Alamouti SFBC and (2,2) QPSK CDD are shown Figure 5.6 for F_c(U,1), F_c(U,2) and F_c(U,4) while F_c(U,8) and F_c(U,16) are shown in Figure 5.7. Despite the adjacent subcarriers in the Alamouti SFBC scheme being less correlated for the increase from one to four multipath taps, the relative performance with respect to CDD improves with this increase. This is mainly due to the CDD scheme being less able to exploit frequency diversity gain as the number of channel taps increases. On the other hand, increasing to 8 multipath taps see that the performance difference between these two schemes start to reduce. In the case of 16 taps scenario, the CDD method actually outperforms the Alamouti SFBC scheme. For higher number of multipath taps, the Alamouti SFBC starts to degrade in performance while CDD reaches its peak performance.

5.4 Conclusion

This chapter considers the Alamouti SFBC and CDD transmit schemes as means to reduce the overhead in the STBC scheme for transmission of small packets, reducing latency. A simplified ZF solution for the Alamouti SFBC has been proposed. The SNR analysis shows that the performance of this scheme is dependent on the correlation between the channels. The simulation results also show that for a non frequency selective channel the error performance is compa-

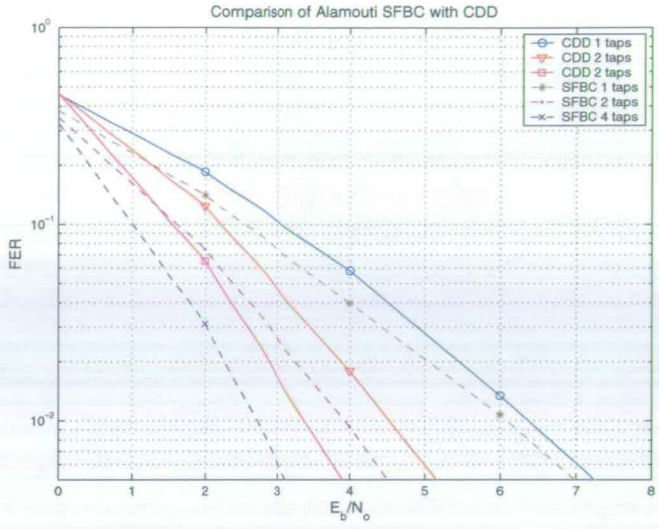

Figure 5.6: *Comparison of (2,2) CDD and (2,2) Alamouti SFBC using QPSK symbols for 1 to 4 taps*

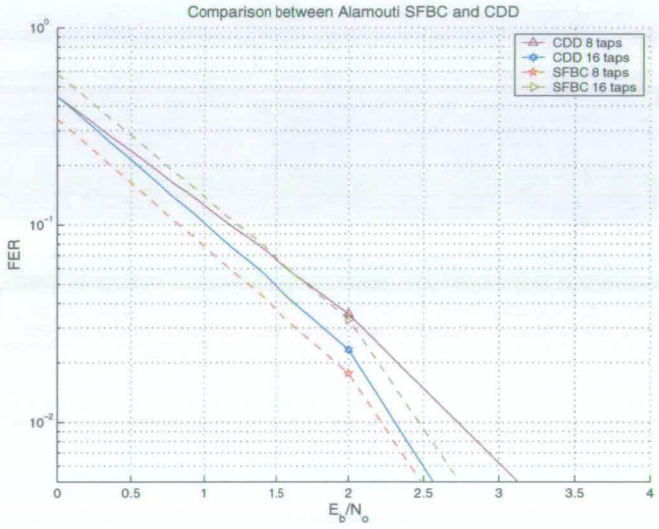

Figure 5.7: *Comparison of (2,2) CDD and (2,2) Alamouti SFBC using QPSK symbols for 8 and 16 taps*

rable to its temporal encoded scheme. However, the SFBC scheme degrades significantly as the number of multipath increases. Despite the partially correlated adjacent subcarriers, this scheme is still able to outperform CDD unless the channel is extremely frequency selective.

Despite the better performance of Alamouti SFBC over CDD, CDD has a significant advantage over Alamouti SFBC in terms of backward compatibility with the legacy terminals, namely

IEEE 802.11a. Hence, in the next chapter we consider CDD not SFBC to provide a benchmark for three transmit antennas schemes.

Chapter 6
Three Transmit Hybrid of Spatial Multiplexing And Transmit Diversity Scheme

6.1 Introduction

In the MIMO study of Chapter 3, it was assumed that an arbitrary number of antennas can be employed at either end of the transmitting or receiving terminal. In practice, low cost MIMO devices implementing more than three antennas can barely be supported at high performance by current microwave and silicon technologies. Due to this restriction, it is currently thought (summer 2004) that all devices supported by IEEE 802.11n will be mandated such that the maximum number of antennas at both the transmitter and receiver are limited to three while higher number of antennas can only be regarded as an optional mode.

In order to meet one of the requirements for the medium access control (MAC) layer which is to support 100 Mbps accounting for the mandated maximum number of antennas, the only known low complexity MIMO scheme supporting this throughput is the V-BLAST technique. Based on results from Chapter 3, it has been shown that V-BLAST with OSIC decoding algorithm does not provide a good solution for high end performance due to the absence of transmit diversity being exploited, especially when the number of Rx is equal to Tx. Despite the fact that Dual Alamouti hybrid structure increases the diversity that is lacking in a V-BLAST scheme, the minimum required number of four Tx does not provide a solution for economically attractive configurations. Therefore, this Dual Alamouti scheme can only be implemented as an optional mode. On the other hand, conventional Alamouti STBC is only feasible for lower rate wireless terminals.

In this chapter, two hybrid transmit schemes implementing three antennas are introduced, one involves concatenating one CDD block with a conventional modulated OFDM stream while the other combines Alamouti STBC with a single QAM stream. Both of these techniques enable the spatial multiplexing scheme to exploit diversity that is absent at the transmitter of a V-BLAST

at low complexity. The hybrid of CDD is chosen over Alamouti SFBC in this chapter due to the CDD backward compatibility with a $2\,Tx$ V-BLAST scheme that will be discussed in detail in Section 6.3.4. Furthermore, it is shown in Section 5.3.3 that the STBC performs similarly to a SFBC scheme in a channel environment of up to 8 multipath equal taps environment, which is the typical scenario of an indoor office environment. Hence, the performance of a STBC hybrid reflects the likely performance of a SFBC. The Alamouti STBC hybrid technique will be discussed in greater details due to its significant performance gain over the CDD hybrid which will be shown in Section 6.4.5, and shall form the basis the transmit structure in future WLAN, IEEE 802.11n, as proposed in this thesis. Several simplified detection algorithms, will be discussed and compared using simulation results. Later on, the design of an adaptive modulation coded scheme (MCS) for future WLAN will be described. MCS is a technique for switching between scheme with respect to several parameters like transmit scheme, detection algorithm, modulation, coding, etc. This switching technique plays a significant role in the system and simulation using the IEEE 802.11n standard MIMO channel model will be presented.

6.2 System Model

The communication system used for generating simulation results follows the transmit and receiver structure in Figure 3.1 and 3.2 respectively. The simulation results generated for this chapter use a frame length of 736 bits, which can be regarded as the minimum physical data size with some allowance for MAC header in a typical WLAN transmission. Similar to previous chapters, the channel is assumed to be static throughout each frame. Contrary to previous chapters where error performance is compared with respect to the E_b/N_o parameter, this chapter compares all performance relative to the power per receive antenna, SNR. The reason for this choosing this parameter is due to the MCS scheme, where this reflects a more realistic WLAN scenario.

6.3 Hybrid of Three Transmit CDD Spatial Multiplexing Scheme (CDDSM)

As previously discussed in Section 5.2, a CDD transmit scheme induces an artificial channel response of higher frequency selectivity between the transmitter and receiver as compared to the

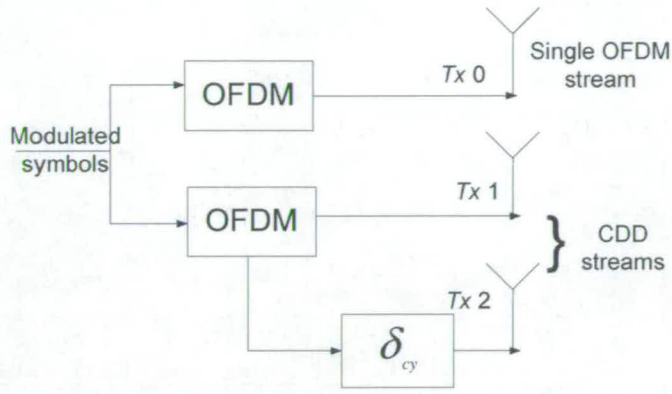

Figure 6.1: *Transmit Structure of CDDSM*

real one. By doing so, this enables the outer channel code coupled with the interleaver to exploit more frequency diversity as a mean to improve the overall system performance. In this section, the CDD hybrid technique, where two antennas formed the basis of a CDD structure spatially multiplexed with a conventional OFDM stream for a third Tx shall be studied. Simulated results comparing its performance with V-BLAST will be shown.

6.3.1 Transmit Structure

The transmit structure of a CDDSM scheme employing three antennas is illustrated in Figure 6.1. Two independent streams of OFDM symbols are transmitted from Tx 0 and Tx 1. A cyclic delay shifted version (δ_{cy}), where δ_{cy} is defined as in Section 5.2, of Tx 1 is then send to Tx 2. This cyclic delay shifted version aims to exploit additional frequency diversity gain by providing more frequency selectivity to the overall channel response of the latter OFDM stream. Hence this scheme can be visualised as a V-BLAST transmit system with an add on transmit diversity normally absent from the conventional V-BLAST transmit scheme [83]. In the later section, all mathematical analysis will assume that Tx 2 is the cyclically delay-shifted OFDM version of the Tx 1 signal.

6.3.2 Receiver Signal Model

The received signal for N receive antennas in an OFDM system for each subcarrier, k_c, transmitted from the 3 Tx CDDSM scheme can be mathematically expressed as:

$$\mathbf{r} = \mathbf{H}\mathbf{x} + \boldsymbol{\eta}$$

$$\begin{bmatrix} r_0 \\ r_1 \\ \vdots \\ \vdots \\ r_{N-1} \end{bmatrix} = \begin{bmatrix} h_{0,0} & h_{0,1} & h_{0,2} \\ h_{1,0} & h_{1,1} & h_{1,2} \\ \ddots & \dots & \dots \\ \vdots & \ddots & \\ h_{N-1,0} & h_{N-1,1} & h_{N-1,2} \end{bmatrix} \begin{bmatrix} x_0 \\ x_1 \\ x_1 \exp(-j\theta_{cy}) \end{bmatrix} + \begin{bmatrix} \eta_0 \\ \eta_1 \\ \vdots \\ \vdots \\ \eta_{N-1} \end{bmatrix} \tag{6.1}$$

where θ_{cy} is the cyclic delay phase defined as in (5.1). The dependence on subcarrier k_c in these equations have not been included for simplicity.

The resultant mathematical expression in (6.1) due to the CDD version from the third antenna can be further simplified as:

$$\begin{bmatrix} r_0 \\ r_1 \\ \vdots \\ \vdots \\ r_{N-1} \end{bmatrix} = \begin{bmatrix} h_{0,0} & h_{0,1} + h_{0,2} \exp(-j\theta_{cy}) \\ h_{1,0} & h_{1,1} + h_{1,2} \exp(-j\theta_{cy}) \\ \vdots & \vdots \\ \vdots & \vdots \\ h_{N-1,0} & h_{N-1,1} + h_{N-1,2} \exp(-j\theta_{cy}) \end{bmatrix} \begin{bmatrix} x_0 \\ x_1 \end{bmatrix} + \begin{bmatrix} \eta_0 \\ \eta_1 \\ \vdots \\ \vdots \\ \eta_{N-1} \end{bmatrix} \tag{6.2}$$

The transition from equation (6.1) to (6.2) implies that spatial diversity of order two is achieved in this scheme. In order to detect the received signal in (6.2) with low complexity, the ZF or MMSE OSIC detector in Section 2.10.1 is suggested. This scheme could provide a significant improvement as compared to 3 Tx V-BLAST OSIC for the same number of Tx used due to the reduction in the number of interfering antennas from three to two. Additionally, the minimum number of receive antennas required to apply the OSIC algorithm is reduced by one to only two, providing an advantage for any space limited and low cost compact wireless terminal.

6.3.3 Simulation Results And Performance Analysis

The performance of (3,3) 64 QAM CDDSM, (2,3) 64 QAM V-BLAST and (3,3) 16 QAM V-BLAST employing the OSIC algorithm is illustrated in Figure 6.2. The scenario uses the F_c(U, A) function. For each of the scheme, code rate, R = 1/2, 2/3 and 3/4 are simulated. For the same code rate, each MIMO scheme attains the same spectral efficiency.

The results show that the (3,3) 16 QAM V-BLAST is significantly worse than the (2,3) 64 QAM V-BLAST due to the absence of diversity in the (3,3) V-BLAST configuration. Therefore, the performance as described later will only assume comparison between the (2,3) V-BLAST and (3,3) CDDSM. At low SNR, (2,3) V-BLAST performs better than (3,3) CDDSM due to the incapability of the channel decoder to exploit frequency diversity. Increases in SNR enables the CDDSM scheme to exploit more frequency diversity which sees the three pairs of curves crossing over one another. The difference in SNR values between both schemes at 1% FER is 1.0 dB, 0.85 dB and 0.45 dB for R values of 1/2, 2/3, 3/4 respectively. This is because at a lower code rate, the redundant bits (which increases for lower code rate) generated are more randomly interleaved, and then allocated to its respective subcarriers. Hence, the probability of one bit (prior to interleaving) being in deep a fade at a particular subcarrier while its adjacent bit allocated at a different subcarrier with higher link quality would be higher when lower code rate is used. Therefore, frequency diversity is more readily achieved.

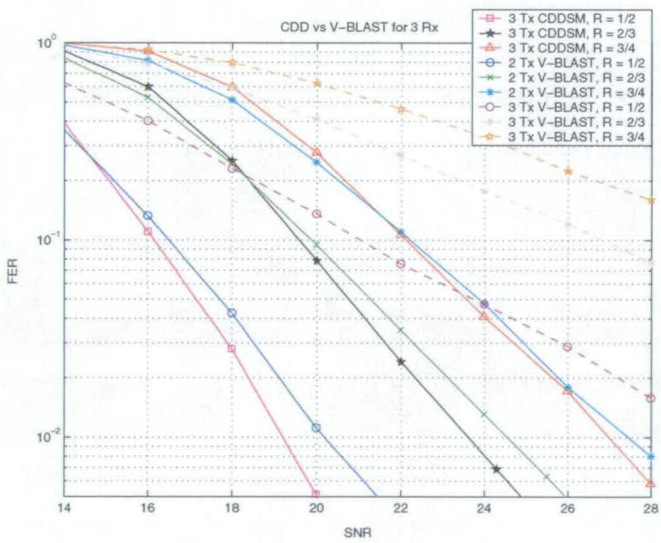

Figure 6.2: *FER vs SNR for 64 QAM (2,3) CDDSM, 16 QAM (3,3) V-BLAST and (2,3) 64 QAM V-BLAST for F_c(U,A) channel*

The performance for both the (2,3) V-BLAST and (3,3) CDDSM schemes with R=1/2 using a 16 QAM constellation in a correlated fading environment is shown in Figure 6.3. In this simulation the antenna spacing at the transmitter is set far apart to minimise its cross-correlation between transmitter due to the V-BLAST have one antenna less than the CDDSM.

This correlated simulation is set up such that half wavelength unit spacing between receive antennas each with 60^o AS. The transmit correlation is not compared and are therefore set to a minimum due to the V-BLAST having one less antenna than the CDDSM scheme. In this case, the spacing between transmitters is spaced by 50λ and an AS of 180^o. The channel function is set to F_c(C, A, 0^o, 180^o, 50λ, 0^o, 60^o, 0.5λ). The cross correlation matrix at receiver $\boldsymbol{\kappa_r}$ is given by:

$$\boldsymbol{\kappa_r} = \begin{bmatrix} 1 & 0.2244 & 0.1637 \\ 0.1637 & 1 & 0.2244 \\ 0.2244 & 0.1637 & 1 \end{bmatrix} \tag{6.3}$$

and the covariance matrix of the V-BLAST and CDDSM $\boldsymbol{\kappa_t}$ at the transmitter are given by:

$$\text{V-BLAST}\,\boldsymbol{\kappa_t} = \begin{bmatrix} 1 & 0.001 \\ 0.001 & 1 \end{bmatrix} \qquad \text{CDDSM}\,\boldsymbol{\kappa_t} = \begin{bmatrix} 1 & 0.001 & 0.0005 \\ 0.0005 & 1 & 0.001 \\ 0.001 & 0.0005 & 1 \end{bmatrix} \tag{6.4}$$

Even though the gradient of the CDDSM gets steeper with respect to increasing SNR, the assumed minimum operating SNR at 1% FER still sees a better performance from V-BLAST relative to CDDSM. This is due to the presence of the third antenna at the transmitter of the CDDSM (V-BLAST has two antennas at the transmitter), that has a correlation effect on the other two CDDSM's antennas. Thus, the effective correlation at the transmitter of the CDDSM is higher than V-BLAST.

6.3.4 Backward Compatibility With V-BLAST System

It might be thought that implementing a CDD system to replace any SISO or SIMO OFDM system could be done with full backward compatibility, e.g. when applied to an 802.11a WLAN system as described in Section 5.2.1. If the CDD system backward compatibility could be fully supported by any single input system, then this would mean that the CDDSM scheme could co-exist with the V-BLAST transmit scheme by means of just a simple switching technique. However, this backward compatibility between CDDSM and V-BLAST is not achievable unless

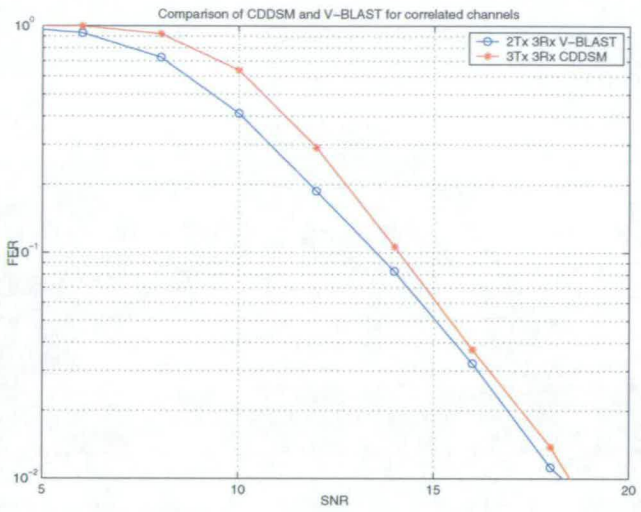

Figure 6.3: *FER vs SNR for 16 QAM (3,3) CDDSM and 16 QAM (2,3) V-BLAST in F_c(C, A, 0^o, 180^o, 50λ, 0^o, 60^o, 0.5λ) channel*

minor change to the receiver are made. The change lies in the channel estimation algorithm, such that the number of multipath channel taps must be increased during the truncation process as discussed in Section 5.2.1.

6.4 Partially Orthogonal Space Time Block Code (POSTBC)

In Chapter 3, it was shown through simulations that Dual Alamouti STBC scheme can significantly outperform V-BLAST and Alamouti STBC. The downside of this transmit technique is that it requires an even number of Tx by concatenating two pairs of Alamouti STBC transmitters. It does not provide a solution for economically attractive modern configurations with an odd number of Tx, especially in the case where three antennas would be the preferable implementation for IEEE 802.11n wireless terminals as speculated. Therefore, this section introduces a 3 Tx hybrid of the Alamouti STBC and QAM scheme where the signals can be decoded by means of a low complexity receiver that can give good performance.

6.4.1 Three Transmit Antenna POSTBC

This scheme comprises the steps of separating modulated data into two categories, encoding the first category of symbols by means of Alamouti STBC and leaving the second category in its

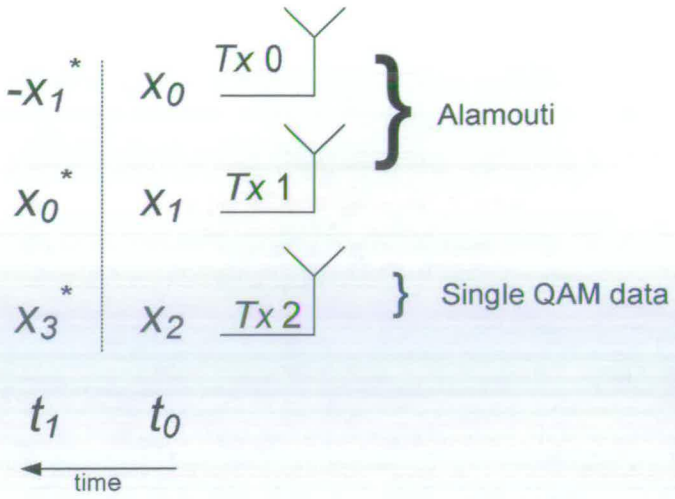

Figure 6.4: *Transmit Structure of POSTBC*

modulated QAM form as shown in Figure 6.4. The first set of symbols, x_0 and x_1, are Alamouti space time encoded and sent to Tx 0 and Tx 1. The second set of symbols, x_2 and x_3^* are sent to Tx 2 in the order of being transmitted at the first and second time interval respectively.

Not only does this transmit scheme provide an option to utilise the robustness of the Alamouti scheme with one less antenna as compared to Dual Alamouti STBC scheme, it also spectrally as efficient as the latter. The overall space time code rate, defined as the number of symbols transmitted per time period, for this 3 Tx transmit scheme is equivalent to 2.

6.4.2 Receive Signal Model

Assuming that three antennas are used at the receiving terminal and that the channel remains static over two transmission symbol periods, the received signal can be expressed as:

$$\mathbf{r} = \mathbf{Hx} + \boldsymbol{\eta}$$

$$\begin{bmatrix} r_{0,0} & r_{0,1} \\ r_{1,0} & r_{1,1} \\ r_{2,0} & r_{2,1} \end{bmatrix} = \begin{bmatrix} h_{0,0} & h_{0,1} & h_{0,2} \\ h_{1,0} & h_{1,1} & h_{1,2} \\ h_{2,0} & h_{2,1} & h_{2,2} \end{bmatrix} \begin{bmatrix} x_0 & -x_1^* \\ x_1 & x_0^* \\ x_2 & x_3^* \end{bmatrix} + \begin{bmatrix} \eta_{0,0} & \eta_{0,1} \\ \eta_{1,0} & \eta_{1,1} \\ \eta_{2,0} & \eta_{2,1} \end{bmatrix} \quad (6.5)$$

where r_{nt} and η_{nt} denotes the received signal and noise respectively from the n^{th} Rx at time t.

The received signal from (6.5) can be rewritten as a vector:

$$\mathbf{r} = \mathbf{H_P x} + \boldsymbol{\eta} \tag{6.6}$$

$$\begin{bmatrix} r_{0,0} \\ r^*_{0,1} \\ r_{1,0} \\ r^*_{1,1} \\ r_{2,0} \\ r^*_{2,1} \end{bmatrix} = \begin{bmatrix} h_{0,0} & h_{0,1} & h_{0,2} & 0 \\ h^*_{0,1} & -h^*_{0,0} & 0 & h^*_{0,2} \\ h_{1,0} & h_{1,1} & h_{1,2} & 0 \\ h^*_{1,1} & -h^*_{1,0} & 0 & h^*_{1,2} \\ h_{2,0} & h_{2,1} & h_{2,2} & 0 \\ h^*_{2,1} & -h^*_{2,0} & 0 & h^*_{2,2} \end{bmatrix} \begin{bmatrix} x_0 \\ x_1 \\ x_2 \\ x_3 \end{bmatrix} + \begin{bmatrix} \eta_{0,0} \\ \eta^*_{0,1} \\ \eta_{1,0} \\ \eta^*_{1,1} \\ \eta_{2,0} \\ \eta^*_{2,1} \end{bmatrix} \tag{6.7}$$

$$= \begin{bmatrix} \mathbf{h_1} & \mathbf{h_2} \\ \mathbf{h_3} & \mathbf{h_4} \\ \mathbf{h_5} & \mathbf{h_6} \end{bmatrix} \begin{bmatrix} x_0 \\ x_1 \\ x_2 \\ x_3 \end{bmatrix} + \begin{bmatrix} \eta_{0,0} \\ \eta^*_{0,1} \\ \eta_{1,0} \\ \eta^*_{1,1} \\ \eta_{2,0} \\ \eta^*_{2,1} \end{bmatrix} \tag{6.8}$$

where each $\mathbf{h}$ represents a 2x2 submatrix of the channel response $\mathbf{H_P}$.

The equation in (6.7) demonstrates an increase in spatial freedom from a three transmit and receive structure to a virtual four transmit six receive case operating at half the symbol rate. Consequently, the minimum number of receive antennas required to detect every symbol efficiently using either the ZF or MMSE estimator is reduced by one to two antennas as compared to V-BLAST for the same number of transmit antennas employed. (Presumably 3 Tx V-BLAST needs 3 RX and 3 Tx POSTBC needs 2 Rx).

6.4.3 Decoding Using OSIC Algorithm

The MMSE OSIC algorithm is recommended as a choice for low decoding complexity. This algorithm chooses the higher SINR of either the Alamouti or QAM stream for detection, quantises it and subtracts the effect of the detected stream from the received signal. This is then followed by detecting the next lower undetected SINR stream. The algorithm implementing OSIC for decoding POSTBC symbols is as follows:

i. Determine the MMSE estimate of the channel matrix $\mathbf{H_P}$.

$$\begin{aligned}
\mathbf{G} &= (\mathbf{H_P}^H\mathbf{H_P} + \sigma_n^2\mathbf{I})^{-1}\mathbf{H_P}^H \\
&= \left(\begin{bmatrix} \mathbf{h}_1^H & \mathbf{h}_3^H & \mathbf{h}_5^H \\ \mathbf{h}_2^H & \mathbf{h}_4^H & \mathbf{h}_6^H \end{bmatrix}\begin{bmatrix} \mathbf{h}_1 & \mathbf{h}_2 \\ \mathbf{h}_3 & \mathbf{h}_4 \\ \mathbf{h}_5 & \mathbf{h}_6 \end{bmatrix} + \sigma_n^2\mathbf{I}_4\right)^{-1}\begin{bmatrix} \mathbf{h}_1^H & \mathbf{h}_3^H & \mathbf{h}_5^H \\ \mathbf{h}_2^H & \mathbf{h}_4^H & \mathbf{h}_6^H \end{bmatrix} \quad (6.9) \\
&= \left(\begin{bmatrix} \mathbf{h}_1^H\mathbf{h}_1 + \mathbf{h}_3^H\mathbf{h}_3 + \mathbf{h}_5^H\mathbf{h}_5 & \mathbf{h}_1^H\mathbf{h}_2 + \mathbf{h}_3^H\mathbf{h}_4 + \mathbf{h}_5^H\mathbf{h}_6 \\ \mathbf{h}_2^H\mathbf{h}_1 + \mathbf{h}_4^H\mathbf{h}_3 + \mathbf{h}_6^H\mathbf{h}_5 & \mathbf{h}_2^H\mathbf{h}_2 + \mathbf{h}_4^H\mathbf{h}_4 + \mathbf{h}_6^H\mathbf{h}_6 \end{bmatrix} + \sigma_n^2\mathbf{I}_4\right)^{-1} \\
&\quad \begin{bmatrix} \mathbf{h}_1^H & \mathbf{h}_3^H & \mathbf{h}_5^H \\ \mathbf{h}_2^H & \mathbf{h}_4^H & \mathbf{h}_6^H \end{bmatrix} \quad (6.10) \\
&= \left(\begin{bmatrix} (c_1 + \sigma_n^2)\mathbf{I}_2 & \mathbf{Z} \\ \mathbf{Z}^H & (c_2 + \sigma_n^2)\mathbf{I}_2 \end{bmatrix}\right)^{-1}\begin{bmatrix} \mathbf{h}_1^H & \mathbf{h}_3^H & \mathbf{h}_5^H \\ \mathbf{h}_2^H & \mathbf{h}_4^H & \mathbf{h}_6^H \end{bmatrix} \quad (6.11)
\end{aligned}$$

where

$$c_1 = |h_{0,0}|^2 + |h_{0,1}|^2 + |h_{1,0}|^2 + |h_{1,1}|^2 + |h_{2,0}|^2 + |h_{2,1}|^2 \quad (6.12)$$

$$c_2 = |h_{0,2}|^2 + |h_{1,2}|^2 + |h_{2,2}|^2 \quad (6.13)$$

Due to the orthogonal structure of Alamouti code and that the QAM symbols do not interfere,

$$\mathbf{Z}\mathbf{Z}^H = c_3\mathbf{I}_2 \quad (6.14)$$

where

$$c_3 = |h_{0,0}^* h_{0,2} + h_{1,0}^* h_{1,2} + h_{2,0}^* h_{2,2}|^2 + |h_{0,1}^* h_{0,2} + h_{1,1}^* h_{1,2} + h_{2,1}^* h_{2,2}|^2 \quad (6.15)$$

Refer to Appendix G for proof.

Hence, the MMSE estimate of the channel matrix, $\mathbf{H_P}$ as defined in equation 6.7 can be analytically derived without full matrix inversion as:

$$\mathbf{G} = \frac{1}{(c_1 + \sigma_n^2)(c_2 + \sigma_n^2) - c_3}\begin{bmatrix} (c_2 + \sigma_n^2)\mathbf{I}_2 & -\mathbf{Z} \\ -\mathbf{Z}^H & (c_1 + \sigma_n^2)\mathbf{I}_2 \end{bmatrix}\begin{bmatrix} \mathbf{h}_1^H & \mathbf{h}_3^H & \mathbf{h}_5^H \\ \mathbf{h}_2^H & \mathbf{h}_4^H & \mathbf{h}_6^H \end{bmatrix} \quad (6.16)$$

Note that the ZF estimate can be easily derived by just removing the σ_n^2 term appearing in equation (6.16).

ii. Calculate the SINR of the $2m^{th}$ stream, where m = 0 and 1 denote the Alamouti and QAM streams respectively, i.e, the x_0 and x_2 streams. At this stage, the SINR of the $(2m+1)^{th}$ stream (x_1 or x_3) is not calculated because this is equal to the SINR of $2m^{th}$ (x_0 or x_2) stream due to the orthogonal structure of Alamouti STBC and non-interfering QAM symbols over two symbol period. Select the stream with the highest SINR.

$$k_{Tx} = \underbrace{\text{argmax}}_{2m}(SINR) \tag{6.17}$$

iii. Determine the weighting matrix for the highest SINR stream

$$\mathbf{w}^T = \mathbf{G}_{k_{Tx}:k_{Tx}+1} \tag{6.18}$$

where $\mathbf{G}_{k_{Tx}:k_{Tx}+1}$ denotes the row vector from row k_{Tx} to $k_{Tx}+1$

iv. Following this, the k_{Tx} and $k_{Tx}+1$ symbols are detected

$$\mathbf{y}_{k_{Tx}:k_{Tx}+1} = \mathbf{w}^T\mathbf{r} \tag{6.19}$$

v. These detected signals are quantised to the constellation in use.

$$\hat{\mathbf{x}}_{k_{Tx}:k_{Tx}+1} = Q(\mathbf{y}_{k_{Tx}:k_{Tx}+1}) \tag{6.20}$$

vi. The effect of the estimated symbols, $\hat{\mathbf{x}}_{k_{Tx}:k_{Tx}+1}$, are then subtracted from the received signal

$$\acute{\mathbf{r}} = \mathbf{r} - \mathbf{H}_{\mathbf{P}k_{Tx}:k_{Tx}+1}\hat{\mathbf{x}}_{k_{Tx}:k_{Tx}+1} \tag{6.21}$$

where $\mathbf{H}_{\mathbf{P}k_{Tx}:k_{Tx}+1}$ denotes the column vector from k_{Tx} to $k_{Tx}+1$

vii. Set k_{Tx} to be index of the other undetected lower SINR stream and determine the weighting matrix, to obtain the MRC matrix.

$$\mathbf{w} = \mathbf{H}_{\mathbf{P}k_{Tx}:k_{Tx}+1}^H \tag{6.22}$$

viii. Repeat the process from Step iv to vii until all symbols are detected

6.4.4 Proposed Decoding Algorithm

In the previous section, it was shown that OSIC algorithm can be a good solution for low complexity implementation. However, due to the features present in this transmit scheme, the OSIC algorithm could be further simplified attaining similar performance. This algorithm is simplified by removing the step for calculating the SINR of both transmitted streams which will be explained later. The proposed algorithm can be summarised as follows:

i. Determine the MMSE estimate of the Alamouti stream.

$$\underbrace{\mathbf{G}}_{0:1} = \frac{1}{(c_1+\sigma_n^2)(c_2+\sigma_n^2)-c_3}\left[\begin{array}{cc}(c_2+\sigma_n^2)\mathbf{I}_2 & -\mathbf{Z}\end{array}\right] \left[\begin{array}{ccc}\mathbf{h}_1^H & \mathbf{h}_3^H & \mathbf{h}_5^H \\ \mathbf{h}_2^H & \mathbf{h}_4^H & \mathbf{h}_6^H\end{array}\right] \tag{6.23}$$

ii. Set $k_{Tx} = 0$, to refer to the Alamouti streams.

$$k_{Tx} = 0 \tag{6.24}$$

iii. Repeat Step iii to vii of the POSTBC OSIC algorithm in Section 6.4.3

iv. Set $k_{Tx} = 2$ to denote the QAM symbols.

$$\mathrm{w} = \mathbf{H}_{\mathbf{P}}{}^{H}_{k_{Tx}:k_{Tx}+1} \tag{6.25}$$

v. Repeat Step iii to vii of the POSTBC OSIC algorithm in Section 6.4.3

The first difference between OSIC and proposed algorithm lies in Step i where the full MMSE estimate of the channel response needs to be calculated for the OSIC while the proposed algorithm only requires the first two rows of the MMSE estimator. Secondly, the proposed algorithm prioritises the Alamouti stream for detection followed by the QAM stream, while the OSIC needs to calculate the SINR of both the Alamouti and non-Alamouti streams and arrange the detection order in accordance to the descending SINR. The SINR is not calculated in the proposed algorithm because the diversity gain from combining the orthogonal Alamouti STBC symbols will most of the time results in higher SINR as compared to the QAM stream.

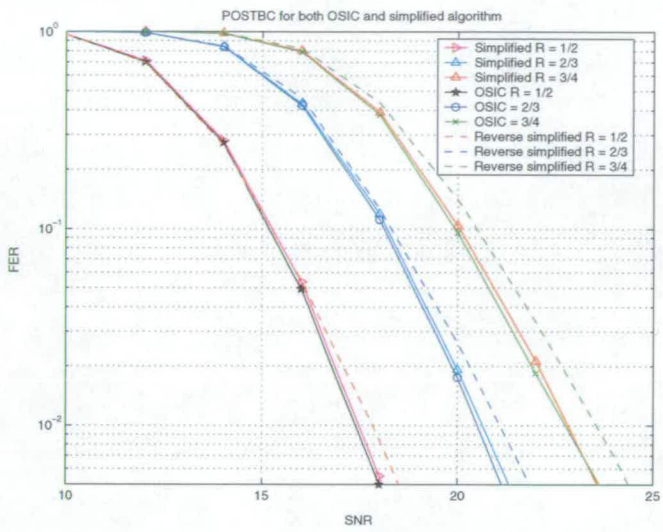

Figure 6.5: *FER vs SNR for 64 QAM (3,3) POSTBC in a F_c(U,A) channel using different SIC detectors*

6.4.5 Simulation Results

Figure 6.5 shows the performance of (3,3) POSTBC implementing both the OSIC and the proposed algorithm for 64 QAM modulated symbols. The channel function is set to F_c(U, A). Both the OSIC and simplified proposed algorithm curves match one another for all different values of the code rate, R. This shows that the proposed algorithm is a simplified version of OSIC algorithm, which is capable of delivering similar performance without the need to order streams for detection in accordance to their calculated SINR. Also shown is the reverse ordering of the proposed algorithm where the QAM stream is detected first followed by the Alamouti STBC stream. As expected the reverse ordered algorithm performs worse than the proposed one.

SNR/dB	Probability of detecting Alamouti first	Probability of detecting QAM first
0	0.8920	0.1080
20	0.9292	0.0708
40	0.9270	0.0730
60	0.9336	0.0664
Average	0.9204	0.0796

Table 6.1: *Probability of Alamouti STBC and QAM streams being detected first in an OSIC algorithm*

To verify further the similarity between the OSIC and the proposed algorithm where the Alam-

outi stream is assumed to be detected first, a counter was added into the simulator of the OSIC receiver to count the frequency of either the Alamouti or QAM stream being detected first. Four different SNRs, each over 64000 random channel realisations are tested and the outcome is tabulated in Table 6.1. The results generated from the counter show that approximately 92% of the ordering results detect the Alamouti STBC symbols followed by the QAM symbols. This confirms the assumption that the Alamouti stream will attain a higher SINR most of the time.

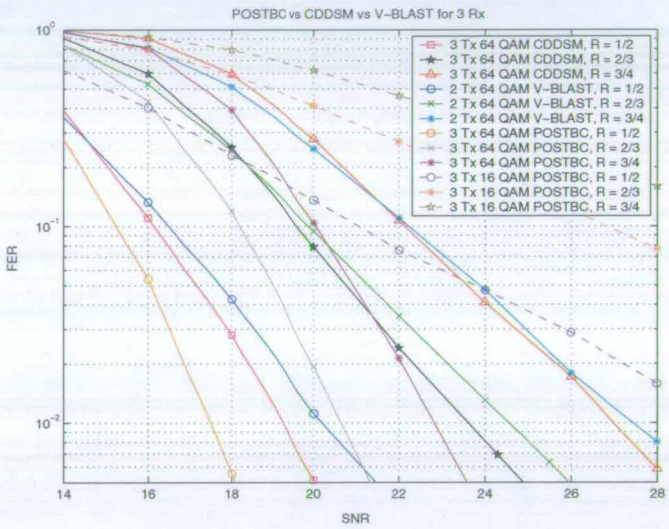

Figure 6.6: *FER vs SNR for (2,3) and (3,3) V-BLAST, (3,3) CDDSM and (3,3) POSTBC in F_c(U, A) channel*

The next simulation illustrated in Figure 6.6 for F_c(U, A) shows the comparison of (3,3) 64 QAM POSTBC implementing the proposed algorithm detector. It is compared with (3,3) 64 QAM CDDSM and (2,3) Tx 64QAM V-BLAST both using OSIC detector. The required SNR at 1% FER for POSTBC is 1.78 dB, 3 dB and 4.3 dB less than that of CDDSM for R values of 1/2, 2/3 and 3/4 respectively. For the same R values, (2,3) 64 QAM and (3,3) 16 QAM V-BLAST perform worse than both CDDSM and POSTBC. The increasing performance gap between both schemes (CDDSM and POSTBC) for higher values of R can be explained from the combination of two factors. These are the incapability of the higher R codes to perform error correction efficiently and the inherent diversity in Alamouti STBC providing a more robust scheme. Prior to soft information bits being fed into the channel decoder, the raw bit error ratios for bits demodulated from the CDDSM or V-BLAST schemes are much higher than that of POSTBC. The majority of these errored bits can be corrected when a low rate code is used. On the other hand, using a higher R value with low error correction capability will leave

most of the erroneous bits uncorrected. Also, decreasing the R value improves the frequency diversity of the OFDM system, irrespective of the MIMO scheme used. This reduces the performance advantage of the inherent transmit diversity gain in the Alamouti structure present at the POSTBC transmitter.

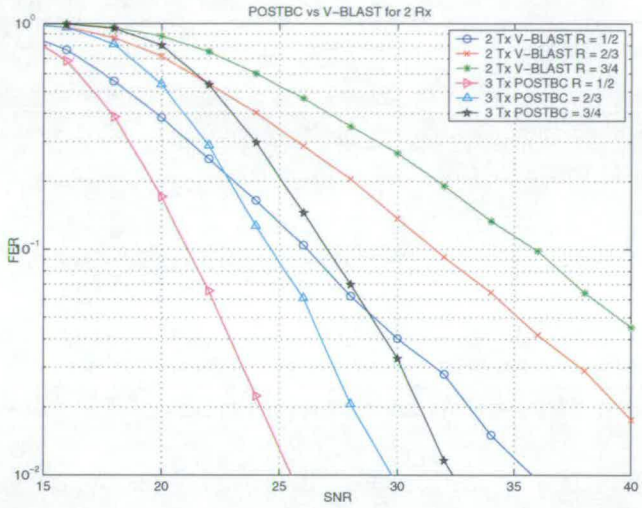

Figure 6.7: *FER vs SNR (2,2) 64 QAM V-BLAST and (3,2) 64 QAM POSTBC in F_c(U, A) channel*

Using the same channel F_c(U, A), the simulation is repeated for (3,2) 64 QAM POSTBC and (2,2) 64 QAM Tx V-BLAST and the results are shown in Figure 6.7. Comparing both schemes for R = 1/2, the SNR difference at 1% FER is 9.50 dB, which is 8.72 dB more when 3 Rx are used as shown in Figure 6.6. The massive performance gap between both schemes is due to the absence of any spatial diversity that is exploitable by the V-BLAST scheme. Hence, the significance of POSTBC is significantly visible when 2 Rx is used as compared to V-BLAST.

The comparison for 16 QAM (3,3) POSTBC and 16 QAM (2,3) V-BLAST for correlated channels are shown in Figure 6.8. The covariance matrix for the 3 Tx and 2 Tx channel are represented in equation (6.4) and the 3 Rx covariance matrix are given in equation (6.3) Contrary to the CDDSM results, the results show that POSTBC still outperform V-BLAST in a correlated fading channel. A more severe correlation model used at both the transmitter and receiver for comparing both schemes will be discussed in Section 6.8 (design of MCS) where a standard 802.11n model is used.

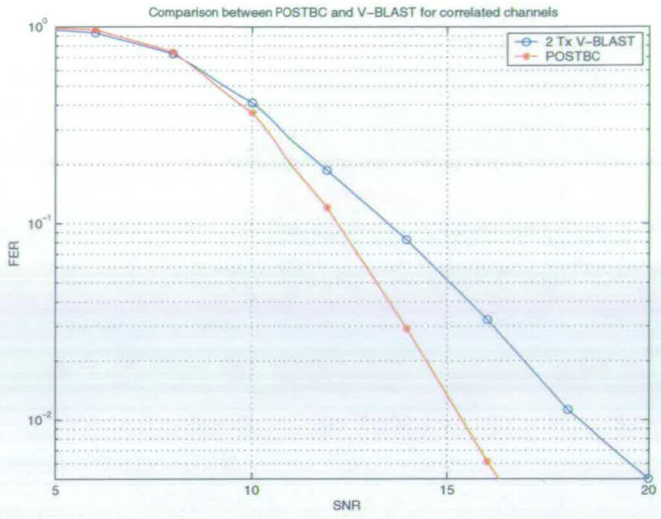

Figure 6.8: *FER vs SNR for 16 QAM (3,3) POSTBC and 16 QAM (2,3) V-BLAST for F_c(C, A, 0^o, 180^o, 50λ, 0^o, 60^o, 0.5λ) channel*

6.4.6 Robustness of Different Antenna Orientations of 3 Tx POSTBC

All studies of POSTBC in previous sections assumed only one typical antenna orientation. However, there exists another possible orientation as shown in Figure 6.9. Antenna orientation 1 is configured such that the two Alamouti Tx are arranged adjacent to each other while orientation 2 configures the structure such that the single non-Alamouti stream is adjacent to both the Alamouti STBC antennas. Initially, it was suggested that orientation 2 might improve the performance by spacing the Alamouti antennas far apart so that the correlation could be minimised and provide a more robust structure when the proposed algorithm is used.

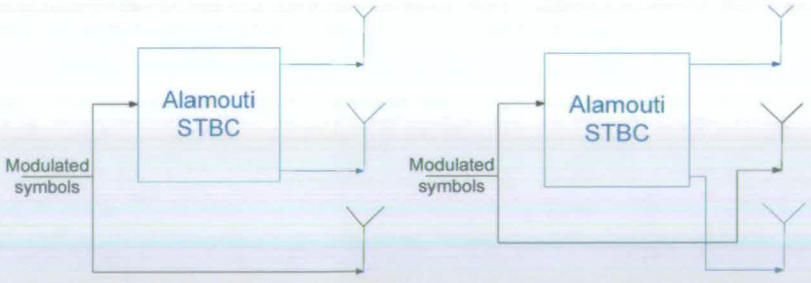

(a) Antenna orientation 1 (b) Antenna orientataion 2

Figure 6.9: *Antenna Orientations of POSTBC*

The 64 QAM POSTBC (3,3) simulation results for both orientations are plotted in Figure 6.10. The channel function F_c(C, A, 60^o, 0^o, 0.5λ, 60^o, 0^o, 0.5λ) is used where the covariance

matrix at both the transmitter and receiver are given in equation (6.3). The observed results do not favour orientation 2 as initially thought. Closer analysis shows that placing the QAM stream between the Alamouti antennas made the separation of Alamouti and QAM streams even harder for the MMSE estimator. This is because allocating the QAM antenna adjacent to both the Alamouti antennas increases the effective correlation between the two different streams. On the other hand, the original arrangement in Figure 6.9(a) only allocated one of Alamouti antennas adjacent to the QAM stream while the second is spaced further apart resulting in a lower overall correlation between the two streams.

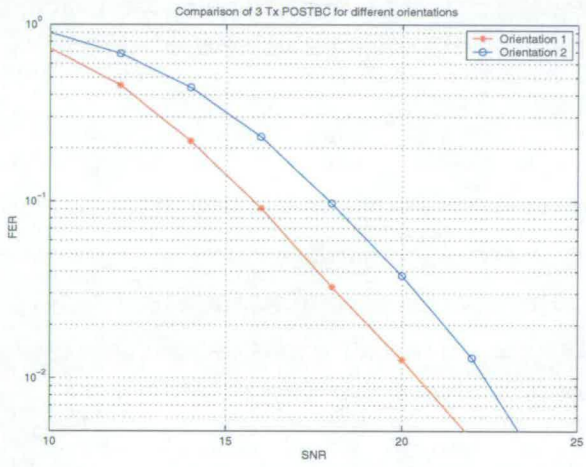

Figure 6.10: *FER vs SNR for 64 QAM (3,3) POSTBC for 2 different antenna orientations in $F_c(U,A)$ channel*

6.5 Bit Loading For POSTBC

In a wireless transmission, terminals may request certain data rates that cannot be matched exactly by using the same modulation constellation on all antennas. It is, however, undesirable to send higher data rates than the terminal would need because this requires a higher channel quality on the communication link to detect the received signal below the desired error probability. Thus, it would be advantageous to apply bit loading, which can use different constellations for the transmit antennas.

To obtain the optimum performance through bit loading [87] different constellations on multiple transmit antennas, it is usual to assign higher constellations to antennas with the better link quality. Doing the opposite will clearly result in poorer performance. Therefore, the channel

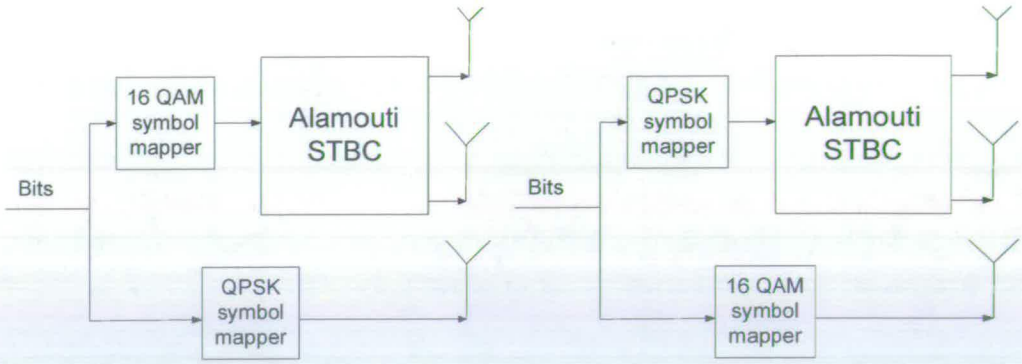

(a) Bit loading concept 1 (b) Bit loading concept 2

Figure 6.11: *Bit loading*

state information (CSI) must be made available at the transmitter prior to bit loading. One way is to ask the receiver to transmit small packets of this information back to the transmitter. In order to accommodate this feedback into the current 802.11 system, drastic changes to the current MAC layer interface is compulsory. Consequently, this changes would destroy the backward compatibility support between the current and next generation 802.11 system.

Bit loading different constellations on multiple antennas on a POSTBC transmit structure could overcome this problem of CSI required at the transmitter. This is based on the assumption that the effective SNR of the Alamouti stream is inherently higher than that of the non-Alamouti one as verified by the results in Table 6.1. In this case, assigning the higher constellation to the Alamouti stream would guarantee that this constellation is transmitted through a link of higher quality for most of the time. Contradictory to this, it cannot be denied that allocating a lower constellation to the Alamouti stream, employing the SIC algorithm to detect the Alamouti stream first will give a more accurate signal subtraction for detecting the non-Alamouti stream. However, this technique compromises on performance by transmitting lower number of bits through a higher link quality.

In order to find out the best bit loading transmit techniques as shown in Figure 6.11, three different systems were set up and simulated.

- System 1

  Bit load 16 QAM onto the Alamouti antennas and QPSK to the non-Alamouti stream. At the receiver, a SIC algorithm that chooses to detect the Alamouti stream first is applied.

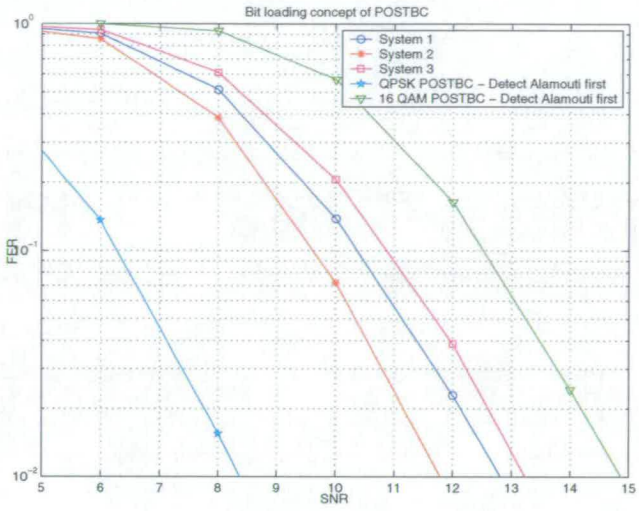

Figure 6.12: *FER vs SNR for R=2/3 (3,3) POSTBC using different bit loading configurations in F_c(U,A) channel*

- System 2

  Bit load 16 QAM onto the Alamouti antennas and QPSK to the non-Alamouti stream. Employs a SIC algorithm that chooses to detect the non-Alamouti stream first at the receiving terminal.

- System 3

  Bit load QPSK onto the Alamouti stream and 16 QAM onto the non-Alamouti stream. Employs a SIC algorithm that chooses to detect the Alamouti stream first.

Figure 6.12 compares the performance of the above three systems using three antennas at the receiving terminal. The channel, F_c(U, A) and the channel code rate, R = 2/3 are used for this simulation. Even though the QPSK symbols transmitted from the Alamouti antennas in system 3 could be detected with a lower error probability, giving a more accurate signal model for the undetected Alamouti streams after subtracting the effect of these detected QPSK symbols, the performance is still poorer than that of system 1. This is because system 3 only detect two bits of the QPSK symbols with higher accuracy while the majority of the bits from the 16 QAM is detected using a less robust system. On the other hand, system 1 detects the 16 QAM bits using the Alamouti scheme which inherently is a more robust system while the remaining less error prone QPSK symbols can be detected accurately from the remaining transmit antenna. On average the diversity gain per bit in system 1 is higher than that of 3.

Comparing system 1 and 2 for the same bit loaded transmitter, the results favours the SIC algorithm where the QPSK symbols are first detected followed by the 16 QAM Alamouti symbols. This is because the error probability is considerably lower in a QPSK constellation and this will provide a better resultant received signal model for the next 16 QAM Alamouti detection after subtracting the effect of the estimated QPSK symbols from the received signal.

Also shown in the figure, is the results of (3,3) POSTBC using only QPSK and 16 QAM constellations. Obviously, the QPSK configuration performs much better than the other results while the 16 QAM configuration requires a higher SNR to achieve 1% FER as compare to system 1, 2 and 3.

In conclusion, a POSTBC bit loading scheme where the higher constellation is assigned to the Alamouti stream while detecting the lower constellation non-Alamouti stream first by means of SIC detector is the preferred choice for implementing a more robust system.

6.6 Simplified Decoding

In this section, simplified decoders that can be applied to POSTBC will be studied. The first detector further simplifies the proposed SIC detector in Section 6.4.4 using only 2 Rx. A simplified joint detector has been proposed in Appendix H. The mathematical analysis that leads to its simplified form has been analytically derived.

6.6.1 Simplified decoding for two receive antennas POSTBC

In this section, a simplified decoding technique for the POSTBC transmit scheme using two antennas at the receiver will be introduced. The analytical derivation shows that the mathematical computation can be reduced as compared to the ZF or MMSE SIC technique as mentioned in the Section 6.4.4 and is capable of delivering reasonable performance. This technique is suitable for use in terminals manufactured at low cost not requiring very high end performance.

The received signal for (3,2) POSTBC is given by:

$$\begin{aligned} \mathbf{r} &= \mathbf{H_P x} + \boldsymbol{\eta} \\ \begin{bmatrix} r_{0,0} \\ r^*_{0,1} \\ r_{1,0} \\ r^*_{1,1} \end{bmatrix} &= \begin{bmatrix} h_{0,0} & h_{0,1} & h_{0,2} & 0 \\ h^*_{0,1} & -h^*_{0,0} & 0 & h^*_{0,2} \\ h_{1,0} & h_{1,1} & h_{1,2} & 0 \\ h^*_{1,1} & -h^*_{1,0} & 0 & h^*_{1,2} \end{bmatrix} \begin{bmatrix} x_0 \\ x_1 \\ x_2 \\ x_3 \end{bmatrix} + \begin{bmatrix} \eta_{0,0} \\ \eta^*_{0,1} \\ \eta_{1,0} \\ \eta^*_{1,1} \end{bmatrix} \end{aligned} \tag{6.26}$$

Introducing the weighting matrix, $\mathbf{w_1}$ and multiply by the received signal.

$$\begin{aligned} \mathbf{r}' &= \mathbf{w}_1 \mathbf{r} \\ &= \begin{bmatrix} h_{1,2} & 0 & h_{0,2} & 0 \\ 0 & h^*_{1,2} & 0 & h^*_{0,2} \end{bmatrix} \\ &\quad \left(\begin{bmatrix} h_{0,0} & h_{0,1} & h_{0,2} & 0 \\ h^*_{0,1} & -h^*_{0,0} & 0 & h^*_{0,2} \\ h_{1,0} & h_{1,1} & h_{1,2} & 0 \\ h^*_{1,1} & -h^*_{1,0} & 0 & h^*_{1,2} \end{bmatrix} \begin{bmatrix} x_0 \\ x_1 \\ x_2 \\ x_3 \end{bmatrix} + \begin{bmatrix} \eta_{0,0} \\ \eta^*_{0,1} \\ \eta_{1,0} \\ \eta^*_{1,1} \end{bmatrix} \right) \end{aligned} \tag{6.27}$$

$$= \begin{bmatrix} c_4 & c_5 & 0 & 0 \\ c^*_5 & -c^*_4 & 0 & 0 \end{bmatrix} \begin{bmatrix} x_0 \\ x_1 \\ x_2 \\ x_3 \end{bmatrix} + \begin{bmatrix} h_{1,2}\eta_{0,0} + h_{0,2}\eta_{1,0} \\ h_{1,2}\eta_{0,1} + h_{0,2}\eta_{1,1} \end{bmatrix} \tag{6.28}$$

where

$$c_4 = h_{1,2}h_{0,0} - h_{0,2}h_{1,0} \tag{6.29}$$

$$c_5 = h_{1,2}h_{0,1} - h_{0,2}h_{1,1} \tag{6.30}$$

Referring to (6.28), multiplying the received signal by the simple weighting matrix, $\mathbf{w_1}$ not only retains the orthogonal Alamouti matrix structure, at the same time the interference from the spatially multiplexed symbols is nulled. The resultant noise remaining spatially white after this multiplication is an additional advantage of this technique. However, this multiplication results in noise enhancement. The covariance matrix of this resultant noise can expressed as:

$$E(\eta\eta^H) = \sigma_n^2(|h_{0,2}|^2 + |h_{1,2}|^2)\mathbf{I}_2 \tag{6.31}$$

The resultant received signal in (6.28) can then be combined to detect x_0 and x_1.

$$\mathbf{r}'' = \begin{bmatrix} c_4 & c_5 \\ c_5^* & -c_4^* \end{bmatrix}^H \mathbf{r}' \tag{6.32}$$

$$= \begin{bmatrix} |c_4|^2 + |c_5|^2 & 0 \\ 0 & |c_4|^2 + |c_5|^2 \end{bmatrix} \begin{bmatrix} x_0 \\ x_1 \end{bmatrix} + \tag{6.33}$$

$$\begin{bmatrix} c_4 & c_5 \\ c_5^* & -c_4^* \end{bmatrix}^H \begin{bmatrix} h_{1,2}\eta_{0,0} + h_{0,2}\eta_{1,0} \\ h_{1,2}\eta_{0,1} + h_{0,2}\eta_{1,1} \end{bmatrix} \tag{6.34}$$

The resultant SNR from symbols x_o and x_1 due to this combining is:

$$\text{SNR} = \frac{|c_4|^2 + |c_5|^2}{\sigma_n^2(|h_{0,2}|^2 + |h_{1,2}|^2)} \tag{6.35}$$

After detecting x_0 and x_1, the effect of this symbols is subtracted from the received signal $\mathbf{r}$. Then, x_2 and x_3 are detected by mean of MRC.

In practice, x_0 and x_1 is detected by as:

$$\begin{bmatrix} \hat{x_0} \\ \hat{x_1} \end{bmatrix} = \left(\mathbf{w}_1 \begin{bmatrix} h_{0,0} & h_{0,1} \\ h_{0,1}^* & -h_{0,0}^* \\ h_{1,0} & h_{1,1} \\ h_{1,1}^* & -h_{1,0}^* \end{bmatrix} \right)^H \mathbf{r} \tag{6.36}$$

where $\hat{x_0}$ and $\hat{x_1}$ are the estimated symbols of x_0 and x_1 respectively.

The number of multiplications needed to generate the pre-multiplying matrix to detect x_0 and x_1 in equation (6.36) is only 32 while using the POSTBC SIC decoder in (6.23) requires 66 multiplications. Hence, the complexity is reduced by a factor of 2.06.

The simulated performance of (3,2) 64 QAM POSTBC applying the MMSE-SIC in Section 6.4.4 and the simplified SIC, both detecting the Alamouti symbols first, is plotted in Figure 6.13. A 1/2 rate channel coder and F_c(U, A) channel function are used. The performance of (2,2) V-BLAST MMSE OSIC is included for comparison. As expected, the MMSE-SIC performs better than the simplified detector due the noise and interference minimising property of the MMSE estimator. However, the performance difference between the MMSE and simplified SIC is only 0.5 dB at 1% FER while they both perform significantly better than the (2,2) V-

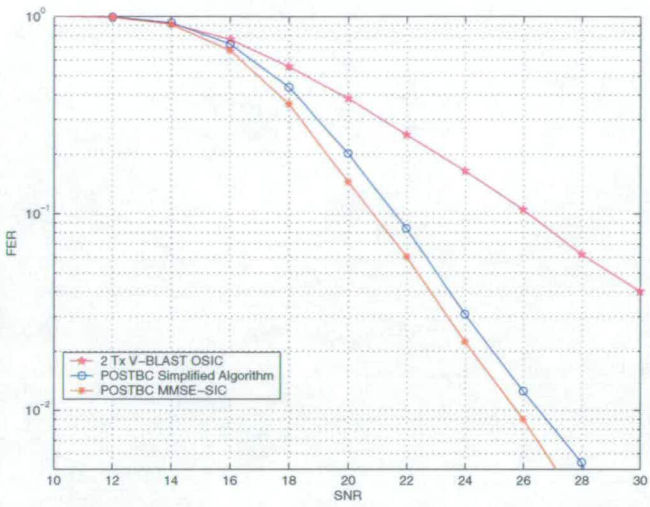

Figure 6.13: *FER vs SNR of R = 2/3 64 QAM (3,2) POSTBC using the simplified detector in a $F_c(U,A)$ channel*

BLAST MMSE OSIC scheme.

6.7 Extending POSTBC For More Than Three Transmit Antennas

In the previous sections, the POSTBC transmit scheme assumes that only three antennas are employed at the transmitter. This section extends the POSTBC transmitting elements to more than three, such that the transmitted symbols are divided into two categories, encoding the first category of symbols to be spatially multiplexed onto M_{al} Alamouti STBC transmit antenna pairs, and the second (non-Alamouti) spatially multiplexed as normal onto the remaining antennas. All streams are then transmitted simultaneously. In order to get an in depth understanding of this POSTBC scheme employing more than three antennas with its detection algorithm, analysis and simulated performance results for four antennas at the transmitter detector is firstly introduced. The generic case where an arbitrary number of transmitting elements are used will be discussed in the later part.

The 4 Tx structure shown in Figure 6.14, encodes the first category of symbols by means of the Alamouti STBC attached to the first two antennas while the remaining two spatially multiplexed antennas transmit the second category of symbols in their QAM modulated form.

The received signal model for this transmit structure assuming the minimum required number

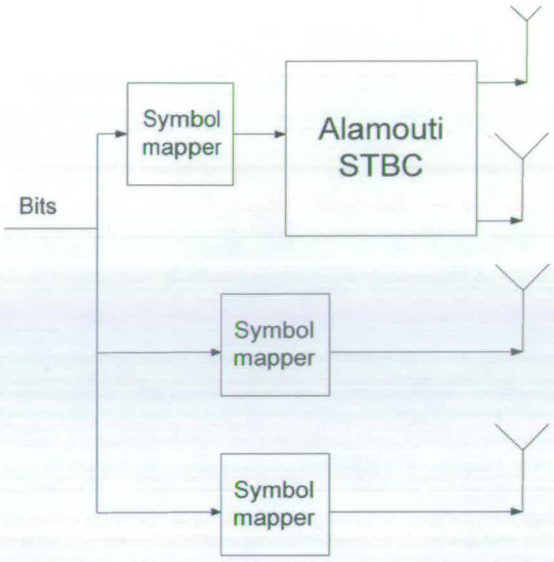

Figure 6.14: *Transmit structure of 4 Tx POSTBC*

of 3 Rx being used can be expressed as:

$$\mathbf{r} = \mathbf{H_P x} + \boldsymbol{\eta}$$

$$\begin{bmatrix} r_{0,0} \\ r^*_{0,1} \\ r_{1,0} \\ r^*_{1,1} \\ r_{2,0} \\ r^*_{2,1} \end{bmatrix} = \begin{bmatrix} h_{0,0} & h_{0,1} & h_{0,2} & 0 & h_{0,3} & 0 \\ h^*_{0,1} & -h^*_{0,0} & 0 & h^*_{0,2} & 0 & h^*_{0,3} \\ h_{1,0} & h_{1,1} & h_{1,2} & 0 & h_{1,3} & 0 \\ h^*_{1,1} & -h^*_{1,0} & 0 & h^*_{1,2} & 0 & h^*_{1,3} \\ h_{2,0} & h_{2,1} & h_{2,2} & 0 & h_{2,3} & 0 \\ h^*_{2,1} & -h^*_{2,0} & 0 & h^*_{2,2} & 0 & h^*_{2,3} \end{bmatrix} \begin{bmatrix} x_0 \\ x_1 \\ x_2 \\ x_3 \\ x_4 \\ x_5 \end{bmatrix} + \begin{bmatrix} \eta_{0,0} \\ \eta^*_{0,1} \\ \eta_{1,0} \\ \eta^*_{1,1} \\ \eta_{2,0} \\ \eta^*_{2,1} \end{bmatrix} \tag{6.37}$$

Similar to the 3 Tx POSTBC detection algorithm, the detector for this 4 Tx version will detect the Alamouti streams first and subtract the effect of the quantised signal from the received signal. However, the remaining two non-Alamouti streams are detected by means of OSIC algorithm in order to achieve a better performance. Assumed that the Alamouti streams are send to the transmitter with index 0 and 1 respectively, the detection algorithm can be described as follows;

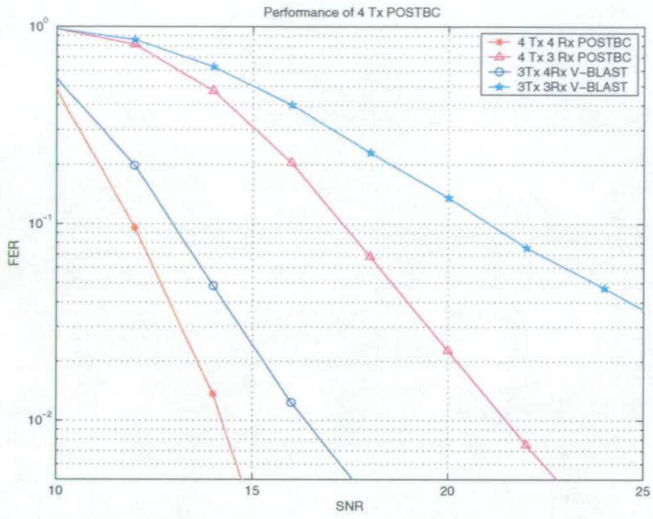

Figure 6.15: *Performance of 4Tx 16 QAM POSTBC with R = 1/2 in F_c(U,A) channel*

i. Calculate the MMSE combiner using the channel matrix $\mathbf{H_P}$ in equation (6.37).

$$\mathbf{G} = \mathbf{H_P}^H(\mathbf{H_P}\mathbf{H_P}^H + \sigma_n^2\mathbf{I})^{-1} \tag{6.38}$$

ii. Set $k_{Tx} = 0$, refers to the Alamouti STBC stream

iii. Determine the weighting matrix for the k_{Tx} and $k_{Tx} + 1$ streams

$$\mathbf{w} = \mathbf{G}_{k_{Tx}:k_{Tx}+1} \tag{6.39}$$

where $\mathbf{G}_{k_{Tx}:k_{Tx}+1}$ denotes the matrix formed by rows k_{Tx} to $k_{Tx} + 1$ of $\mathbf{G}$

iv. Detect the k_{Tx} and $k_{Tx} + 1$ symbols.

$$\mathbf{y}_{k_{Tx}:k_{Tx}+1} = \mathbf{wr} \tag{6.40}$$

v. Quantise these symbols to the nearest points in their respective constellations.

$$\hat{\mathbf{x}}_{k_{Tx}:k_{Tx}+1} = Q(\mathbf{y}_{k_{Tx}:k_{Tx}+1}) \tag{6.41}$$

vi. The effects of the estimated symbols, $\hat{\mathbf{x}}_{k_{Tx}:k_{Tx}+1}$, are then subtracted from the received

signal

$$\hat{\mathbf{r}} = \mathbf{r} - \mathbf{H_P}_{k_{Tx}:k_{Tx}+1}\hat{\mathbf{x}}_{k_{Tx}:k_{Tx}+1} \tag{6.42}$$

where $\mathbf{H_P}_{k_{Tx}:k_{Tx}+1}$ denotes the matrix formed by columns k_{Tx} to $k_{Tx}+1$ of $\mathbf{H_P}$

vii. Null the columns of the k_{Tx} and $k_{Tx}+1$ streams.

$$\mathbf{H_P^-} = \mathbf{H_P} - [0\,0\,\ldots\mathbf{H_P}_{k_{Tx}:k_{Tx}+1}\ldots\,0\,0]. \tag{6.43}$$

viii. Calculate the MMSE estimated of the nulled channel.

$$\mathbf{G} = (\mathbf{H_P^-})^H(\mathbf{H_P^-}(\mathbf{H_P^-})^H + \sigma_n^2\mathbf{I})^{-1} \tag{6.44}$$

ix. Calculate the SINR of the $2m^{th}$ stream and choose the one with the highest SINR.

$$k_{Tx} = \underbrace{\text{argmax}}_{2m}(SINR) \tag{6.45}$$

x. Repeat this process from step iv until all streams have been detected.

The performance of the 16 QAM 4 Tx POSTBC scheme is compared to the 16 QAM 3 Tx V-BLAST OSIC technique using 3 and 4 Rx respectively. The simulated results for both schemes attaining the same spectral efficiency are shown in Figure 6.15. The channel is set to E_c(U, A) and R = 1/2 is used for every scheme. Using either four or three antennas at the receiver favours the POSTBC transmit scheme with the latter showing significant improvement due to the absence of transmit diversity available for exploitation in the (3,3) V-BLAST scheme.

In practice this POSTBC can be extended to M_{al} Alamouti and M_q non-Alamouti transmitters as shown in Figure 6.16.

The suggested linear detection algorithm chooses to detect every Alamouti stream first followed by the non-Alamouti streams both by means of OSIC technique. A descriptive flowchart to illustrate the process of this algorithm is shown in Figure 6.17.

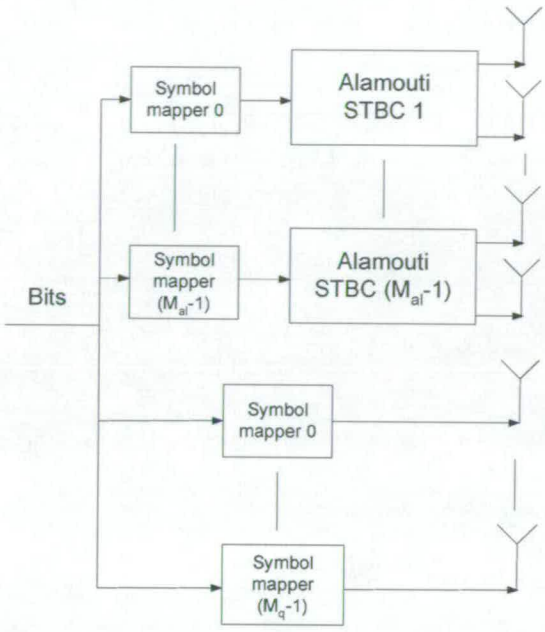

Figure 6.16: *Transmit structure of M Tx POSTBC*

6.8 Modulation Coded Scheme(MCS)

The concept of MCS involves switching between modes to enable a terminal to maximise its achievable throughput. The switching criteria can be selected based on several parameters like SNR, channel quality or several good acknowledgements received from the MAC. The latter option shall not be discussed in detail here. A pictorial example to illustrate the concept of MCS is depicted in Figure 6.18. Due to the longer path length taken by a radio signal to travel from the access point (AP) to mobile terminal (MT) 1 as compared to MT 2, the expected received SNR would be lower. Hence, the overall expected data received over the same period would be lower from MT 1.

The operational modes selected by the switching scheme can vary as a function of channel code rates, modulation schemes and even transmission schemes coupled with their detection algorithms. In this section, the combinations of all these functions that best suit IEEE 802.11n will be studied. Initial studies account for the best MIMO schemes that maximises the throughput supported only for IEEE 802.11n terminals only . Later design considers some additional factors like legacy terminal compatibility, resource saving and latency, based on a summary of all comparisons compiled in this thesis.

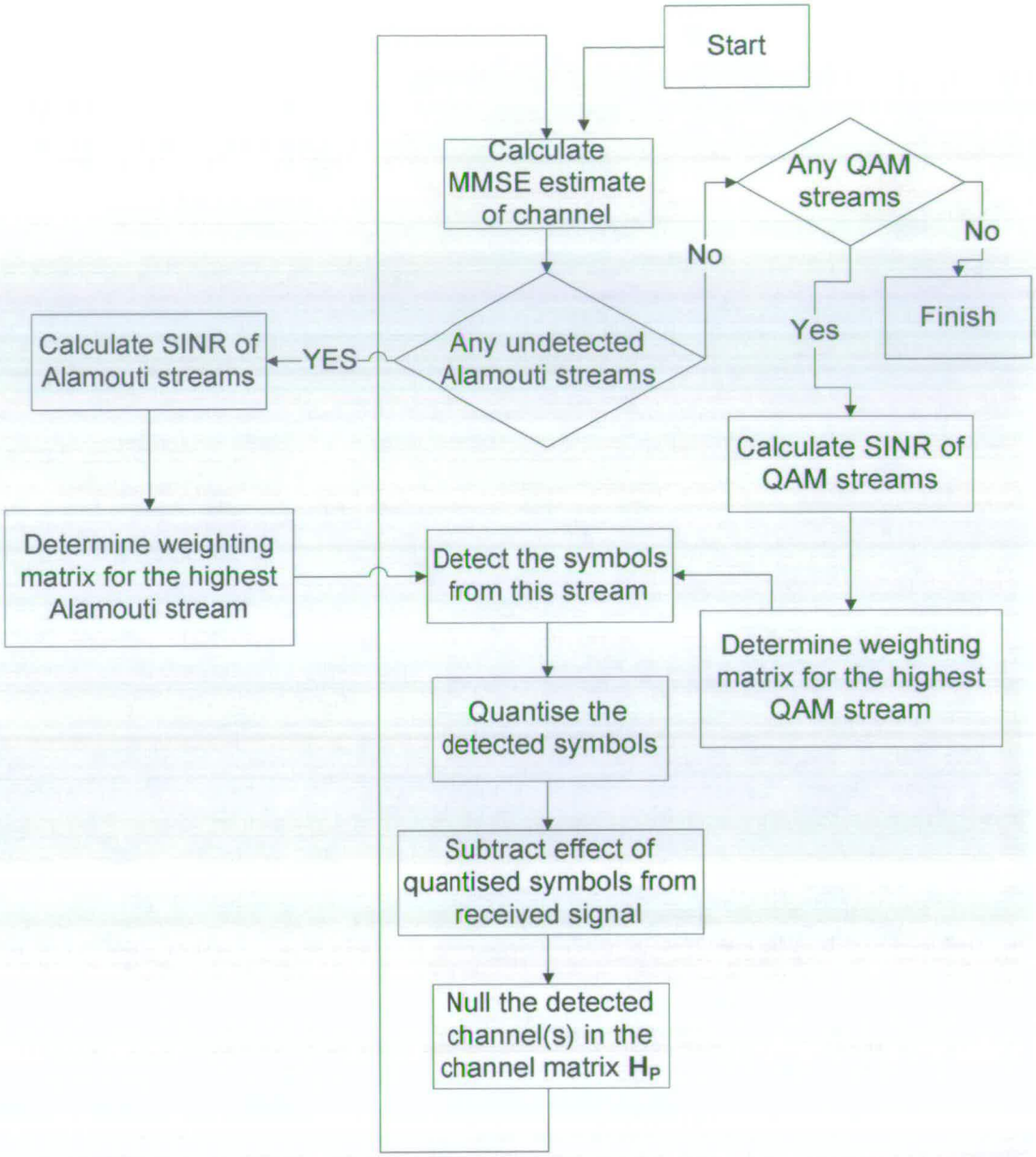

Figure 6.17: *Descriptive flowchart algorithm for detecting M Tx POSTBC*

6.8.1 Design Of MCS For IEEE 802.11n Terminals

From Chapter 3 and Section 6.4, it was assumed that 3 Tx POSTBC, 2 and 3 Tx V-BLAST and 2 Tx Alamouti STBC can be implemented at reasonable performance with the use of just low complexity decoder. In this MCS study, the above systems will be considered for

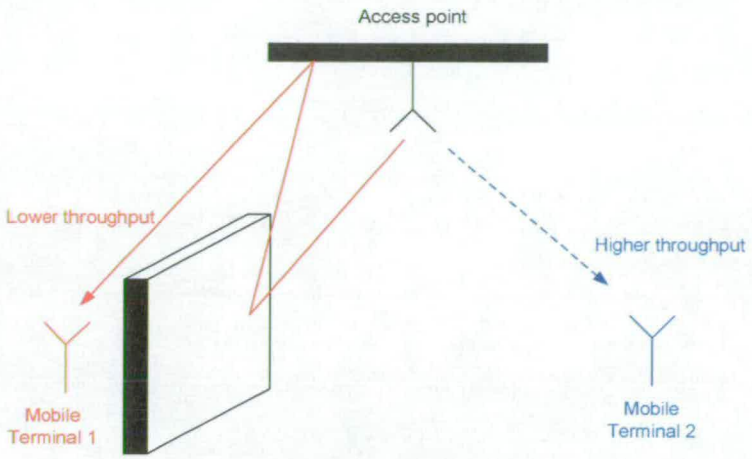

Figure 6.18: *Concept of MCS*

switching modes in an IEEE 802.11n system. The Alamouti STBC uses the decoder in Section 2.11.2, V-BLAST the MMSE OSIC and POSTBC the MMSE SIC detector in Section 6.4.4. This simulation uses the standard IEEE 802.11n channel model D (F_c(C, D)) with an available bandwidth of 20 MHz. It will be assumed that the throughput produced from the 20 MHz channel can be doubled when considering a 40 MHz channel (or two 20 MHz channels paired together).

6.8.2 Design Criterion

The primary requirement for the IEEE 802.11n proposal was to design a system such that a maximum data rate of 100 Mbps could be supported by the receiving terminals (including MAC overhead). On the basis of this requirement, the MCS modes will be designed with the following restrictions and assumptions:

i. The 100 Mbps MAC throughput shall be achieved given a 40 MHz bandwidth allocated in the 5.2 GHz unlicensed spectrum (However, due to the provided channel data being available with 50 ns delay spread (20MHz) channel, it can be assumed that the throughput shown in the later results can be doubled to reflect its throughput in a 40 MHz channel).

ii. Bits can only be modulated by means of BPSK, QPSK, 16 QAM and 64 QAM symmetric constellations.

iii. Any type of channel code with different code rates can be used. For simplicity, in the

later simulated results all bits are encoded with a convolutional encoder.

iv. The maximum number of antennas at terminals are set to three.

v. The MAC throughput efficiency is assumed to be 50% of that for the physical layer (PHY).

vi. Only 48 out of the 64 subcarriers are mapped with information symbols, while the last 16 IFFT samples are repeated for the cyclic prefix.

The MAC throughput can be calculated as:

$$\text{Throughput} = \frac{(1 - \text{FER}) * \text{CBTPS} * R * 0.5 * \frac{48}{64}}{T_s} \tag{6.46}$$

where CBTPS is defined as the coded bits transmitted per OFDM symbol and T_s is one OFDM symbol period, calculated as:

$$\begin{aligned} T_s &= \frac{1}{20MHz}(64 \text{ IFFT samples} + 16 \text{ cyclic prefix}) \\ &= 4.0\,\mu s \end{aligned} \tag{6.47}$$

6.8.3 MCS Design On the Basis Alamouti STBC, V-BLAST and POSTBC

This MCS design has the choice of switching between three selected MIMO schemes, namely, Alamouti STBC, V-BLAST and POSTBC, with different channel code rates adapted to suit the required throughput. This design considers two different scenarios, one of which where the receiving terminals are equipped with two antennas and the other with three. The choice of modes available from different combinations of MIMO schemes and channel code rates, with some schemes' data rate coinciding with one another, are tabulated in Table 6.2. These data rates are maximum possible values given the parameters used. The choice of these data rates are randomly chosen such that steps of switching from one mode to another is reasonably met. The process of eliminating the poorer schemes will then be determined by comparing these simulated results.

Tx	R	MIMO	Modulation	MAC Throughput/Mbps (20 MHz channel)	MAC Throughput/Mbps (40 MHz channel)
2	1/2	Alamouti	BPSK	3.0	6.0
2	3/4	Alamouti	BPSK	4.5	9.0
2	1/2	Alamouti	QPSK	6.0	12.0
2	3/4	Alamouti	QPSK	9.0	18.0
2	1/2	Alamouti	16 QAM	12.0	24.0
2	2/3	Alamouti	16 QAM	16.0	32.0
2	3/4	Alamouti	16 QAM	18.0	36.0
2	1/2	Alamouti	64 QAM	18.0	36.0
2	2/3	Alamouti	64 QAM	24.0	48.0
2	3/4	Alamouti	64 QAM	27.0	54.0
2	1/2	V-BLAST	BPSK	6.0	12.0
2	3/4	V-BLAST	BPSK	9.0	18.0
2	1/2	V-BLAST	QPSK	12.0	24.0
2	3/4	V-BLAST	QPSK	18.0	36.0
2	1/2	V-BLAST	16 QAM	24.0	48.0
2	3/4	V-BLAST	16 QAM	36.0	72.0
2	2/3	V-BLAST	64 QAM	48.0	96.0
2	3/4	V-BLAST	64 QAM	54.0	108.0
3	2/3	V-BLAST	16 QAM	48.0	96.0
3	3/4	V-BLAST	16 QAM	54.0	108.0
3	2/3	V-BLAST	64 QAM	72.0	144.0
3	1/2	POSTBC	BPSK	6.0	12.0
3	3/4	POSTBC	BPSK	9.0	18.0
3	1/2	POSTBC	QPSK	12.0	24.0
3	3/4	POSTBC	QPSK	18.0	36.0
3	1/2	POSTBC	16 QAM	24.0	48.0
3	3/4	POSTBC	16 QAM/QPSK	27.0	54.0
3	3/4	POSTBC	16 QAM	36.0	72.0
3	2/3	POSTBC	64/16 QAM	40.0	80.0
3	2/3	POSTBC	64 QAM	48.0	96.0
3	3/4	POSTBC	64 QAM	54.0	108.0

Table 6.2: *Simulated MCS list*

6.8.4 Simulation Results and Analysis

The simulation results for the MCS in Table 6.2 for 2 and 3 Rx are shown in Figure 6.19 and 6.20 respectively. The plotted curves shows only the envelopes of interest where switching between modes could take place. For the full range simulation, refer to Appendix I.

The simulated results using 2 Rx in Figure 6.19 show the Alamouti STBC curves is positioned

furthest to the left relative to the other 2 MIMO schemes for throughputs less than 27 Mbps, indicating that Alamouti STBC is the best scheme for low data rates. Terminals demanding a higher throughput than 27 Mbps would need to switch transmission mode to the 3 Tx POSTBC as this scheme achieves a much higher throughput than a 2 Tx V-BLAST for the same received SNR.

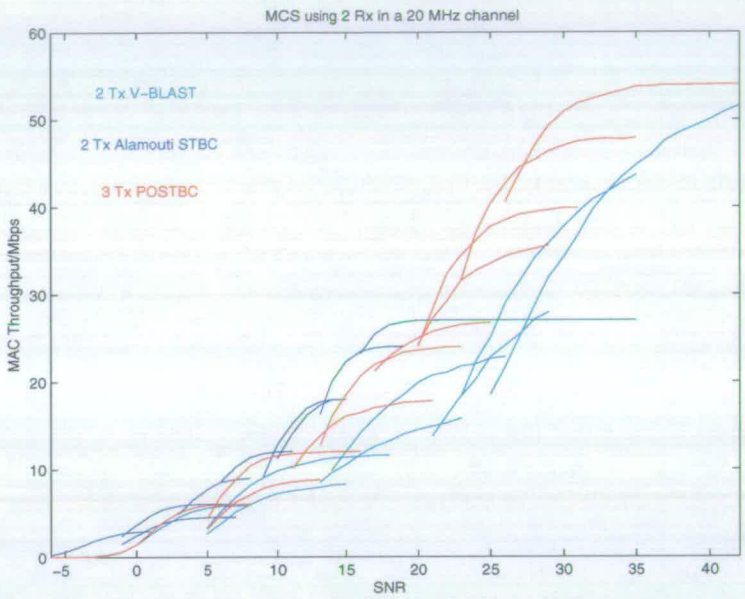

Figure 6.19: *MAC throughput vs SNR of the MCS using 2 Rx in F_c(C,D) channel*

Contrary to the above results as shown in Figure 6.20, for receiving terminals employing 3 Rx, throughput within the range of 10 to 27 Mbps, sees the 3 Tx POSTBC performing slightly better than the Alamouti STBC. The lower rates below 10 Mbps still favour Alamouti STBC. On the other hand, the V-BLAST performance for receiving terminals implementing three antennas draws closer to that of POSTBC as compared to the situation for two receive antennas with the latter achieving a slightly higher throughput.

From these observed results, it is possible to eliminate the poorer schemes from the full MCS list drafted in Table 6.2. Two sets of MCS MIMO modes capable of delivering the best performance, by switching among themselves on the basis of achievable throughput, are given in Table 6.3 and 6.4 for receiving terminals employing two and three antennas respectively. The performance of the chosen tabulated MCS lists for 2 and 3 Rx are shown in Figure 6.21(a) and 6.21(b) respectively.

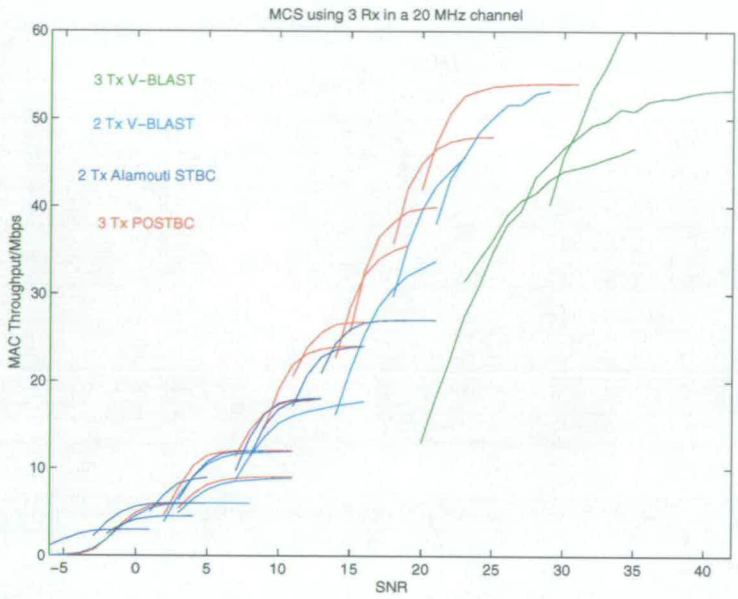

Figure 6.20: *MAC throughput vs SNR of the MCS using 3 Rx in F_c(C,D) channel*

Modes	Tx	R	MIMO	Modulation	MAC Throughput/Mbps (20 MHz channel)	MAC Throughput/Mbps (40 MHz channel)
M2a	2	1/2	Alamouti	BPSK	3.0	6.0
M2b	2	1/2	Alamouti	QPSK	6.0	12.0
M2c	2	3/4	Alamouti	QPSK	9.0	18.0
M2d	2	1/2	Alamouti	16 QAM	12.0	24.0
M2e	2	3/4	Alamouti	16 QAM	18.0	36.0
M2f	2	2/3	Alamouti	64 QAM	24.0	48.0
M2g	2	3/4	Alamouti	64 QAM	27.0	54.0
M2h	3	2/3	POSTBC	64/16 QAM	40.0	80.0
M2i	3	2/3	POSTBC	64 QAM	48.0	96.0
M2j	3	3/4	POSTBC	64 QAM	54.0	108.0

Table 6.3: *MCS list for terminals employing 2 Rx*

6.8.5 Coverage of IEEE 802.11n

While switching among the MCS list design in Table 6.3 and 6.4 enables peak MAC data rates of over 100 Mbps, it more meaningful to find out the range within which MTs can be situated to establish a communication link with its AP at the different data rates. To determine the range of radius covered by a WLAN AP, the standard path loss propagation model proposed in [88] will be used. This model consists of the free space path loss L_{FS} (slope of 2) up to a breakpoint distance (d_{BP}) and slope of 3.5 after the breakpoint distance [89]. This model was chosen such

Modes	Tx	R	MIMO	Modulation	MAC Throughput/Mbps (20 MHz channel)	MAC Throughput/Mbps (40 MHz channel)
M3a	2	1/2	Alamouti	BPSK	3.0	6.0
M3b	2	1/2	Alamouti	QPSK	6.0	12.0
M3c	2	3/4	Alamouti	QPSK	9.0	18.0
M3d	3	1/2	POSTBC	QPSK	12.0	24.0
M3e	3	3/4	POSTBC	QPSK	18.0	36.0
M3f	3	1/2	POSTBC	16 QAM	24.0	48.0
M3g	3	3/4	POSTBC	16 QAM/QPSK	27.0	54.0
M3h	3	3/4	POSTBC	16 QAM	36.0	72.0
M3i	3	2/3	POSTBC	64/16 QAM	40.0	80.0
M3j	3	2/3	POSTBC	64 QAM	48.0	96.0
M3k	3	3/4	POSTBC	64 QAM	54.0	108.0

Table 6.4: *MCS list for terminals employing 3 Rx*

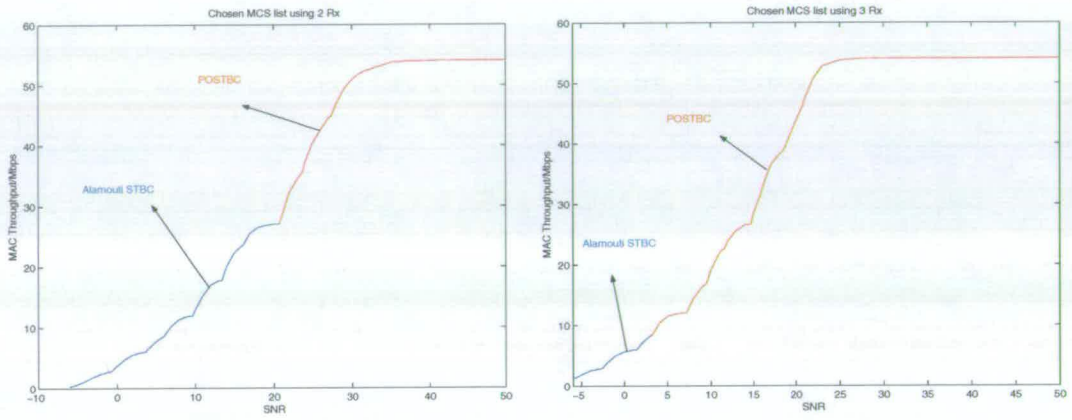

(a) MCS list for 2 Rx

(b) MCS list for 3 Rx

Figure 6.21: *MAC throughput vs SNR of the chosen MCS using 2 and 3 Rx in F_c(C,D) channel*

that the path loss model is given as:

$$L_{PL}(d) = L_{FS}(d) \qquad d \geq_{BP} \tag{6.48}$$

$$L_{PL}(d) = L_{FS}(d) + 35log_{10}\left(\frac{d}{d_{BP}}\right) \qquad d > d_{BP} \tag{6.49}$$

where L_{FS} is governed by the Friss relationship [74]:

$$L_{FS} = \frac{P_{Tx}}{P_Rx} = \frac{16\pi^2 d^2 L_{sys}}{G_{Tx} G_{Rx} \lambda^2} \tag{6.50}$$

where G_{Tx} and G_{Rx} is the antenna gain at the transmitter and receiver respectively, L_{sys} is the system loss and d is the distance between the transmitter and receiver. In this simulation G_{Tx}, G_{Rx} and L_{sys} are assumed to be unity while the typical transmitted power in a WLAN, P_{Tx}, to be 200 mW and noise -100 dBm.

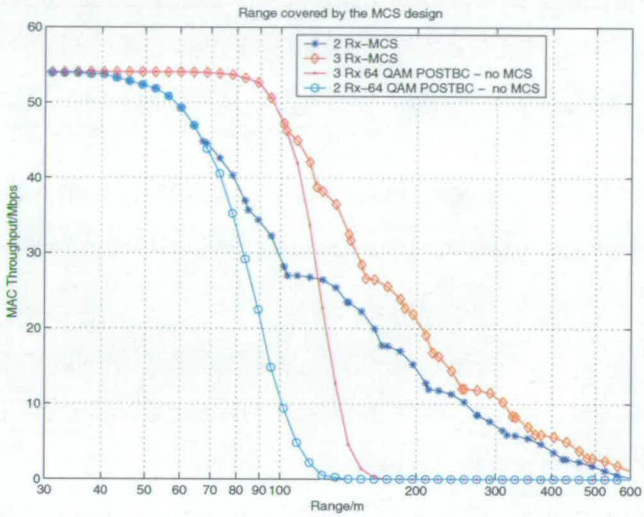

Figure 6.22: *MAC throughput vs Range covered by the 802.11n AP in F_c(C,D) channel*

The range of radius covered by a WLAN AP with respect to its achievable throughput for 2 and 3 Rx employed following the standard IEEE 802.11n path loss model is plotted in Figure 6.22. The selected transmission modes to cover this range are selected on the basis of MCS list in Table 6.3 and 6.4. Included as a comparison is the maximum achievable throughput transmission scheme, 64 QAM POSTBC with R = 3/4 which is labelled 'no MCS', highlighting the single mode transmission scheme for all ranges without switching. It can be seen that the MCS list provides a much wider range of coverage, e.g. 250 m and 310 m for a data rate of 10 Mbps with 2 and 3 Rx respectively. The single mode only manages to cover a range of 100m and 150m for the same throughput using 2 and 3 Rx respectively. Adding an extra antenna at the receiver provides a significant advantage with respect to the throughput achieved, especially in the lower range of distance. For example, there is a 20 Mbps difference in MAC data rate at a range of 100 m. Comparing the MCS with different antennas employed at the receiving

terminal, the 2 Rx case is more sensitive to switching than the 3 Rx case. The 3 Rx case is able to operate in its single mode for up to 100 m before any switching is required while the 2 Rx case would requires three mode changes within this 0-100 m range of distance.

6.8.6 Issues To Consider For WLAN Implementing MIMO Schemes

From the perspective of end users, it is important to consider issues of backward compatibility because legacy terminals will not be completely phased out once the next generation WLAN is introduced. To ensure the latest legacy terminals (IEEE 802.11a) can be supported, the transmitter can either switch to a SISO system or a MIMO system depending on the MT type. To tackle this issue, switching the transmission mode to CDD is suggested. The CDD scheme provides some improvement to the current IEEE 802.11a OFDM system performance by creating more frequency selectivity between communication link. This assumes that an improved time domain channel estimator considering more multipath channel taps or that a frequency domain channel estimator is used.

The second issue is to consider the problem introduced when Alamouti STBC transmit scheme is selected for transmission. In spite of its high performance, the allocation of one information symbol per two OFDM symbols for transmission is an absolute waste of resources especially for small packet transmissions. More importantly, the receiver would need to buffer the first time interval signal and waits for the second one to arrive before detection can take place. This process introduces a latency phenomenon in the system which can be significantly visible in a real time communication. The best solution to this problem is to replace the orthogonal temporal encoded symbols with frequency encoding suggested in Chapter 5. Eventhough Alamouti SFBC compromises its performance for latency and available resources, this scheme still deliver a considerable high performance in comparison to other transmit schemes.

Taking these two issues into consideration, improvements to the suggested IEEE 802.11n MCS design are depicted in the flowchart of Figure 6.23.

When a request to send (RTS) signal is received at the transmitter, the first decision is made to determine the nature of the requesting terminal, i.e., an IEEE 802.11n or legacy terminal. If the terminal belongs to an IEEE 802.11a system, then the AP switches its mode to enable CDD transmission. Otherwise, it would decide if latency introduced and resource saving is an issue for the system. If so, it switches its mode to encode data by means of Alamouti SFBC and send

them for transmission. On the other hand, it will move down the hierarchy to determine the number of antennas available at the receiving terminal. Then, it would transmit in one of its available modes from Table 6.3 and 6.4 according to the number of receive antennas and the quality of the link as determined by the switching parameter in used.

6.9 Conclusion

This chapter introduces two 3 Tx hybrid schemes where one involves spatial multiplexing CDD and the other Alamouti STBC with a conventional QAM stream. The aforementioned scheme can only work well when a low channel code rate, R, is used as compared to the conventional V-BLAST OSIC scheme. Regardless of scenario, the latter hybrid scheme outperforms both V-BLAST and CDDSM schemes attaining the same spectral efficiency. This hybrid scheme is robust due to the presence of an orthogonal space time code that inherently provides a source of diversity gain. One of the advantages from this scheme is its ability to achieve high performance through the use of linear MMSE-SIC detector. This detection algorithm is simplified from the conventional OSIC algorithm such that the ordering of antennas for detection in accordance to their SNR can be omitted. A simpler detection algorithm which leads to a slight degradation in performance with the use of just two antennas at the receiving terminal is also introduced. Extending this hybrid concept to more than three antennas strongly favours this scheme as compared to a 3 Tx V-BLAST MMSE-OSIC scheme for the same spectral efficiency attained by both systems.

Two advantageous implementations of this hybrid concept are also illustrated. The first one is where bits are loaded differently onto the two different stream of antennas. The preferred configuration is to assign a higher constellation to the Alamouti STBC stream and the lower to the non-Alamouti encoded stream. By doing so, it will be guaranteed that the higher constellation is always assigned to the higher SNR stream most of the time without the need for channel feedback information. To further enhance the bit loading performance, the SIC detector is chosen to detect the more robust non-Alamouti lower constellation first.

The other implementation of this hybrid scheme is its proposed inclusion into an IEEE 802.11n WLAN switched transmission MCS mode. This hybrid scheme can be very useful for terminals requiring intermediate or higher data rates where higher throughputs can be efficiently delivered compared to the 2 Tx V-BLAST MIMO schemes. The importance of this hybrid scheme can

be further highlighted for terminals employing 2 Rx where the V-BLAST scheme's achievable throughput is unable to match that of the hybrid scheme, while Alamouti STBC is incapable of efficient high data rate transmission.

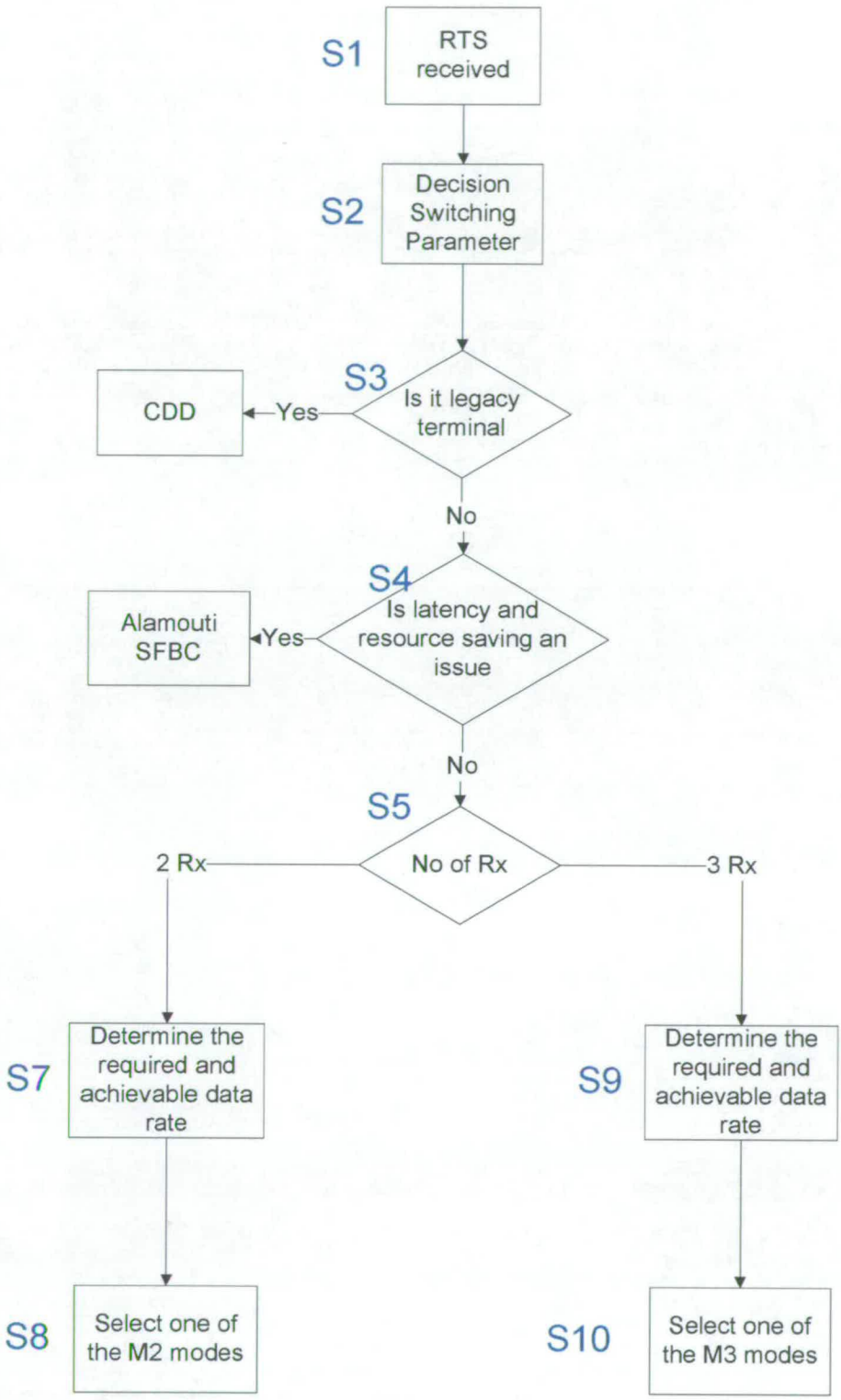

Figure 6.23: *WLAN modes upon terminal requesting for transmission*

Chapter 7
Conclusion

In this thesis, the physical layer for future WLAN, particularly IEEE 802.11n, has been developed and studied. Several techniques have been proposed to increase the data rate for the IEEE 802.11n as an improvement to the IEEE 802.11a standard. The most obvious way is to apply MIMO and diversity techniques so that spectral efficiency improvements to the current standard can be realised. Several novel hybrid techniques have been proposed and also the possibility of future MIMO WLAN supporting multiple users are investigated. A summary of the key results from different chapters and possible future research directions as a result of this PhD work will be discussed.

7.1 Summary Of Results

Chapter 2

Several modulation schemes, namely SC-FE, OFDM, MC-CDMA and flash OFDM have been compared to select the best modulation scheme for future WLAN. SC-FE, which has the same complexity as OFDM is only good when lower order modulation and high code rates are used. Typically, future WLAN systems would prefer the use of higher order modulation to increase system throughput and low code rate to improve error performance. In this case OFDM is preferred. Although MC-CDMA and flash OFDM outperform the stand alone OFDM, both of these schemes attain considerably less spectral efficiency which will limit future WLAN from supporting high data throughput. Moreover, flash OFDM introduces latency in the uplink transmission.

Chapter 3

The three MIMO techniques suggested to fulfil the high throughput criterion for IEEE 802.11n, namely, V-BLAST, Alamouti STBC and Dual Alamouti STBC were studied. Their capacity analysis for 2 Rx and 4 Rx in an uncorrelated environment strongly favours Dual Alamouti STBC in all cases. For low capacity using 2 Rx, Alamouti STBC achieves a higher capacity

than V-BLAST. When 4 Rx are used, V-BLAST capacity improves significantly due to the extra diversity exploited in this scheme. In the correlated fading analysis, Dual Alamouti STBC is seen to be more robust than V-BLAST due to the inherent diversity at its transmitter. The simulation results using low complexity physically reliable decoders with respect to three parameters, spectral efficiency, number antennas and channel correlations were studied. Similar results were observed as compared to the theoretical capacity analysis with two exceptions. In the case of 2 Rx used, V-BLAST performs significantly worse than the other two schemes. Also, 2 Rx Alamouti STBC outperforms Dual Alamouti STBC and V-BLAST.

Chapter 4

Two interference models, synchronous and asynchronous have been modelled. Bit error probability and signal model analysis for these models are presented. Then, two interference mitigation techniques, interference cancellation (IC) and interference suppression (IS) were introduced. Application of these two mitigation techniques into a two users synchronised transmission scenario was investigated. This study shows that the IC technique is preferred over IS provided the spatial degrees of freedom is available at the receiver and that the channel of the interferer can be estimated. On the other hand, IS technique is preferred for asynchronous interference due to the absence of interferer's channel information. The simulation results using IS technique to mitigate synchronous and asynchronous interference for the same system set up gives the same error performance.

Chapter 5

A simplified ZF detector was developed for the Alamouti SFBC technique which can replace its temporal encoded version to avoid latency and redundancy in small packet transmission. Using the simplified ZF solution, Alamouti SFBC behaves similarly to its temporal encoded version for low frequency selective channel. However, SFBC degrades as the number of multipath taps increases. On the other hand, this scheme is more robust than CDD in most channel conditions, though CDD performs better in a very frequency selective channel.

Chapter 6

Lastly, the physical size of future WLAN mobile devices is restricted to only three antennas to reduce manufacturing cost. Two techniques, CDDSM and POSTBC were proposed. Even though CDDSM performs better than the V-BLAST, its performance were seen to be significantly poorer than POSTBC. The newly developed Alamouti transmitter prioritised SIC detector was proposed for POSTBC and its performance is similar to that of the OSIC algorithm. A

more simplified decoder was developed and only slight degradation was observed as compared to the Alamouti prioritised SIC detector. Bit loading concept on POSTBC where the higher constellation is loaded onto the Alamouti transmitter and the lower one to the spatial multiplexed QAM modulator without channel feedback information at the transmitter was suggested to achieve a better performance. To further enhance this configuration, the ordered SIC detector where the QAM stream is always detected first has been proposed. A modulation coded scheme (MCS) technique, where switching between modes of Alamouti STBC and POSTBC is permitted, was designed. The simulation results show that for lower throughput, switching to Alamouti STBC is preferred while POSTBC is preferred over V-BLAST at higher throughput. The range covered by the MCS design shows that switching between modes increases coverage and improves system throughput as compared to the non-switching case, especially when 2 Rx are used. However, switching is less significant for the 3 Rx case if a smaller range (approximately 100 m) of radius is to be served by the AP. Based on this MCS criterion, two additional schemes for a full MCS design taking into account latency and small packet transmission supported by Alamouti SFBC and CDD for backward compatibility has been proposed.

7.2 Future Work

Two area of work as a result of this PhD work are suggested.

- Simulation for the proposed joint detector in Appendix H

  This joint detector increases the spatial freedom at the expense of coloured noise. This trade off will not be known unless a simulation is performed. The comparison with the full optimum APP solution and 2 Tx APP V-BLAST will decide if this detector is worth proposing for future WLAN where the receiver has high signal processing capability. Also, suboptimal APP detectors like sphere decoding [90] can be applied.

- Frequency encoded POSTBC

  In Chapter 5, the performance of Alamouti SFBC is similar to that of Alamouti STBC for very low frequency selective channel while its performance is better than CDD for most channel conditions. Changing the POSTBC from temporal to frequency interleaving is an area to exploit to see if the same error performance as in Chapter 3 is still observed due to the extra interfering QAM antenna. The performance of this frequency encoded version can be compared to CDDSM as a potential candidate to reduce the latency effect

and save resources for small packet transmission.

References

[1] W. H. Press, B. P. Flannery, S. A. Teukolsky, and W. T. Vetterling, *Numerical Recipes in C: The Art of Scientific Computing*. Cambridge University Press, 1993.

[2] D. Falconer, S. L. Ariyavisitakul, A. Benyamin-Seeyar, and B. Edison, "Frequency domain equalization for single-carrier broadband wireless systems," *IEEE Communications Magazine*, vol. 40, pp. 58–66, April 2002.

[3] P. E. Mogensen and J. Wigard, "On antenna-and frequency diversity in GSM related systems (GSM-900, DCS-1800, and PCS1900," *Personal Indoor and Mobile Radio Communications Conference*, vol. 3, pp. 1272–1276, Oct 1996.

[4] V. K. Garg, S. Halpern, and K. F. Smokik, "Third generation (3G) mobile communicaitons systems," *IEEE International Conference on Personal Wireless Communication*, pp. 39–43, Feb 1999.

[5] "http://grouper.ieee.org/groups/802/11/."

[6] "http://grouper.ieee.org/groups/802/16/."

[7] "http://www.ieee802.org/15/."

[8] K. Siwiak, *Ultra-Wideband Radio Technology*. John Wiley and Sons Ltd, 2004.

[9] "www.ieee802.org."

[10] R. V. Nee and R. Prasad, *OFDM For Wireless Multimedia Communications*. Artech House, 1st ed., 2000.

[11] L. Hanzo, W. Webb, and T. Keller, *Single and Multi Carrier Quadrature Amplitude Modulation, Principle and Applications for Personal Communications WLANs and Broadcasting*. John Wiley and Sons, 2nd ed., 2000.

[12] J. G. Proakis, *Digital Communications*. McGraw Hill, 4th ed., 2000.

[13] A. R. S. Bahai, B. R. Saltzberg, and A. Bahai, *Multi-Carrier Digital Communications - Theory and Applications of OFDM (Information Technology: Transmission, Processing & Storage*. Kluwer Academic/Plenum, 2000.

[14] J. Heiskala and J. Terry, *OFDM Wireless LANs: A Theoretical and Practical Guide*. Kluwer Academic/Plenum, 2nd ed., 2001.

[15] L. Hanzo, M. Munster, B. J. Choi, and T. Keller, *OFDM and MC-CDMA for BroadBand Multi-User Communications, WLANs and Broadcasting*. John Wiley & Sons, 2003.

[16] M. Engels and M. Engels, *Wireless OFDM Systems: How To Make Them Work*. Kluwer Academic, 2002.

[17] L. Hanzo and L. L. Y. E. L. J. K. Yen, *Single and Multi-Carrier DS-CDMA: Multi-User Detection, Space-Time Spreading, Synchronisation, Networking and Standards*. John Wiley & Sons, 2003.

[18] K. Fazel and S. Kaiser, *Multi-Carrier and Spread Spectrum Systems*. John Wiley & Sons, 2003.

[19] K. Fazel and S. Kaiser, *Multi-Carrier Spread-Spectrum: Fourth International Workshop Germany, September 17-19 2003*. Kluwer Academics, 2003.

[20] A. Czylwik, "Synchronization for single carrier modulation with frequency domain equalization," *IEEE Vehicular Technology Conference*, vol. 3, pp. 2277–2281, May 1998.

[21] A. Czylwik, "Low overhead pilot-aided synchronization for single carrier modulation with frequency domain equalization," *IEEE Global Telecommunications Conference*, vol. 4, pp. 2068–2073, Nov 1998.

[22] N. Al-Dhahir, "Single-carrier frequency-domain equalization for space-time block-coded transmissions over frequency-selective fading channels," *IEEE Communications Letters*, vol. 5, pp. 304–306, July 2001.

[23] J. Coon, S. Armour, M. Beach, and J. McGeehan, "Adaptive frequency-domain equlaization for single-carrier MIMO systems," *IEEE International Communications Conference*, vol. 4, pp. 2487–2491, June 2004.

[24] J. Coon, J. Siew, M. Beach, A. Nix, S. Armour, and J. McGeehan, "A comparison of MIMO-OFDM and MIMO-SCFDE in WLAN environments," *IEEE Global Telecommunications Conference*, vol. 6, pp. 3296–3301, Dec 2003.

[25] "OFDM for Mobile Data Communicaitions," *http://www.flarion.com/viewpoint/white_papers.asp*.

[26] A. Czylwik, "Comparison between adaptive OFDM and single carrier modulated with frequency domain equalization," *IEEE Vehicular Technology Conference*, vol. 2, pp. 865–869, 1997.

[27] H. Sari, G. Karam, and I. Jeanclaud, "Frequency-domain equalization of mobile radio and terrestrial broadcast channels," *IEEE Global Telecommunications Conference*, vol. 1, pp. 1–5, 1994.

[28] M. V. Clark, "Adaptive frequency-domain equalization and diversity combining for broadband wireless communications," *IEEE Selected Areas in Communications Journal*, vol. 16, pp. 1385–1395, October 1998.

[29] J. Linder, M. Nold, W. G. Teich, and M. Schreiner, "MC-CDMA and OFDMA for indoor communications: the influence of multiple receiving antennas," *IEEE Spread Spectrum Techniques and Applications*, vol. 1, pp. 189–194, 1998.

[30] C. Ibar and Y. Bar-Ness, "Comparing the performance of coded multiuser OFDM and coded MC-CDMA over fading channels," *IEEE Golbal Telecommunications Conference*, vol. 2, pp. 881–885, 2001.

[31] H. Atarashi and M. Sawahashi, "Variable spreading factor orthogonal frequency and code divsion multiplexing(VSF-OFCDM)," *Kluwer Academic Publishers*, pp. 113–122, September 2001.

[32] P. W. Wolniansky, G. J. Foschini, G. D. Golden, and R. A. Valenauela, "V-BLAST:An architecture for realizing very high data rates over the rich-scattering wireless channel," *Signals, Systems, and Electronics, ISSSE-98*, pp. 295–300, September 1998.

[33] G. D. Golden, C. J. Foschini, R. A. Valenauela, and P. W. Wolniansky, "Detection algorithm and initial laboratory results using V-BLAST space-time communication architecture," *Electronics Letter*, vol. 35, pp. 14–16, January 1999.

[34] F. J. Foschini, G. D. Golden, R. A. Valenzuela, and P. W. Wolniansky, "Simplified processin for high spectral efficiency wireless communication employing multi-element arrays," *IEEE Journal on Selected Areas in Communications*, pp. 1841–1852, Nov 1999.

[35] S. M. Alamouti, "A simple transmit diversity technique for wireless communications," *IEEE Journal Selected Areas in Communications*, vol. 16, pp. 1451–1458, October 1998.

[36] A. F. Naguib, N. Seshadri, and A. R. Calderbank, "Applications of space-time block codes and interference suppression for high capacity and high data rate wireless systems," *Signals, Systems & Computers Conference*, vol. 2, pp. 1803–1810, Nov 1998.

[37] A. Naguib, N. Seshadri, and A. R. Calderbank, "Increasing data rate over wireless channels," *IEEE Signal Processing Magazine*, vol. 17, pp. 76–92, May 2000.

[38] A. F. Naguib, "Combined interference suppression and frequency domain equalization for space-time block coded transmission," *IEEE International Communications Conference*, vol. 2, pp. 596–603, June 2003.

[39] D. M, M. B, de Courville M, M. M, S. S, and L. P, "A MMSE successive interference cancellation scheme for a new adjustable hybrid spread OFDM system," *IEEE Vechicular Technology Conference Proceedings*, vol. 2, pp. 745–749, Spring 2000.

[40] S. Baro, G. Bauch, A. Pavlic, and A. Semmler, "Improving BLAST performance using space time block codes and turbo decoding," *IEEE Global Telecommunications Conference*, vol. 2, pp. 1067–1071, August 2000.

[41] R. S. Blum, G. Y. Li, J. H. Winters, and Q. Yan, "Improved space-time coding for MIMO-OFDM communications," *IEEE Transactions on Communications*, vol. 49, pp. 1873–1878, November 2001.

[42] M. Kang and M. S. Alouini, "Performance anaylsis of MIMO systems with cochannel intereference over rayleigh fading channels," *IEEE International Communications Conference*, vol. 1, pp. 391–395, April/May 2002.

[43] M. Kang and M. S. Alouini, "Quadratic forms in complex Gaussian matrices and performance analysis of MIMO systems with co-channel interference," *IEEE International Information Theory Symposium*, p. 160, 2002.

[44] D. C. Popescu and C. Rose, "Multiuser MIMO systems and interference avoidance," *IEEE International Acoustics, Speech and Signal Processing Conference*, vol. 1, pp. 45–49, May 2002.

[45] L. Ren, S. Xi, M. Song, and J. Song, "Interference cancellation technology in MIMO mobile cellular communication systems," *IEEE Electrical and Computer Engineering Canadian Conference*, vol. 3, pp. 1941–1944, May 2003.

[46] H. Dai and A. F. Molisch, "Multiuser detection for interference limited MIMO systems," *IEEE Vechicular Technology Conference*, vol. 1, pp. 45–49, Spring 2002.

[47] L. Giangaspero, L. Agarossi, G. Paltenghi, S. Okamura, M. Okada, and S. Komaki, "Co-channel intereference cancellation based on MIMO OFDM systems," *IEEE Wireless Communications*, vol. 9, Dec 2002.

[48] J. Li, K. B. Letaief, and Z. Cao, "Co-channel interference cancellation for space-time coded OFDM systems," *IEEE Wireless Communications*, vol. 1, pp. 41–49, Jan 2003.

[49] K. B. Letaif, E. Choi, J. Y. Ahn, and R. Chen, "Joint maximum likelihood detection and interference cancellation for MIMO/OFDM systems," *IEEE Vechicular Technology Conference*, vol. 1, pp. 612–616, Oct 2003.

[50] G. Bauch, "Space-time block codes versus space-frequency block codes," *IEEE Vechicular Technology Conference*, vol. 1, pp. 567–571, Spring 2003.

[51] S. Kaiser, "Space frequency block codes and code division multiplexing in OFDM systems," *IEEE Global Telecommunications Conference*, vol. 4, pp. 2360–2364, Dec 2003.

[52] K. F. Lee and D. B. Williams, "A space-frequency transmitter frequency technique for OFDM systems," *IEEE Global Telecommunications Conference*, vol. 3, pp. 1473–1477, Dec 2000.

[53] B. Qzbek, D. L. Ruyet, and M. Bellanger, "On space-frequency block codes for unequal channels," *COST 273 Workshop On Broadband Local Access*, pp. 3/1–3/6, May 2003.

[54] A. Dammann, R. Raulefs, and S. Kaiser, "Beamforming in combination with space-time diversity for braadband OFDM systems," *IEEE International Communications Conference*, vol. 1, pp. 165–171, April/May 2002.

[55] S. Kaiser, "Spatial transmit divesity techniques for broadband OFDM systems," *IEEE Global Telecommunications Conference*, vol. 3, pp. 1824–1828, Nov/Dec 2000.

[56] A. Dammann and S. Kaiser, "Standard conformable antenna diversity techniques for OFDM and its application to the DVB-T system," *IEEE Global Telecommunications Conference*, vol. 5, pp. 3100–3105, Nov 2001.

[57] J. Khun-Jush, P. Schramm, U. Wachsmann, and F. Wenger, "Structure and performance of the HIPERLAN/2 physical layer," *IEEE Vechicular Technology Conference*, vol. 5, pp. 2667 – 2671, Fall 1999.

[58] B. P. Crow, I. Widjaja, J. G. Kim, and P. T.Sakai, "IEEE 802.11 wireless local area networks," *IEEE Personal Communications*, vol. 35, pp. 116–126, September 1997.

[59] "IEEE standard 802.11, part11: Wireless LAN medium access control(MAC) and physical layer(PHY) specifications," 1999.

[60] http://grouper.ieee.org/groups/802/11/main.html, "General introduction to IEEE 802.11 standards."

[61] B. J. Choi, *Multi-Carrier Code Division Multiple Access*. PhD thesis, University of Southampton, June 2001.

[62] N. Yee and J. P. Linnartz, "Multi-carrier CDMA in an indoor wireless radio channel," *Report from University of Carlifornia at Berkeley*.

[63] "http://buffy.eecs.berkeley.edu/~linnartz/wireless/indexmccdma.html," Links to MC-CDMA.

[64] R. Prasad and S. Hara, "An overview of multi-carrier CDMA," *IEEE Spread Spectrum Techniques and Applications Proceedings*, vol. 1, pp. 107–114, 1996.

[65] www.flarion.com, "Website of Flarion."

[66] C. Z. W. H. Sweatman, B. Mulgrew, J. S. Thompson, and P. M. Grant, "Multiuser detection for CDMA antenna array receivers using spatial equivalence classes," *IEE Proceedings on Communications*, vol. 147, pp. 105–113, April 2000.

[67] C. Z. W. H. Sweatman, J. S. Thompson, and P. M. G. B. Mulgrew, "Multiuser detection for CDMA antenna array receivers," *IEEE Global Telecommunications Conference*, vol. 1, pp. 237–240, Nov 1998.

[68] N. Oikonomopoulos and P. A. Cosimini, "System level performance of multi-user detection for W-CDMA," *IEE 3G 2002 Mobile Communication Technologies Conference*, pp. 276–280, May 2002.

[69] A. C. McCormick, P. M. Grant, and J. S. Thompson, "Hybrid uplink multi-carrier CDMA interference cancellation receiver," *IEE Communication Proceedings*, vol. 148, pp. 119–124, April 2001.

[70] G. J. Foschini and M. J. Gans, "On limits of wireless communications in a fading environment when using multiple antennas," *Wireless Personal Communications*, vol. 6, pp. 311–335, 1998.

[71] I. E. Telatar, "Capacity of multi-antennas Gaussian channels," *AT&T Bell Labs internal report*, June 1995.

[72] M. S, "Multi-user detection for DS-CDMA communications," *IEEE Communications Magazine*, vol. 34, pp. 124–136, Oct 1996.

[73] J. H. Winters, J. Salz, and R. D. Gitlin, "The impact of antenan diversity on the capacity of wireless communication systems," *IEEE Transactions on Communications*, vol. 42, pp. 1740–1751, Feb/Mar/April 1994.

[74] S. R. Saunders, *Antennas and Propagation for Wireless Communication Systems*. John Wiley and Sons, 1st ed., 1999.

[75] J. P. Kermoal, L. Schumacher, K. I. Pedersen, P. E. Mogensen, and F. Frederiksen, "A stochastic MIMO radio channel model with experimental validation," *IEEE Journal on Selected Areas in Communications*, vol. 20, pp. 1211–1226, Aug 2002.

[76] L. Schumacher, K. I. Pedersen, and P. E. Mogensen, "From antenna spacings to theoretical capacities - guidelines for simulating MIMO systems," *IEEE Personal, Indoor and Mobile Radio Communications*, vol. 2, pp. 587–592, Sept 2002.

[77] W. M. Younis, A. H. Sayed, and N. Al-Dhahir, "Efficient adaptive receivers for joint equalization and interference cancellation in multiuser space-time block-coded systems," *IEEE Transactions on Signal processing*, vol. 51, pp. 2849–2862, November 2003.

[78] D. Chizhik, F. Rashid-Fanokhi, J. Ling, and A. Lozano, "Antenna separation and capacity of BLAST in correlated channels," *IEEE Antennas and Propagation for Wireless Communications Conference*, pp. 183–185, Nov 2000.

[79] M. M. Wang, X. Weimin, and T. Brown, "Soft decision metric generation for QAM with channel estimation," *IEEE Transactions on Communications*, vol. 50, pp. 1058–1061, July 2002.

[80] J. H. Winters, "Smart antenna for wireless systems," *IEEE Personal Communications*, vol. 5, pp. 23–27, February 1998.

[81] Z. Guo and W. Zhu, "Performance study of OFDMA vs. ofdm/sdma," *IEEE Vechicular Technology Conference*, vol. 1, pp. 171–174, Sept 2002.

[82] P. Vandenamellel, L. V. D. Perre, M. G. E. Engels, B. Gyselinckx, and H. J. D. Man, "A combined OFDM/SDMA approach," *IEEE Journal on Selected Areas in Communications*, vol. 18, pp. 2312–2321, Nov 2000.

[83] P. W. Wolniansky, G. J. Foschini, G. D. Golden, and R. A. Valenauela, "V-BLAST:An architecture for realizing very high data rates over the rich-scattering wireless channel," *Signals, Systems, and Electronics, ISSSE-98*, pp. 295–300, September 1998.

[84] L. Ren, S. Xi, and J. Song, "Interference cancellation technology in MIMO cellular communications systems," *IEEE Electrical and Computer Engineering, CCECE*, vol. 3, pp. 1941–1944, May 2003.

[85] Y. Li, "Simplified channel estimation for OFDM systems with multiple transmit antennas," *Wireless Communications, IEEE Transactions*, vol. 1, pp. 67–75, January 2002.

[86] T. A. Tran and A. B. Sesay, "A generalized linear quasi-ML decoder of OSTBCs for wireless communications over time-selective fading channels," *IEEE Transactions on Wireless Communications*, May.

[87] J. Gao and M. Faulkner, "On implementation of bit-loading algorithms for OFDM systems with multiple-input multiple-output," *IEEE Vehicular Technology Conference Proceedings*, vol. 1, pp. 199–203, September 2002.

[88] "IEEE P802.11, Wireless LANs, TGn channel models, doc.: IEEE 802.11-03/940r2," January 2004.

[89] V. Rhodes, "Path loss proposal for the IEEE 802.11 HTSG channel model ad hoc group," January 2004.

[90] E. Viterbo and J. Bouros, "A universal lattice code decoder for fading channels," *IEEE Transactions on Information Theory*, vol. 45, pp. 1639–1642, July 1999.

Appendix A
Power Delay Profile of Hiperlan Channel A

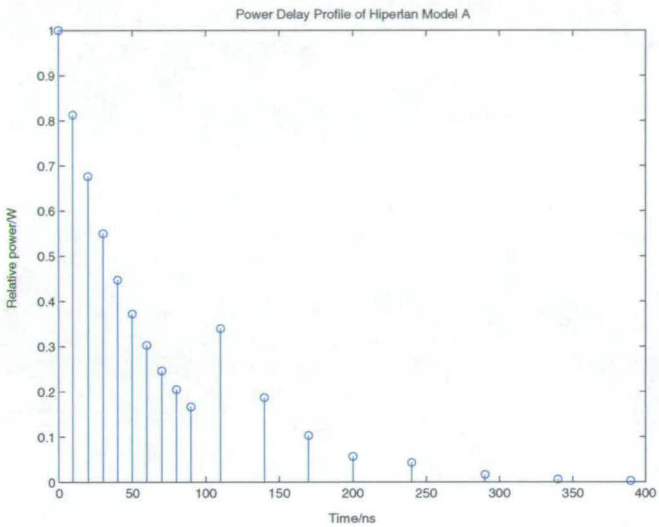

Figure A.1: *Power Delay Profile of Hiperlan Model A*

Appendix B
Comparison Between OFDM and SC-FE From Exisiting Literatures

This appendix provides detailed explanation upon which the comparison between OFDM and SC-FE has been summarised in Section 2.3

The comparison is made in [26] of 16QAM SC-LE, 16QAM OFDM and adaptive OFDM modulation from the range tabulated in Table B.1. This adaptive modulation works to optimise the power spectrum and distribution of bits simultaneously. This results in the same signal-to-noise-ratio (SNR) margin across all sub-carriers. The scenario assumes a non line-of-sight (NLOS) indoor environment. No outer coding is employed. For a BER value of 10^{-3}, 16QAM OFDM requires a SNR value of 38.2 dB, which is 7.4 dB higher than SC-LE. The adaptive modulated OFDM system requires only 25.5 dB.

Modulation schemes	Number of bits
2-PSK	1
4-PSK	2
8QAM	3
16QAM	4
32QAM	5
64QAM	6
128QAM	7
256QAM	8

Table B.1: *Modulation schemes used for adaptive OFDM*

In contrast to uncoded systems, [27] shows a similar comparison but this time with a forward error correcting code (FEC). The FEC employed is a convolutional code with code rate 1/2 and constraint length 7. This coding is applied with frequency domain interleaving to allow SNR averaging. The impulse response of the channel is represented by (0.04, -0.05, 0.07, -0.21, -0.5, 0.72, 0.36, 0.0 0.21, 0.03, 0.07). For a BER value of 10^{-3}, uncoded OFDM requires an SNR of approximately 15 dB, SC-LE 9.2 dB while coded OFDM 5 dB and coded SC-LE 4.8 dB.

In [2], the performance of three coded systems, namely SC-LE, OFDM and SC-DFE are investigated for three different code rates with QPSK. The SNR results for a BER value of 10^{-3} are tabulated in Table B.2. The performance of OFDM is slightly better than SC-LE for low code rates. This is because the OFDM system is able to exploit more frequency diversity from the outer channel coder. However, as the code rate increases, SC-LE eventually outperforms OFDM. This paper also shows that SC-DFE outperforms the former two on all occasions at the expense of higher complexity. Using higher code rate leads to an increase in transmission power as the required SNR to achieve the desired error probability is higher. The simulation is performed in a SUI-5 channel which is a test channel model for the IEEE 802.16 standard. IEEE 802.16 is a standard defined for wireless access to home users.

Technique	rate 2/3	rate 3/4	rate 7/8
OFDM	16.9 dB	19.8 dB	23.6 dB
SC-LE	17.1 dB	18.9 dB	21.2 dB
SC-DFE	11.8 dB	16.8 dB	18.3 dB

Table B.2: *SNR comparison between the 3 techniques for various convolutional code rate with BER value of* 10^{-3} *for QPSK modulated data*

Also in [2], the effect of different modulation schemes with code rate 1/2 for the SUI-5 model using the three previously mentioned receivers is investigated. The results are shown in Figure B.1. This graph illustrates that for low order modulation schemes, the discussion in the previous paragraph holds. However as the modulation order increases, the BER performance of OFDM moves closer to SC-DFE. The graph shows that for a 64 QAM modulated data, the performance of OFDM is similar to SC-DFE. This graph also shows that the BER performance of SC-LE degrades with higher order modulation as compared to OFDM.

SC-LE without coding can outperform OFDM significantly. However, in WLAN the use of FEC to correct channel errors combined with the use of high modulation order to increase data throughput is desirable. In this case, OFDM would be the ideal choice for a better performance.

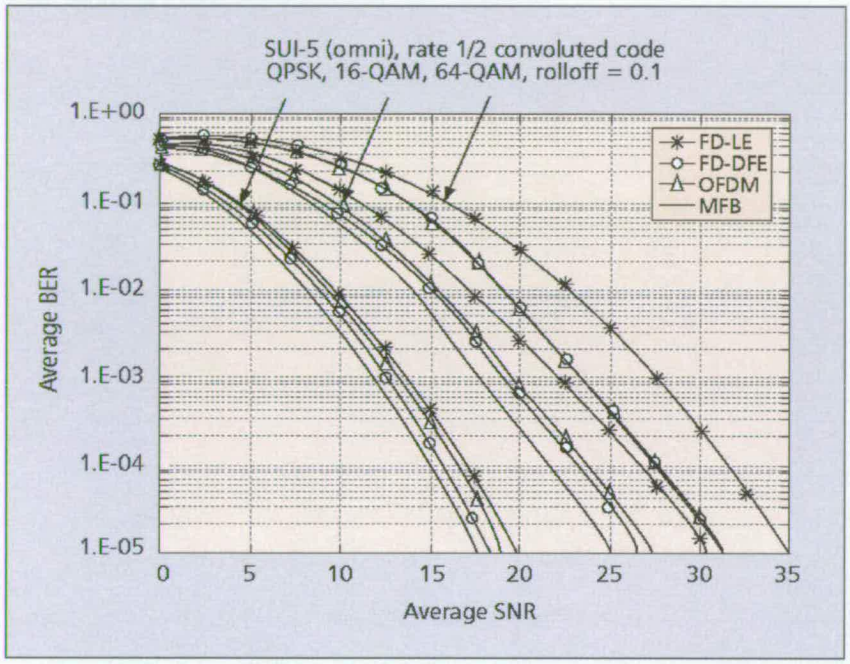

Figure B.1: *Comparison between SC-LE, OFDM and SC-DFE for various modulation schemes, figure copied from [2]*

Appendix C

Comparison Between OFDM and MC-CDMA From Exisiting Literatures

This appendix provides detailed explanation upon which the comparison between OFDM and MC-CDMA has been summarised in Section 2.6

Based on three papers [29–31], this section compares some properties of MC-CDMA and orthogonal frequency division multiple access (OFDMA). The performance of OFDMA can be thought to be similar to that of an OFDM system supporting multiple users.

A comparison on the effect of the number of receive antennas [29] comparing the performance of both systems without coding is simulated in an indoor environment. The SNR values corresponding to 1% BER from the graphs in this paper are tabulated in Table C.1. The results show that MC-CDMA has a multiple dB advantage over OFDMA in a single antenna system because of the inherent frequency diversity gain in MC-CDMA. However, as the number of antennas increases, this advantage gradually diminishes. In the paper, with the use of 4 antennas, MC-CDMA with a higher complexity is 0.1 dB better than OFDMA. This is because for a fixed power transmission, MC-CDMA can exploit frequency selective fading much more effectively than OFDMA in a single antenna system. However, this effect will decrease when multiple antennas are used as OFDMA can now exploit spatial diversity effectively. Hence when multiple antennas are implemented, OFDMA is preferable, having a low complexity and cost.

No. of receiver antennas	OFDMA	MC-CDMA
1	15 dB	10 dB
2	14 dB	8.7 dB
3	8.2 dB	7.6 dB
4	7.7 dB	7.6 dB

Table C.1: *Comparison of the SNR needed for OFDMA and MC-CDMA as the number of receiver antennas vary for a BER value of* 10^{-2}

During a transmission, it is preferable to load the system fully to maximise capacity. In this paper [30] the effect of loading on both systems in a frequency selective channel, where 32 users represent a full load is analysed. Each carrier is assumed to be narrowband and is modelled as a flat fading channel. A convolutionally coded BPSK signal of rate 1/2 with generator (133, 171) was used in the simulation. Table C.2 shows some results from the graph in the paper of BER vs number of users for SNR value 8 dB. These values are plotted in Figure C.1. When the system is fully loaded, the performance of MC-CDMA is very similar to OFDMA. On the other hand, with partial loading, MC-CDMA significantly outperforms the BER performance of OFDMA. With partial loading, the interference between spreading codes is less, therefore the performance is better. The absence of spreading sequence means that OFDMA is insensitive to of system loading.

No. of users	BER of OFDMA	BER of MC-CDMA
5	5e-3	7e-5
10	5e-3	1.8e-4
15	5e-3	4.5e-4
20	5e-3	9.5e-4
25	5e-3	2e-3
30	5e-3	3e-3
32	5e-3	4.2e.3

Table C.2: *Comparison of OFDMA with MC-CDMA for various loading*

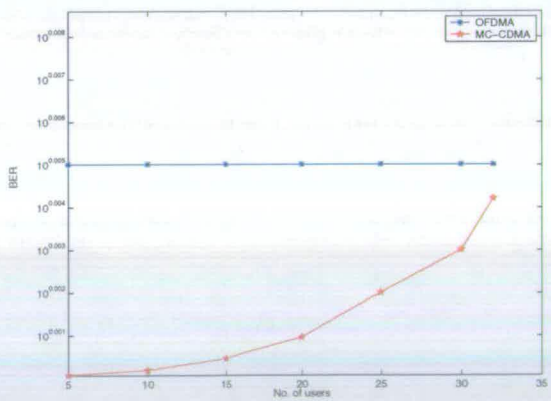

Figure C.1: *Comparison of OFDMA and MC-CDMA for various loading*

Lastly [31] discusses the issue of multiple cell systems. The channel model in this simulation uses 3 path groups, with each path group comprising 8 independent Rayleigh fading paths. In the multi-cell environment, a hexagonal layout is assumed, where users are uniformly distrib-

uted. The propagation model has distance dependent path loss with decay factor of 4.0 and log-normally distributed random path loss (shadowing) with 8 dB standard deviation and correlation factor of 0.5 among cells. When MC-CDMA is used in the simulation, a frequency reuse of 1 among the neighbouring 6 cells is assumed. When OFDM is used, a frequency reuse of 3 cells is assumed with interference coming from the nearest 6 neighbouring cells. Turbo coding with code rate 1/2 and constraint length 4 is applied to all QPSK modulated data. In the isolated cell simulation, for a BER value of 10^{-3}, OFDM has a SNR value of 7.6 dB which is 1.2 dB better than MC-CDMA with processing gain G_p=4. OFDM outperforms MC-CDMA in an isolated cell due to the absence of inter-code interference in OFDM. In the multi-cell scenario, the link capacity is compared. Due to the three cell frequency reuse in OFDM, MC-CDMA has a capacity 1.36 times higher than that of OFDM. This is because the effect of inter-cell interference is more significant as compared to inter-code interference in a multi cell environment, MC-CDMA allows universal frequency reuse, regardless of the number of cells.

To summarise the comparison, MC-CDMA can exploit frequency diversity more effectively than OFDM unless multiple antennas are used. However, the capacity of multiple users OFDM and MC-CDMA systems is very similar. Also, in a large environment which consists of several cells, MC-CDMA is more efficient because of universal frequency reuse in every cell.

Appendix D
Coefficients of BEP of QAM constellations

BPSK	$\{(1,2)\}$
QPSK	$\{(1,1)\}$
16QAM	$\{(\frac{3}{4},\frac{1}{5}),(\frac{2}{4},\frac{3^2}{5}),(-\frac{1}{4},\frac{5^5}{5})\}$
64QAM	$\{(\frac{7}{12},\frac{1}{21}),(\frac{6}{12},\frac{3^2}{21}),(\frac{-1}{12},\frac{5^2}{21}),(\frac{1}{12},\frac{9^2}{21}),(\frac{-1}{12},\frac{13^2}{21})\}$

Appendix E

Generation of Correlation Matrix For Space Time Block Code

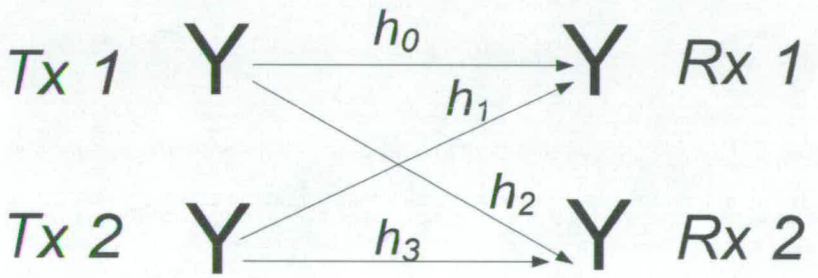

Figure E.1: *(2,2) Alamouti STBC*

Assume a (2,2) Alamouti STBC structure as in Figure E.1, the channel spanned by this configuration can be expressed as:

$$\mathbf{H_A} = \begin{bmatrix} h_0 & h_1 \\ h_1^* & -h_0^* \\ h_2 & h_3 \\ h_3^* & -h_2^* \end{bmatrix} \tag{E.1}$$

Given that the covariance matrix at the receiver can be expressed as :

$$\kappa_r = E(|\mathbf{H_A}^H \mathbf{H_A}|^2) \tag{E.2}$$

where $E(|.|)$ denotes the expectation of the absolute values of every element in the matrix.

Expanding equation (E.2)

$$\begin{aligned}\kappa_r &= E\left(\left\|\begin{bmatrix} h_0 & h_1 \\ h_1^* & -h_0^* \\ h_2 & h_3 \\ h_3^* & -h_2^* \end{bmatrix}\begin{bmatrix} h_0^* & h_1 & h_2^* & h_3 \\ h_1^* & -h_0 & h_3^* & -h_2 \end{bmatrix}\right\|\right) \\ &= E\left(\left\|\begin{bmatrix} A & 0 & B & C \\ 0 & A & -C^* & B^* \\ B^* & -C & D & 0 \\ C^* & B & 0 & D \end{bmatrix}\right\|\right) \end{aligned} \tag{E.3}$$

where

$$\begin{aligned} A &= |h_o|^2 + |h_1|^2 \\ B &= h_o h_2^* + h_1 h_3^* \\ C &= h_0 h_3 - h_1 h_2 \\ D &= |h_2|^2 + |h_3|^2 \end{aligned} \tag{E.4}$$

From equation (E.4), it is obvious that both A and D are non-zero values, which is the autocorrelation for both Rx 1 and Rx 2. Given the relationship between two correlated values a and b are as follows:

$$E(|ab^*|) = c \tag{E.5}$$

$$E(|ab|) = 0 \tag{E.6}$$

where c is a non-zero value.

Therefore, B will result in a non-zero value which is the cross-correlation coefficient between two channels while C goes to zero.

Hence, the equation in (E.3) can be further formulated to obtained the normalised covariance

matrix at the reciever as:

$$\boldsymbol{\kappa_r} = \begin{bmatrix} \kappa_{0,0} & 0 & \kappa_{0,1} & 0 \\ 0 & \kappa_{0,0} & 0 & \kappa_{0,1} \\ \kappa_{0,1} & 0 & \kappa_{1,1} & 0 \\ 0 & \kappa_{0,1} & 0 & \kappa_{1,1} \end{bmatrix} \tag{E.7}$$

Appendix F
Improvement In Diversity Gain For Different Gains' Factors

This appendix shows the decrease in performance for subsequent gain in diversity order.

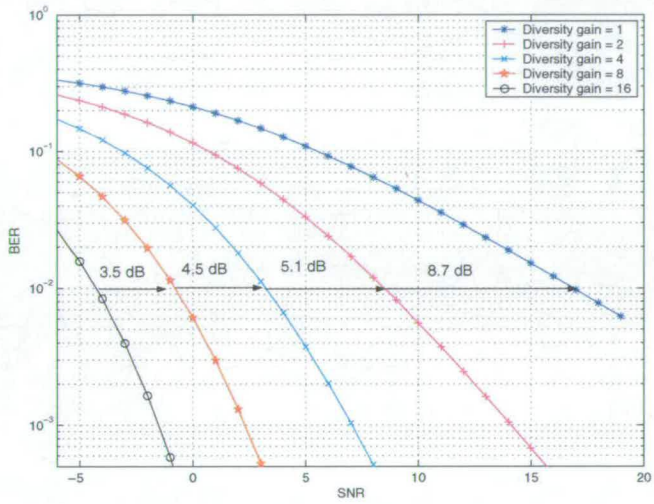

Figure F.1: *Diversity gain for a QPSK system*

Figure F.1 shows the theoretical performance of a 1 Tx QPSK system in a Rayleigh fading scenerio. At the receiver MRC is employed to achieved a 2^N fold diversity gain. It can be seen that as the diversity order increases from 1 to 16 in steps of 2^N, the diversity order decreases gradually from 8.7 dB, 5.1 dB, 4.5 dB to 3.6 dB. Therefore it increasing diversity higher than four does not gives much significant improvement in performance.

Appendix G
Proof Of Orthogonality Structure in the MMSE POSTBC

From equation (6.11),

$$\mathbf{Z} = \mathbf{h}_1^H \mathbf{h}_2 + \mathbf{h}_3^H \mathbf{h}_4 + \mathbf{h}_5^H \mathbf{h}_6 \tag{G.1}$$

where

$$\mathbf{h}_1^H \mathbf{h}_2 = \begin{bmatrix} h_{0,0}^* & h_{0,1} \\ h_{0,1}^* & -h_{0,0} \end{bmatrix} \begin{bmatrix} h_{0,2} & 0 \\ 0 & h_{0,2}^* \end{bmatrix} \tag{G.2}$$

$$= \begin{bmatrix} h_{0,0}^* h_{0,2} & h_{0,1} h_{0,2}^* \\ h_{0,1}^* h_{0,2} & -h_{0,0} h_{0,2} \end{bmatrix} \tag{G.3}$$

$$\mathbf{h}_3^H \mathbf{h}_4 = \begin{bmatrix} h_{1,0}^* & h_{1,1} \\ h_{1,1}^* & -h_{1,0} \end{bmatrix} \begin{bmatrix} h_{1,2} & 0 \\ 0 & h_{1,2}^* \end{bmatrix} \tag{G.4}$$

$$= \begin{bmatrix} h_{1,0}^* h_{1,2} & h_{1,1} h_{1,2}^* \\ h_{1,1}^* h_{1,2} & -h_{0,0} h_{1,2} \end{bmatrix} \tag{G.5}$$

$$\mathbf{h}_3^H \mathbf{h}_4 = \begin{bmatrix} h_{1,0}^* & h_{1,1} \\ h_{1,1}^* & -h_{1,0} \end{bmatrix} \begin{bmatrix} h_{1,2} & 0 \\ 0 & h_{1,2}^* \end{bmatrix} \tag{G.6}$$

$$= \begin{bmatrix} h_{1,0}^* h_{1,2} & h_{1,1} h_{1,2}^* \\ h_{1,1}^* h_{1,2} & -h_{1,0} h_{1,2} \end{bmatrix} \tag{G.7}$$

$$\mathbf{h}_5^H \mathbf{h}_6 = \begin{bmatrix} h_{2,0}^* & h_{2,1} \\ h_{2,1}^* & -h_{2,0} \end{bmatrix} \begin{bmatrix} h_{2,2} & 0 \\ 0 & h_{2,2}^* \end{bmatrix} \tag{G.8}$$

$$= \begin{bmatrix} h_{2,0}^* h_{2,2} & h_{2,1} h_{2,2}^* \\ h_{2,1}^* h_{2,2} & -h_{2,0} h_{2,2} \end{bmatrix} \tag{G.9}$$

Expanding equation (G.1),

$$\mathbf{Z} = \begin{bmatrix} h_{0,0}^* h_{0,2} + h_{1,0}^* h_{1,2} + h_{2,0}^* h_{2,2} & h_{0,1} h_{0,2}^* + h_{1,1} h_{1,2}^* + h_{2,1} h_{2,2}^* \\ h_{0,1}^* h_{0,2} + h_{1,1}^* h_{1,2} + h_{2,1}^* h_{2,2} & -h_{0,0} h_{0,2}^* - h_{1,0} h_{1,2}^* - h_{2,0} h_{2,2}^* \end{bmatrix} \tag{G.10}$$

and that

$$\mathbf{Z}^H = \begin{bmatrix} h_{0,0} h_{0,2}^* + h_{1,0} h_{1,2}^* + h_{2,0} h_{2,2}^* & h_{0,1} h_{0,2}^* + h_{1,1} h_{1,2}^* + h_{2,1} h_{2,2}^* \\ h_{0,1}^* h_{0,2} + h_{1,1}^* h_{1,2} + h_{2,1}^* h_{2,2} & -h_{0,0}^* h_{0,2} - h_{1,0}^* h_{1,2} - h_{2,0}^* h_{2,2} \end{bmatrix} \tag{G.11}$$

Therefore

$$\mathbf{Z}\mathbf{Z}^H = c_3 \mathbf{I}_2 \tag{G.12}$$

where

$$c_3 = |h_{0,0}^* h_{0,2} + h_{1,0}^* h_{1,2} + h_{2,0}^* h_{2,2}|^2 + |h_{0,1}^* h_{0,2} + h_{1,1}^* h_{1,2} + h_{2,1}^* h_{2,2}|^2 \tag{G.13}$$

Appendix H
Simplified Joint Detection

Applying the APP optimum detector directly to equation (6.7) would require jointly detecting N_{cons}^4 bits to decode all transmitted bits per subcarrier. This exhaustive search increases exponentially as the modulation order gets higher. Premultiplying a weighting matrix, that will be introduced in this section, allows this exhaustive search to be reduced significantly from N_{cons}^4 to $2N_{cons}^2$. This reduction is significant especially when a high order modulation is used. The weighting matrix is chosen such that the resultant channel from one of the Alamouti symbols is decoupled from both the other Alamouti symbol and one of the other non-Alamouti symbols. The two groups of decoupled symbols can then be decoded independently from each other.

An example of the selected weighting matrix when multiplied by the received signal, decouples x_0 and x_2 from x_1 and x_3 is:

$$\mathbf{w}_{APP} = \begin{bmatrix} h_{1,1} & 0 & -h_{0,1} & 0 & 0 & 0 \\ h_{2,1} & 0 & 0 & 0 & -h_{0,1} & 0 \\ 0 & 0 & h_{2,1} & 0 & -h_{1,1} & 0 \\ 0 & h_{1,1}^* & 0 & -h_{0,1}^* & 0 & 0 \\ 0 & h_{2,1}^* & 0 & 0 & 0 & -h_{0,1}^* \\ 0 & 0 & 0 & h_{2,1}^* & 0 & -h_{1,1}^* \end{bmatrix} \tag{H.1}$$

Multiplying $\mathbf{w}_{APP}$ by the received signal (6.7) yields

$$\mathbf{w}_{APP}\mathbf{r} = \begin{bmatrix} c_6 & 0 & c_7 & 0 \\ c_8 & 0 & c_9 & 0 \\ c_{10} & 0 & c_{11} & 0 \\ 0 & c_{12} & 0 & c_{13} \\ 0 & c_{14} & 0 & c_{15} \\ 0 & c_{16} & 0 & c_{17} \end{bmatrix} \begin{bmatrix} x_0 \\ x_1 \\ x_2 \\ x_3 \end{bmatrix} + \mathbf{w}_{APP}\boldsymbol{\eta} \tag{H.2}$$

Referring to equation (H.2), it can be seen that x_0 and x_2 can be jointly detected independently

from x_1 and x_3 (and vice versa). This weighting matrix when multiplied by the received signal adds an extra spatial freedom to the number available received streams relative to the transmitted streams, as compared to the jointly detecting the symbols directly from (6.5), where three unknowns are jointly detected from three available signals. However, the trade off with this reduced APP detection results in the noise being coloured. The weighting matrix chosen merely shows one example of jointly detecting x_0 and x_2 and x_1 and x_3 concurrently. The weighting matrix can be modified such the a permutation of any two symbols, one from the Alamouti and the other from the non-Alamouti streams can be selected for joint detection. Increasing the number of receive antennas would create more spatial degrees of freedom at the receiver relative to the transmitter.

Appendix I
Full Range MCS simulation

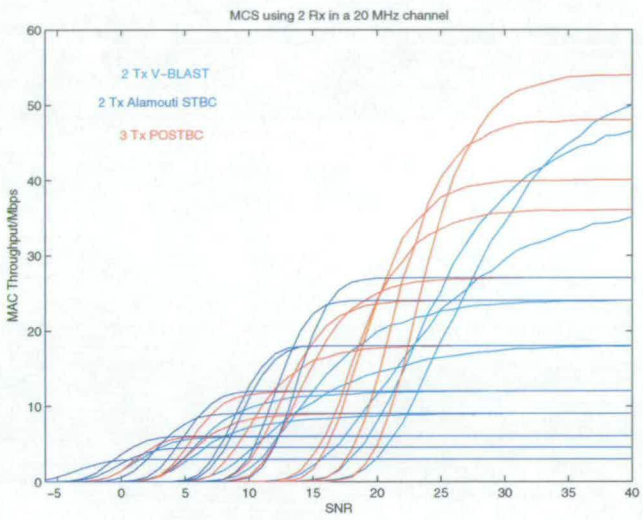

Figure I.1: *MAC throughput vs SNR of the MCS using 2 Rx in F_c(C,D) channel*

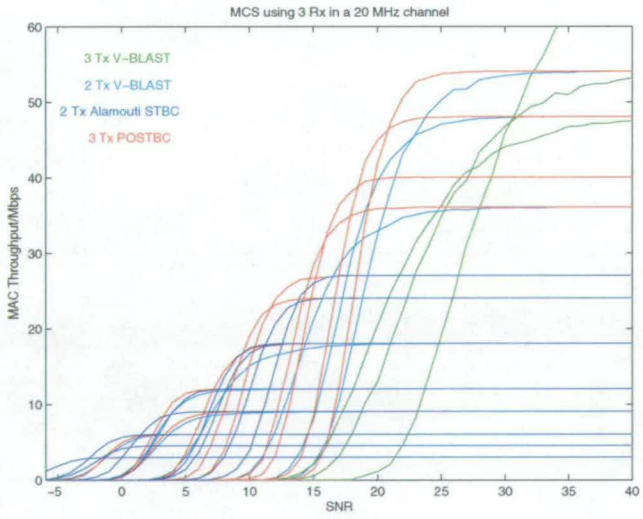

Figure I.2: *MAC throughput vs SNR of the MCS using 3 Rx in F_c(C,D) channel*

Appendix J
List of Publications

Patent

- H.S. Tan and Y. Sun , "Spatial Multiplexing for MIMO devices", UK patent, 0410644.9, filed 12th May 2004

Journal

- H.S. Tan, Y. Sun and J.S. Thompson, "Space Time Hybrid Transmit Diversity For Future Wireless LAN", submitted to IEEE Transaction on Communcations.

Conference

- H.S.Tan, Y.Sun and J.S. Thompson, "Performance Analysis of Layered Space Time Block Code For Future Wireless LAN", accepted for publication in IEEE VTC Fall 2004
- H.S.Tan, Y.Sun and J.S. Thompson, "Comparison of Robustness of MIMO Schemes In the Presence of Interference", accepted for publication in ISWCS 2004
- H.S.Tan, J.S. Thompson and D.G.M. Cruickshank "On the performance of opportunistic beamforming", Proc.of IEE 3G 2003, pg 428-431.
- H.S. Tan and J.S. Thompson, "Diversity technique for smart antennas using maximal ratio combining" Proc. of PG Net 2002
- Y.Sun, H.S. Tan and J.S. Thompson, "Analysis of Space-Time and Space-Frequency Transmitter Diversity Techniques for Boradband OFDM systems", submitted to PIMRC 2005.
- J.S. Thompson, H.S.Tan and Y.Sun, "Investigation of Hybrid MIMO Techniques", accepted for IEE 3G 2004
- H.S. Tan, Y. Sun and J.S. Thompson, "Non-orthogonal Space Time Transmit Diversity For Future Wireless LAN", submitted to IEEE Globecom 2005.

Performance Analysis of Layered Space-Time Block Code For Future WLAN

H.S. Tan*, Y. Sun† and J.S. Thompson‡
* ‡ Institute of Digital Communications
School of Engineering and Electronics, University of Edinburgh,
King's Buildings, Mayfield Road, Edinburgh EH9 3JL, United Kingdom
Email hst@ee.ed.ac.uk, jst@ee.ed.ac.uk
* † Toshiba Research Europe Limited, 32 Queens Square
Bristol BS1 4ND, United Kingdom
Email Sun@toshiba-trel.com

Abstract— **The demand for high data rates and low implementation complexity form two of the prerequisites for future wireless local area networks. The V-BLAST architecture and the Alamouti space time block code are two strong candidates for this particular implementation. The drawback of V-BLAST is its poor performance in correlated fading channels and for Alamouti STBC, the spectral efficiency is generally poorer than V-BLAST. Trying to overcome these problems leads to the hybrid V-BLAST/Alamouti scheme. Instead of decoupling antennas for separate detection, each transmitted stream is treated as a layer and detected successively using the ordered successive interference cancellation algorithm. In this paper, we investigate the frame error performance of this hybrid scheme with respect to three parameters, namely fading channel correlation, number of receive antennas used and spectral efficiency. The hybrid's error performance is compared to the V-BLAST and the Alamouti STBC schemes.**

I. Introduction

Support for high data rates and low implementation complexity form two of the prerequisites for future wireless local area networks (WLAN), and in particular for candidate architectures for the IEEE 802.11n working group. Spatial multiplexing and space time block code (STBC) techniques by virtue of their multiple input and multiple output (MIMO) structure are attractive schemes to fulfil the two requirements. Specifically, Alamouti STBC [1], V-BLAST [6] and Damen STBC [2] are three MIMO candidates that can achieve favourable link layer performance. Despite its high performance and data rate, Damen codes are not considered further here due to the use of a non linear lattice decoding receiver.

It is known that V-BLAST is potentially vulnerable to correlated fading channels, while Alamouti STBC is incapable of achieving high spectral efficiency as compared to V-BLAST. This leads to the hybrid of these two MIMO schemes which has been proposed in [4] to exploit the diversity gain and high spectral efficiency of both schemes. By doing so, the number of receive antennas to successfully separate the transmitted streams using the zero forcing (ZF) or minimum mean square error (MMSE) estimate is halved compared to V-BLAST for the same number of transmitters.

In this paper, we study the performance of this hybrid V-BLAST/Alamouti scheme implemented in a wireless LAN environment. Instead of decoupling the Alamouti pair for individual decoding, we suggest as in [5] that each transmit antenna(Tx) can be treated as a layer and successively decoded by means of the ordered successive interference cancellation (OSIC) algorithm. We call this technique layered Alamouti STBC (LASTBC). The frame error ratio (FER) performance of LASTBC will be compared with V-BLAST and Alamouti STBC with respect to three parameters, namely, spectral efficiency, number of receive antennas employed and the channel correlation, which will be significant when considering future MIMO wireless LAN implementation.

Section II describes the channel and system model used in this study. The MIMO schemes are also introduced in here while their simulation performance based on the above criteria are illustrated in Section III. Lastly, the conclusions are presented in Section IV.

II. System Model

Consider a MIMO OFDM system with M and N transmitting and receiving antennas respectively, - the (M, N) system. The received signal at each subcarrier can be expressed as:

$$\mathbf{r} = \mathbf{H}\mathbf{x} + \boldsymbol{\eta} \tag{1}$$

where $\mathbf{r}$ and $\boldsymbol{\eta}$ are the received signal and noise vector of size Nx1 respectively. The vector $\mathbf{x}$ is the Mx1 transmitted signal vector and $\mathbf{H}$ the size NxM channel matrix.

Prior to the space-time encoding, blocks of randomly generated binary data are encoded using a rate R = 1/2, octal polynomials 133 171 convolutional code with a random interleaver. These coded bits are QAM mapped, OFDM modulated and encoded with its respective MIMO technique. A 20 MHz bandwidth quasi-static WLAN non line of sight (NLOS) channel with 10 ns sub-symbol spaced taps are used

in the simulator. At the receiver, the transmitted streams are spatially and temporally processed and decoded for a-posteriori information input to the Viterbi decoder.

A. Alamouti STBC

The Alamouti STBC two transmitter scheme encodes every two symbols spatially and temporally such that the resultant transmission matrix posses an orthogonal structure. The received signal in equation (1) can be mathematically formulated as:

$$\begin{bmatrix} r_{0,0} \\ r_{0,1} \\ \vdots \\ r_{N-1,0} \\ r_{N-1,1} \end{bmatrix} = \begin{bmatrix} h_{0,0} & h_{0,1} \\ h^*_{0,1} & -h^*_{0,1} \\ \vdots & \vdots \\ h_{N-1,0} & h_{N-1,1} \\ h^*_{N-1,1} & -h^*_{N-1,1} \end{bmatrix} \begin{bmatrix} x_0 \\ x_1 \end{bmatrix} + \begin{bmatrix} \eta_{0,0} \\ \eta_{0,1} \\ \vdots \\ \eta_{N-1,0} \\ \eta_{N-1,1} \end{bmatrix} \tag{2}$$

where $h_{n,m}$ is the channel response due to transmit antenna m at receiver n, x_m is the transmitted symbol from antenna m while $r_{n,t}$ and $\eta_{n,t}$ are the received signal and noise at receive antenna n during time t respectively.

The received signal in equation (2) can be combined to obtain an estimate for the transmitted symbols as:

$$\hat{\mathbf{x}} = \mathbf{H}^H \mathbf{r} \tag{3}$$

$$\begin{bmatrix} \hat{x}_0 \\ \hat{x}_1 \end{bmatrix} = \begin{bmatrix} \sum_{N-1}^{n=0} \sum_{m=0}^{1} |h_{n,m}|^2 & 0 \\ 0 & \sum_{N-1}^{n=0} \sum_{m=0}^{1} |h_{n,m}|^2 \end{bmatrix} \begin{bmatrix} x_0 \\ x_1 \end{bmatrix} + \mathbf{H}^H \eta \tag{4}$$

These estimated symbols can then be detected using the maximum likelihood (ML) detector given by:

$$\hat{d} = \underbrace{\text{argmin}}_{d_c} \left| \hat{x}_m - \left(\sum_{N-1}^{n=0} \sum_{m=0}^{1} h_{n,m} \right) d_c \right|^2 \tag{5}$$

where C is the total number of constellation points and $\mathbf{d} = [d_1 d_2 ..... d_C]$ is the vector of all possible points in the constellation.

B. V-BLAST

The V-BLAST scheme consists of M spatially multiplexed QAM modulators each attached to a transmit antenna. The received signal in equation (1) can be expressed as:

$$\begin{bmatrix} r_0 \\ \vdots \\ r_{N-1} \end{bmatrix} = \begin{bmatrix} h_{0,0} & \cdots & h_{0,M-1} \\ \vdots & \ddots & \\ h_{N-1,0} & \cdots & h_{N-1,M-1} \end{bmatrix} \begin{bmatrix} x_0 \\ \vdots \\ x_{M-1} \end{bmatrix} + \begin{bmatrix} \eta_0 \\ \vdots \\ \eta_{N-1} \end{bmatrix} \tag{6}$$

where $h_{n,m}$ is the channel response due to transmit antenna m at receiver n, x_m is the transmitted symbol from antenna m while r_n and η_n are the received signal and noise at receive antenna n respectively.

The received signal can be successively detected by employing the MMSE-OSIC [3] detector provided $N \geq M$. The OSIC algorithm is described as follows:

i) Determine the MMSE estimate of the channel matrix, $\mathbf{H}$ in equation (6). This is given by:

$$\mathbf{G} = (\mathbf{H}^H \mathbf{H} + \sigma_n^2 \mathbf{I})^{-1} \mathbf{H}^H \tag{7}$$

where σ_n^2 is the noise variance.

ii) Calculate the SNR of the m streams (m = 0 to M-1). Select the stream with the highest SNR

$$k = \underbrace{\text{argmax}}_{m}(\text{SNR}) \tag{8}$$

iii) Determine the weighting matrix of the highest SNR stream

$$\mathbf{w} = \mathbf{G}_m \tag{9}$$

where $\mathbf{G}_m$ denotes the m^{th} row vector

iv) Detect the m^{th} symbol.

$$y_m = \mathbf{w}\mathbf{r} \tag{10}$$

v) This decision statistic is quantised to its respective constellation point.

$$\hat{x}_m = Q(y_m) \tag{11}$$

vi) The effect of this estimated symbol is then subtracted from the received signal

$$\acute{\mathbf{r}} = \mathbf{r} - \mathbf{H}_m \hat{x}_m \tag{12}$$

where $\mathbf{H}_m$ is the m^{th} column vector of $\mathbf{H}$

vii) Null the m^{th} column of the channel matrix, $\mathbf{H}$

$$\mathbf{H}^- = \mathbf{H} - [0\,0 \ldots \mathbf{H}_m \ldots 0\,0] \tag{13}$$

viii) Calculate the MMSE estimate of the nulled channel

ix) Repeat the process from step (ii) until all the streams are detected.

C. LASTBC

The LASTBC scheme exploits the advantages of both the Alamouti STBC and V-BLAST schemes by concatenating blocks of Alamouti STBC. The received signal by concatenating two blocks of Alamouti STBC can be expressed as:

$$\begin{bmatrix} \mathbf{r}'_0 \\ \mathbf{r}'_1 \\ \vdots \\ \mathbf{r}'_{N-1} \end{bmatrix} = \begin{bmatrix} \mathbf{h}'_{0,0} & \mathbf{h}'_{0,1} \\ \mathbf{h}'_{1,0} & \mathbf{h}'_{1,1} \\ \vdots & \vdots \\ \mathbf{h}'_{N-1,0} & \mathbf{h}'_{N-1,1} \end{bmatrix} \begin{bmatrix} \mathbf{x}'_0 \\ \mathbf{x}'_1 \end{bmatrix} + \begin{bmatrix} \eta'_0 \\ \eta'_1 \\ \vdots \\ \eta'_{N-1} \end{bmatrix} \tag{14}$$

where

$$\mathbf{r'}_n = \begin{bmatrix} r_{n,\tau_0} \\ r^*_{n,\tau_1} \end{bmatrix} \qquad \boldsymbol{\eta}'_n = \begin{bmatrix} \eta_{n,\tau_0} \\ \eta^*_{n,\tau_1} \end{bmatrix}$$

$$\mathbf{x'}_m = \begin{bmatrix} x_{2m} \\ x_{2m+1} \end{bmatrix} \qquad \mathbf{h'}_{n,m} = \begin{bmatrix} h_{n,2m} & h_{n,2m+1} \\ h^*_{n,2m+1} & -h^*_{n,2m} \end{bmatrix}$$

where τ_t is the time index. Similarly the received signal in equation (14) can be detected using the OSIC algorithm as described in the previous subsection II.B. In this case, the ordering of streams for detection is based on a per Alamouti STBC block.

Assuming the minimum number of two antennas are used, the MMSE solution can be represented as [7]:

$$\mathbf{G} = \begin{bmatrix} \boldsymbol{\alpha}\boldsymbol{\beta}^* & -\boldsymbol{\alpha}\boldsymbol{\beta}^*\mathbf{h'}_{0,1}\mathbf{h'}^{-1}_{1,1} \\ -\boldsymbol{\gamma}\boldsymbol{\theta}^*\mathbf{h'}_{1,0}\mathbf{h'}^{-1}_{0,0} & \boldsymbol{\gamma}\boldsymbol{\theta}^* \end{bmatrix} \qquad (15)$$

where

$$\boldsymbol{\beta} = \mathbf{h'}_{0,0} - \mathbf{h'}_{0,1}\mathbf{h'}^{-1}_{1,1}\mathbf{h'}_{1,0}\,, \quad \boldsymbol{\theta} = \mathbf{h'}_{1,1} - \mathbf{h'}_{1,0}\mathbf{h'}^{-1}_{0,0}\mathbf{h'}_{0,1}$$

$$\boldsymbol{\alpha} = (\boldsymbol{\beta}^*\boldsymbol{\beta} + \sigma_n^2\mathrm{I})^{-1}, \quad \boldsymbol{\gamma} = (\boldsymbol{\theta}^*\boldsymbol{\theta} + \sigma_n^2\mathrm{I})^{-1}$$

III. Simulation Results

The results comparing Alamouti STBC, V-BLAST and LASTBC attaining spectral efficiencies of 2, 4 and 6 bits/s/Hz employing both two and four receive antennas are shown in Figure 1, 2 and 3 respectively.

Irrespective of the spectral efficiency attained by any of the three MIMO schemes, the 2 receive antennas V-BLAST scheme performs significantly worse than the other two schemes. The is due to the absence of transmit diversity in the V-BLAST scheme. Comparing the 4 receive antennas case for both the V-BLAST and LASTBC achieving 2, 4 and 6 bits/s/Hz, the SNR difference between both schemes at 1% or 10 % FER is approximately similar to each other with the performance favouring the LASTBC scheme. However, this difference becomes more apparent when 2 receive antennas are used at the receiving terminals. The difference in values at 10% FER are 4.7 dB, 6.2 dB and 7.3 dB for spectral efficiency 2, 4 and 6 bits/s/Hz respectively.

Eventhough the 4 receive antennas case of LASTBC scheme achieves a diversity double that of V-BLAST, the performance gain is not as significant as the 2 antennas case due to V-BLAST achieving an approximate diversity order of four fold. Further increase in diversity order higher than four would only achieve a slight enhancement in performance. Due to the lack of diversity being exploited in the V-BLAST 2 receive antenna case, its relative performance to LASTBC scheme is seen to be more sensitive to spectral efficiency. This is because the higher spectrally efficient system requires a larger constellation that results in more interference between the transmitted streams. In this case, the transmit diversity inherent in the LASTBC scheme is fully utilised to minimise the error probability.

The Alamouti STBC scheme performs better than both the V-BLAST and LASTBC schemes when two antennas are used at the receiver. The achievable diversity gain from the LASTBC scheme is minimum when two receive antennas are used, in addition to interference between the two Alamouti concatenated pairs. As the number of receive antennas increases, the LASTBC and V-BLAST schemes become more robust than Alamouti STBC because the latter scheme requires a larger constellation size to achieve the same spectral efficiency as compared to the other two MIMO techniques.

The results for comparing the 16 QAM (2,4) Alamouti STBC, QPSK (2,4) V-BLAST, BPSK (4,4) V-BLAST and QPSK (4,4) LASTBC schemes in a correlated fading channel are illustrated in Figure 4. In this simulation, the angular spread (AS) at the receiver is varied while the transmitter is fixed at an AS of 90^o. Note that there is an inverse relationship between correlation and AS so that low angular spread implies high correlation and vice versa. As expected, V-BLAST performance is significantly affected by low AS while Alamouti STBC is fairly robust to variations in correlation. The plots show that at low correlation (AS $>$ 100^o), the FER performance for LASTBC is approximately 2.0 dB better than the other techniques. However, at very low angular spread the LASTBC scheme suffers some degradation compared to Alamouti STBC. Comparing V-BLAST and LASTBC, LASTBC attains similar performance to Alamouti STBC at an AS of 50^o while V-BLAST requires a much higher AS of 115^o at the receiver to achieve similar performance. The robustness to correlation is due to the orthogonal nature of Alamouti STBC which makes each stream from the same Alamouti pair non-interfering unlike V-BLAST where every stream interferes with one another.

Similar simulations to the previous correlation study is shown in Figure 5, but this time the receiver correlation is fixed at an AS of 90^o while the transmit correlations are varied. The relative performance of each scheme is ordered similar to the previous case. Unlike the previous case, the (2,4) V-BLAST required SNR is observed to be less than the LASTBC for very low AS, approximately 30^o and less. This is because the number of transmit elements is doubled in the latter scheme, hence increasing its effective correlation as compared to two antenna transmit V-BLAST. Also, the LASTBC scheme requires an AS of 60^o to equal and outperform the performance of Alamouti STBC, which is 10^o more than the previous case. This can be explained by the MMSE beamformer being less able to spatially separate the more correlated transmitted streams.

IV. Conclusion

This paper compares the performance of three well known MIMO schemes, namely V-BLAST, Alamouti STBC and LASTBC which are potential candidates for future wireless LANs. The three parameters used for comparison are spectral efficiency, number of receive antennas and correlation. At low spectral efficiency, Alamouti STBC is preferred over the other two when two antennas are implemented at the receiver. Consequently, LASTBC becomes the best scheme when four antennas are available due to more diversity exploited and the setback suffered by Alamouti STBC when using a larger constellation size to attain the same spectral efficiency. The V-BLAST technique is significantly poorer than LASTBC and STBC when two receive antennas are used. Additionally, its relative performance gap to LASTBC widen as the spectral efficiency increases. Under the influence of correlation, V-BLAST requires a much lower channel correlation factor before it can achieve similar performance to or outperform the Alamouti STBC as compared to LASTBC. Also, LASTBC is more susceptible and less robust to variations in the AS at the transmitter than receiver.

Acknowledgment

HS Tan would like to express his sincere gratitude to Toshiba Research Europe Ltd Telecommunication Research Laboratory (Bristol) for funding his work.

References

[1] S. M. Alamouti, "A simple transmit diversity technique for wireless communications," *IEEE Journal Selected Areas in Communications*, vol. 16, no. 8, pp. 1451–1458, October 1998.

[2] M. O. Damen, A. Tewfik, and J. C. Belflore, "A construction of space-time code based on number theory," *IEEE Transactions on Infomation Theory*, vol. 48, no. 3, pp. 753–760, March 2002.

[3] M. Debbah, B. Muquet, M. deCourville, M. Muck, S. Simoens, and P. Loubaton, "A MMSE successive interference cancellation scheme for a new adjustable hybrid spread OFDM system," *IEEE Vechicular Technology Conference Proceedings*, vol. 2, pp. 745–749, Spring 2000.

[4] A. F. Naguib, N. Seshadri, and A. R. Calderbank, "Increasing data rate over wireless channels," *IEEE Signal Processing Magazine*, vol. 17, no. 3, pp. 76–92, May 2000.

[5] S. Rouquette-Leveil, K. Gosse, X. Zhuang, and F. W. Vook, "Spatial division multiplexing of space-time block codes," *International Conference on Communication Technology Proceedings, ICCT*, vol. 2, pp. 1343–1347, April 2003.

[6] P. W. Wolniansky, G. J. Foschini, G. D. Golden, and R. A. Valenauela, "V-BLAST:An architecture for realizing very high data rates over the rich-scattering wireless channel," *Signals, Systems, and Electronics,1998.ISSSE98 URSI International Symposium*, pp. 295–300, September 1998.

[7] W. M. Younis, A. H. Sayed, and N. Al-Dhahir, "Efficient adaptive receivers for joint equalization and interference cancellation in multiuser space-time block-coded systems," *IEEE Transactions on Signal processing*, vol. 51, no. 11, pp. 2849–2862, November 2003.

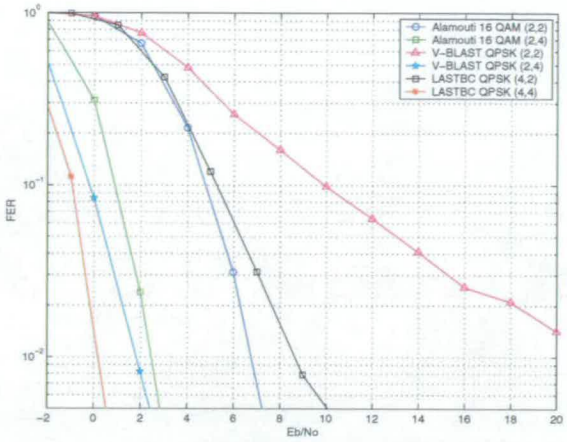

Fig. 1. FER vs SNR for spectral efficiency 2 bits/s/Hz

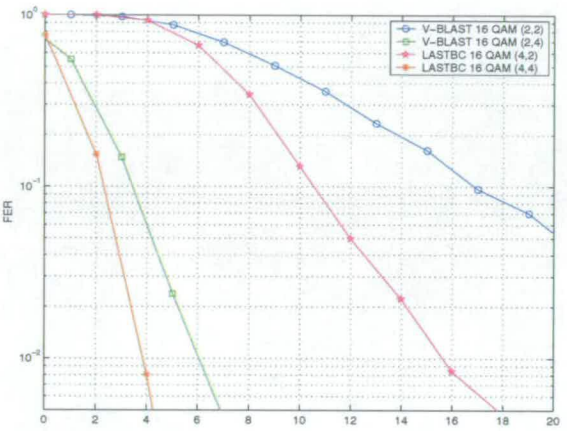

Fig. 2. FER vs SNR for spectral efficiency 4 bits/s/Hz

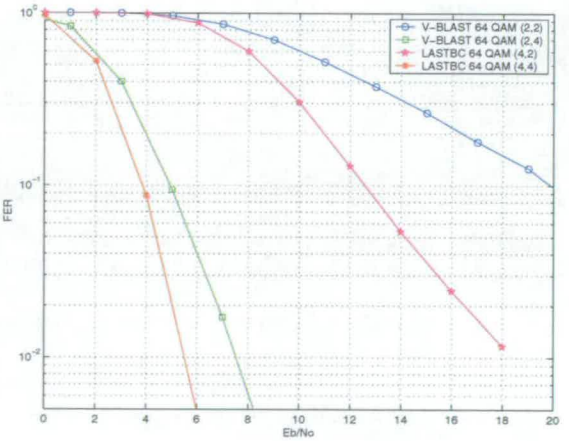

Fig. 3. FER vs SNR for spectral efficiency 6 bits/s/Hz

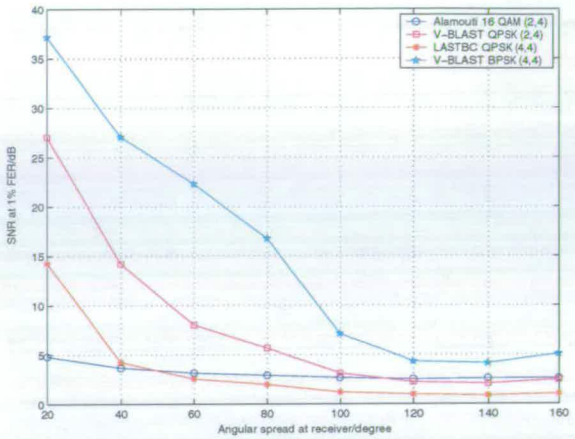

Fig. 4. Comparison of 3 MIMO schemes for different AS at the receiver

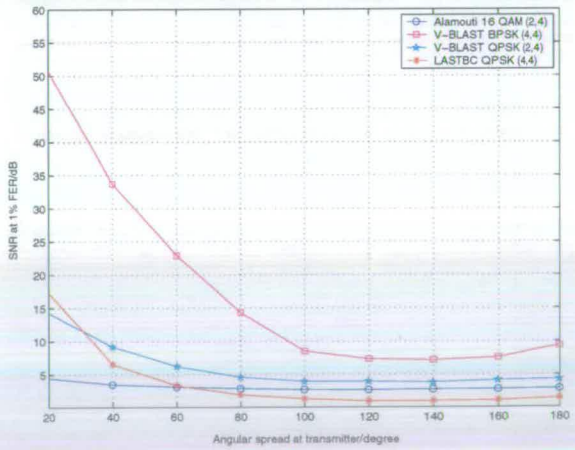

Fig. 5. Comparison of 3 MIMO schemes for different AS at the transmitter

Analysis of Sapce-Time and Space-Frequency Transmitter Diversity Techniques for Broadband OFDM Systems

Y. Sun[§], H. S. Tan[*] & J. S. Thompson[+]
[§*]Toshiba Research Europe Limited, 32 Queen Square, Bristol BS1 4ND, UK
[*+]IDCOM, School of Engineering & Electronics, University of Edinburgh, Edinburgh, EH9 3JL, UK

***Abstract*-Space-time and space-frequency diversity techniques become attractive for broadband orthogonal frequency division multiplexing (OFDM) systems due to their efficient implementation and high diversity gain. Two techniques that have been recently proposed for OFDM systems are cyclic delayed diversity (CDD) and space-frequency block coding (SFBC). This paper analyses these two different diversity concepts and their practical application. Also, a simplified algorithm for SFBC decoding is presented to push the frequency diversity gain even higher but with less complexity.**

***Keywords*-SFBC, CDD, STBC, space-frequency diversity, STBC, space-time diversity, diversity, diversity gain**

I. INTRODUCTION

The fundamental difficulty of a reliable wireless transmission is time-varying multipath fading. OFDM is a suitable technique for broadband transmission in multipath fading environments [1] and is being implemented in wireless local area network (WLAN) standards such as IEEE802.11a and IEEE802.11n. For many scattering environments, spatial diversity is an effective way to improve the system performance. Space-time block coding (STBC) was firstly proposed by Alamouti [2] in order to get the benefits of channel coding in combination with spatial diversity. Also, space-time coded OFDM (ST-OFDM) [3] and STBC-OFDM [4] were proposed for wideband transmissions.

Theoretically the STBC-OFDM can achieve optimal diversity gain. However, in spite of its high performance gain, STBC-OFDM has two major weaknesses for realistic applications. The first is the need to allocate two OFDM symbols for spatial-temporal encoding, which can be a waste of resources for the transmission of small packets. Secondly, the detection could only take place after one delayed OFDM symbol period, which results in a latency problem.

To overcome the necessity to use two successive symbols for coding, SFBC-OFDM was proposed [5] to send combined symbols sent on different subcarriers in OFDM systems. For the SFBC-OFDM, the feature of OFDM is exploited that two adjacent narrowband subcarriers can be assumed to be affected by the same channel coefficients and thus it requires only one OFDM symbol for detection and avoids coherence time restrictions and reduces the system delay [6].

However, the STBC designed to achieve full spatial diversity in the narrowband case will in general not achieve full space-frequency diversity [5], especially employing the Alamouti scheme [2] across OFDM multicarriers. Even though the Alamouti scheme continues to achieve second-order diversity in the broadband OFDM cases, it fails to exploit the additionally available frequency diversity, due to the unequal channels [7]

Alternatively, in order to exploit the frequency diversity gain, another ST diversity scheme for OFDM, cyclic delay diversity (CDD), has been proposed [8] and the scheme can be shown to be equal to phase diversity (PD) and conditionally equal to delay diversity (DD) as described in [9]. However, our recent study shows that the capability of CDD to exploit the frequency diversity gain is limited to certain channel conditions, which will be described in this paper.

In contrast, the frequency diversity gain can be further exploited for SFBC-OFDM. In this paper, the performance in terms of signal noise ratio (SNR) gain will be analyzed for different values of subcarrier correlation. It is shown that the gain loss is due to the variability in channel conditions. Therefore, we are presenting our study of algorithms to combat the variability and a simplified algorithm is proposed to obtain higher frequency diversity gain with lower complexity.

This paper will also discuss the tradeoff between these different techniques and the paper is organized as follows: the next section describes the SFBC-OFDM. Investigation of algorithms to exploit further frequency diversity gain for SFBC-OFDM and the simplified method is described in section III. Section IV presents the SNR analysis of under differently correlated subcarriers. Section V discusses the capability of CDD to exploit frequency diversity gain and backward compatibility issues. Numerical studies and conclusions that follow wrap up this paper.

II. SPACE FREQUENCY BLOCK CODE OFDM

The SFBC-OFDM technique employing the Alamouti scheme is encoded over two transmit antennas such that the k_{2n} subcarriers consist of the original transmitted symbols, while the conjugated symbols are allocated to the k_{2n+1} subcarriers. Fig. 1 depicts a block diagram of the transmit structure of the SFBC-OFDM and the mapping scheme for SFBC with 2 transmitter antennas is shown in Table 1.

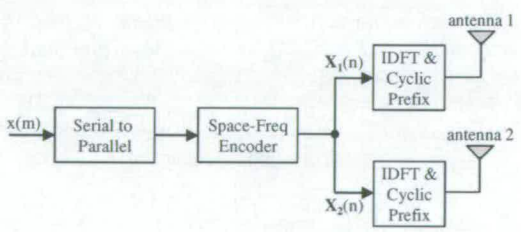

Fig. 1. Transmit structure of SFBC-OFDM

TABLE 1
MAPPING SCHEME WITH SFBC AND 2 TX-ANTENNAS

	antenna 1	antenna 2
subcarrier k_{2n}	x_{2m}	x_{2m+1}
subcarrier k_{2n+1}	x^*_{2m+1}	$-x^*_{2m}$

At each of the N receiver antennas, the signals are OFDM demodulated and the $(2, N)$ MIMO received signal at each subcarrier can be represented as

$$\mathbf{r} = \mathbf{H}\mathbf{x} + \boldsymbol{\eta}. \quad (1)$$

The received signal in (1) can be expressed for this case as

$$\begin{bmatrix} \dot{\mathbf{r}}_1 \\ \dot{\mathbf{r}}_2 \\ \vdots \\ \dot{\mathbf{r}}_N \end{bmatrix} = \begin{bmatrix} \dot{\mathbf{h}}_{1,1} \\ \dot{\mathbf{h}}_{2,1} \\ \vdots \\ \dot{\mathbf{h}}_{N,1} \end{bmatrix} \dot{\mathbf{x}} + \begin{bmatrix} \dot{\boldsymbol{\eta}}_1 \\ \dot{\boldsymbol{\eta}}_2 \\ \vdots \\ \dot{\boldsymbol{\eta}}_N \end{bmatrix} = \mathbf{H}_F \dot{\mathbf{x}} + \dot{\boldsymbol{\eta}}, \quad (2)$$

where

$$\dot{\mathbf{r}}_n = \begin{bmatrix} r_n(k_{2c}) \\ r_n(k_{2c+1})^* \end{bmatrix}, \quad \dot{\boldsymbol{\eta}}_n = \begin{bmatrix} \eta_n(k_{2c}) \\ \eta_n(k_{2c+1})^* \end{bmatrix}, \quad \dot{\mathbf{x}} = \begin{bmatrix} x_{2m}(2k_c) \\ x_{2m+1}(2k_c) \end{bmatrix}$$

$$\text{and } \dot{\mathbf{h}}_{n,m} = \begin{bmatrix} h_{n,2m}(k_{2c}) & h_{n,2m+1}(k_{2c}) \\ h^*_{n,2m+1}(k_{2c+1}) & -h^*_{n,2m}(k_{2c+1}) \end{bmatrix}, \quad (3)$$

where $r_n(k_c)$ and $\eta_n(k_c)$ are the received signal and noise of subcarrier k_c at receive antenna n, $x_m(k_c)$ is the transmitted symbol at transmit antenna m mapped onto subcarrier k_c and $h_{n,m}(k_c)$ is the channel response from subcarrier k_c at receive antenna n due to transmit antenna m.

Conventionally, it was assumed that the channels between adjacent subcarriers are highly correlated. Hence, the symbols can be detected using the MRC technique as

$$\hat{\dot{\mathbf{x}}} = \mathbf{H}_F^H \mathbf{r} = \mathbf{H}_F^H \mathbf{H}_F \dot{\mathbf{x}} + \mathbf{H}_F^H \dot{\boldsymbol{\eta}}, \quad (4)$$

where $\hat{\dot{\mathbf{x}}}$ is the estimated symbol vector expressed as

$$\hat{\dot{\mathbf{x}}} = \begin{bmatrix} \hat{x}_{2m}(2k_c) \\ \hat{x}_{2m+1}(2k_c) \end{bmatrix}, \text{ and } \begin{matrix} h_{n,2m}(k_{2c}) = h_{n,2m}(k_{2c+1}) \\ h_{n,2m+1}(k_{2c}) = h_{n,2m+1}(k_{2c+1}). \end{matrix} \quad (5)$$

However, this method of detection, assuming that adjacent subcarriers' channels are highly correlated, is only applicable for channels characterised by low frequency selectivity. This algorithm is referred as the conventional Alamouti detection algorithm (CADA) in this paper.

III. Exploiting Frequency Diversity Gain for SFBC-OFDM

For the conventional SFBC detection as described in previous section (referred to CADA) the performance will degrade in heavily frequency-selective channels where the assumption of constant channel coefficients over a space-frequency block code matrix is not justified. Therefore, the SFBC-OFDM case calls for improved detection algorithms.

In the case where channels are highly frequency selective, it no longer fulfils the equalities in (5) and the full rank of channels as in (3) has to be used. It is well known that the zero-forcing (ZF) algorithm is a straightforward equaliser method to cope with this requirement, which can be applied to solve (2) with knowledge of the channel matrices in (3). With this, the detected symbols can be expressed as

$$\hat{\dot{\mathbf{x}}} = \mathbf{G}_F \mathbf{H}_F \dot{\mathbf{x}} + \mathbf{G}_F \dot{\boldsymbol{\eta}} \quad (6)$$

$$\text{and } \mathbf{G}_F = \left(\mathbf{H}_F^H \mathbf{H}_F\right)^{-1} \mathbf{H}_F^H. \quad (7)$$

Although the method in (7) allows for four different channels coefficients, $h_{n,2m}(k_{2c})$, $h_{n,2m+1}(k_{2c})$, $h^*_{n,2m}(k_{2c+1})$ and $h^*_{n,2m+1}(k_{2c+1})$ for the two subcarriers per decoding process, the zero-forcing (ZF) beamformer consists of several multiplications to form a $2\times 2N$ size channel matrix. The solution in (9) can be further developed by concatenating the adjoint channel matrix of the response at each receiver as

$$\mathbf{G}_S = \left[adj(\dot{\mathbf{h}}_{1,1}), adj(\dot{\mathbf{h}}_{2,1}) \ldots adj(\dot{\mathbf{h}}_{N,1})\right], \quad (8)$$

where $adj(A)$ is the adjoint matrix of A, which can be expressed as

$$A = \begin{bmatrix} a_{1,1} & a_{1,2} \\ a_{2,1} & a_{1,1} \end{bmatrix}, \quad adj(A) = \begin{bmatrix} a_{2,2} & -a_{1,2} \\ -a_{2,1} & a_{1,1} \end{bmatrix}.$$

Multiplying $\mathbf{G}_s$ in (8) by the received signal in (2) yields the equivalent ZF solution as

$$\hat{\dot{\mathbf{x}}} = \mathbf{G}_S \left(\mathbf{H}_F \dot{\mathbf{x}} + \dot{\boldsymbol{\eta}}\right)$$

$$= \left[adj(\dot{\mathbf{h}}_{1,1}), adj(\dot{\mathbf{h}}_{2,1}), \ldots, adj(\dot{\mathbf{h}}_{N,1})\right] \left(\begin{bmatrix} \dot{\mathbf{h}}_{1,1} \\ \dot{\mathbf{h}}_{2,1} \\ \vdots \\ \dot{\mathbf{h}}_{N,1} \end{bmatrix} \dot{\mathbf{x}} + \begin{bmatrix} \dot{\boldsymbol{\eta}}_1 \\ \dot{\boldsymbol{\eta}}_2 \\ \vdots \\ \dot{\boldsymbol{\eta}}_N \end{bmatrix} \right)$$

$$= \begin{bmatrix} -\alpha_{s1} & 0 \\ 0 & -\alpha_{s2} \end{bmatrix} \begin{bmatrix} x_m(2k_c) \\ x_m(2k_c+1) \end{bmatrix} + \mathbf{G}_S \dot{\boldsymbol{\eta}}, \quad (9)$$

where $\alpha_{S1} = \sum_{n=1}^{N} \sum_{m=1}^{2} h^*_{n,2m}(k_{2c+1}) h_{n,2m}(k_{2c})$

$$\alpha_{S2} = \sum_{n=1}^{N} \sum_{m=1}^{2} h_{n,2m+1}(k_{2c+1}) h^*_{n,2m+1}(k_{2c+1}).$$

Hence, as illustrated in (9), the equivalent ZF solution can be obtained without performing the full pseudo inverse as shown in (7). In this case the complexity can be reduced by the number of multiplications required to generate the ZF solution in (7).

The ZF is a common algorithm [10] in modern communications theory and its obvious disadvantage is its noise enhancement. However, we will prove in next section that the simplified algorithm is exploiting the frequency diversity gain for the SFBC-OFDM and has superior performance compared to the CADA.

IV. SNR Analysis Under Differently Correlated Subcarriers

In order to verify the system performance for different correlation coefficients between subcarriers, the SNR parameter, which has direct impact on the performance, will be analyzed.

Consider a (2,1) STBC-OFDM system; the SNR for each of the two transmitted orthogonal symbols can be expressed as follows,

$$SNR = \frac{|h_{1,1}|^2 + |h_{1,2}|^2}{\sigma_n^2}. \quad (10)$$

Given the same system, but for the frequency encoded version, there are two detection algorithms, CADA and simplified ZF, as described in previous sections.

Assuming $\begin{bmatrix} v_1 & v_2 \\ v_3 & v_4 \end{bmatrix} = \begin{bmatrix} h_{1,1}(2k) & h_{1,2}(2k) \\ h_{1,2}(2k+1) & h_{1,1}(2k+1) \end{bmatrix}$, for the CADA, the combined received signal can expressed as

$$\begin{bmatrix} \hat{x}_1(2k) \\ \hat{x}_2(2k) \end{bmatrix} = \begin{bmatrix} v_1 & v_2 \\ v_2^* & -v_1 \end{bmatrix}^H \left(\begin{bmatrix} v_1 & v_2 \\ v_3 & -v_4^* \end{bmatrix} \begin{bmatrix} x_1(2k) \\ x_2(2k) \end{bmatrix} + \begin{bmatrix} \eta_1(2k) \\ \eta_1^*(2k+1) \end{bmatrix} \right)$$
$$= \begin{bmatrix} \left(|v_1|^2 + v_2 v_3^*\right) x_1(2k) + \left(v_1^* v_2 - v_2 v_4^*\right) x_2(2k) \\ \left(v_1 v_2^* - v_1 v_3^*\right) x_1(2k) + \left(|v_2|^2 + v_{12} v_4^*\right) x_2(2k) \end{bmatrix}$$
$$+ \begin{bmatrix} v_1 \eta_1(2k) + v_2 \eta_1^*(2k+1) \\ v_2^* \eta_1(2k) - v_1 \eta_1^*(2k+1) \end{bmatrix}, \quad (11)$$

It is shown clearly in (11) that interference is introduced due to the unequal channels between adjacent subcarriers.

To analyse the SNR performance, the adjacent subcarrier coefficients from both transmit antennas are varied simultaneously to produce different correlation factors, κ. We assume

$$E\left(|v_1|^2\right) = E\left(|v_2|^2\right) = E\left(|v_3|^2\right) = E\left(|v_4|^2\right) = 1,$$

and

$$E\left(|v_1 v_4^*|^2\right) = E\left(|v_4 v_1^*|^2\right) = \kappa_1,$$
$$E\left(|v_2 v_3^*|^2\right) = E\left(|v_3 v_2^*|^2\right) = \kappa_2,$$

where κ_1 and κ_2 are the correlation coefficients between the adjacent subcarriers at transmit antenna $m = 1$ and $m = 2$ respectively.

If we treat the interference as white noise, the SNR of $\hat{x}_1(2k)$ in (11) can be derived as

$$SNR_{CADA-x_1} = \frac{(1+\kappa_2)P_1}{\sigma_n^2 + (1-\kappa_1)P_2}, \quad (12)$$

where P_1 and P_2 represent the signal power at antennas 1 and 2 respectively.

Similarly, the SNR of $x_2(2k)$ is

$$SNR_{CADA-x_2} = \frac{(1+\kappa_1)P_2}{\sigma_n^2 + (1-\kappa_2)P_1}. \quad (13)$$

In contrast, for the proposed simplified ZF (SZF) algorithm, the combined received signal can expressed as

$$\begin{bmatrix} \hat{x}_1(2k) \\ \hat{x}_2(2k) \end{bmatrix} = \begin{bmatrix} -v_4^* & -v_2 \\ -v_3^* & v_1 \end{bmatrix} \left(\begin{bmatrix} v_1 & v_2 \\ v_3 & -v_4^* \end{bmatrix} \begin{bmatrix} x_1(2k) \\ x_2(2k) \end{bmatrix} + \begin{bmatrix} \eta_1(2k) \\ \eta_1^*(2k+1) \end{bmatrix} \right)$$
$$= \begin{bmatrix} -v_4^* v_1 - v_2 v_3^* & 0 \\ 0 & -v_3^* v_2 - v_4 v_1^* \end{bmatrix} \begin{bmatrix} x_1(2k) \\ x_2(2k) \end{bmatrix}$$
$$+ \begin{bmatrix} -v_4^* \eta_1(2k) - v_2 \eta_1(2k+1) \\ -v_3^* \eta_1(2k) + v_1 \eta_1(2k+1) \end{bmatrix}, \quad (14)$$

The SNR of $x_1(2k)$ & $x_2(2k)$ in (14) can be also derived as

$$SNR_{SZF-x_1} = \frac{(1+\kappa_1\kappa_2)P_1}{\sigma_n^2}, \quad (15)$$

$$SNR_{SZF-x_2} = \frac{(1+\kappa_1\kappa_2)P_2}{\sigma_n^2}. \quad (16)$$

The normalised achievable SNR with respect to its correlation factor $\kappa_1 = \kappa_2$, power $P_1 = P_2 = 1$ and $\sigma_n^2 = 1$ is shown in Fig. 2.

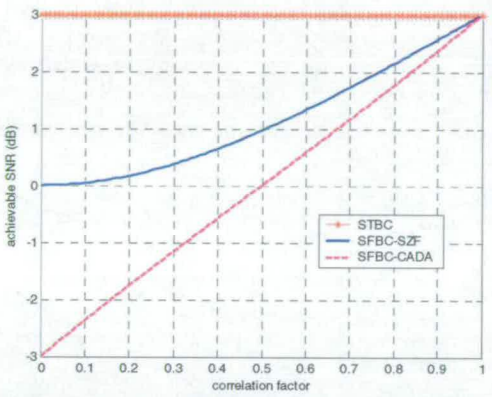

Fig. 2. Achievable relative SNR for different correlated adjacent subcarriers

From the above figure it can be seen that the SNR increases as the adjacent subcarriers become more correlated with each other. When $\kappa_1 = \kappa_1 = 1$, i.e., adjacent subcarriers are fully correlated, the performance of both SFBC detection algorithms equals that of STBC. On the other hand, if $\kappa_1 = \kappa_1 = 0$, i.e., adjacent subcarriers are uncorrelated, SFBC-SZF is 3dB worse than STBC, however, it is 3dB better than SFBC-CADA. For later comparison between the proposed SZF and CDD, we introduce CDD in next section before the numerical study.

V. Cyclic Delay Diversity and its Backward Compatibility

As discussed previously, CDD is another scheme to exploit frequency diversity gain. Fig. 3 shows a two transmit CDD scheme for simplicity without loss generality.

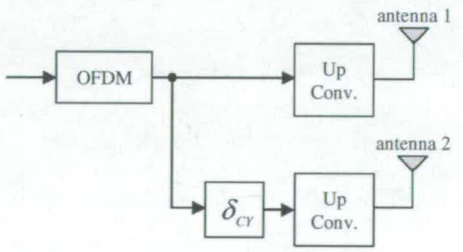

Fig. 3. Transmit Structure of CDD

Transmit antenna 1 consists of a conventional OFDM system while transmit antenna 2 is a cyclically delay shifted ver-

sion of transmit antenna 1 by a factor of δ_{CY}, where δ_{CY} is defined as the cyclic delay shift. The cyclically delayed version of antenna 2 is obtained by replicating the last δ_{CY} samples of the OFDM symbol and prefixing them at the beginning of the OFDM symbol. Hence, the frequency domain symbol at each subcarrier, k_c, is phase shifted by a factor of θ_{CY}, where

$$\theta_{cy} = \frac{2\pi k_c S_{cy}}{K_c} \quad (17)$$

where k_c is the subcarrier index and K_c is the FFT size. The phase shifted signal induces an artificial channel with higher frequency selectivity so that more frequency diversity can be exploited from the OFDM system coupled with its outer channel code.

Assuming that two antennas are used, the received signal can be expressed as

$$\begin{bmatrix} r_1 \\ r_2 \end{bmatrix} = \begin{bmatrix} h_{1,1} & h_{1,2} \\ h_{2,1} & h_{2,2} \end{bmatrix} \begin{bmatrix} x \\ x\exp(-j\theta_{cy}) \end{bmatrix} + \begin{bmatrix} \eta_1 \\ \eta_2 \end{bmatrix}$$
$$= \begin{bmatrix} h_{1,1} + h_{1,2}\exp(-j\theta_{cy}) \\ h_{2,1} + h_{2,2}\exp(-j\theta_{cy}) \end{bmatrix} [x] + \begin{bmatrix} \eta_1 \\ \eta_2 \end{bmatrix}$$
$$= \mathbf{H}_c \mathbf{x} + \boldsymbol{\eta}, \quad (18)$$

where r_n and η_n are the received signal and noise at the nth antenna, x is the transmitted signal and $h_{n,m}$ is the channel response at nth received antenna from mth transmit antenna.

The received signal at the two antennas can be further enhanced by maximum ratio combining (MRC) to obtain the estimated symbol as

$$\hat{x} = \mathbf{H}_c^H \mathbf{H}_c x + \mathbf{H}_c^H \eta$$
$$= (c_1 + c_2)x + \sqrt{c_1}\eta_1 + \sqrt{c_2}\eta_2, \quad (19)$$

where

$$c_1 = \left|h_{1,1} + h_{1,2}\exp(-j\theta_{cy})\right|^2$$
$$c_2 = \left|h_{2,1} + h_{2,2}\exp(-j\theta_{cy})\right|^2.$$

In addition to the advantages of good resource management and latency reduction as compared to Alamouti STBC, CDD supports backward compatibility with the current WLAN single input single output (SISO) system, i.e., IEEE 802.11a. Consider a 2-*Tx* CDD source received by an IEEE 802.11a single antenna, the received signal as seen by the receiver can be expressed as

$$[r] = [h_{1,1} + h_{1,2}\exp(-j\theta_{cy})][x] + [\eta]. \quad (20)$$

Although, the transmitted signals come from two different antennas, the receiver adds the two channel responses as shown in (20), viewing it as a signal from a single source. Hence, the transmitted CDD signal can be detected by a legacy terminal.

VI. Numerical Study

Here, we present two-case studies for comparison. In these studies, we use a (2, 2) MIMO system with QPSK modulation and half-rate convolutional coding. The MIMO channel has a uniform, Rayleigh fading multipath power delay profile (p-1 represents 1-path, p-16 represents 16-paths, etc). Each multipath is spaced at the sampling period (T_s) of OFDM symbol. Also, the acronym SFBC-OFDM specifies the use of the SFBC-SZF algorithm. For the (2, 2) CDD system, the impact of delay, δ_{CY}, on system performance is also studied, which is depicted in Fig. 4. It shows that the significant gain can be achieved in a small multipath environment, e.g. 2-path. For fair comparison, δ_{CY} is set to $8T_s$ in the system simulation.

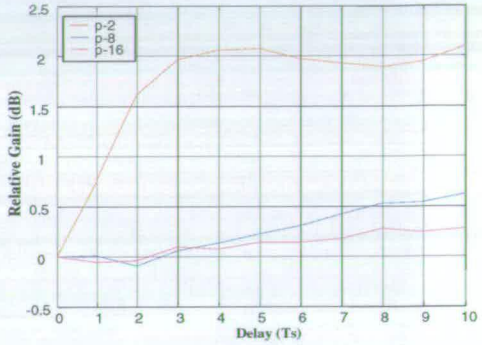

Fig. 4. (2,2) CDD receive gain vs delay

Case-1: Comparison between STBC and SFBC:

The results for comparing STBC and SFBC is shown in Fig. 5 for p-1, p-2 and p-4 while p-8 and p-16 results are in Fig. 6.

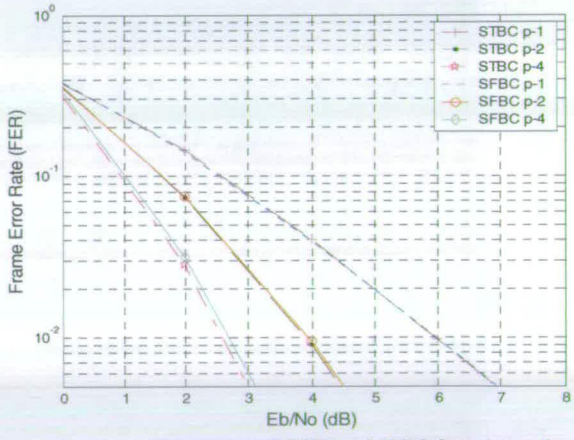

Fig. 5. Comparison of STBC and SFBC for p-1 to p-4

When the channel is flat fading, the performance of the temporal and frequency coded system is similar to each other. This is because the adjacent channel subcarriers are fully correlated with one another. However, the performance advantage of STBC over SFBC increases for subsequent increments in the number of channel taps. Even though the SFBC 16 taps system can exploit more frequency diversity inherent in the OFDM transmission, coupled with the channel decoder, the performance for this scenario is worse than the 8 taps STBC system. This is due to the uncorrelated adjacent subcarriers, which destroy the orthogonality of the Alamouti code.

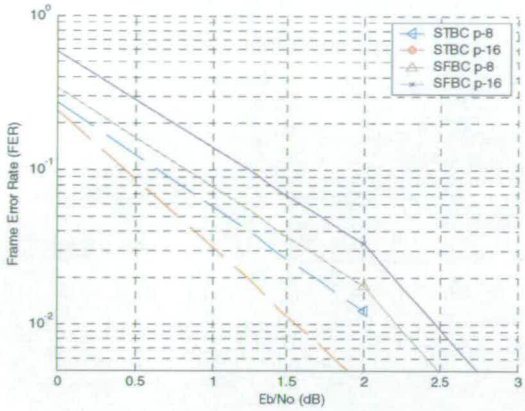

Fig. 6. Comparison of STBC and SFBC for p-8 and p16

CASE-2: COMPARISON BETWEEN SFBC AND CDD:

The next set of results comparing SFBC and CDD is shown Fig. 7 for p-1, p-2 and p-4 while p-8 and p-16 results are shown in Fig. 8.

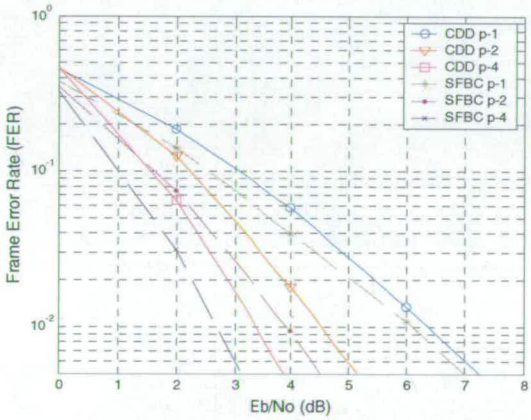

Fig. 7. Comparison of CDD and SFBC for p-1 to p-4

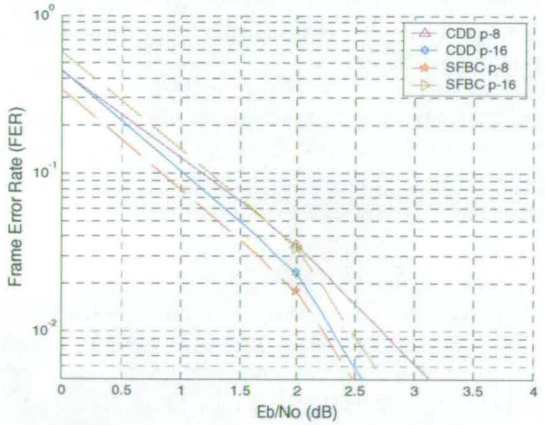

Fig. 8. Comparison of CDD and SFBC for p-8 and p-16

Despite the adjacent subcarriers in the SFBC scheme being less correlated for the increase from p-1 to p-4 multipath taps, the relative performance with respect to CDD improves with this increment. This is mainly due to the CDD scheme being less able to exploit frequency diversity gain as the number of channel taps increases. On the other hand, when increasing to p-8 taps we see that the performance difference between these two schemes starts to reduce. In the case of 16 taps scenario, the CDD method actually outperforms the SFBC scheme. For higher number of multipath taps, the SFBC starts to degrade in performance while CDD reaches its peak performance.

VII. CONCLUSIONS

This paper investigates the SFBC-OFDM and CDD transmit schemes as means to reduce the two symbol overhead and latency in the STBC-OFDM scheme. A simplified ZF solution for the SFBC-OFDM has been proposed. The SNR analysis shows that the correlation between the channels has impacts on this scheme, however, it outperforms conventional SFBC detection (by 3dB with fully uncorrelated adjacent subcarriers). The simulation results also show that for a low frequency selective channel the error performance is comparable to its temporal encoded scheme. However, the SFBC scheme degrades as the number of multipath increases. Despite the partially correlated adjacent subcarriers, this scheme is still able to outperform CDD unless the channel is extremely frequency selective. Despite the better performance of SFBC over CDD, CDD has a significant advantage over SFBC in terms of backward compatibility with the legacy terminals, such as IEEE 802.11a.

ACKNOWLEDGMENT

The authors would like to thank all their colleagues for their help and support with this work.

REFERENCES

[1] S. B. Weinstein and P. M. Ebert, "Data transmission by frequency division multiplexing using the discrete fourier transform", IEEE Trans Comm, vol. COM-19, no. 15, pp. 628-634, October 1971.

[2] S. M. Alamouti, "A simple trasmit diversity technique for wireless communications", IEEE Jnl of Sel Area in Comms, vol. 16, no. 8, pp. 1451-1458, October 1998.

[3] D. Agrawal, V. Tarokh, A. Naguib and N. Seshadri, "Space-time coded OFDM for high data-rate wireless communication over wideband", IEEE Vechicular Technology Conf, vol. 3, pp. 2232-2236, May 1998.

[4] S. Mudulodu and A. Paulraj, "A transmit diversity scheme for frequency-selective fading channels", IEEE Globecom Conf, pp. 1089-1093, December 2000.

[5] H. Bölcskei & A. J. Paulraj, "Space-frequency coded broadband OFDM systems", Wireless Comms and Networking Conf, vol. 1, pp. 1-6, Sept. 2000

[6] S. Kaiser, "Space frequency block codes and code division multiplexing in OFDM systems," IEEE Globecom Conf, vol. 4, pp. 2360–2364, December 2003.

[7] B. Qzbek, D. L. Ruyet, and M. Bellanger, "On space-frequency block codes for unequal channels," COST 273 Workshop On Broadband Local Access, pp. 3/1–3/6, May 2003.

[8] A. Dammann & S. Kaiser, "Standard conformable antenna diversity techniques for OFDM and its application to the DVB-T system", IEEE Globecom Conf, vol. 5, pp. 3100–3105, Nov 2001.

[9] S. Kaiser, "Spatial transmit diversity techniques for broadband OFDM system", IEEE Globecom Conf, pp. 1824-1828, November 2000.

[10] J. G. Proakis, *Digital Communications*, third edtion, McGraw-Hill , Inc. USA, 1995.

Comparison Of Robustness Of MIMO Schemes In The Presence Of Interference

H.S. Tan*, Y. Sun†, J.S. Thompson‡ and D.G.M. Cruickshank§
* ‡ §Institute of Digital Communications
School of Engineering and Electronics, University of Edinburgh,
King's Buildings, Mayfield Road, Edinburgh EH9 3JL, United Kingdom
Email hst@ee.ed.ac.uk, jst@ee.ed.ac.uk, dgmc@ee.ed.ac.uk
* † Toshiba Research Europe Limited, 32 Queens Square
Bristol BS1 4ND, United Kingdom
Email Sun@toshiba-trel.com

Abstract— **Multiuser interference (MUI) is a major problem in an orthogonal frequency division multiplexing (OFDM) multiple access system due the the absence of unique spreading codes being assigned to different users for separation at the receiver. In our paper, we propose the use of spatial separation techniques to separate users at the receiver. The two proposed interference mitigation techniques, defined as interference cancellation(IC) and interference suppression(IS), can be employed to mitigate interference. However, depending on the scenario and restrictions imposed on either of these two techniques, this requires careful consideration especially in a multiple input multiple output (MIMO) system. Two particular MIMO schemes, V-BLAST and Dual Alamouti space time block code (STBC), which are strong candidates for future wireless systems, will be introduced. Their robustness in the presence of interference will be compared and the selection of appropriate interference mitigation techniques will be suggested. Results obtained from our simulator will be shown to support this study.**

I. Introduction

MUI [4], [8] in a multiple access system acts as a limiting factor for achieving maximum capacity in a wireless system. In the event that this interference is not properly mitigated, it appears as coloured noise and can cause severe degradation to the overall system performance. A code division multiple access (CDMA) system supporting multiple users transmission can mitigate MUI efficiently because the receiver is able to identify each user's unique code and decorrelates the desired user from others. However, this is not as straightforward in an OFDM multiple access scheme employed in a wireless system where no spreading codes are assigned to each individual user. Furthermore, systems supporting high data rate implementing MIMO techniques cause more problems in mitigating interference because more spatial degrees of freedom are required at the receiver.

The robustness of two MIMO schemes namely, V-BLAST [7] and Dual Alamouti STBC [3], in the presence of interference will be studied. V-BLAST is a spatial multiplexing scheme where each transmit antenna consists of a conventional QAM modulator. The receiver can employ minimum mean square error (MMSE) ordered successive interference cancellation (OSIC) algorithm to spatially separate and detect the transmitted streams. This detector delivers good performance at linear complexity while achieving high data rates. The drawback of this transmit scheme is the absence of diversity exploitable at the transmitter. This leads to the Dual Alamouti STBC scheme where two Alamouti STBC [1] transmitters are concatenated to exploit both high data rate transmission and transmit diversity gain. The OSIC algorithm can also be applied to this case where the Alamouti pair with the highest signal-to-noise-ratio (SNR) is detected first. Not only does this provide additional transmit diversity gain, the minimum number of receive antennas required to successfully detect both pairs of Alamouti encoded streams is halved as compared to the V-BLAST scheme employing the same number of transmitters. The performance in [6] is shown to favour the latter scheme in a single user environment.

In a multiuser environment, the two interference mitigation techniques suggested are extensions to that of [2], [4], [7] where multiple users are considered. In order to mitigate interference efficiently, two types of interference mitigation techniques will be defined and considered, namely interference cancellation (IC) and interference suppression (IS). IC processing is similar to that of OSIC algorithm where transmitted signals from each antenna of all users are ordered according to the highest SNR, detected and removed from the received signal. On the other hand, IS processing only detects the desired user signals while nulling its interferers.

In this paper, these two interference mitigation techniques applied to V-BLAST and Alamouti STBC multiuser environment will be studied. The channel and MIMO system model used in this study will be described in Section II. The MUI mitigation techniques are suggested in Section III. Simulation results showing the robustness of these MIMO schemes are illustrated in Section IV. Lastly, the conclusions are presented in Section V.

II. System Model

Consider a MIMO OFDM system with M and N transmitting and receiving antennas respectively - the (M,N) system. The received signal at each subcarrier can be expressed as:

$$\mathbf{r} = \mathbf{H}\mathbf{x} + \boldsymbol{\eta} \tag{1}$$

where $\mathbf{r}$ and $\boldsymbol{\eta}$ is the received signal and noise vector of size Nx1 respectively, $\mathbf{x}$ is the Mx1 transmitted signal vector and $\mathbf{H}$ the size NxM channel matrix.

The channel is assumed to be static over one transmission packet. Each wireless channel between the n^{th} and m^{th} antennas is assumed to be Rayleigh flat faded [5]. The probability density function of the received signal envelope, γ is given by:

$$\rho(\gamma) = \begin{cases} \frac{\gamma}{\alpha^2}\exp[\frac{\gamma^2}{2\alpha^2}] & \text{for } \gamma \geq 0 \\ 0 & \text{otherwise} \end{cases} \tag{2}$$

where $2\alpha^2$ is the predetection mean power of the signal path.

A. V-BLAST

The V-BLAST scheme consists of M spatially multiplexed QAM modulators each attached to a transmit antenna. The received signal in equation (1) can be expressed as:

$$\begin{bmatrix} r_0 \\ \vdots \\ r_{N-1} \end{bmatrix} = \begin{bmatrix} h_{0,0} & \cdots & h_{0,M-1} \\ \vdots & \ddots & \\ h_{N-1,0} & \cdots & h_{N-1,M-1} \end{bmatrix} \begin{bmatrix} x_0 \\ \vdots \\ x_{M-1} \end{bmatrix} + \begin{bmatrix} \eta_0 \\ \vdots \\ \eta_{N-1} \end{bmatrix} \tag{3}$$

where $h_{n,m}$ is the channel response due to transmit antenna m at receiver n, x_m is the transmitted symbol from antenna m while r_n and η_n are the received signal and noise at receive antenna n respectively.

The received signal can be successively detected by employing the MMSE-OSIC [2] detector provided $N \geq M$. The OSIC algorithm is described as follows:

i) Determine the MMSE estimate of the channel matrix, $\mathbf{H}$ in equation (3). This is given by:

$$\mathbf{G} = (\mathbf{H}^H\mathbf{H} + \sigma_n^2\mathbf{I})^{-1}\mathbf{H}^H \tag{4}$$

where σ_n^2 is the noise variance.

ii) Calculate the SNR of the m streams (m = 0 to M-1). Select the stream with the highest SNR

$$k = \underbrace{\text{argmax}}_{m}(\text{SNR}) \tag{5}$$

iii) Determine the weighting matrix of the highest SNR stream

$$\mathbf{w} = \mathbf{G}_m \tag{6}$$

where $\mathbf{G}_m$ denotes the m^{th} row vector

iv) Detect the m^{th} symbol.

$$y_m = \mathbf{w}\mathbf{r} \tag{7}$$

v) This decision statistic is quantised to its respective constellation point.

$$\hat{x}_m = Q(y_m) \tag{8}$$

vi) The effect of this estimated symbol is then subtracted from the received signal

$$\acute{\mathbf{r}} = \mathbf{r} - \mathbf{H}_m\hat{x}_m \tag{9}$$

where $\mathbf{H}_m$ is the m^{th} column vector of $\mathbf{H}$

vii) Null the m^{th} column of the channel matrix, $\mathbf{H}$

$$\mathbf{H}^- = \mathbf{H} - [0\,0\ldots\mathbf{H}_m\ldots0\,0] \tag{10}$$

viii) Calculate the MMSE estimate of the nulled channel

ix) Repeat the process from step (ii) until all the streams are detected.

B. Dual Alamouti STBC

The Dual Alamouti STBC scheme exploits the advantages of both the Alamouti STBC and V-BLAST schemes by concatenating two blocks of Alamouti STBC. The received signal can be expressed as:

$$\begin{bmatrix} \mathbf{r'}_0 \\ \mathbf{r'}_1 \\ \vdots \\ \mathbf{r'}_{N-1} \end{bmatrix} = \begin{bmatrix} \mathbf{h'}_{0,0} & \mathbf{h'}_{0,1} \\ \mathbf{h'}_{1,0} & \mathbf{h'}_{1,1} \\ \vdots & \vdots \\ \mathbf{h'}_{N-1,0} & \mathbf{h'}_{N-1,1} \end{bmatrix} \begin{bmatrix} \mathbf{x'}_0 \\ \mathbf{x'}_1 \end{bmatrix} + \begin{bmatrix} \boldsymbol{\eta}'_0 \\ \boldsymbol{\eta}'_1 \\ \vdots \\ \boldsymbol{\eta}'_{N-1} \end{bmatrix} \tag{11}$$

where

$$\mathbf{r'}_n = \begin{bmatrix} r_{n,\tau_0} \\ r_{n,\tau_1} \end{bmatrix} \qquad \boldsymbol{\eta}'_n = \begin{bmatrix} \eta_{n,\tau_0} \\ \eta_{n,\tau_1} \end{bmatrix}$$

$$\mathbf{x'}_m = \begin{bmatrix} x_{2m} \\ x_{2m+1} \end{bmatrix} \qquad \mathbf{h'}_{n,m} = \begin{bmatrix} h_{n,2m} & h_{n,2m+1} \\ h^*_{n,2m+1} & -h^*_{n,2m} \end{bmatrix}$$

where τ_t is the time index. Similarly the received signal in equation (11) can be detected using the OSIC algorithm as described in the previous section.

III. Interference Mitigation Techniques

In the presence of multiuser synchronous interference, the received signal can be mathematically modelled as:

$$\mathbf{r} = \mathbf{H_D}\mathbf{x_D} + \sum_{o=1}^{O}\mathbf{H_{Io}}\mathbf{x_{Io}} + \boldsymbol{\eta} \tag{12}$$

where $\mathbf{H_D}$ and $\mathbf{H_I}$ is the channel response of the desired user and interferer respectively, $\mathbf{x_D}$ and $\mathbf{x_{Io}}$ the data vector of the desired user and interferer respectively and O is the total number of multiuser interferers in the system.

The signal model in equation (12) can be translated to its matrix form as:

$$\mathbf{r} = \begin{bmatrix} \mathbf{H_D} & \mathbf{H_{I_1}} & \mathbf{H_{I_2}} & \cdots & \mathbf{H_{I_O}} \end{bmatrix} \begin{bmatrix} \mathbf{x_D} \\ \mathbf{x_{I_1}} \\ \mathbf{x_{I_2}} \\ \vdots \\ \mathbf{x_{I_O}} \end{bmatrix} + \boldsymbol{\eta}$$

$$= \begin{bmatrix} \mathbf{H_D} & \mathbf{H_{OI}} \end{bmatrix} \begin{bmatrix} \mathbf{x_D} \\ \mathbf{x_{OI}} \end{bmatrix} + \boldsymbol{\eta} \quad (13)$$

where $\begin{bmatrix} \mathbf{H_D} & \mathbf{H_{I_1}} & \mathbf{H_{I_2}} & \cdots & \mathbf{H_{I_O}} \end{bmatrix}$ is the column concatenation of the desired user's channel with the interferers' channels and $\begin{bmatrix} \mathbf{x_D} & \mathbf{x_{I_1}} & \mathbf{x_{I_2}} & \cdots & \mathbf{x_{I_O}} \end{bmatrix}^T$ is the row concatenation of the desired user's data with the interferers' data. Also define:

$$\mathbf{H_{OI}} = \begin{bmatrix} \mathbf{H_{I_1}} & \mathbf{H_{I_2}} & \cdots & \mathbf{H_{I_O}} \end{bmatrix}, \qquad \mathbf{x_{OI}} = \begin{bmatrix} \mathbf{x_{I_1}} \\ \mathbf{x_{I_2}} \\ \vdots \\ \mathbf{x_{I_O}} \end{bmatrix}$$

Under the influence of MUI, the system performance can severely degrade when no interference mitigation is applied to the system. Two of the well known techniques suggested for mitigating this interference are IC and IS.

IC is defined such that both the desired user's and the interferers' data are being detected and cancelled from the received signal. The MMSE beamformer or weighting matrix can be mathematically expressed as:

$$\mathbf{G} = [\mathbf{H_D}\mathbf{H_{OI}}]^H \left((\mathbf{H_D})^H \mathbf{H_D} + \sum_{o=1}^{O} \frac{P_{Io}}{P_D} (\mathbf{H_{Io}})^H \mathbf{H_{Io}} + \frac{\sigma_n^2}{P_D} \mathbf{I} \right)^{-1} \quad (14)$$

where P_D and P_{Io} is the power transmitted by the desired user and o interferer respectively.

IS is defined in such a way that the interference is only suppressed from the desired user's data and left undetected. The beamformer for this technique is expressed as:

$$\mathbf{G} = (\mathbf{H_D})^H ((\mathbf{H_D})^H \mathbf{H_D} + \sum_{o=1}^{O} \frac{P_{Io}}{P_D} (\mathbf{H_{Io}})^H \mathbf{H_{Io}} + \frac{\sigma_n^2}{P_D} \mathbf{I})^{-1} \quad (15)$$

With these two suggested interference mitigation techniques, the interference can be removed by means of the OSIC algorithm.

The advantage of IS over IC is the ability to perform its operation without the need to estimate the interferers' channel irrespective of them being synchronous or asynchronous. Synchronous interference is defined such that the start and end of one transmission burst coincides with that of the desired user while asynchronous interference can start and finish at any time. The interferers' channel information using the MMSE detector can be estimated from the covariance matrix of the received signal assuming that the channels among the desired user and interferers are independent of one another.

$$\begin{aligned} E(\mathbf{r}\mathbf{r}^H) &= E((\mathbf{H_D}\mathbf{x_D} + \mathbf{H_{OI}}\mathbf{x_{OI}} + \boldsymbol{\eta}) \\ &\quad (\mathbf{H_D}\mathbf{x_D} + \mathbf{H_{OI}}\mathbf{x_{OI}} + \boldsymbol{\eta})^H) \\ &= \mathbf{H_D}\mathbf{x_D}\mathbf{x_D}^H\mathbf{H_D}^H + \\ &\quad \mathbf{H_{OI}}\mathbf{x_{OI}}\mathbf{x_{OI}}^H\mathbf{H_{OI}}^H + \sigma_n^2\mathbf{I} \\ &= \mathbf{H_D}\mathbf{H_D}^H + \mathbf{H_{OI}}\mathbf{H_{OI}}^H + \sigma_n^2\mathbf{I} \quad (16) \end{aligned}$$

IV. Simulation

The scenario where one V-BLAST and Dual Alamouti STBC user is being interfered by one synchronous interferer using the same transmission scheme with uncoded BPSK OFDM modulated data has been simulated. The 2 transmit and 4 receive antennas MMSE V-BLAST system and 4 transmit and 4 receive antennas MMSE Dual Alamouti STBC scheme using IC technique are shown in Figure 1 and 2 respectively. The results displayed in all the figures show the bit error ratio (BER) vs SNR performance for various interference-to-noise ratio (INR). The INR is defined as the INR at each receive antenna due to one interfering transmit antenna.

It is observed from the figures that employing the IC scheme gives better BER performance for higher INR values. This is because at high INR values, the interference is easily detected and cancelled from the received signal with a high degree of accuracy. Hence, this provides a more accurate received signal model when the desired user's signals are to be detected. The overlapping of BER curves for very high INR values is due to the saturation effect where the interferer's signal is completely cancelled.

In Figure 2, the crossover between the INR -10 dB and 0 dB curves is observed. This is because at lower SNR, the higher INR interferer can be detected and subtracted more successfully from the received signal, hence improving the BER performance slightly. As the SNR increases the optimal ordering priority switches from the interferer to the desired user's data. This time, the higher SNR desired user's data will be detected first while spatially suppressing the interferer. The optimal ordering around the crossover region would be a mixture between these two extreme cases.

The simulated results for the same set up as before using the IS technique for (2,4) V-BLAST, (4,4) Dual Alamouti STBC are shown in Figure 3 and 5 respectively. Contrary to IC technique, the mitigation performance degrades as INR values increase. This is because the interference is not cancelled and its presence is only treated as coloured noise by

the user. The results shown in Figure 4 is for a (4,4) system so that the total number of transmitters is greater than the number of receivers. The results illustrate that for low INR values, the BER performance is still tolerable while the IC technique will completely malfunction in this case. However, the BER performance degrades significantly at high INRs.

Table I and II shows the results of both V-BLAST and Dual Alamouti STBC employing the IC and IS algorithm to mitigate interference respectively. Provided that the number of receive antennas is sufficient, the IC mitigation technique is the preferred choice for a more robust system. Despite the total number of interfering elements being greater in Dual Alamouti STBC than V-BLAST, the Dual Alamouti STBC is more robust to interference given the same number of receive antennas employed in both schemes.

Interferer's INR/dB	BPSK Dual Alamouti (4,4)/dB	BPSK BLAST (2,4)/dB
0	0.3	2.3
10 → 30	-0.45	0.8

TABLE I

COMPARISON OF REQUIRED SNR USING IC AT BER 10^{-2}

Interferer's INR/dB	BPSK Dual Alamouti (4,4)/dB	BPSK BLAST (2,4)/dB
-10	0.75	1.30
0	2.78	3.30
10	4.20	5.50
20	4.50	6.50
30	4.50	7.10

TABLE II

COMPARISON OF REQUIRED SNR USING IS AT BER 10^{-2}

V. CONCLUSION

Two interference mitigation techniques are investigated in this paper which can be used to mitigate interference at low complexity. IC is preferred over IS because the interference signals can be cancelled from the received signal. However, this technique will not operate properly when the number of spatial degrees of freedom at the receiver is insufficient or the interferers' signal is not synchronous with the user's one. In this case, the IS technique is a much simpler approach, at the cost of some degradation in performance. Comparing V-BLAST and Dual Alamouti STBC, the latter scheme is more robust to interference irrespective of the interference mitigation technique used.

ACKNOWLEDGMENT

HS Tan would like to express his sincere gratitude to Toshiba Research Europe Ltd Telecommunication Research Laboratory (Bristol) for funding his work.

REFERENCES

[1] S. M. Alamouti, "A simple transmit diversity technique for wireless communications," *IEEE Journal Selected Areas in Communications*, vol. 16, no. 8, pp. 1451–1458, October 1998.

[2] M. Debbah, B. Muquet, M. deCourville, M. Muck, S. Simoens, and P. Loubaton, "A MMSE successive interference cancellation scheme for a new adjustable hybrid spread OFDM system," *IEEE Vechicular Technology Conference Proceedings*, vol. 2, pp. 745–749, Spring 2000.

[3] A. F. Naguib, N. Seshadri, and A. R. Calderbank, "Increasing data rate over wireless channels," *IEEE Signal Processing Magazine*, vol. 17, no. 3, pp. 76–92, May 2000.

[4] L. Ren, S. Xi, and J. Song, "Interference cancellation technology in MIMO cellular communications systems," *IEEE Electrical and Computer Engineering, CCECE*, vol. 3, pp. 1941–1944, May 2003.

[5] B. Sklar, "Rayleigh fading channels in mobile digital communications systems part i: Characteristics," *IEEE Communications Magazine*, vol. 35, no. 7, pp. 90 – 100, July 1997.

[6] H. S. Tan, Y. Sun, and J. S. Thompson, "Performance analysis of layered space time block code for future wireless LAN," *accepted for publication in IEEE Vehicular Technology Conference 2004, Fall.*

[7] P. W. Wolniansky, G. J. Foschini, G. D. Golden, and R. A. Valenauela, "V-BLAST:An architecture for realizing very high data rates over the rich-scattering wireless channel," *Signals, Systems, and Electronics,1998.ISSSE98 URSI International Symposium*, pp. 295–300, September 1998.

[8] S. Ye and R. S. Blum, "Optimized signaling for MIMO interference systems with feedback," *IEEE Transactions on Signal Processing*, vol. 51, no. 11, pp. 2839–2848, November 2003.

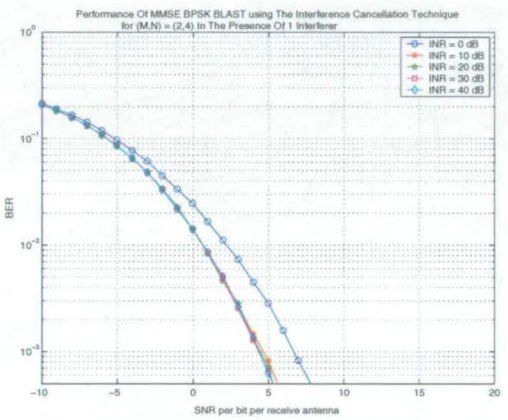

Fig. 1. BER vs SNR for MMSE V-BLAST interference cancellation

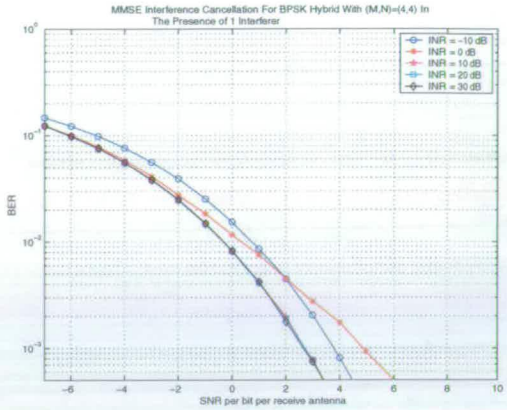

Fig. 2. BER vs SNR for MMSE Dual Alamouti interference cancellation

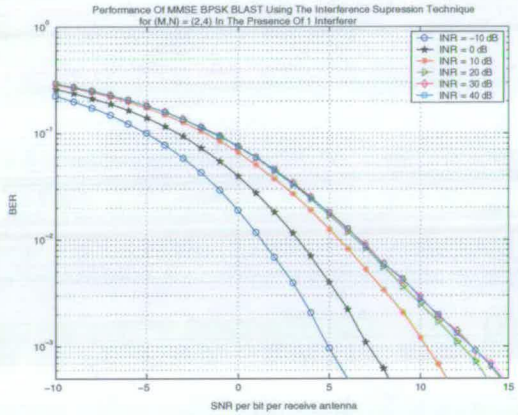

Fig. 3. BER vs SNR for MMSE V-BLAST interference suppression for (M, N)=(2,4)

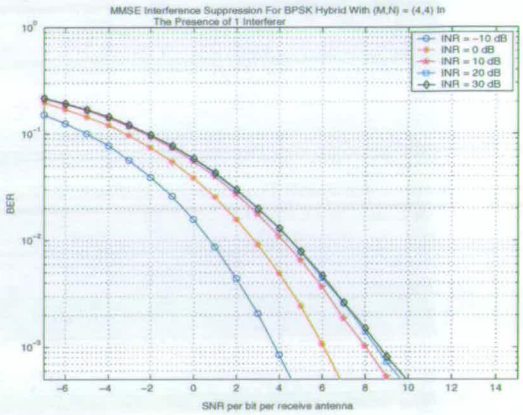

Fig. 5. BER vs SNR for MMSE hybrid interference suppression (M, N) = (4,4)

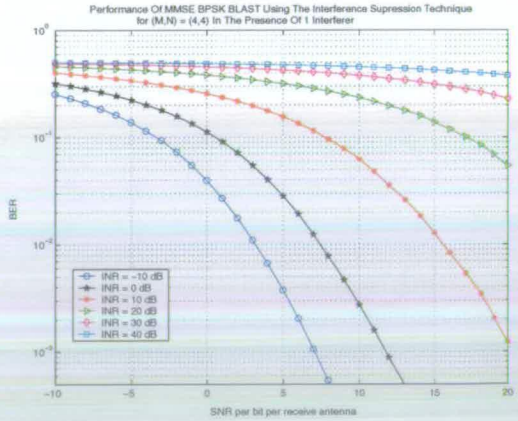

Fig. 4. BER vs SNR for MMSE V-BLAST interference suppression for (M, N)=(4,4)

HS Tan, JS Thompson and DGM Cruickshank
Institute of Digital Communications, University of Edinburgh

Abstract— Opportunistic beamforming(OB) which exploits the advantages of both multiuser diversity and proportional fairness(PF) scheduling is shown to increase the downlink throughput of a system. In this paper, simulation results of delay and throughput performance with respect to the rate of antenna pattern updates are described. A channel model is used which includes shadowing effects, path loss and Rayleigh fading. The results indicate a favourable throughput performance with increasing antenna update rates while the delay performance shows a trade off between average delay and 90 percentile values in which the latter favour the use of OB.

I. INTRODUCTION

PF scheduling can be used in the downlink of a code division multiple access(CDMA) system, such as 1xEV-DO [1], to increase the data throughput. The scheduler works in such a way that it transmits data to the user with the highest priority. This priority is calculated and updated for every time slot based on the signal-to-noise ratio(SNR) of each individual user in the system. Thus, this scheduler tends to favour users with higher SNR. However, users with low SNR who are constantly waiting would have their priority increased for every update until they are scheduled. The multiuser diversity gain, which provided by PF, can be defined as the increase in system throughput as the number of users increase. The diversity gain can be increased by adding more users to the system because the scheduler would have a higher probability of picking a user whose channel SNR is significantly higher than the average. On the other hand, as PF is dependent on the channel dynamics, this scheduler may not work well in a slow fading channel as deep channel fades may last for a significant period of time. Rician fading statistics may also reduce the dynamic range of the fading, reducing multiuser diversity gain [2].

Recently, [2] has proposed a new technique to mitigate problems of slow fading and Rician fading channels. This technique, called opportunistic beamforming(OB), employs multiple antennas at the base station transmitter to improve performance. The power and phase of each element is varied randomly at a rate higher than the channel changes to induce a fast fading channel characteristic. By doing so, the scheduler would see a larger range of SNR values which change more quickly over time.

So far the work done on this area is mainly focused on the throughput performance with different channel characteristics and the use of OB to improve the throughput. The paper extends the discussion of OB with respect to the rate of antenna pattern update. In this paper, the throughput performance with respect to the antenna pattern update rate will be analysed. Another parameter that has not been covered in [2] is the delay characteristics associated with each data packet which will be investigated in this paper. Section 2 describes the simulation scenario. The following two sections introduce the concept of PF scheduling, multiuser diversity and OB. Simulations on the antenna pattern update rate are studied and analysed in section 5. Lastly, conclusions to sum up the performance of OB are presented.

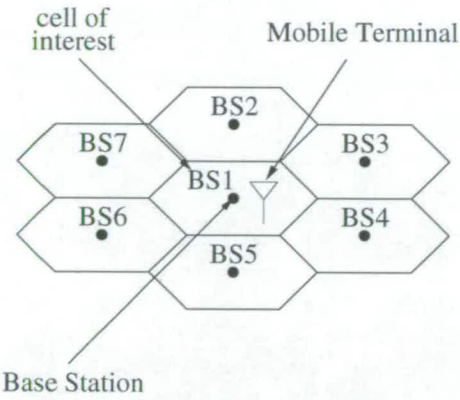

Fig. 1. Layout of the cell scenario

II. SIMULATION SCENARIO

The simulation scenario involves a cell surrounded by 1 tier of neighbouring cells. The centre cell serves as the focus for simulation results as shown in Figure 1. The simulated transmission scheme is based on the 1xEV-DO [1] wireless system, in which packets of data transmitted are classified into 9 different data rates depending on the measured signal-to-interference-noise ratio(SINR) at the mobile terminal. Each time slot is 1.67 ms. The tabular form of this transmission scheme is summarised in Table 1 in [1]. The SINR of the received signal at mobile station(MS) n from base station(BS) 1 can be expressed as (similar to [3]):

$$SINR = \frac{P_{1n}}{\sum_{m=2}^{7} P_{mn} + \sigma^2} \quad (1)$$

where P_{mn} is the received signal power by MS n from BS m and σ^2 is the variance of the complex additive white Gaussian noise(AGWN). The scalar P_{mn} includes the effect of path loss, lognormal shadowing and Rayleigh fading. The attenuation of the received signal from MS which includes the effect of Rayleigh fading is assumed to be(with slight modification of equation (1) in [3]) is:

$$\alpha_{mn} = \beta 10^{\frac{\zeta_{mn}}{10}} (d_{mn})^4 \quad (2)$$

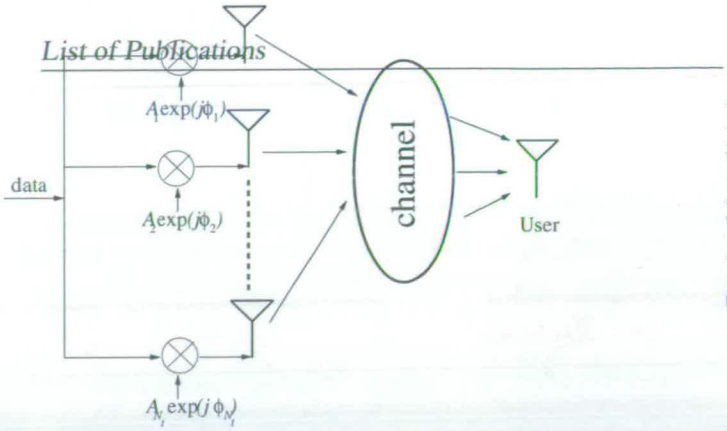

Fig. 2. Opportunistic Beamforming

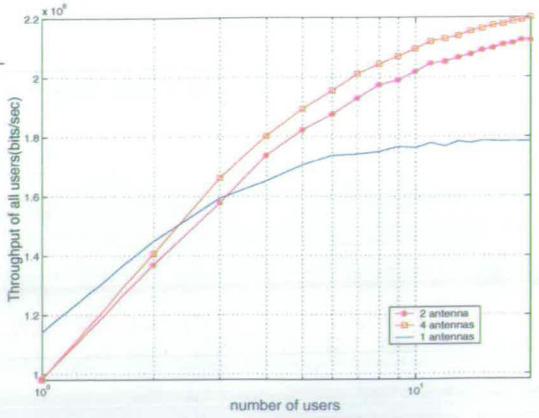

Fig. 3. Throughput vs number of users

where β is the Rayleigh fading coefficient, d_{mn} is the distance from BS m to MS n and ζ is the shadowing coefficients. The coefficients ζ_{mn} are modified to introduce correlation as described in [3]. Note that this model assumes flat fading conditions.

III. PF AND MULTIUSER DIVERSITY

PF [1,4] tracks the data request rate of every user in the system. The user I with the highest priority $c_i(t)$ would be scheduled for transmission. The priority for the *ith* user is calculated as follows:

$$c_i(t) = \frac{DRC_i(t)}{R_i(t)} \tag{3}$$

where DRC_i is the data request rate of of user i and $R_i(t)$ the throughput rate is expressed as follows [2]

$$R_i(t+1) = \begin{cases} (1-\frac{1}{t_c})R_i(t) + \frac{1}{t_c}DRC_i(t) & i = I \\ (1-\frac{1}{t_c})R_i(t) & i \neq I \end{cases} \tag{4}$$

where t_c is the past window length of the filter and I is the number of the user selected by the scheduler for transmission to at time t. The DRC is dependent on the received SINR. In general, a stronger SINR leads to a higher DRC. This scheduling algorithm also introduces fairness in such a way that users with low SINR will have their throughput rates, $R_i(t)$ decrease each time slot whenever they are not transmitted to, hence increasing their priority $c_i(t)$. In this way, the PF algorithm is dependent on two parameters, the DRC which favours high SINR and R to introduce fairness to users with low SINR. Eventually, those users with weak SINR, e.g., at the edge of the cell, will obtain the highest priority and have their chance for transmission. Thus, the average latency of the system is reduced.

The algorithm is summarised in the following steps:
i. Determine the DRC of each user.
ii. Calculate the priority of each user.
iii. Transmit to the user with the highest priority.
iv. Update the throughput rate, R.
v. Repeat for the next time slot.

As already shown in [2], multiuser diversity gain is obtained through the use of PF techniques. This is because the throughput of the system increases as the number of users increase. The amount of multiuser diversity gain is dependent on the channel dynamics. In a fast fading environment, PF can achieve significant gains due to a large range of possible channel amplitudes. On the other hand, where the channel fluctuation is small due to very slow fading or Rician channel conditions, this diversity gain cannot be fully achieved [2].

IV. OPPORTUNISTIC BEAMFORMING

As mentioned in the previous section, multiuser diversity is not fully exploited when the channel variations are small. A newly proposed technique [2] called opportunistic beamforming, aims to mitigate the problem of slow fading and Rician fading channel characteristics. OB exploits the advantages of both PF and multiuser diversity by employing multiple antennas at the base station transmitter. Each antenna's power and phase is varied randomly(as shown in Figure 2) at a rate higher than the channel rate to induce more channel fluctuation. By doing so, the channel characteristic is transformed from a slow to a fast fading type. The sum of all the antennas output power is kept constant such that

$$S = \sum_{j=1}^{N_t} |A_j \exp^{j\phi}|^2 \tag{5}$$

where N_t is the number of antennas at the transmitter, S is the total transmit power, A_j and ϕ_j is the amplitude and phase for the jth antenna respectively. Both $|A_j|^2$ and ϕ_j are uniformly distributed, with ranges 0 to 1 and 0 to 2π respectively. The amplitude coefficients are subsequently normalised to ensure that S in equation (5) is constant.

The main advantage of OB is to increase the system throughput in a slow fading environment. However, it

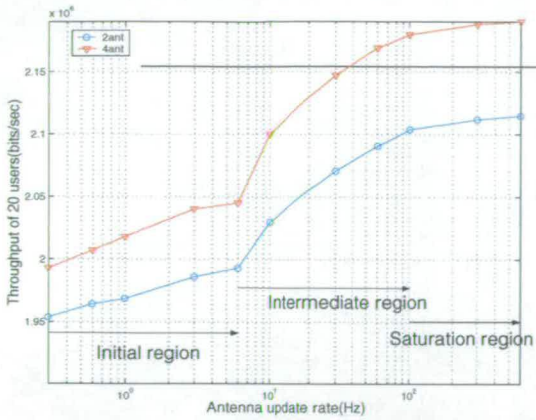

Fig. 4. Throughput vs antenna updates rate

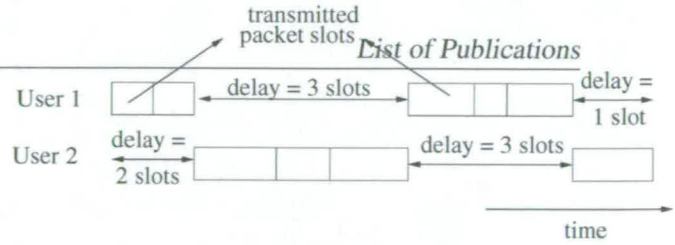

accumulated delay of user 1 = 4

accumulated delay of user 2 = 5

Fig. 5. Delay scenario for 2 users

would be less advantageous to apply OB to a fast fading channel as the difference in throughput performance would be negligible.

V. SIMULATION RESULTS

In order to understand the throughput performance gain through the use of OB, simulation results comparing the performance of OB and PF techniques is illustrated in Figure 3. The antennas' power/phase are updated at a rate of 100 Hz, 10 times the channel fading rate, 10 Hz, for the OB 2 and 4 antennas cases. The simulation is performed for 20 users over 10000 time slots. The value of t_c in (4) is set to be 1000.

The throughput is defined as the average rate of data size transmitted which can be expressed as:

$$\text{Throughput} = \frac{1}{t_{tot}} \sum_{t=1}^{t_{tot}} DRC(t) \qquad (6)$$

where t_{tot} is the total time slots used by the BS for transmitting data.

The use of extra antennas in the OB technique sees an improvement in the system throughput performance for more than 3 users. The cell throughput improves as the number of users increases. This highlights the multiuser diversity gain which is obtained from the PF scheduling.

A. Antenna Update Rate And Delay

As illustrated in Figure 3, the use of OB can provide a significant increase in throughput gain. In this section, the impact on the system performance is studied with respect to the antenna update rate, i.e., how frequently the power/phase at each antenna changes. The simulation parameters are identical to Figure 3 except that the channel Doppler is set to be 6 Hz.

Apart from the throughput performance, the delay performance in terms of the average and 90 percentile delay will be investigated. For each packet transmitted to a given user, the delay is defined as the number of idle packet slots that have occurred since the last packet was sent to the same user. Figure 5 illustrates the delay scenario for 2 users. It can be seen that the delay is measured in packet slots as the time between two packet transmissions to the same user.

A.1 Throughput Performance

The throughput performance for 2 and 4 antennas is shown in Figure 4. This throughput performance can be categorised into 3 regions: initial(antenna update rate $<$ channel Doppler rate), intermediate(antenna update rate $\geq$ channel Doppler rate) and saturation region(antenna update rate $>>$ channel Doppler rate) as shown in the figure.

When the antenna update rate is less than the channel Doppler rate, a moderate increase in throughput with respect to the antenna rate is observed. Further increases in antenna update rate above the channel Doppler rate, defined as the intermediate region, results in a greater increase in the throughput which signifies the value of the OB technique. Subsequent increases in the antenna update rate cause the throughput to reach its maximum limit.

From this simulation result, a 100 Hz antenna update rate would be sufficient to achieve a good throughput performance. In this particular scenario, to achieve the saturation throughput performance, the required ratio of antenna update rate to slot rate is 0.167.

A.2 Delay Performance

Two different statistical parameters for the delay performance through the use of OB techniques with respect to antenna update rate are studied. 4 antennas are implemented at the transmitter. The average delay is a measure of the average waiting time for every user between each transmission. The 90 percentile value gives a more accurate measure of the worst case delay performance. Comparing the average and 90 percentile delay values gives an impression of the range of delay values that can occur. This provides some indication of the quality of service that each user in the system can expect. The average delay and 90 percentile delay values are illustrated in Figure 6 and 7 respectively.

Simulation results given in Figure 6 have shown that the average delay increases as the antenna update rate

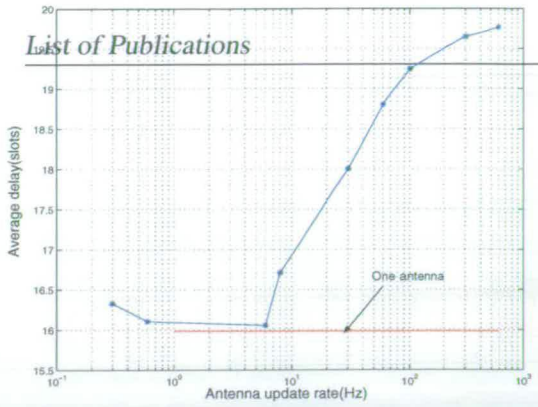

Fig. 6. Average delay performance of OB

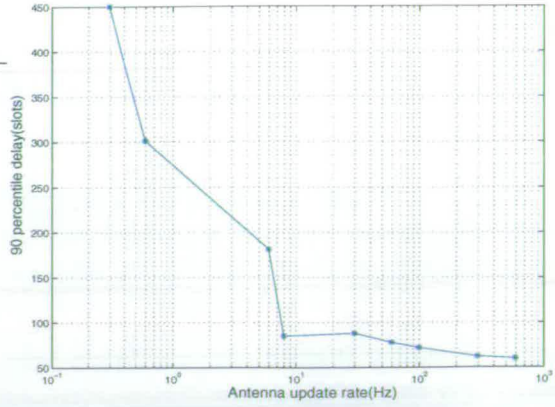

Fig. 7. 90 percentile performance of OB

gets higher. In the region where OB plays a significant role in the system throughput(antenna update rate $\geq$ channel Doppler rate), a slight increase in the average delay is observed. This increase in average delay coincides with the increase in throughput performance. Also shown in this graph is the average delay value with just 1 transmitter antenna, where a lower average delay value than that of the 4 antennas case is seen. The average delay increases because switching between users takes place more quickly with higher antenna update rates.

The 90 percentile delay performance shows the opposite behaviour to the average delay where OB is seen to reduce the delay, rather than increase it. Simulation results given in Figure 7 indicate that the 90 percentile performance for high antenna pattern update rate values(where OB plays an important role to increase the system throughput) looks to be fairly constant and is much lower than the corresponding value for small antenna update rates. In conclusion, a good 90 percentile performance can be achieved by just adjusting the antenna rate slightly above the channel rate.

A trade off in the delay performance between the average delay and 90 percentile is seen. The increase in OB average delay is about 25% compared to the 1 antenna PF case. On the other hand, an order of magnitude improvement in the 90 percentile delay performance clearly will reduce delay jitter significantly. Thus OB can provide a more uniform quality of service than the case when it is not used. Clearly, the worst case delay performance is much better with the use of OB.

VI. CONCLUSION

The simulations in this paper show that the OB throughput performance becomes better for antenna pattern update rates above the channel Doppler rate. On the other hand a mixed system delay performance is observed through the use of OB. Despite the slightly poorer average delay values, the enormous gain in the 90 percentile values shows that OB significantly reduces delay jitter. In general, both the system throughput and delay performance favour the use of OB. OB would be preferred for non real time transmission,(e.g. indoor office scenario) to realise the high throughput achieved for fast data download. In addition to this, data packets are transmitted in a more uniform fashion due to faster switching between users in PF scheduling.

VII. ACKNOWLEDGEMENT

Hwa Sin Tan would like to thank Toshiba Research Europe Ltd (TREL),Telecommunication Research Laboratory for his student sponsorship.

REFERENCES

[1] JH Rhee, TH Kim, and DK Kim, "A wireless fair scheduling alogrithm for 1xEV-DO system", *IEEE Vehicular Technology Conference*, vol. 2, pp. 743–746, Fall 2001.

[2] P Viswanath, D.N.C Tse, and R Laroia, "Opportunistic beamforming using dumb antennas", *IEEE Transactions on Information Theory*, vol. 8, pp. 1277–1294, June 2002.

[3] R Stuetzle and A Paulraj, "Modeling of forward link performance in IS-95 CDMA networks", *IEEE 4th International Symposium On Spread Spectrum Techniques and Applications*, vol. 3, pp. 1058–1062, September 1996.

[4] JM Holtzman, "Asymptotic analysis of proportional fair algorithm", *IEEE 4th International Symposium On Personal, Indoor and Mobile Radio Communications*, vol. 2, pp. F–33–F–37, September/October 2001.

Diversity Technique For Smart Antennas Using Maximal Ratio Combining

Hwa Sin Tan and John Thompson
Department of Electronics and Electrical Engineering, University of Edinburgh,
King's Building, Mayfield Road, Edinburgh EH9 3JL.
email:Hwa.Sin.Tan@ee.ed.ac.uk

Abstract

Smart antenna technologies are potential candidates in future wireless communications for capacity increase and interference cancellation. Diversity is one of the techniques which can be exploited in smart antenna technology. The correlation of signals arriving at the antennas plays an important role in Bit Error Ratio(BER) performance. We will investigate two scenarios, one where signals at the antennas are assumed to be completely correlated whilst the other uncorrelated. Mathematical equations supported by software simulations based on four modulation techniques, namely, BPSK, QPSK, 16QAM and 64QAM, are presented.

1 Introduction

Smart antennas [1–7] are one of the leading technologies in future wireless systems. A smart antenna system combines multiple antenna elements with a signal-processing capability to optimize its radiation and/or reception pattern automatically in response to signal environment [8]. When implemented at the transmitter, the signals at each antenna are multiplied with a coefficient to form beams directing the transmission towards the desired location. Similarly, at the receiver, the signals that arrive at each antenna are multiplied with an assigned weight, then summed for an optimal output.

Smart antennas steer higher power beams toward the location of the users and null their interferers with low power beams. This property increases Signal-to-Interference-Noise-Ratio(SINR) by its virtue of noise and interference reduction. The effect of multipath propagation is minimised by forming narrow beams to reduce delay spread. Another fundamental advantage of employing smart antennas is to increase diversity gain, which will be discussed in detail in the later section. The above mentioned advantages lead to an increase in system capacity, improvement in error rate performance, enhanced date rate and spectral efficiency and increased coverage. However, the implementation of smart antennas increases both hardware and software complexities.

In this paper, we will investigate the difference in diversity gain that can be achieved in two different scenarios, i.e., correlated and uncorrelated fading signals arriving at the antennas. Two common types of smart antennas will be discussed in section 2. Section 3 discusses the different diversity techniques that can be achieved in smart antennas while the following section shows the mathematical equations of BER probability. Section 5 comments on the simulation results while section 6 concludes the paper.

2 Smart Antennas- Multibeam and Adaptive Array Combining

A multibeam configuration as shown in Figure 1a is a 'fixed' antenna system where M beam patterns are formed by an array of antennas. A multibeam system has the ability to increase uplink SINR and to reduce interference on both up and downlink.

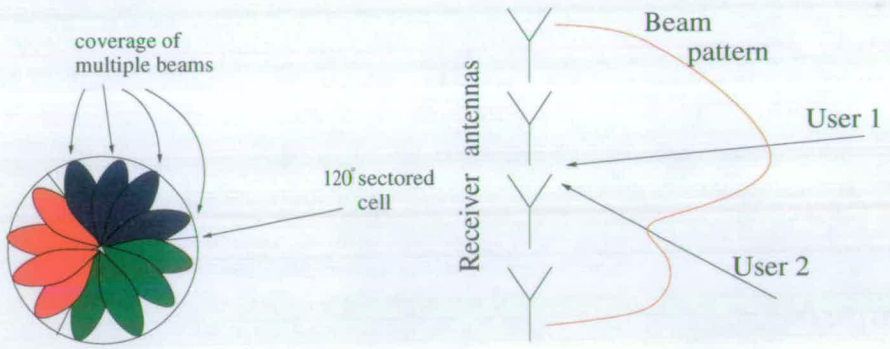

(a) Beams distribution in Multibeam

(b) Amplitude of Rayleigh variable

Figure 1: Smart antennas

Locking onto the wrong beam due to multipath and interference from other users is one of the disadvantages. Also, scalloping (signals arriving between beams) might decrease the antenna gain by approximately 3-4 dB [5].

Multibeam systems perform poorly in a large angular spread environment, e.g., indoor, due to the need of several beams to be utilised to capture all the signal energy. Therefore, the concept of adaptive array combining may be preferable for such environments. A picture of an adaptive antenna receiver is shown Figure 1b.

The receiver antennas detect all signals that arrive, and then multiply, and combine them to maximise the SINR. Hence, multipath propagation is exploited to improve performance. With

M antennas, the array can cancel interference from up to M-1 users, though this causes noise enhancement. In a large angular spread environment, irrespective of the location of the user and interferer, this technique is still able to cancel interference due to multipath scattering of signals. The equivalent cancellation operation could be much more difficult if multibeam were deployed.

In a line-of-sight(LOS) environment, adaptive antennas can again form M-1 nulls for M-1 interferers. However, in this particular environment, a multibeam system would be preferred due to its reduced complexity.

3 Diversity

Diversity [5], [7] is a technique to exploit low signal correlation at different antennas. Signals propagating in a radio environment are preferred to be uncorrelated with one another when they arrive at the receiver. This is because the probability that all signals will simultaneously fall into a deep fade is smaller for uncorrelated signals. Three of the diversity techniques that can be achieved are angle, polarisation and space diversity.

Angle diversity is achieved by forming adjacent narrow beams, in which arriving signals at the different beams have low fading correlation. This technique works best in an environment with large angle spread. Polarisation diversity uses two orthogonal polarised antennas, e.g., vertical and horizontal polarisation which have low correlation between them. Spatial diversity is gained by spacing antenna elements far apart for low fading correlation.

Several combining methods [7] can be performed at the receiver to achieve diversity gain. Selection diversity selects the antenna with highest signal-to-noise ratio(SNR) to minimise BER performance. Equal-gain combining(EGC) adds up all the antennas' signals at the receiver. EGC weighs all branches equally irrespective of the channel condition, which might reduce the combined output SNR. Hence, the preferred method would be maximal ratio combining(MRC) where all branches are weighted according to their channel amplitude and phase. The simulations performed in the following section will be based on the MRC technique.

4 Theoretical Analysis of MRC

The mathematical expression of bit error probability(BEP) supported by simulation results will be shown in this section. The BEP equation of four modulation schemes, i.e., BPSK, QPSK, 16QAM and 64QAM will be evaluated to achieve the desired equation for employing multiple antennas at receiver in a Rayleigh flat fading channel. In this study, average received power in each antenna branch is assumed to be equal. With Rayleigh fading, the probability density function(pdf) of the received signal envelope(r) is [9]:

$$\rho(r) = \begin{cases} \frac{r}{\sigma^2} \exp[\frac{r^2}{2\sigma^2}] & \text{for } r \geq 0 \\ 0 & \text{otherwise} \end{cases}$$

where $2\sigma^2$ is the predetection mean power of the multipath signal.

The average BEP for m-ary QAM is expressed [10] as

$$P_{e,m}(\overline{\gamma}) = \int_0^\infty \sum_i A_i Q(\sqrt{a_i \gamma}) f_{\overline{\gamma}} d\gamma \quad (1)$$

$$= \sum_i A_i P_e(\overline{\gamma}; a_i) \quad (2)$$

where $\overline{\gamma}$ is the SNR per symbol and the parameters (A_i, a_i) are tabulated as in [10].

m	modulation	coefficients
2	BPSK	$\{(1,2)\}$
4	QPSK	$\{(1,1)\}$
16	16QAM	$\{(\frac{3}{4},\frac{1}{5}), (\frac{2}{4},\frac{3^2}{5}), (-\frac{1}{4},\frac{5^5}{5})\}$
64	64QAM	$\{(\frac{7}{12},\frac{1}{21}), (\frac{6}{12},\frac{3^2}{21}), (\frac{-1}{12},\frac{5^2}{21}), (\frac{1}{12},\frac{9^2}{21}), (\frac{-1}{12},\frac{13^2}{21})\}$

Table 1: Coefficients of $(A_i, a_i)$for equation (2)

while the $P_e(\overline{\gamma}; a_i)$ can be expressed as

$$P_e(\overline{\gamma}; a_i) = \frac{1}{2}\left(1 - \sqrt{\frac{a_i \gamma}{2 + a_i \gamma}}\right) \quad (3)$$

Consider now a Single Input Multiple Output(SIMO) system, where signals arrive at a set of N antennas. If the N antennas' signals at the receiver are assumed to be completely correlated, the expression in (3) can be expanded to obtain the BEP as:

$$P_{e,m}(\overline{\gamma}) = \sum_i \frac{1}{2} A_i \left(1 - \sqrt{\frac{a_i N \gamma}{2 + a_i\ N\gamma}}\right) \quad (4)$$

while the BEP for uncorrelated signals [11] is given by

$$P_e(\overline{\gamma}; a_i) = \left[\frac{1}{2}(1-\mu)\right]^N \sum_{k=0}^{N-1} \binom{N-1+k}{k} \left[\frac{1}{2}(1+\mu)\right]^k \quad (5)$$

where $\mu = \sqrt{\overline{\gamma}/(1+\overline{\gamma})}$.

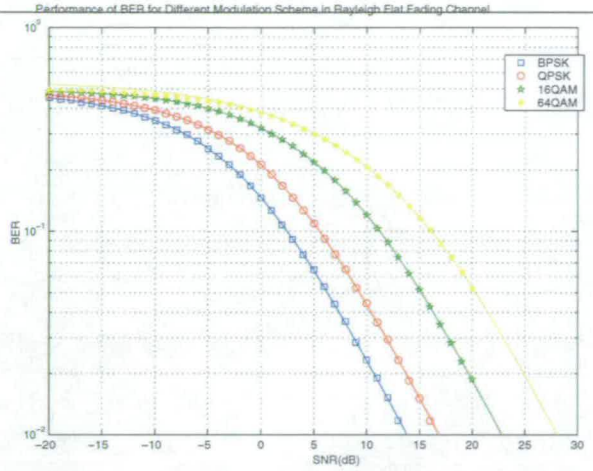

Figure 2: Performance of different modulation schemes in Rayleigh flat fading channel

5 Results

Figure 2, 3a and 3b show the results for m-QAM Single Input Single Output(SISO), BPSK SIMO correlated signals and BPSK SIMO uncorrelated signals respectively. Simulation results are shown as markers, while theoretical results are shown as solid lines. All figures show a good match between theory and simulation.

In Figure 2, for a BER of 10^{-2}, BPSK requires 3 dB, 9.1 dB and 14.3 dB less SNR than QPSK, 16QAM and 64QAM respectively. It is clear from these results that there exists a trade off between BER performance and data rate. Figure 3a for BPSK correlated signals, shows that for every increase in the number of antennas by a factor of 2, there is only a 3dB increase in SNR for a particular BER value. Figure 3b for uncorrelated signals, for a BER value of 10^{-2}dB, there is a diversity gain of 8.3 dB, 5.3 dB, 4.0 dB and 3.5 dB between N=1 and N=2, N=2 and N=4, N=4 and N=8 and N=8 and N=16 respectively. These diversity gains for uncorrelated signals do not appear in correlated ones because uncorrelated signals are less likely to suffer deep fades at the same time in a radio channel. It is apparent that the subsequent gain becomes less as N increases. A comparison between Figure 3a and 3b shows that for a BER value of 10^{-2}, uncorrelated signals outperformed correlated ones by 2.3 dB, 4.5 dB, 5.5 dB and 6.2 dB for N = 2, 4, 8 and 16 antennas respectively. These results instigate the fact that increasing the number of antenna elements improve the BER performance.

6 Conclusion

This paper shows that antenna diversity can significantly improve BER performance provided received signals between diversity branches are uncorrelated. In fact, [12] has mentioned that good diversity gain can be obtained provided the correlation value is low, e.g. <0.7. With the use

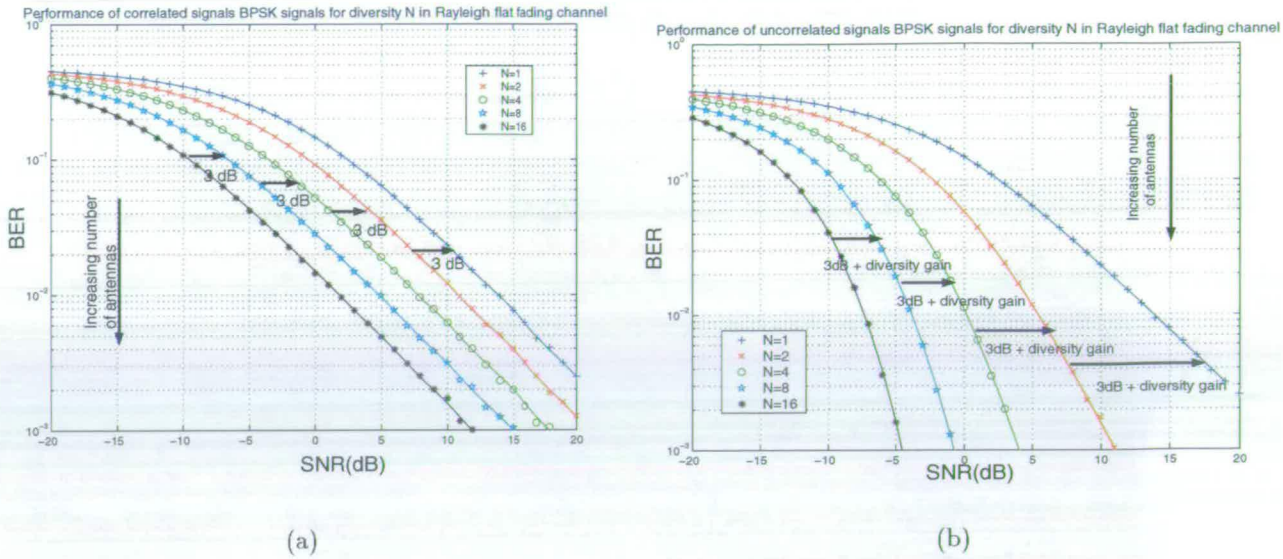

(a) (b)

Figure 3: Performance of signals in a Rayleigh flat fading channel employing N antennas for (a) BER vs SNR for correlated BPSK signals, (b) BER vs SNR for uncorrelated BPSK signals.

of diversity techniques such as those mentioned in section 3, this technique can be fully exploited for minimum BER. However, the number of elements are restricted to the available space in a mobile handset. While BER performance can be improved by increasing diversity, the next issue is to increase capacity in a wireless local area networks(WLAN) [13], [14]. One of the ways is to implement an orthogonal multicarrier based Multiple Input Multiple Output(MIMO) system. Techniques such as BLAST [15] and beamforming will be studied and investigated in depth to see how space time processing can be used to improve system performance.

7 Acknowledgement

Hwa Sin Tan would like to thank Toshiba Research Europe Ltd (TREL),Telecommunication Research Laboratory for his student sponsorship.

References

[1] Seshaiah Ponnekanti, "An overview of smart antenna technology for heterogeneous networks", *IEEE Communications Surveys*, vol. 2, Fourth Quarter 1999.

[2] Per H. Lehne and Magne Pettersen, "An overview of smart antenna technology for mobile communications systems", *IEEE Communications Surveys*, vol. 2, Fourth Quarter 1999.

[3] Richard B.Ertel, Paulo Cardieri, Kevin W. Sowerby, Theodore S. Rappaport, and Jeffrey H. Reed, "Overview of spatial channel models for antenna array communication systems", *IEEE Personal Communications*, vol. 5, pp. 10–22, February 1998.

[4] John S. Thompson, Peter M. Grant, and Bernard Mulgrew, "Smart antenna arrays for CDMA systems", *IEEE Personal Communications*, vol. 3, pp. 16 – 25, October 1996.

[5] Jack H. Winters, "Smart antenna for wireless systems", *IEEE Personal Communications*, vol. 5, pp. 23–27, February 1998.

[6] Ryuji Kohno, "Spatial and temporal communication theory using adaptive antenna array", *IEEE Personal Communications*, vol. 5, pp. 28–35, February 1998.

[7] Simon R Saunders, *Antennas and Propagation for Wireless Communication Systems*, John Wiley and Sons, first edition, 1999.

[8] "http://www.stanford.edu/~azizn/".

[9] Bernard Sklar, "Rayleigh fading channels in mobile digital communications systems part i: Characteristics", *IEEE Communications Magazine*, vol. 35, pp. 90 – 100, July 1997.

[10] Byoung Jo Choi, *Multi-Carrier Code Division Multiple Access*, PhD thesis, University of Southampton, June 2001.

[11] John G. Proakis, *Digital Communications*, McGraw Hill, fourth edition, 2000.

[12] W.C.Y.Lee, "Effects on correlation between two mobile radio base station antennas", *IEEE Transactions on Communications*, vol. 21, pp. 1214–1223, November 1973.

[13] Jamshid Khun-Jush, Peter Schramm, Udo Wachsmann, and Fabian Wenger, "Structure and performance of the HIPERLAN/2 physical layer", *IEEE Vechicular Technology Conference*, vol. 5, pp. 2667 – 2671, Fall 1999.

[14] "IEEE standard 802.11, part11: Wireless LAN medium access control(MAC) and physical layer(PHY) specifications", 1999.

[15] A Lozano, F.R Farrokhi, and R.A Valenzuela, "Lifting the limits on high speed wirelss data access using antenna arrays", *IEEE Communications Magazine*, vol. 39, pp. 156–162, Sept 2001.

INVESTIGATION OF HYBRID MIMO TECHNIQUES

John S. Thompson(†), Hwa Sin Tan(†) and Yong Sun(‡)
(†) Institute for Digital Communications, School of Engineering and Electronics
The University of Edinburgh, Edinburgh, EH9 3JL, UK.
(‡) Toshiba Research Laboratory, Queens Square, Bristol, BS1 4ND, UK
Email: John.Thompson@ed.ac.uk

Keywords: antenna arrays, multiple input–multiple output, V-BLAST, Alamouti scheme.

ABSTRACT

This paper compares and investigates the performance of wireless local area network systems using multiple input–multiple output (MIMO) techniques. In particular, two different algorithms, V-BLAST and space–time block coding (STBC), are described. A third hybrid approach, which incorporates elements of both V-BLAST and STBC is also introduced. All three techniques are compared using both theoretical Shannon capacity analysis and by simulation results for the bit error ratio performance of the three methods. It is shown that the hybrid method attains superior diversity gain performance to V-BLAST and can outperform V-BLAST at spectral efficiencies of practical interest.

I. INTRODUCTION

Multiple antennas are a new solution for high data rate wireless local area networks (WLANs) [1]. They are preferable to increasing the sensitivity of the receiver or increasing the power of the transmitted signal. The latter technique is not effective because the increase in attainable channel capacity is only a logarithmic function of the increase in signal-to-noise ratio (SNR) for the received signal. Moreover, this technique is limited by thermal noise and maximum limits on radiating power in the WLAN frequency bands. This leads to alternative solutions where multiple antennas are deployed at both the transmitter and receiver. The implementation of multiple transmit (Tx) antennas increases the data rate, while the multiple receive (Rx) antennas support the signal processing required to separate the transmitter antennas.

Multiple input-multiple output (MIMO) systems are an effective way to achieve high data rate and spectrally efficient WLANs, as their capacity increase is linearly proportional to the number of antennas employed at the transmitter and receiver. Three different MIMO signal processing techniques will be studied in this paper. These include spatial multiplexing, i.e. an implementation of the vertical Bell Labs layered space-time (V-BLAST) algorithm [1], space-time block coding (STBC) [2] and a hybrid of the BLAST and STBC schemes [3]. The V-BLAST algorithm aims to maximise the capacity by using a combination of spatial processing and subtractive cancellation to remove co-channel interference, provided that the number of antennas at the receiver is greater or equal to that of the transmitter. Conversely, the STBC or Alamouti scheme exploits the diversity against fading that is available from employing multiple antennas at the transmitter and possibly at the receiver. We also consider in this paper a third technique, which is called the Dual Alamouti technique. This method combines elements of both spatial multiplexing (V-BLAST) and STBC to try to exploit the advantages of both higher data rates and increased diversity gain.

In this paper, the Shannon capacity of the three techniques will be investigated theoretically. This analysis will also be complemented by detailed simulation studies of the algorithms, investigating the bit error ratio performance of the three receivers. The results will show that in some cases the Dual Alamouti algorithm can significantly outperform the V-BLAST and STBC techniques. The remainder of this paper is structured as follows. Section II of the paper will describe the system model that is used in the paper. Section III will describe the algorithms to be compared. Section IV will investigate Shannon capacity results for the three techniques. Section V will present simulation results and finally section VI will present conclusions to the paper.

II. SYSTEM MODEL

In this paper, we consider a single user wireless channel, where the transmitter employs M separate Tx antennas and the receiver uses N Rx antennas. This configuration is denoted as the (M, N) MIMO system. The M Tx antennas transmit M synchronous data streams at the same radio carrier frequency. The channel is assumed to be frequency-flat Rayleigh fading. Assuming ideal demodulation to baseband, the receiver signal can be expressed as:

$$\mathbf{r}(k) = \sqrt{P_T/M}\mathbf{H}\mathbf{a}(k) + \boldsymbol{\eta}(k), \qquad (1)$$

where P_T is the power at the transmitter and k denotes the time index. The vector $\mathbf{r}(k)$ is the size N received signal vector $\{r_1(k), r_2(k)...r_N(k)\}^T$ where $r_n(k)$ denotes the received signal at Rx antenna n. Further, $\mathbf{a}(k)$ is the quadrature amplitude modulation (QAM) transmission vector $\{a_1(k), a_2(k)...a_M(k)\}^T$ of size M, where $a_m(k)$ denotes the transmitted QAM symbol at antenna m. The matrix $\mathbf{H}$ is the $N \times M$ channel matrix where the element at row n and column m, $h_{n,m}$ denotes the channel response at receiver n due to

transmitter m. The NM channels $h_{n,m}$ are statistically independent, identically distributed random variables. The vector $\boldsymbol{\eta(k)}$, which equals $\{\eta_1(k), \eta_2(k)...\eta_N(k)\}^T$, represents additive white Gaussian noise at the receiver with zero mean and variance σ^2 where η_n is the noise received at the n-th antenna. A block diagram of the system under consideration can be seen in Fig 1.

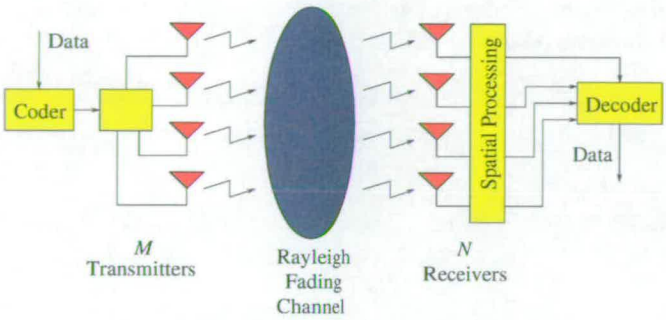

Fig. 1. A diagram of a single user multiple input–multiple output wireless system using M transmit and N receive antennas.

III. MIMO ALGORITHMS UNDER CONSIDERATION

In this section, the three main algorithms will be introduced and explained in turn. These are the V-BLAST algorithm, the Alamouti scheme and the Dual Alamouti MIMO scheme.

A. V-BLAST

V-BLAST[1] is a spatial multiplexing transmission scheme that has the capability to support high data rates which are linearly proportional to the number of Tx and Rx antennas. The architecture of V-BLAST consists of M spatially multiplexed data streams at the transmitter, which are measured at N Rx antennas. For successful operation of the algorithm, it is usually required that $N \geq M$.

The V-BLAST signal processor operates using M detection cycles, one for each Tx antenna. The ordering algorithm selects the antenna with the strongest SNR, followed by the next strongest, until every antenna signal has been detected. Reconstructed signals for the detected antennas are then subtracted from the received signal to remove interference to the remaining undetected antennas. During the detection process, except for the antenna signal to be detected, the interference from antennas yet to be detected must be suppressed. This operation is performed by linearly weighting the received signals to satisfy the minimum mean squared error(MMSE) criterion[4]. The MMSE detector is defined as:

$$\mathbf{G}_1 = \mathbf{H}^H(\mathbf{H}\mathbf{H}^H + \frac{\sigma^2}{P_T/M}\mathbf{I_M})^{-1}, \tag{2}$$

where $\mathbf{I}_M$ is the $M \times M$ identity matrix. The subscript notation $\mathbf{G}_1$ indicates that this matrix is used in the first detection cycle. This $M \times N$ matrix $\mathbf{G}_1$ pre-multiplies the received signal to separate spatially each antenna's signal from all others. This means that data detection can be performed independently on each of the M outputs from the multiplication. In order to determine which transmit antenna has the best SNR at the ith iteration, the following formula for the mth antenna is used:

$$\mathrm{SNR}_i(m) = \frac{|\alpha|^2 E(|a_m|^2)}{\beta_i}, \tag{3}$$

where α and β are defined as:

$$\begin{aligned} \alpha &= \mathbf{G}_i(m)\mathbf{H}(m) \\ \beta_i &= |\mathbf{G}_i(m)|^2\sigma^2 + \sum_{\substack{p=1 \\ p\neq k_1\cdots k_{i-1}}}^{M} |\mathbf{G}_i(m)\mathbf{H}(p)|^2 E(|a_p|^2). \end{aligned} \tag{4}$$

The vector $\mathbf{G}_i(m)$ is the m-th *row* of $\mathbf{G}_i$ calculated after $(i-1)$ detection cycles. Similarly, the vector $\mathbf{H}(m)$ is the mth *column* of $\mathbf{H}$.

The optimal ordering for detection and symbol cancellation makes V-BLAST different from the conventional linear combinatorial nulling. Let $S = \{k_1, k_2, ...k_M\}$ be a permutation of integers from 1 to M specifying the order of detecting the symbol vector $\mathbf{a}$. The soft decision statistic for the mth antenna at iteration i can be formed by multiplying the nulling vector and received signal:

$$y(k_i) = \mathbf{G}_i(k_i) \times \mathbf{r}_i, \tag{5}$$

where $\mathbf{r}_i$ denotes the received signal after subtracting $(i-1)$ previously detected signals . The decision statistic is then quantised in accordance to the constellation in use:

$$\hat{a}(k_i) = \mathrm{Q}[y(k_i)], \tag{6}$$

where Q[ ] is the slicer to its respective constellation in use. The detected data are subtracted from the received signal while the column vectors of $\mathbf{H}$ due to the detected symbols are nulled. Finally, the received signal is updated for the next iteration as follows:

$$\mathbf{r}_{i+1} = \mathbf{r}_i - \hat{a}(k_i) \times \mathbf{H}_i(k_i), \tag{7}$$

where $\mathbf{H}_i(k_i)$ denotes the k_ith column of $\mathbf{H}_i$ after zeroing $(i-1)$ columns matching the $(i-1)$ previously detected signals. The subtraction of the detected data from the received signal aims to minimise errors in the subsequent detection process, provided the detected data possesses a certain degree of accuracy. At the end of the ith detection cycle, the matrix $\mathbf{H}_{i+1}$ is formed by setting column k_i of the matrix $\mathbf{H}_i$ to zero. The MMSE matrix $\mathbf{G}_{i+1}$ must then be re-calculated using equation (2) with $(\mathbf{H}_{i+1})$ used in place of $\mathbf{H}$.

B. Alamouti Scheme

This particular scheme is restricted to using $M = 2$ antennas at the transmitter but can use any number of Rx antennas N. Two QAM symbols a_1 and a_2 for transmission by the Alamouti scheme are encoded in both the space and time domain at the two Tx antennas over two consecutive symbol periods as shown in (8).

$$\mathbf{A} = [\acute{\mathbf{a}}(1)\acute{\mathbf{a}}(2)] = \begin{bmatrix} a_1 & -a_2^* \\ a_2 & a_1^* \end{bmatrix}. \tag{8}$$

In order to decode the signal, the received signal can be expressed as:

$$\begin{aligned} \acute{\mathbf{r}} &= \sqrt{\frac{P_T}{2}}\mathbf{H}_A\acute{\mathbf{a}}(1)+\acute{\boldsymbol{\eta}} \\ \begin{bmatrix} \acute{\mathbf{r}}_1 \\ \acute{\mathbf{r}}_2 \\ \vdots \\ \vdots \\ \acute{\mathbf{r}}_N \end{bmatrix} &= \sqrt{\frac{P_T}{2}}\begin{bmatrix} \mathbf{H}_{A,1} \\ \mathbf{H}_{A,2} \\ \vdots \\ \vdots \\ \mathbf{H}_{A,N} \end{bmatrix}\acute{\mathbf{a}}(1)+\begin{bmatrix} \acute{\eta}_1 \\ \acute{\eta}_2 \\ \vdots \\ \vdots \\ \acute{\eta}_N \end{bmatrix}, \end{aligned} \quad (9)$$

where $\acute{\mathbf{r}}_n = [r_n(0), r_n(1)^*]^T$ is the received signal vector at receiver n during symbol periods $k = 0$ and 1. Similarly, $\acute{\boldsymbol{\eta}}_n = [\eta_n(0), \eta_n(1)^*]^T$ denotes the noise samples at antenna n for the two symbol periods.. The matrix $\mathbf{H}_{A,n}$ is defined as:

$$\mathbf{H}_{A,n} = \begin{bmatrix} h_{n,1} & h_{n,2} \\ -h_{n,2}^* & h_{n,1}^* \end{bmatrix}. \quad (10)$$

Decoding the data is achieved be done by multiplying the received signal with the Hermitian transpose of the channel matrix $\mathbf{H}_A$ as:

$$\begin{aligned} \hat{\mathbf{a}}(1) &= \mathbf{H}_A^H\acute{\mathbf{r}} = \sqrt{\frac{P_T}{2}}\mathbf{H}_A^H\mathbf{H}_A\acute{\mathbf{a}}(1)+\mathbf{H}_A^H\acute{\boldsymbol{\eta}} \\ &= \sqrt{\frac{P_T}{2}}\begin{bmatrix} \gamma & 0 \\ 0 & \gamma \end{bmatrix}\begin{bmatrix} a_1 \\ a_2 \end{bmatrix}+\mathbf{H}_A^H\acute{\boldsymbol{\eta}}. \end{aligned} \quad (11)$$

In this equation $\gamma = \sum_{m=1}^{2}\sum_{n=1}^{N}|h_{(n,m)}|^2$.

C. Dual Alamouti Scheme

In the previous section on the Alamouti scheme, it is seen that for 2 Tx antennas to achieve full diversity, the spectral efficiency of the system is the same as that of a single transmitter antenna. In order to improve on the spectral efficiency of the system, a 4 Tx structure is now considered, where the Alamouti scheme is applied separately to two pairs of antennas. This means that two data streams are spatially multiplexed on two different pairs of antennas. The received signal for this transmitter configuration may be written in a similar manner to (9):

$$\begin{aligned} \mathbf{r}' &= \sqrt{\frac{P_T}{4}}\mathbf{H}_D\mathbf{a}(1)+\boldsymbol{\eta}' \\ \begin{bmatrix} \acute{\mathbf{r}}_1 \\ \acute{\mathbf{r}}_2 \\ \vdots \\ \acute{\mathbf{r}}_N \end{bmatrix} &= \sqrt{\frac{P_T}{4}}\begin{bmatrix} \mathbf{H}_{A,1} & \mathbf{H}_{B,1} \\ \mathbf{H}_{A,2} & \mathbf{H}_{B,2} \\ \vdots & \vdots \\ \mathbf{H}_{A,N} & \mathbf{H}_{B,N} \end{bmatrix}\mathbf{a}(1)+\begin{bmatrix} \acute{\eta}_1 \\ \acute{\eta}_2 \\ \vdots \\ \acute{\eta}_N \end{bmatrix} \end{aligned} \quad (12)$$

In this equation,the vector $\mathbf{a}(1) = [a_1, a_2, a_3, a_4]^T$, where the quantities a_3 and a_4 represent the QAM symbols for the second Alamouti-encoded data stream which are transmitted simultaneously with a_1 and a_2. The matrix $\mathbf{H}_{B,m}$ is defined as:

$$\mathbf{H}_{B,n} = \begin{bmatrix} h_{n,3} & h_{n,4} \\ -h_{n,4}^* & h_{n,3}^* \end{bmatrix}, \quad (13)$$

Unlike equation (11), the two symbol pairs (a_1, a_2) and (a_3, a_4) interfere with one another, so simple linear decoding is no longer optimal. However, the form of equation (12) means that the V-BLAST algorithm can be applied directly to detect the data symbols $a_1 - a_4$. As with the Alamouti scheme, the structure of the Dual Alamouti scheme means that a_1 and a_2 do not interfere with one another, which is also the case for a_3 and a_4. The dimension of $\mathbf{r}'$ in equation (12) is $2N$, which means that the transmissions of 4 Tx antennas can be successfully decoded with only 2 Rx antennas.

IV. SHANNON CAPACITY COMPARISONS

In this section, Shannon capacity results for the three algorithms under consideration will be revised. Under the assumption of unit bandwidth, the Shannon capacity of the MIMO system shown in equation (1) is given by the formula [5]:

$$C_1 = \log_2 \det\left(\mathbf{I}_M + \frac{P_T}{M\sigma^2}\mathbf{H}^H\mathbf{H}\right) \quad \text{(bits/sec/Hz)}. \quad (14)$$

In this formula, det( ) denotes the matrix determinant operation. This formula assumes that the transmitter possesses no knowledge of the channel matrix $\mathbf{H}$. It has been shown, in for example [6], that the MMSE V-BLAST detector can achieve the full Shannon capacity C_1. This holds under the constraint that at capacity, decoding of each transmitter's signal can be performed error-free, so that the subtractive cancellation process in equation (7) is performed perfectly.

In order to calculate the capacity of the Alamouti scheme, we can notice that equation (9) has the same general form as (1). So, equation (14) can also be applied to this system. However, the vector $\mathbf{r}'$ is measured over two consecutive symbol periods. For consistent results, the effective bandwidth of the system must be divided by two in compensation. So, the following result is obtained [7]:

$$C_2 = \frac{1}{2}\log_2 \det\left(\mathbf{I}_2 + \frac{P_T}{2\sigma^2}\mathbf{H}_A^H\mathbf{H}_A\right) = \log_2\left(1+\frac{P_T\gamma}{2\sigma^2}\right). \quad (15)$$

The RHS of this equation may be obtained from the LHS by noticing the orthogonal structure of the matrix product $\mathbf{H}_\mathbf{A}^\mathbf{H}\mathbf{H}_\mathbf{A}$ in equation (11).

Again, the capacity of the Dual Alamouti scheme may be obtained by noticing that equation (12) has the same general form as (1). As with the Alamouti scheme, the bandwidth must be scaled by a factor of two to compensate for $\mathbf{r}'$ being measured over two consecutive symbol periods. This time, the resulting capacity equation is:

$$C_3 = \frac{1}{2}\log_2 \det\left(\mathbf{I}_4 + \frac{P_T}{4\sigma^2}\mathbf{H}_D^H\mathbf{H}_D\right). \quad (16)$$

The matrix $\mathbf{H}_D$ is defined in equation (12). The equations for $C_1 - C_3$ may be evaluated to compare the achievable Shannon capacities of the three systems.

V. SIMULATION RESULTS

In this section results are initially presented for the Shannon capacity of the different schemes. Then, results are presented

for the bit error ratio (BER) vs SNR performance of the different schemes, to compare with the capacity results.

A. Capacity Results

In this section, the results obtained from evaluating the formulas for $C_1 - C_3$ in section IV are compared. This is done by generating 10,000 sample $\mathbf{H}$ matrices and using these to evaluate the channel capacity at different SNRs. The results are presented as 1% outage capacities — that is, the capacity that is exceeded for 99% of all channel realisations.

The results for two Rx antennas are presented in Fig 2 (a). In this case, it can be seen that the (4,2) Dual Alamouti scheme provides a distinct performance advantage over the (2,2) V-BLAST or Alamouti schemes at high SNRs. In part (b) of the figure, results for four Rx antennas are presented. It can be seen that at lower SNRs, the (4,4) V-BLAST and Dual Alamouti schemes achieve similar capacity results. However, at higher SNRs, (4,4) V-BLAST begins to out-perform the Dual Alamouti scheme. Both of these techniques perform better than (2,4) Alamouti or V-BLAST.

B. Frame Error Ratio Results

Results for the BER vs SNR performance of the different schemes will now be considered. In all of these simulations, a rate 1/2, constraint length 7 code was employed, using soft decision Viterbi decoding. A frame length of 3066 data bits was used at the transmitter for encoding and transmission.

The first results presented in Fig 3 compare the performance of the three schemes for a spectral efficiency of 2 bits/s/Hz. Looking first to the schemes with 2 Rx antennas, it can be seen that the (2,2) V-BLAST method provides the poorest performance. The (2,2) Alamouti scheme performs slightly better, while the (4,2) Dual Alamouti scheme provides the best performance. Moving on to 4 Rx antennas, it can be seen that (2,4) Alamouti provides the poorest performance, while (2,4) V-BLAST slightly outperforms (4,4) V-BLAST. Again the (4,4) Dual Alamouti scheme provides the best performance of all techniques considered.

The spectral efficiency of the MIMO system was increased to 4 bits/s/Hz for the second set of simulations, the results of which are shown in Fig 4. In this case, results are only shown for V-BLAST and Dual Alamouti, as the Alamouti scheme would require to use at least 256 QAM to achieve the desired spectral efficiency. Again, it can be seen that for 2 Rx antennas, the Dual Alamouti scheme performs significantly better than V-BLAST. For 4 Rx antennas, the Dual Alamouti and V-BLAST schemes achieve similar performances for 4 transmit antennas.

Finally, the simulations were updated to consider a somewhat higher spectral efficiency of 6 bits/s/Hz. The simulation results for this case are shown in Fig 5. Again, results are only shown for V-BLAST and Dual Alamouti, as the Alamouti scheme would require to use at least 4096 QAM. For two Rx antennas, it can again be seen that the (4,2) Dual Alamouti scheme achieves a significant performance advantage over the (2,2) V-BLAST configuration. For four Rx antennas, the (4,4) Dual Alamouti scheme performs better than either (2,4) or (4,4) V-BLAST at low SNRs.

(a)

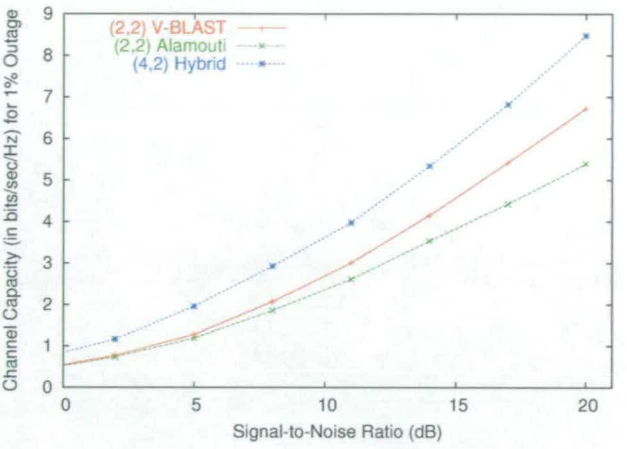

(b)

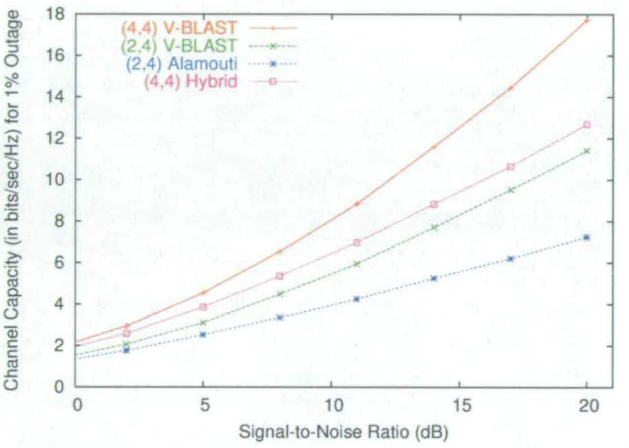

Fig. 2. Shannon capacity vs SNR performance of the three schemes under consideration for (a) 2 Rx and (b) 4 Rx antennas.

VI. CONCLUSIONS

This paper has compared the performance of V-BLAST, the Alamouti STBC and the hybrid Dual Alamouti scheme. Results for the Shannon capacity of the three systems shows that for 2 receive antennas, the Dual Alamouti scheme provides the best performance. In the case of 4 receive antennas, the V-BLAST algorithm attains the best spectral efficiency at high SNRs. Simulation results for the bit error ratio performance of the algorithms using convolutionally coded modulation have also been presented for spectral efficiencies of 2, 4 and 6 bits/s/Hz. These confirm the superiority of the Dual Alamouti scheme for 2 receive antennas. They also show that for 4 receive antennas, the Dual Alamouti scheme attains similar bit error ratio performance to V-BLAST.

ACKNOWLEDGEMENTS

HS Tan gratefully acknowledges the funding of his PhD research by Toshiba Research Laboratory, Bristol.

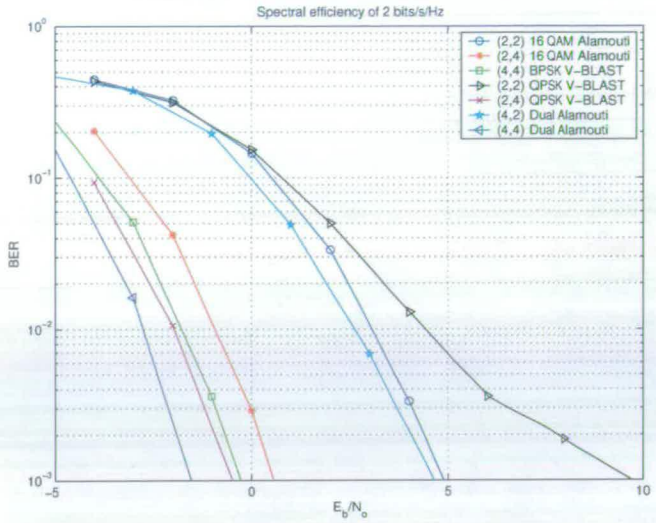

Fig. 3. BER vs SNR performance of the three schemes under consideration for a spectral efficiency of 2 bit/s/Hz, with 2 or 4 Rx antennas.

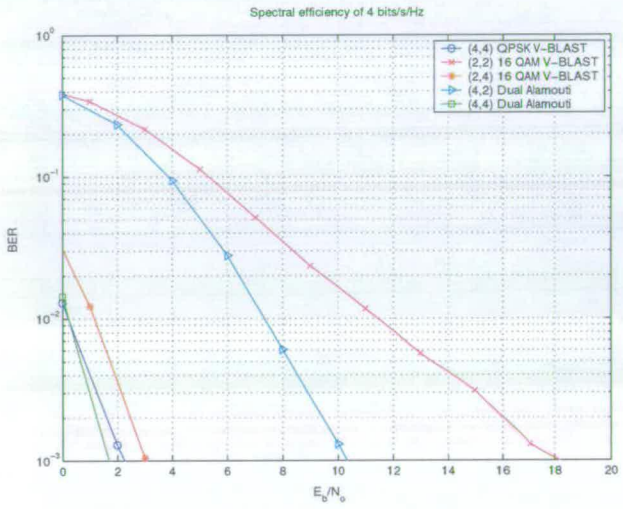

Fig. 4. BER vs SNR performance of the three schemes under consideration for a spectral efficiency of 4 bit/s/Hz, with 2 or 4 Rx antennas.

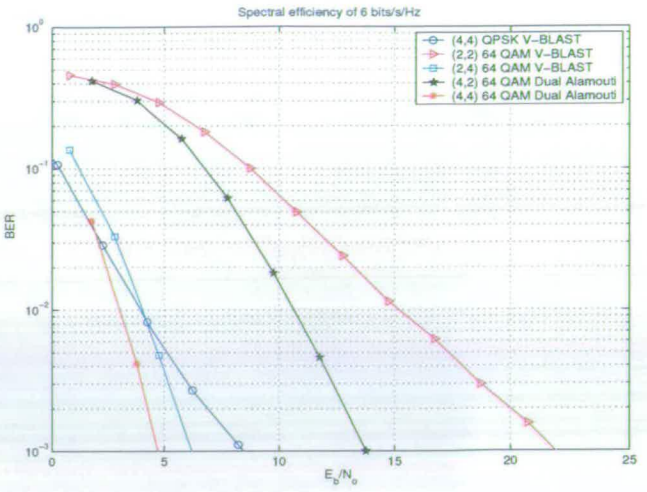

Fig. 5. BER vs SNR performance of the three schemes under consideration for a spectral efficiency of 6 bit/s/Hz, with 2 or 4 Rx antennas.

References

[1] G.D. Golden, G.J. Foschini, R.A. Valenzuela and P.W. Wolniansky, "Detection algorithm and initial laboratory results using V-BLAST space-time communication architecture", *IEE Electronics Letters*, Vol 35(1), pp 14–16, January 1999.

[2] S.M. Alamouti, "A simple transmit diversity technique for wireless communications", *IEEE Journal on Selected Areas in Communications*, Vol 16(8), pp 1451–58, October 1998.

[3] A.F. Naguib et al, "Increasing data rate over wireless channels", *IEEE Signal Processing Magazine*, Vol 17, May 2000.

[4] M. Debbah, B. Muquet, M. de Courville, M. Muck, S. Simoens, and P. Loubaton, "A MMSE successive interference cancellation scheme for a new adjustable hybrid spread OFDM system", *In Proceedings IEEE Vehicular Technology Conference (VTC) Spring 2000, Tokyo (Japan)*, pp 745-749, May 2000.

[5] G.J. Foschini, "Layered space–time architecture for wireless communication in a fading environment when using multi–element antennas", *Bell Labs Technical Journal*, pp 41–59, Autumn 1996.

[6] S.L. Ariyavisitakul, "Turbo Space Time Processing to Improve Wireless Channel Capacity", *IEEE Transactions on Communications*, Vol 48(8), pp 1347-1359, August 2000.

[7] C. Papadias, "On the spectral efficiency of space-time spreading schemes for multiple antenna CDMA systems", *In Proceedings of the IEEE Asilomar Conference on Signals, Systems and Computers, Pacific Grove (USA),*, pp 639–643, November 1999.

INVESTIGATION OF HYBRID MIMO TECHNIQUES

John S. Thompson(†), Hwa Sin Tan(†) and Yong Sun(‡)
(†) Institute for Digital Communications, School of Engineering and Electronics
The University of Edinburgh, Edinburgh, EH9 3JL, UK.
(‡) Toshiba Research Laboratory, Queens Square, Bristol, BS1 4ND, UK
Email: John.Thompson@ed.ac.uk

Keywords: antenna arrays, multiple input–multiple output, V-BLAST, Alamouti scheme.

ABSTRACT

This paper compares and investigates the performance of wireless local area network systems using multiple input–multiple output (MIMO) techniques. In particular, two different algorithms, V-BLAST and space–time block coding (STBC), are described. A third hybrid approach, which incorporates elements of both V-BLAST and STBC is also introduced. All three techniques are compared using both theoretical Shannon capacity analysis and by simulation results for the bit error ratio performance of the three methods. It is shown that the hybrid method attains superior diversity gain performance to V-BLAST and can outperform V-BLAST at spectral efficiencies of practical interest.

I. INTRODUCTION

Multiple antennas are a new solution for high data rate wireless local area networks (WLANs) [1]. They are preferable to increasing the sensitivity of the receiver or increasing the power of the transmitted signal. The latter technique is not effective because the increase in attainable channel capacity is only a logarithmic function of the increase in signal-to-noise ratio (SNR) for the received signal. Moreover, this technique is limited by thermal noise and maximum limits on radiating power in the WLAN frequency bands. This leads to alternative solutions where multiple antennas are deployed at both the transmitter and receiver. The implementation of multiple transmit (Tx) antennas increases the data rate, while the multiple receive (Rx) antennas support the signal processing required to separate the transmitter antennas.

Multiple input-multiple output (MIMO) systems are an effective way to achieve high data rate and spectrally efficient WLANs, as their capacity increase is linearly proportional to the number of antennas employed at the transmitter and receiver. Three different MIMO signal processing techniques will be studied in this paper. These include spatial multiplexing, i.e. an implementation of the vertical Bell Labs layered space-time (V-BLAST) algorithm [1], space-time block coding (STBC) [2] and a hybrid of the BLAST and STBC schemes [3]. The V-BLAST algorithm aims to maximise the capacity by using a combination of spatial processing and subtractive cancellation to remove co-channel interference, provided that the number of antennas at the receiver is greater or equal to that of the transmitter. Conversely, the STBC or Alamouti scheme exploits the diversity against fading that is available from employing multiple antennas at the transmitter and possibly at the receiver. We also consider in this paper a third technique, which is called the Dual Alamouti technique. This method combines elements of both spatial multiplexing (V-BLAST) and STBC to try to exploit the advantages of both higher data rates and increased diversity gain.

In this paper, the Shannon capacity of the three techniques will be investigated theoretically. This analysis will also be complemented by detailed simulation studies of the algorithms, investigating the bit error ratio performance of the three receivers. The results will show that in some cases the Dual Alamouti algorithm can significantly outperform the V-BLAST and STBC techniques. The remainder of this paper is structured as follows. Section II of the paper will describe the system model that is used in the paper. Section III will describe the algorithms to be compared. Section IV will investigate Shannon capacity results for the three techniques. Section V will present simulation results and finally section VI will present conclusions to the paper.

II. SYSTEM MODEL

In this paper, we consider a single user wireless channel, where the transmitter employs M separate Tx antennas and the receiver uses N Rx antennas. This configuration is denoted as the (M, N) MIMO system. The M Tx antennas transmit M synchronous data streams at the same radio carrier frequency. The channel is assumed to be frequency-flat Rayleigh fading. Assuming ideal demodulation to baseband, the receiver signal can be expressed as:

$$\mathbf{r}(k) = \sqrt{P_T/M}\mathbf{H}\mathbf{a}(k) + \boldsymbol{\eta}(k), \qquad (1)$$

where P_T is the power at the transmitter and k denotes the time index. The vector $\mathbf{r}(k)$ is the size N received signal vector $\{r_1(k), r_2(k)...r_N(k)\}^T$ where $r_n(k)$ denotes the received signal at Rx antenna n. Further, $\mathbf{a}(k)$ is the quadrature amplitude modulation (QAM) transmission vector $\{a_1(k), a_2(k)...a_M(k)\}^T$ of size M, where $a_m(k)$ denotes the transmitted QAM symbol at antenna m. The matrix $\mathbf{H}$ is the $N \times M$ channel matrix where the element at row n and column m, $h_{n,m}$ denotes the channel response at receiver n due to

transmitter m. The NM channels $h_{n,m}$ are statistically independent, identically distributed random variables. The vector $\boldsymbol{\eta(k)}$, which equals $\{\eta_1(k), \eta_2(k)...\eta_N(k)\}^T$, represents additive white Gaussian noise at the receiver with zero mean and variance σ^2 where η_n is the noise received at the n-th antenna. A block diagram of the system under consideration can be seen in Fig 1.

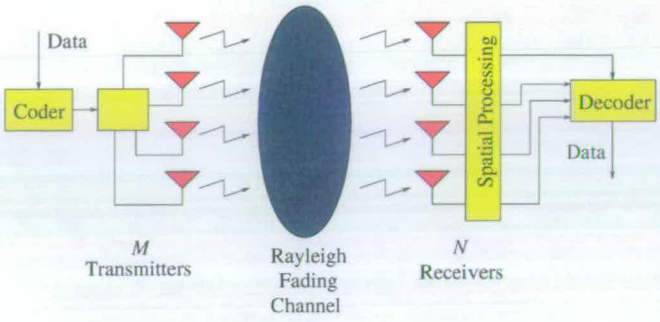

Fig. 1. A diagram of a single user multiple input–multiple output wireless system using M transmit and N receive antennas.

III. MIMO ALGORITHMS UNDER CONSIDERATION

In this section, the three main algorithms will be introduced and explained in turn. These are the V-BLAST algorithm, the Alamouti scheme and the Dual Alamouti MIMO scheme.

A. V-BLAST

V-BLAST[1] is a spatial multiplexing transmission scheme that has the capability to support high data rates which are linearly proportional to the number of Tx and Rx antennas. The architecture of V-BLAST consists of M spatially multiplexed data streams at the transmitter, which are measured at N Rx antennas. For successful operation of the algorithm, it is usually required that $N \geq M$.

The V-BLAST signal processor operates using M detection cycles, one for each Tx antenna. The ordering algorithm selects the antenna with the strongest SNR, followed by the next strongest, until every antenna signal has been detected. Reconstructed signals for the detected antennas are then subtracted from the received signal to remove interference to the remaining undetected antennas. During the detection process, except for the antenna signal to be detected, the interference from antennas yet to be detected must be suppressed. This operation is performed by linearly weighting the received signals to satisfy the minimum mean squared error(MMSE) criterion[4]. The MMSE detector is defined as:

$$\mathbf{G}_1 = \mathbf{H}^H(\mathbf{H}\mathbf{H}^H + \frac{\sigma^2}{P_T/M}\mathbf{I_M})^{-1}, \tag{2}$$

where $\mathbf{I}_M$ is the $M \times M$ identity matrix. The subscript notation $\mathbf{G}_1$ indicates that this matrix is used in the first detection cycle. This $M \times N$ matrix $\mathbf{G}_1$ pre-multiplies the received signal to separate spatially each antenna's signal from all others. This means that data detection can be performed independently on each of the M outputs from the multiplication. In order to determine which transmit antenna has the best SNR at the ith iteration, the following formula for the mth antenna is used:

$$\mathrm{SNR}_i(m) = \frac{|\alpha|^2 E(|a_m|^2)}{\beta_i}, \tag{3}$$

where α and β are defined as:

$$\begin{aligned} \alpha &= \mathbf{G}_i(m)\mathbf{H}(m) \\ \beta_i &= |\mathbf{G}_i(m)|^2\sigma^2 + \sum_{\substack{p=1 \\ p\neq k_1\cdots k_{i-1}}}^{M} |\mathbf{G}_i(m)\mathbf{H}(p)|^2 E(|a_p|^2). \end{aligned} \tag{4}$$

The vector $\mathbf{G}_i(m)$ is the m-th *row* of $\mathbf{G}_i$ calculated after $(i-1)$ detection cycles. Similarly, the vector $\mathbf{H}(m)$ is the mth *column* of $\mathbf{H}$.

The optimal ordering for detection and symbol cancellation makes V-BLAST different from the conventional linear combinatorial nulling. Let $S = \{k_1, k_2, ...k_M\}$ be a permutation of integers from 1 to M specifying the order of detecting the symbol vector $\mathbf{a}$. The soft decision statistic for the mth antenna at iteration i can be formed by multiplying the nulling vector and received signal:

$$y(k_i) = \mathbf{G}_i(k_i) \times \mathbf{r}_i, \tag{5}$$

where $\mathbf{r}_i$ denotes the received signal after subtracting $(i-1)$ previously detected signals . The decision statistic is then quantised in accordance to the constellation in use:

$$\hat{a}(k_i) = \mathrm{Q}[y(k_i)], \tag{6}$$

where Q[ ] is the slicer to its respective constellation in use. The detected data are subtracted from the received signal while the column vectors of $\mathbf{H}$ due to the detected symbols are nulled. Finally, the received signal is updated for the next iteration as follows:

$$\mathbf{r}_{i+1} = \mathbf{r}_i - \hat{a}(k_i) \times \mathbf{H}_i(k_i), \tag{7}$$

where $\mathbf{H}_i(k_i)$ denotes the k_ith column of $\mathbf{H}_i$ after zeroing $(i-1)$ columns matching the $(i-1)$ previously detected signals. The subtraction of the detected data from the received signal aims to minimise errors in the subsequent detection process, provided the detected data possesses a certain degree of accuracy. At the end of the ith detection cycle, the matrix $\mathbf{H}_{i+1}$ is formed by setting column k_i of the matrix $\mathbf{H}_i$ to zero. The MMSE matrix $\mathbf{G}_{i+1}$ must then be re-calculated using equation (2) with $(\mathbf{H}_{i+1})$ used in place of $\mathbf{H}$.

B. Alamouti Scheme

This particular scheme is restricted to using $M = 2$ antennas at the transmitter but can use any number of Rx antennas N. Two QAM symbols a_1 and a_2 for transmission by the Alamouti scheme are encoded in both the space and time domain at the two Tx antennas over two consecutive symbol periods as shown in (8).

$$\mathbf{A} = [\hat{\mathbf{a}}(1)\hat{\mathbf{a}}(2)] = \begin{bmatrix} a_1 & -a_2^* \\ a_2 & a_1^* \end{bmatrix}. \tag{8}$$

In order to decode the signal, the received signal can be expressed as:

$$\begin{aligned} \acute{\mathbf{r}} &= \sqrt{\frac{P_T}{2}}\mathbf{H}_A\acute{\mathbf{a}}(1)+\acute{\boldsymbol{\eta}} \\ \begin{bmatrix} \acute{\mathbf{r}}_1 \\ \acute{\mathbf{r}}_2 \\ \vdots \\ \vdots \\ \acute{\mathbf{r}}_N \end{bmatrix} &= \sqrt{\frac{P_T}{2}} \begin{bmatrix} \mathbf{H}_{A,1} \\ \mathbf{H}_{A,2} \\ \vdots \\ \vdots \\ \mathbf{H}_{A,N} \end{bmatrix} \acute{\mathbf{a}}(1) + \begin{bmatrix} \acute{\eta}_1 \\ \acute{\eta}_2 \\ \vdots \\ \vdots \\ \acute{\eta}_N \end{bmatrix}, \end{aligned} \quad (9)$$

where $\acute{\mathbf{r}}_n = [r_n(0), r_n(1)^*]^T$ is the received signal vector at receiver n during symbol periods $k = 0$ and 1. Similarly, $\acute{\boldsymbol{\eta}}_n = [\eta_n(0), \eta_n(1)^*]^T$ denotes the noise samples at antenna n for the two symbol periods.. The matrix $\mathbf{H}_{A,n}$ is defined as:

$$\mathbf{H}_{A,n} = \begin{bmatrix} h_{n,1} & h_{n,2} \\ -h_{n,2}^* & h_{n,1}^* \end{bmatrix}. \quad (10)$$

Decoding the data is achieved be done by multiplying the received signal with the Hermitian transpose of the channel matrix $\mathbf{H}_A$ as:

$$\begin{aligned} \hat{\mathbf{a}}(1) &= \mathbf{H}_A^H\acute{\mathbf{r}} = \sqrt{\frac{P_T}{2}}\mathbf{H}_A^H\mathbf{H}_A\acute{\mathbf{a}}(1)+\mathbf{H}_A^H\acute{\boldsymbol{\eta}} \\ &= \sqrt{\frac{P_T}{2}} \begin{bmatrix} \gamma & 0 \\ 0 & \gamma \end{bmatrix} \begin{bmatrix} a_1 \\ a_2 \end{bmatrix} + \mathbf{H}_A^H\acute{\boldsymbol{\eta}}. \end{aligned} \quad (11)$$

In this equation $\gamma = \sum_{m=1}^{2}\sum_{n=1}^{N}|h_{(n,m)}|^2$.

C. Dual Alamouti Scheme

In the previous section on the Alamouti scheme, it is seen that for 2 Tx antennas to achieve full diversity, the spectral efficiency of the system is the same as that of a single transmitter antenna. In order to improve on the spectral efficiency of the system, a 4 Tx structure is now considered, where the Alamouti scheme is applied separately to two pairs of antennas. This means that two data streams are spatially multiplexed on two different pairs of antennas. The received signal for this transmitter configuration may be written in a similar manner to (9):

$$\begin{aligned} \mathbf{r}' &= \sqrt{\frac{P_T}{4}}\mathbf{H}_D\mathbf{a}(1)+\boldsymbol{\eta}' \\ \begin{bmatrix} \acute{\mathbf{r}}_1 \\ \acute{\mathbf{r}}_2 \\ \vdots \\ \acute{\mathbf{r}}_N \end{bmatrix} &= \sqrt{\frac{P_T}{4}} \begin{bmatrix} \mathbf{H}_{A,1} & \mathbf{H}_{B,1} \\ \mathbf{H}_{A,2} & \mathbf{H}_{B,2} \\ \vdots & \vdots \\ \mathbf{H}_{A,N} & \mathbf{H}_{B,N} \end{bmatrix} \mathbf{a}(1) + \begin{bmatrix} \acute{\boldsymbol{\eta}}_1 \\ \acute{\boldsymbol{\eta}}_2 \\ \vdots \\ \acute{\boldsymbol{\eta}}_N \end{bmatrix} \end{aligned} \quad (12)$$

In this equation,the vector $\mathbf{a}(1) = [a_1, a_2, a_3, a_4]^T$, where the quantities a_3 and a_4 represent the QAM symbols for the second Alamouti-encoded data stream which are transmitted simultaneously with a_1 and a_2. The matrix $\mathbf{H}_{B,m}$ is defined as:

$$\mathbf{H}_{B,n} = \begin{bmatrix} h_{n,3} & h_{n,4} \\ -h_{n,4}^* & h_{n,3}^* \end{bmatrix}, \quad (13)$$

Unlike equation (11), the two symbol pairs (a_1, a_2) and (a_3, a_4) interfere with one another, so simple linear decoding is no longer optimal. However, the form of equation (12) means that the V-BLAST algorithm can be applied directly to detect the data symbols $a_1 - a_4$. As with the Alamouti scheme, the structure of the Dual Alamouti scheme means that a_1 and a_2 do not interfere with one another, which is also the case for a_3 and a_4. The dimension of $\mathbf{r}'$ in equation (12) is $2N$, which means that the transmissions of 4 Tx antennas can be successfully decoded with only 2 Rx antennas.

IV. SHANNON CAPACITY COMPARISONS

In this section, Shannon capacity results for the three algorithms under consideration will be revised. Under the assumption of unit bandwidth, the Shannon capacity of the MIMO system shown in equation (1) is given by the formula [5]:

$$C_1 = \log_2 \det\left(\mathbf{I}_M + \frac{P_T}{M\sigma^2}\mathbf{H}^H\mathbf{H}\right) \quad \text{(bits/sec/Hz)}. \quad (14)$$

In this formula, det( ) denotes the matrix determinant operation. This formula assumes that the transmitter possesses no knowledge of the channel matrix $\mathbf{H}$. It has been shown, in for example [6], that the MMSE V-BLAST detector can achieve the full Shannon capacity C_1. This holds under the constraint that at capacity, decoding of each transmitter's signal can be performed error-free, so that the subtractive cancellation process in equation (7) is performed perfectly.

In order to calculate the capacity of the Alamouti scheme, we can notice that equation (9) has the same general form as (1). So, equation (14) can also be applied to this system. However, the vector $\mathbf{r}'$ is measured over two consecutive symbol periods. For consistent results, the effective bandwidth of the system must be divided by two in compensation. So, the following result is obtained [7]:

$$C_2 = \frac{1}{2}\log_2 \det\left(\mathbf{I}_2 + \frac{P_T}{2\sigma^2}\mathbf{H}_A^H\mathbf{H}_A\right) = \log_2\left(1+\frac{P_T\gamma}{2\sigma^2}\right). \quad (15)$$

The RHS of this equation may be obtained from the LHS by noticing the orthogonal structure of the matrix product $\mathbf{H_A^H H_A}$ in equation (11).

Again, the capacity of the Dual Alamouti scheme may be obtained by noticing that equation (12) has the same general form as (1). As with the Alamouti scheme, the bandwidth must be scaled by a factor of two to compensate for $\mathbf{r}'$ being measured over two consecutive symbol periods. This time, the resulting capacity equation is:

$$C_3 = \frac{1}{2}\log_2 \det\left(\mathbf{I}_4 + \frac{P_T}{4\sigma^2}\mathbf{H}_D^H\mathbf{H}_D\right). \quad (16)$$

The matrix $\mathbf{H}_D$ is defined in equation (12). The equations for $C_1 - C_3$ may be evaluated to compare the achievable Shannon capacities of the three systems.

V. SIMULATION RESULTS

In this section results are initially presented for the Shannon capacity of the different schemes. Then, results are presented

for the bit error ratio (BER) vs SNR performance of the different schemes, to compare with the capacity results.

A. Capacity Results

In this section, the results obtained from evaluating the formulas for $C_1 - C_3$ in section IV are compared. This is done by generating 10,000 sample $\mathbf{H}$ matrices and using these to evaluate the channel capacity at different SNRs. The results are presented as 1% outage capacities — that is, the capacity that is exceeded for 99% of all channel realisations.

The results for two Rx antennas are presented in Fig 2 (a). In this case, it can be seen that the (4,2) Dual Alamouti scheme provides a distinct performance advantage over the (2,2) V-BLAST or Alamouti schemes at high SNRs. In part (b) of the figure, results for four Rx antennas are presented. It can be seen that at lower SNRs, the (4,4) V-BLAST and Dual Alamouti schemes achieve similar capacity results. However, at higher SNRs, (4,4) V-BLAST begins to out-perform the Dual Alamouti scheme. Both of these techniques perform better than (2,4) Alamouti or V-BLAST.

B. Frame Error Ratio Results

Results for the BER vs SNR performance of the different schemes will now be considered. In all of these simulations, a rate 1/2, constraint length 7 code was employed, using soft decision Viterbi decoding. A frame length of 3066 data bits was used at the transmitter for encoding and transmission.

The first results presented in Fig 3 compare the performance of the three schemes for a spectral efficiency of 2 bits/s/Hz. Looking first to the schemes with 2 Rx antennas, it can be seen that the (2,2) V-BLAST method provides the poorest performance. The (2,2) Alamouti scheme performs slightly better, while the (4,2) Dual Alamouti scheme provides the best performance. Moving on to 4 Rx antennas, it can be seen that (2,4) Alamouti provides the poorest performance, while (2,4) V-BLAST slightly outperforms (4,4) V-BLAST. Again the (4,4) Dual Alamouti scheme provides the best performance of all techniques considered.

The spectral efficiency of the MIMO system was increased to 4 bits/s/Hz for the second set of simulations, the results of which are shown in Fig 4. In this case, results are only shown for V-BLAST and Dual Alamouti, as the Alamouti scheme would require to use at least 256 QAM to achieve the desired spectral efficiency. Again, it can be seen that for 2 Rx antennas, the Dual Alamouti scheme performs significantly better than V-BLAST. For 4 Rx antennas, the Dual Alamouti and V-BLAST schemes achieve similar performances for 4 transmit antennas.

Finally, the simulations were updated to consider a somewhat higher spectral efficiency of 6 bits/s/Hz. The simulation results for this case are shown in Fig 5. Again, results are only shown for V-BLAST and Dual Alamouti, as the Alamouti scheme would require to use at least 4096 QAM. For two Rx antennas, it can again be seen that the (4,2) Dual Alamouti scheme achieves a significant performance advantage over the (2,2) V-BLAST configuration. For four Rx antennas, the (4,4) Dual Alamouti scheme performs better than either (2,4) or (4,4) V-BLAST at low SNRs.

(a)

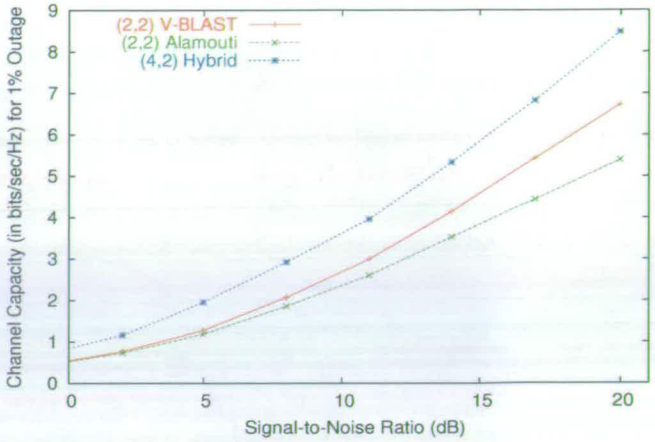

(b)

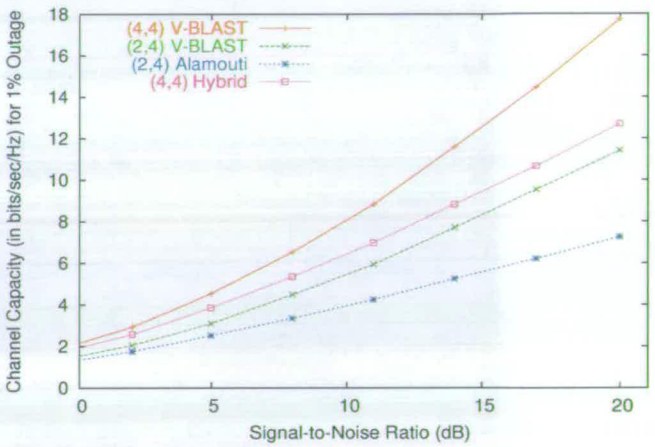

Fig. 2. Shannon capacity vs SNR performance of the three schemes under consideration for (a) 2 Rx and (b) 4 Rx antennas.

VI. CONCLUSIONS

This paper has compared the performance of V-BLAST, the Alamouti STBC and the hybrid Dual Alamouti scheme. Results for the Shannon capacity of the three systems shows that for 2 receive antennas, the Dual Alamouti scheme provides the best performance. In the case of 4 receive antennas, the V-BLAST algorithm attains the best spectral efficiency at high SNRs. Simulation results for the bit error ratio performance of the algorithms using convolutionally coded modulation have also been presented for spectral efficiencies of 2, 4 and 6 bits/s/Hz. These confirm the superiority of the Dual Alamouti scheme for 2 receive antennas. They also show that for 4 receive antennas, the Dual Alamouti scheme attains similar bit error ratio performance to V-BLAST.

ACKNOWLEDGEMENTS

HS Tan gratefully acknowledges the funding of his PhD research by Toshiba Research Laboratory, Bristol.

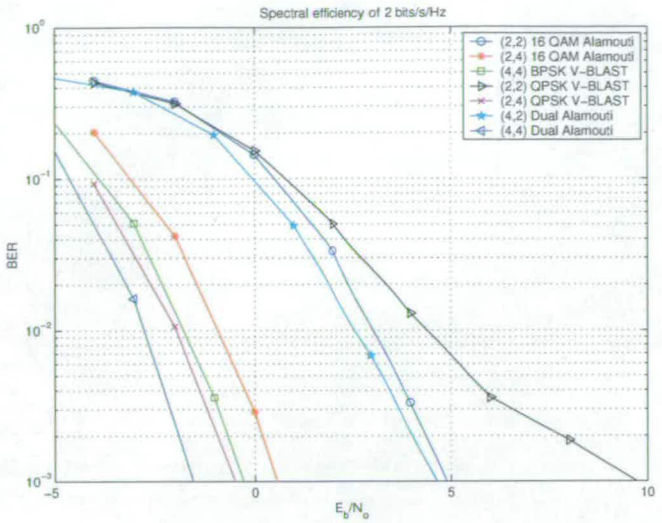

Fig. 3. BER vs SNR performance of the three schemes under consideration for a spectral efficiency of 2 bit/s/Hz, with 2 or 4 Rx antennas.

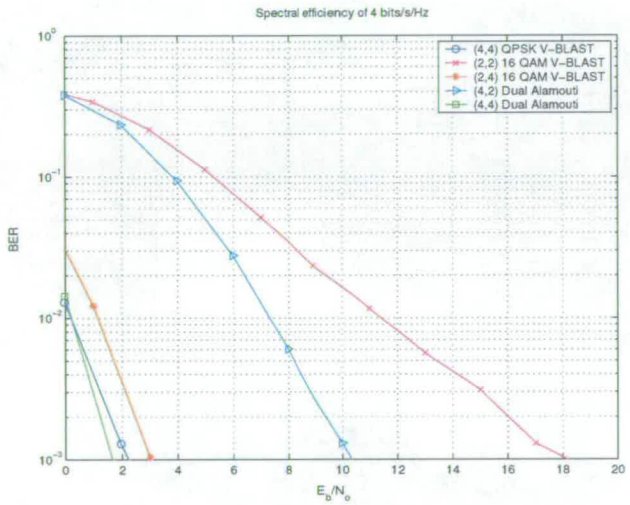

Fig. 4. BER vs SNR performance of the three schemes under consideration for a spectral efficiency of 4 bit/s/Hz, with 2 or 4 Rx antennas.

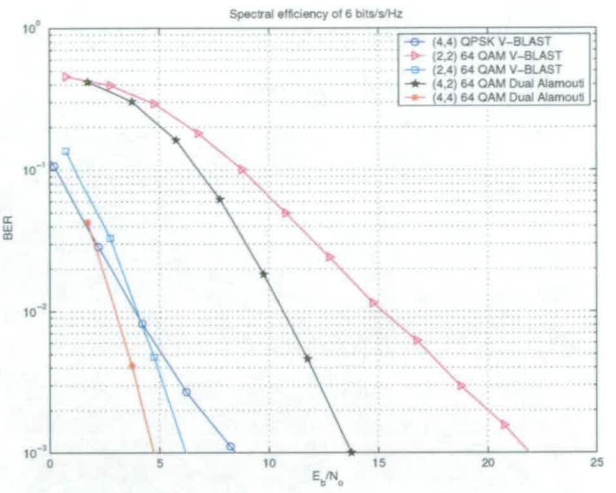

Fig. 5. BER vs SNR performance of the three schemes under consideration for a spectral efficiency of 6 bit/s/Hz, with 2 or 4 Rx antennas.

REFERENCES

[1] G.D. Golden, G.J. Foschini, R.A. Valenzuela and P.W. Wolniansky, "Detection algorithm and initial laboratory results using V-BLAST space-time communication architecture", *IEE Electronics Letters*, Vol 35(1), pp 14–16, January 1999.

[2] S.M. Alamouti, "A simple transmit diversity technique for wireless communications", *IEEE Journal on Selected Areas in Communications*, Vol 16(8), pp 1451–58, October 1998.

[3] A.F. Naguib et al, "Increasing data rate over wireless channels", *IEEE Signal Processing Magazine*, Vol 17, May 2000.

[4] M. Debbah, B. Muquet, M. de Courville, M. Muck, S. Simoens, and P. Loubaton, "A MMSE successive interference cancellation scheme for a new adjustable hybrid spread OFDM system", *In Proceedings IEEE Vehicular Technology Conference (VTC) Spring 2000, Tokyo (Japan)*, pp 745-749, May 2000.

[5] G.J. Foschini, "Layered space–time architecture for wireless communication in a fading environment when using multi–element antennas", *Bell Labs Technical Journal*, pp 41–59, Autumn 1996.

[6] S.L. Ariyavisitakul, "Turbo Space Time Processing to Improve Wireless Channel Capacity", *IEEE Transactions on Communications*, Vol 48(8), pp 1347-1359, August 2000.

[7] C. Papadias, "On the spectral efficiency of space-time spreading schemes for multiple antenna CDMA systems", *In Proceedings of the IEEE Asilomar Conference on Signals, Systems and Computers, Pacific Grove (USA),*, pp 639–643, November 1999.